



MDOT State Study 286 - Performance Evaluation of Highway Slopes on Yazoo Clay

FINAL REPORT



Mohammad Sadik Khan, Ph.D., P.E.

Farshad Amini, Ph.D., P.E.

Masoud Nobahar

Department of Civil and Environmental Engineering,

Jackson State University,

1400 J.R. Lynch Street, JSU Box 17068

Jackson, MS 39217-0168, USA

June 30, 2020

FHWA Technical Report Documentation Page

1. Report No. FHWA/MDOT-RD-20-286	2. Government Accession No.	3. Recipient's Catalog No.	
4. Title and Subtitle Performance Evaluation of Highway Slopes on Yazoo Clay		5. Report Date: June 30, 2020	
7. Author(s) Mohammad Sadik Khan, Ph.D., P.E. https://orcid.org/0000-0002-0150-6105 Farshad Amini, Ph.D., P.E., F.ASCE https://orcid.org/0000-0003-2899-0045 Masoud Nobahar https://orcid.org/0000-0001-8457-7234		6. Performing Organization Code Leave blank but delete this	
		8. Performing Organization Report No. State Study 286	
9. Performing Organization Name and Address Mississippi Department of Transportation PO Box 1850 Jackson, MS 39215-1850		10. Work Unit No. (TRAIS)	
		11. Contract or Grant No. SPR-2017(028)/107691-1011000	
12. Sponsoring Agency Name and Address		13. Type Report and Period Covered Feb 27, 2018 to June 30, 2020	
		14. Sponsoring Agency Code	
15. Supplementary Notes			
<p>16. Abstract</p> <p>Slope failures are frequent in highway embankments on expansive Yazoo clay in Mississippi due to frequent seasonal rainfall events associated with temperature and humidity variation causing expensive maintenance problems for the Mississippi Department of Transportation (MDOT). This State Study 286 was conducted to understand the performance of highway slopes containing Yazoo clay. Six repaired highway slopes were instrumented comprehensively to monitor the moisture, matric suction, and temperature variation, as well as monitoring the slope deformation using vertical inclinometers. Besides field monitoring, numerical modeling using the Finite Element Method (FEM) was conducted to evaluate the effect of rainfall frequency and duration (based on historical rainfall data of Mississippi) on the water infiltration and corresponding change in the factor of safety of the highway slope. Based on the field monitoring results, the data of volumetric moisture content and matric suction readings were observed constant throughout all six slopes. Certain peaks and drops in the moisture content were also observed during the summer months. The numerical modeling analyses indicates the rainfall during late summer to early fall is the most critical time in which a perched water condition will develop. As the wet-dry cycle soften the shear strength of high plastic clay to fully softened state the presence of perched water creates a slope condition vulnerable to a creeping slide failure. Based on this research, it is observed that slope failures of Highway embankments containing highly plastic clays such as Yazoo clay takes place due to the development of perched water conditions after five to seven years of construction. It is highly recommended to consider including a perched water zone up to the depth of the active zone along with the development of fully soften shear strength condition in the slope stability analysis of any slope containing high volume change clays, such as Yazoo clay.</p>			
17. Key Words Expansive Soil, Performance, Instrumentation, FEM Analysis		18. Distribution Statement Unclassified	
19. Security Classif. Unclassified	20. Security Classif. Unclassified	21. No. of Pages: 254	22. Price

DISCLAIMER

Jackson State University and the Mississippi Department of Transportation do not endorse service providers, products, or manufacturers. Trade names or manufacturers' names appear herein solely because they are considered essential to the purpose of this report. The contents of this report do not necessarily reflect the views and policies of the sponsor agency.

MDOT STATEMENT OF NONDISCRIMINATION

The Mississippi Department of Transportation (MDOT) operates its programs and services without regard to race, color, national origin, sex, age or disability in accordance with Title VI of the Civil Rights Act of 1964, as amended and related statutes and implementing authorities.

MISSION STATEMENTS

The Mississippi Department of Transportation (MDOT)

MDOT is responsible for providing a safe intermodal transportation network that is planned, designed, constructed and maintained in an effective, cost efficient and environmentally sensitive manner.

The Research Division

MDOT Research Division supports MDOT's mission by administering Mississippi's State Planning and Research (SP&R) Part II funds in an innovative, ethical, accountable, and efficient manner, including selecting and monitoring research projects that solve agency problems, move MDOT forward, and improve the network for the traveling public.

ACKNOWLEDGMENTS

The authors sincerely appreciate the contribution of Griffin Sullivan, P.E., Mike Stroud, P.E., of MDOT Material Division and Cindy Smith, P.E. and Alex Middleton, P.E. of Research Division throughout the study. Authors also sincerely acknowledge the contribution of Sean Ferguson, P.E. in setting up this study.

TABLE OF CONTENT

DISCLAIMER.....	ii
MDOT STATEMENT OF NONDISCRIMINATION.....	iii
MISSION STATEMENTS.....	iii
ACKNOWLEDGMENTS.....	iv
EXECUTIVE SUMMARY.....	xxii
Chapter 1 : INTRODUCTION.....	1
1.1 Background.....	1
1.2 Problem Statement.....	2
1.3 Research Objective and Major Tasks.....	6
Chapter 2 : LITERATURE REVIEW.....	7
2.1 Expansive Soil.....	7
2.2 Identification of Expansive Clay.....	7
2.2.1 Identification by Atterberg Limits.....	7
2.2.2 Clay Minerals and Its Effect on the plasticity.....	8
2.2.3 Indirect Measurement of Potential Swell.....	9
2.2.4 Variation of Shear Strength of Highly Plastic Clay soil.....	13
2.2.5 Climate and hydrological condition.....	15
2.3 Yazoo Clay.....	16
2.3.1 Engineering Aspects of Yazoo Clay.....	17
2.3.2 Synopsis of Regional Observations.....	20
2.3.3 Extended Mohr-Coulomb failure envelope.....	22
2.3.4 Effect of the wet-dry cycle of Yazoo clay.....	23
2.3.5 Progressive change on Shear Strength.....	28
2.3.6 Permeability.....	34

Chapter 3 : SITE LOCATION AND SITE INVESTIGATION	39
3.1 Site Selection	39
3.2 Slope 1: I220N Ramp Toward I55N Highway Slope	40
3.2.1 Investigation of CPT Testing	41
3.2.2 Soil Parameters from CPT	44
3.3 Slope 2: Metro Center Highway Slope	46
3.3.1 Investigation of CPT Testing	50
3.3.2 Soil Parameters from CPT	50
3.4 Slope 3: Terry Road Site Highway Slope	53
3.4.1 Investigation of CPT Testing	56
3.4.2 Soil Parameters from CPT	56
3.5 Slope 4: Highland Drive Highway Slope.....	59
3.5.1 Investigation of CPT Testing	61
3.5.2 Soil Parameters from CPT	62
3.6 Slope 5: Sowell Road Highway Slope	65
3.6.1 Investigation of CPT Testing	67
3.6.2 Soil Parameters from CPT	68
3.7 Slope 6: McRaven Road Highway Slope.....	71
3.7.1 Investigation of CPT Testing	73
3.7.2 Soil Parameters from CPT	74
Chapter 4 : FIELD INSTRUMENTATION AND MONITORING.....	77
4.1 Field Instrumentation	77
4.2 Slope 1: I220N Ramp Toward I55N Highway Slope	79
4.2.1 Field Monitoring Results	82
4.3 Slope 2: Metro Center Highway Slope	88

4.3.1 Field Monitoring Results	89
4.4 Slope 3: Terry Road Highway Slope	95
4.4.1 Field Monitoring Results	96
4.5 Slope 4: Highland Drive Highway Slope.....	102
4.5.1 Field Monitoring Results	103
4.6 Slope 5: Sowell Road Highway Slope	109
4.6.1 Field Monitoring Result.....	110
4.7 Slope 6: McRaven Road Highway Slope.....	117
4.7.1 Field Monitoring Results	118
4.8 I220S Ramp Toward I20E/US49S Highway Slope	124
4.9 Discussion	125
4.9.1 Determination of Active Zone	125
Chapter 5 : NUMERICAL INVESTIGATION.....	133
5.1 Finite Element Method (FEM).....	133
5.1.1 Flow Analysis	133
5.1.2 Coupled flow-deformation and safety Analysis.....	133
5.2 Slope 1: I220N Ramp Toward I55N Highway Slope	134
5.2.1 Flow Analysis	134
5.2.2 FEM Flow Analysis Results	136
5.3 Slope 2: Metro Center Highway Slope	138
5.3.1 Coupled Flow-Deformation and Safety Analysis	138
5.3.2 FEM Flow Analysis Results	139
5.3.3 Stability Analysis.....	147
5.3.4 FEM Stability Analysis Results	147
5.4 Slope 3: Terry Road Highway Slope	155

5.4.1 Flow Analysis	155
5.4.2 Comparison of Flow Analysis Results between Slope 1, Slope 3 and Slope 6.....	159
5.4.3 Stability Analysis	161
5.5 Slope 4: Highland Drive Highway Slope.....	163
5.5.1 Flow Analysis	163
5.6 Sowell Road Highway Slope	166
5.6.1 Field Investigation Results.....	166
5.6.2 Coupled Hydro-Mechanical and Stability Analysis.....	168
5.6.3 Stability Analysis Results	174
5.6.4 Effect of Uniaxial Geogrid- Soil Interaction.....	174
5.7 McRaven Road Highway Slope.....	176
5.7.1 Flow Analysis	176
5.7.2 Stability Analysis	180
Chapter 6 : CONCLUSIONS	182
6.1 Conclusion	182
6.2 Major Findings.....	182
REFERENCES	184

LIST OF FIGURES

Figure 1.1	(a) Total Precipitation map (b) Drought map (c) Yazoo clay profile in Mississippi (d) Shallow slope failure	2
Figure 1.2	Comparisons of peak, residual and fully softened shear strength (redrawn after Skempton, 1977)	3
Figure 1.3	Instrumentation results at the crest of the slope (a) daily rainfall data (b) Moisture content and matric suction at 1.2 m depth (Hossain et al., 2016)	4
Figure 1.4	(a) Schematic of rainfall intrusion through desiccation crack (b) Boundary conditions for the flow model (c) Suction profile of slope before rainfall (d) Suction profile 16 hours after rainfall (e) Suction profile 2 days after rainfall (f) Suction profile 7 days after rainfall (Khan et al., 2016).....	5
Figure 2.1	Atterberg limits description, volume change and generalized stress-strain response of expansive soils (redrawn After Holtz and Kovacs (1981))	8
Figure 2.2	Diagram of the structures of (a) Kaolinite, (b) Illite, and (c) montmorillonite (Das, 2010).....	9
Figure 2.3	Scanning Electron Microscope Image (a) Kaolinite, and (b) Illite (Das, 2010).....	9
Figure 2.4	The plot of clay minerals on Casagrande’s chart (redrawn after Chleborad et al. (2008)).....	10
Figure 2.5	Chart for evaluation of potential expansiveness (Seed et al. (1960))	11
Figure 2.6	Classification chart for swelling potential proposed by Carter and Bentley (1991).....	12
Figure 2.7	Comparisons of peak, residual and fully softened shear strength (Skempton (1970))	13
Figure 2.8	Shear strength envelopes regarding effective stress (a) Beaumont clay (b) Paris clay (Kayyal and Wright (1991)).....	15
Figure 2.9	Boundary boxes of the Jackson Formation, including Yazoo clay and its geological equivalents, in Mississippi, Alabama, and Louisiana (after USGS 2010).....	16
Figure 2.10	Box plots showing a range of depths for visually-classified samples (Lee (2012))	18
Figure 2.11	Volume change percent (VC%) values for all Yazoo clay data in the 5-county area of central Mississippi, plotted by elevation above mean sea level (MSL) (Lee (2012)).....	19
Figure 2.12	Regional weathered plus un-weathered Yazoo clay VC % and Atterberg limit values, averaged by 5-ft (1.524m) depth intervals (Lee (2012)).....	20

Figure 2.13 Dry density versus natural water content for all Yazoo clay data in the 5-county area of central Mississippi (Lee (2012))	20
Figure 2.14 Extended Mohr-Coulomb failure envelope for unsaturated soils (Fredlund and Rajardjo, 1993)	23
Figure 2.15 Soil water retention curve of Yazoo clay (Nobahar et al., 2019)	23
Figure 2.16 Vertical deformation curve of Yazoo clay sample at (a) 3 wet-dry cycles (b) 5 wet-dry cycles (c) 7 wet-dry cycles	25
Figure 2.17 Change in void ratio with different wet-dry cycles	26
Figure 2.18 Change in pore space of Yazoo clay using SEM imaging after the sample subjected to (a) 3 wet-dry cycles (b) 5 wet-dry cycles (c) 7 wet-dry cycles.....	27
Figure 2.19 Mohr-coulomb failure envelopes of the samples subjected to different wet-dry cycles	28
Figure 2.20 Peak drained shear strength curves for three applied normal stresses.....	29
Figure 2.21 Sample preparation from the slurry mix to fully soften shear strength, (a) Shredding (b) Slaking (c) Blending and (d) Sieving	30
Figure 2.22 Fully soften shear strength curves for three applied normal stresses	31
Figure 2.23 Shear Stress variations with time for residual shear strength test (a) Normal Stress of 25kPa (b) Normal Stress of 50kPa and (c) Normal Stress of 100kPa	32
Figure 2.24 Residual shear strength curves for three applied normal stresses.....	33
Figure 2.25 Mohr-coulomb failure envelopes of the samples subjected to different wet-dry cycles	33
Figure 2.26 Propagation of desiccation at different wet-dry cycle (a) 1N (b) 2N (3N).....	34
Figure 2.27 Laboratory hydraulic conductivity set up (a) Mini disk Infiltrometer (b) Testing of the samples using Mini Disk Infiltrometer.....	35
Figure 2.28 Change in Hydraulic conductivity of different initial moisture contents at different wet-dry cycle	36
Figure 2.29 Laboratory hydraulic conductivity set up (a) Yazoo clay soil sample with instrumented moisture sensors (b) Drying cycle simulation process with the instrumented samples	36
Figure 2.30 Variation of volumetric moisture content overtime at 3N wet-dry cycle (a) change in volumetric moisture content for 20% and 25% initial moisture contents at different sample depth (b) change in volumetric moisture content for 10%, 15% and 35% initial moisture contents.....	37

Figure 3.1	I220N Ramp Toward I55N highway slope location and side view.....	40
Figure 3.2	Assigning CPT location at I220N Ramp Toward I55N highway slope	42
Figure 3.3	Conducting CPT test at I220N Ramp Toward I55N highway slope	43
Figure 3.4	Piezo Cone Penetration Test (CPT) results at the crest of highway slope I220N Ramp Toward I55N at CPT 1.....	43
Figure 3.5	I220N Ramp Toward I55N highway slope CPT analyzed results for peak friction angle (a) crest of the slope (b) middle of the slope (c) toe of the slope	44
Figure 3.6	I220N Ramp Toward I55N highway slope CPT analyzed results for undrained shear strength (a) crest of the slope (b) middle of the slope (c) toe of the slope	45
Figure 3.7	I220N Ramp Toward I55N highway slope CPT analyzed results for dry unit weight (a) crest of the slope (b) middle of the slope (c) toe of the slope	45
Figure 3.8	I220N Ramp Toward I55N highway slope CPT analyzed results for Young’s modulus (a) crest of the slope (b) middle of the slope (c) toe of the slope	46
Figure 3.9	Metro center highway slope location and side view.....	47
Figure 3.10	CPT and Boring Locations at Slope 2	49
Figure 3.11	Field Activity of CPT test at Metro center highway slope	50
Figure 3.12	Piezo Cone Penetration Test (CPT) results at the crest of highway slope Metro Center	50
Figure 3.13	Metro center highway slope CPT analyzed results for peak friction angle (a) crest of the slope (b) middle of the slope (c) toe of the slope.....	51
Figure 3.14	Metro center highway slope CPT analyzed results for undrained shear strength (a) crest of the slope (b) middle of the slope (c) toe of the slope	51
Figure 3.15	Metro center highway slope CPT analyzed results for dry unit weight (a) crest of the slope (b) middle of the slope (c) toe of the slope	52
Figure 3.16	Metro center highway slope CPT analyzed results for Young’s modulus (a) crest of the slope (b) middle of the slope (c) toe of the slope.....	52
Figure 3.17	Terry road highway slope location and side view	53
Figure 3.18	CPT and Borehole locations at Terry Road Site.....	55
Figure 3.19	Piezo Cone Penetration Test (CPT) results at the crest of highway slope Terry Road	56

Figure 3.20 Terry road highway slope CPT analyzed results for peak friction angle (a) crest of the slope (b) middle of the slope (c) toe of the slope.....	57
Figure 3.21 Terry road highway slope CPT analyzed results for undrained shear strength (a) crest of the slope (b) middle of the slope (c) toe of the slope	57
Figure 3.22 Terry road highway slope CPT analyzed results for dry unit weight (a) crest of the slope (b) middle of the slope (c) toe of the slope	58
Figure 3.23 Terry road highway slope CPT analyzed results for Young’s modulus (a) crest of the slope (b) middle of the slope (c) toe of the slope	58
Figure 3.24 Highland drive highway slope location and side view	59
Figure 3.25 CPT location at Slope 4.....	61
Figure 3.26 Field activity of CPT at Highland drive highway slope	62
Figure 3.27 Piezo Cone Penetration Test (CPT) results at the crest of Slope 4.....	62
Figure 3.28 Highland drive highway slope CPT analyzed results for peak friction angle (a) crest of the slope (b) middle of the slope (c) toe of the slope	63
Figure 3.29 Highland drive highway slope CPT analyzed results for undrained shear strength (a) crest of the slope (b) middle of the slope (c) toe of the slope	63
Figure 3.30 Highland drive highway slope CPT analyzed results for dry unit weight (a) crest of the slope (b) middle of the slope (c) toe of the slope.....	64
Figure 3.31 Highland drive highway slope CPT analyzed results for Young’s modulus (a) crest of the slope (b) middle of the slope (c) toe of the slope.....	64
Figure 3.32 Sowell road highway slope location and side view	65
Figure 3.33 Assigning CPT location at Sowell road highway slope.....	67
Figure 3.34 (a) Field Activities, (b) CPT results at the crest of Slope 5.....	68
Figure 3.35 Sowell road highway slope CPT analyzed results for peak friction angle (a) crest of the slope (b) middle of the slope (c) toe of the slope.....	69
Figure 3.36 Sowell road highway slope CPT analyzed results for undrained shear strength (a) crest of the slope (b) middle of the slope (c) toe of the slope	69
Figure 3.37 Sowell road highway slope CPT analyzed results for dry unit weight (a) crest of the slope (b) middle of the slope (c) toe of the slope	70

Figure 3.38 Sowell road highway slope CPT analyzed results for Young’s modulus (a) crest of the slope (b) middle of the slope (c) toe of the slope.....	70
Figure 3.39 McRaven Road highway slope location and side view	71
Figure 3.40 Assigning CPT location at McRaven Road highway slope.....	73
Figure 3.41 Conducting CPT test at McRaven Road highway slope.....	74
Figure 3.42 Piezo Cone Penetration Test (CPT) results at the crest of highway slope McRaven Road....	74
Figure 3.43 McRaven Road highway slope CPT analyzed results for peak friction angle (a) crest of the slope (b) middle of the slope (c) toe of the slope	75
Figure 3.44 McRaven Road highway slope CPT analyzed results for undrained shear strength (a) crest of the slope (b) middle of the slope (c) toe of the slope	75
Figure 3.45 McRaven Road highway slope CPT analyzed results for dry unit weight (a) crest of the slope (b) middle of the slope (c) toe of the slope.....	76
Figure 3.46 McRaven Road highway slope CPT analyzed results for Young’s modulus (a) crest of the slope (b) middle of the slope (c) toe of the slope	76
Figure 4.1 (a) Instrumentation layout at each slope, (b) image of individual sensors	77
Figure 4.2 Field sensor preparation.....	78
Figure 4.3 Field sensor color-coding set up.....	79
Figure 4.4 Layout of the instrumentation at Slope 1.....	80
Figure 4.5 Slope 1 sensor installation	81
Figure 4.6 Slope 1 slope inclinometer installation.....	82
Figure 4.7 Horizontal displacements of the Inclinometer 1 at Slope 1	83
Figure 4.8 Variation of lateral deformation at the top of inclinometer at Slope 1 as-built section.....	83
Figure 4.9 Horizontal displacements of the Inclinometer 2 at Slope 1	84
Figure 4.10 SI2 Variation of lateral deformation at Slope 1 repaired section	84
Figure 4.11 In situ variation of (a) matric suction (b) moisture content with rainfall across instrumentation 1 at Slope 1	85
Figure 4.12 In situ variation of (a) matric suction (b) moisture content with rainfall across instrumentation 2 at Slope 1	85

Figure 4.13 In situ variation of (a) matric suction (b) moisture content with rainfall across instrumentation 3 at Slope 1	86
Figure 4.14 Combined air and soil temperature variation Slope 1 (a) at the crest (b) at the middle (c) at the toe	87
Figure 4.15 Instrumentation layout at Slope 2	88
Figure 4.16 Field Activities photo at Slope 2.	88
Figure 4.17 Incliner casing at Slope 2.....	89
Figure 4.18 Horizontal displacements of the Incliner 1 at Slope 2.....	90
Figure 4.19 Variation of lateral deformation at the top of Incliner 1 at Slope 2.....	90
Figure 4.20 Horizontal displacements of the Incliner 2 at Slope 2.....	91
Figure 4.21 Variation of lateral deformation at the top of Incliner 2 at Slope 2.....	91
Figure 4.22 In situ variation of (a) matric suction (b) moisture content with rainfall across instrumentation 1 at Slope 2.....	92
Figure 4.23 In situ variation of (a) matric suction (b) moisture content with rainfall across instrumentation 2 at Slope 2.....	93
Figure 4.24 In situ variation of (a) matric suction (b) moisture content with rainfall across instrumentation 3 at Slope 2.....	93
Figure 4.25 Combined air and soil temperature variation (a) at the crest (b) at the middle (c) at the toe of the slope at Metro Center highway slope	94
Figure 4.26 Instrumentation layout at Slope 3.....	95
Figure 4.27 Field Instrumentation Activities at Slope 3	96
Figure 4.28 Incliner casting at Slope 3	96
Figure 4.29 Horizontal displacements of the Incliner 1 at Slope 3.....	97
Figure 4.30 Variation of lateral deformation at the to of Incliner 1 at Slope 3.....	97
Figure 4.31 Horizontal displacements of the Incliner 2 at Slope 3.....	98
Figure 4.32 Variation of lateral movement at the top of Incliner 2 at Slope 3.	98
Figure 4.33 In situ variation of (a) matric suction (b) moisture content with rainfall across instrumentation 1 at Terry Road highway slope.....	99

Figure 4.34 In situ variation of (a) matric suction (b) moisture content with rainfall across instrumentation 2 at Terry Road highway slope.....	100
Figure 4.35 In situ variation of (a) matric suction (b) moisture content with rainfall across instrumentation 3 at Terry Road highway slope.....	100
Figure 4.36 Combined air and soil temperature variation at Slope 3 (a) at the crest (b) at the middle (c) at the toe	101
Figure 4.37 Instrumentation layout at Slope 4.....	102
Figure 4.38 Field installation of the sensors at Slope 4	102
Figure 4.39 Installation of vertical inclinometer at Slope 4.....	103
Figure 4.40 Horizontal displacements of the Inclinometer 1 at Slope 4.....	104
Figure 4.41 Variation of lateral deformation at the top of Inclinometer 1 at Slope 4.....	104
Figure 4.42 Soil Erosion at the slope surface at Slope 4.....	105
Figure 4.43 In situ variation of (a) matric suction (b) moisture content with rainfall across instrumentation 1 at Slope 4.....	106
Figure 4.44 In situ variations of (a) matric suction (b) moisture content with rainfall across instrumentation 2 at Slope 4.....	106
Figure 4.45 In situ variation of (a) matric suction (b) moisture content with rainfall across instrumentation 3 at Slope 4.....	107
Figure 4.46 Combined air and soil temperature variation at Slope 4 (a) at the crest (b) at the middle (c) at the toe	108
Figure 4.47 Instrumentation layout at Slope 5.....	109
Figure 4.48 Installation of sensors at Slope 5	110
Figure 4.49 Slope 5 slope inclinometer installation.....	110
Figure 4.50 Horizontal displacements of the Inclinometer 1 at Slope 5.....	111
Figure 4.51 Variation of lateral deformation at the top of Inclinometer 1 at Slope 5.....	111
Figure 4.52 Horizontal displacements of the Inclinometer 2 at Slope 5.....	112
Figure 4.53 Landslides at Slope 5.....	113

Figure 4.54 In situ variation of (a) matric suction (b) moisture content with rainfall across instrumentation 1 at Slope 5	114
Figure 4.55 In situ variation of (a) matric suction (b) moisture content with rainfall across instrumentation 2 at Slope 5	115
Figure 4.56 In situ variation of (a) matric suction (b) moisture content with rainfall across instrumentation 3 at Slope 5	115
Figure 4.57 Combined air and soil temperature variation at Slope 5 (a) at the crest (b) at the middle (c) at the toe	116
Figure 4.58 Instrumentation layout at Slope 6.....	117
Figure 4.59 Slope 6 sensor installation	118
Figure 4.60 Slope 6 slope inclinometer installation.....	118
Figure 4.61 Horizontal displacements of the Inclinometer 1 at Slope 6.....	119
Figure 4.62 Variation of lateral deformation at the top of Inclinometer 1 at Slope 6.....	119
Figure 4.63 Horizontal displacements of the Inclinometer 2 at Slope 6.....	120
Figure 4.64 Variation of lateral deformation at the top of Inclinometer 2 at Slope 6.....	120
Figure 4.65 In situ variation of (a) matric suction (b) moisture content with rainfall across instrumentation 1 at Slope 6.....	121
Figure 4.66 In situ variation of (a) matric suction (b) moisture content with rainfall across instrumentation 2 at Slope 6.....	122
Figure 4.67 In situ variation of (a) matric suction (b) moisture content with rainfall across instrumentation 3 at Slope 6.....	122
Figure 4.68 Combined air and soil temperature variation at Slope 6 (a) at the crest (b) at the middle (c) at the toe	123
Figure 4.69 Horizontal Displacement at Slope 7	124
Figure 4.70 Variation of lateral deformation at Slope 7	124
Figure 4.71 Moisture variation along with depth at I220N ramp toward I55N site slope (a) at the crest (b) at the middle of the slope	125
Figure 4.72 Suction variation along with depth at I220N ramp toward I55N site slope (a) at the crest (b) at the middle	126

Figure 4.73 Moisture variation along with depth at Metro Center site slope (a) at the crest (b) at the middle of the slope	126
Figure 4.74 Suction variation along with depth at Metro Center site slope (a) at the crest (b) at the middle	127
Figure 4.75 Moisture variation along with depth at McRaven Road site slope (a) at the crest (b) at the middle of the slope	127
Figure 4.76 Suction variation along with depth at McRaven Road site slope (c) at the crest (d) at the middle	128
Figure 4.77 Field SWRC instrumentation data at I220N ramp toward I55N highway slope	129
Figure 4.78 Field SWRC instrumentation data at Metro Center highway slope.....	130
Figure 4.79 Field SWRC instrumentation data at Terry Road highway slope.....	130
Figure 4.80 Field SWRC instrumentation data at Highland Drive highway slope.....	131
Figure 4.81 Field SWRC instrumentation data at Sowell Road highway slope	131
Figure 4.82 Field SWRC instrumentation data at McRaven Road highway slope.....	132
Figure 5.1 Natural daily precipitation input as a discharge function for Slope 1	134
Figure 5.2 FEM soil model with the boundary conditions of Slope 1	134
Figure 5.3 Field and numerical model comparison (a) Selected rainfall event (b) Numerical modeling (c) Vol. moisture content (d) Matric suction	136
Figure 5.4 FEM flow analysis results (Depth of moisture variation profiles) for I220N Ramp Toward I55N highway slope for Max of 2 in (50.8 mm) daily rainfall (a) Before rainfall (b) 30 min after rainfall (c) 60 min after rainfall (d) 12 hrs after rainfall (e) 1 day after rainfall (f) 3 days after rainfall (g) 7 days after rainfall (h) 15 days after rainfall.....	137
Figure 5.7 FEM flow analysis results (Depth of moisture variation profiles) for Metro Center highway slope for Max of 2 in (50.8 mm) daily rainfall (a) Prior to rainfall (b) 30 min after rainfall (c) 60 min after rainfall (d) 12 hrs after rainfall (e) 1 day after rainfall (f) 3 days after rainfall (g) 7 days after rainfall (h) 15 days after rainfall.....	141
Figure 5.8 PDS based IDF curves of Jackson, Mississippi (NOAA, 2014).....	142
Figure 5.9 Suction profile variation of 3H:1V slope made of Yazoo clay (a) Flow functions to simulate the rainfall in FEM analysis (b) Suction profile before rainfall (c) Suction profile after rainfall-30 min (d) Suction profile after rainfall-60 min (e) Suction profile after rainfall-12 hours (f) Suction profile after rainfall-3 days.....	143

Figure 5.10 Suction variation for total rainfall amount of 4.7 in with fully softened shear strength, 2H:1V slope (a) Before rainfall (b) After 3 days rainfall (c) After 7 days rainfall, 3H:1V slope (d) Before rainfall (e) After 3 days rainfall (f) After 7 days rainfall, 4H:1V slope (g) Before rainfall (h) After 3 days rainfall (i) After 7 days rainfall.....	144
Figure 5.11 Variation of change in suction near the crest with Fully Softened Shear Strength at topsoil layer (a) with 234.1 mm (9.2 in) total rainfall of the slope 2H:1V (c) with 234.1 mm (9.2 in) total rainfall of the slope 3H:1V (e) with 234.1 mm (9.2 in) total rainfall of the slope 4H:1V (b) with 98.5 mm (4 in) total rainfall of the slope 2H:1V (d) with 98.5 mm (4 in) total rainfall of the slope 3H:1V (f) with 98.5 mm (4 in) total rainfall of the slope 4H:1V.....	146
Figure 5.12 Change in suction at the crest, middle, and toe of the slope with Fully Softened Shear Strength at topsoil layer (a) with 234.1 mm (9.2 in) total rainfall of the slope 2H:1V (c) with 234.1 mm (9.2 in) total rainfall of the slope 3H:1V (e) with 234.1 mm (9.2 in) total rainfall of the slope 4H:1V (b) with 98.5 mm (4 in) total rainfall of the slope 2H:1V (d) with 98.5 mm (4 in) total rainfall of the slope 3H:1V (f) with 98.5 mm (4 in) total rainfall of the slope 4H:1V.....	147
Figure 5.13 Change in factor of safety for 4.7 in/hr. (126.2 mm/hr.) with 2 hours of rainfall (a) before rainfall (b) Case I (c) Case II (d) Case III (e) Case IV.....	149
Figure 5.14 Changes in factor of safety for 4.7 in/hr. (126.2 mm/hr.) with 2 hours of rainfall (a) prior to rainfall (b) 2 hours rainfall duration (c) after 1-day (d) after 3-day.....	150
Figure 5.15 Change in the factor of safety.....	151
Figure 5.16 Slip surface for total rainfall amount of 4.7 in for fully softened shear strength, 2H:1V slope (a) Prior to rainfall (b) After 3 days rainfall (c) After 7 days rainfall, 3H:1V slope (d) Prior to rainfall (e) After 3 days rainfall (f) After 7 days rainfall, 4H:1V slope (g) Prior to rainfall (h) After 3 days rainfall (i) After 7 days rainfall.....	152
Figure 5.17 Change in the factor of safety with different total rainfall for peak shear strength.....	153
Figure 5.18 Change in the factor of safety with different total rainfall for fully softened shear strength.	154
Figure 5.19 Change in the factor of safety with different total rainfall for residual shear strength.....	155
Figure 5.20 Natural daily precipitation input as a discharge function for Terry Road highway slope.....	156
Figure 5.21 FEM soil model with the boundary conditions for Terry road highway slope.....	156
Figure 5.22 FEM flow analysis results (Depth of moisture variation profiles) for Slope 3 for Max of 2 in (50.8 mm) daily rainfall (a) Prior to rainfall (b) 30 min after rainfall (c) 60 min after rainfall (d) 12 hrs after rainfall (e) 1 day after rainfall (f) 3 days after rainfall (g) 7 days after rainfall (h) 15 days after rainfall.....	158

Figure 5.23 Numerical variation of matric suction (a) Wet period (b) Dry period, Numerical variation of moisture content (c) Wet period (d) Dry period at Slope 1, Slope 3, and Slope 6 159

Figure 5.24 Field-Numerical Modeling comparison (a) Slope 1 (b) Slope 3 (c) Slope 6 160

LIST OF TABLES

Table 2.1	Potential swell based on plasticity (Holtz and Gibbs (1956)).....	10
Table 2.2	Identification of potential swell based on plasticity (Carter and Bentley (1991))	10
Table 2.3	Summary of Shear Strength Parameters from drained direct shear tests on specimens subjected to wetting and drying cycles (Rogers and Wright (1986))	14
Table 2.4	Yazoo clay average index property values (Lee (2012))	18
Table 2.5	Yazoo clay soil properties.....	24
Table 2.6	Laboratory study of the effect of the wet-dry cycle on Yazoo clay	24
Table 2.7	Yazoo clay sample chemical composition based on SEM data	26
Table 2.8	Soil Properties.....	28
Table 2.9	Peak, fully soften and Residual Shear Strength of Yazoo clay.....	34
Table 2.10	Laboratory Hydraulic Conductivity values at different wet-dry cycles.....	35
Table 2.11	Variation of VMC and hydraulic conductivity in response to water infiltration and number of wet-dry cycles respectively with 20% initial moisture content.....	38
Table 2.12	Variation of VMC and hydraulic conductivity in response to water infiltration and number of wet-dry cycles respectively with 25% initial moisture content.....	38
Table 3.1	Selected highway site slopes locations	39
Table 3.2	I220N Ramp Toward I55N highway slope investigation details	40
Table 3.3	Metro center highway slope investigation details.....	48
Table 3.4	Terry road highway slope investigation details	53
Table 3.5	Highland drive highway slope investigation details	60
Table 3.6	Sowell road highway slope investigation details	66
Table 3.7	McRaven Road highway slope investigation details	72
Table 4.1	Different Instrumentation for Data Collection.....	77
Table 4.2	Schedule of sites instrumentation	79

Table 4.3	Schedule of the site monitoring program.....	79
Table 4.4	Field Soil Water Retention Curve fitted parameters.....	129
Table 5.1	Soil parameters for FEM analysis.....	135
Table 5.2	Soil parameters for FEM analysis.....	139
Table 5.3	Variation in shear strength of Yazoo clay.....	151
Table 5.4	Wet-Dry Cycle Shear Strength Values for Yazoo clay (Soil 1 in Table 5.2)	148
Table 5.5	Soil parameters for FEM analysis.....	157
Table 5.6	Soil parameters for FEM analysis.....	164
Table 5.7	Soil parameters for FEM analysis.....	171
Table 5.8	Soil parameters for FEM analysis.....	177

EXECUTIVE SUMMARY

Slope failures are frequent in highway embankments on expansive Yazoo clay in Mississippi due to frequent seasonal rainfall events associated with temperature and humidity variation causing expensive maintenance problems for the Mississippi Department of Transportation (MDOT). This State Study 286 was conducted to understand the performance of highway slopes containing Yazoo clay. The objective of the study was to investigate the infiltration behavior of the slope on expansive Yazoo clay during rainfall using field monitoring and to evaluate its impact on the performance and safety of the slope. Six repaired highway slopes were instrumented comprehensively to monitor the moisture, matric suction, and temperature variation, as well as monitoring the slope deformation using vertical inclinometers. Besides field monitoring, advanced numerical modeling using the Finite Element Method (FEM) was conducted to evaluate the effect of rainfall frequency and duration (based on historical rainfall data of Mississippi) on the water infiltration and corresponding change in the factor of safety of the highway slope. Based on the field monitoring results, the data of volumetric moisture content and matric suction readings were observed constant throughout all six slopes. Certain peaks and drops in the moisture content were also observed during the summer months. This occurred due to the formation of shrinkage cracks because of the shrink/swell potential of the highly plastic clay and resulted in increasing vertical permeability which allows more rainfall infiltration during summer to early fall. Because of the low horizontal permeability of Yazoo Clay soils the infiltrated water stayed in the slope, which eventually creates a perched water condition. The existence of the perched water condition within the highway slopes containing Yazoo clay makes the condition vulnerable to the initiation of landslides.

The six highway slopes (labelled Slope 1 through Slope 6) investigated under State Study 286 each contained an as-built section and a repaired section. The repaired sections had either H-pile as a reinforcement or remove and replace types of remediation. The portion of the slopes that is repaired with reinforcement (such as H-pile) resisted any sliding. The section of the slopes that has no reinforcement or any other means of repair remediation has shown shallow sliding movement up to 6 feet deep, as evidenced in Slope 3 (Terry Road) and Slope 6 (McRaven Road). Moreover, Slope 5 (Sowell Road) has experienced a sliding movement up to 12 feet deep beyond the H-pile reinforcement. The advanced numerical modeling analyses indicates the rainfall during late summer to early fall is the most critical time in which a perched water condition will develop. In addition, the study revealed that high intensity, short-duration rainfall contributes less than the low intensity, long-duration rainfall to vertical infiltration behavior which eventually creates a perched water condition. As the wet-dry cycle soften the shear strength of high plastic clay to fully softened state the presence of perched water creates a slope condition vulnerable to a creeping slide failure. Based on this research, it is observed that slope failures of Highway embankments containing highly plastic clays such as Yazoo clay takes place due to the development of perched water conditions after five to seven years of construction. It is highly recommended to consider including a perched water zone up to the depth of the active zone along with the development of fully soften shear strength condition in the slope stability analysis of any slope containing high volume change clays, such as Yazoo clay.

Chapter 1: INTRODUCTION

1.1 Background

Slopes and embankments are integral components of any transportation infrastructure. Many of the slopes in the transportation infrastructure of Mississippi are constructed using marginal high-volume change (HVC) soils found in many locations statewide, similar to the type of soil focused on in this research study, known as Yazoo clay. All of the HVC soils are known for their expansive capacity and also known to be susceptible to both shallow and deep-seated landslides. Slopes and embankment landslides often cause significant hazards to transportation infrastructure and generally require more extensive and expensive remediation repairs (Loehr and Bowers, 2007; Loehr et al., 2007; Hossain et al., 2017; Khan et al., 2019).

For example, in the Mississippi Yazoo clay belt, Mississippi receives an average annual rainfall intensity higher than other neighboring states resulting in a variation of rainfall, temperature, and soil condition, as presented in Figure 1.1, which eventually works as a stressor to cause shallow slope failure. Historically, this rainfall has caused much damage to Mississippi transportation infrastructures such as highways, embankments, and slopes. During the 1960s many of the highway slopes and embankments in Mississippi were constructed using the marginal HVC type clay soil. Due to the high-volume change characteristics of HVC clays, shallow to deep-seated slope failure has become widespread in highway slopes and embankments of Mississippi, especially in the Jackson metroplex. Typically, these slope failures occur as pore water pressures increase which cause a reduction of soil shearing strength capacities due to the progressive wetting of the slopes near-surface soil. Soil moisture vacillations further deteriorate this condition due to seasonal climatic variations that typically result in the HVC soils shrink-swell behavior. Besides slope failure, HVC clay has a detrimental effect on the roads, foundations, and related infrastructure in the central Mississippi region (Douglas et al., 2000; Lee et al., 2012).

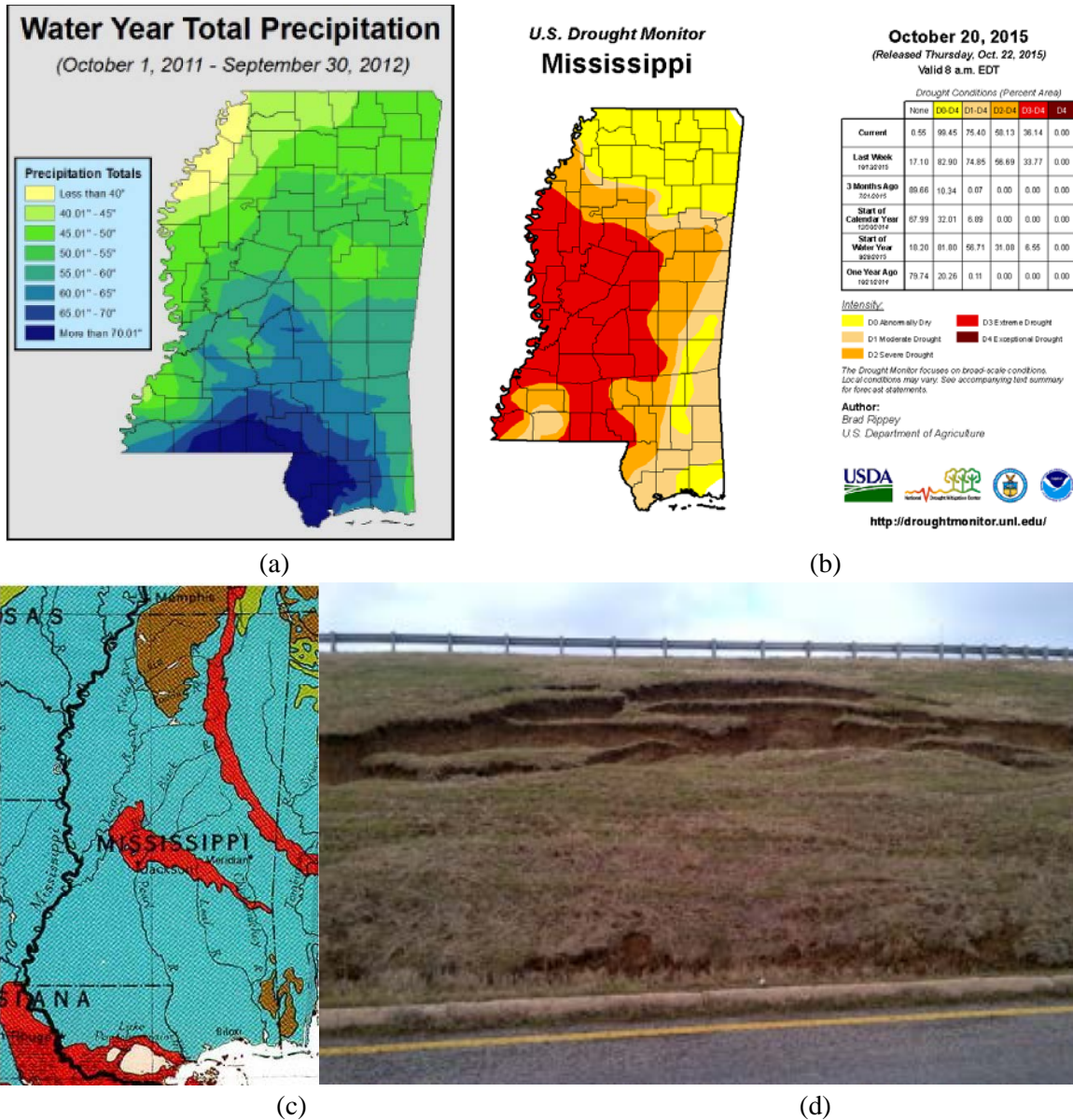


Figure 1.1 (a) Total Precipitation map (b) Drought map (c) Yazoo clay profile in Mississippi (d) Slope failure in Highway Embankment.

1.2 Problem Statement

The Yazoo Formation containing HVC Yazoo clay is geologically defined within the Jackson group and has been identified throughout the southeastern and southwestern United States. The upper stratigraphy of the Jackson group that contains the Yazoo Formational clay (or its geological equivalent) extends in regional locations across Alabama, Louisiana, and Mississippi. The regional extent of the Yazoo clay lies within the central Mississippi counties of Yazoo, Holmes, Hinds, Rankin, Madison, Scott, Newton, Smith, Jasper, and Wayne. The horizontal width of the surface outcrop varies from approximately 35 miles on the west to less than 10 miles on the east, whereas; the metropolitan Jackson area is located directly on top of the Yazoo Formation clay (Lee 2012).

Yazoo Clay is a highly plastic clay and subject to very high-volume change capacity (Douglas and Dunlap, 2000, Lee 2012). The average composition of the Yazoo clay is 28% smectite (probably montmorillonite), 24% kaolinite, 22% quartz, 15% calcite, 8% illite, 2% feldspar, and 1% gypsum based on recent x-ray diffraction results (Taylor 2005). The Yazoo clay in the Jackson area consists of a weathered upper zone overlying an un-weathered lower zone of HVC clays. The upper zone weathered portion of the Yazoo clay varies in-depth, however, mostly extends to a depth of around 30 feet (Taylor 2005). In geotechnical engineering practice, the magnitude of the liquid limit and plasticity index coupled with the proximity of the natural in-situ water content in close vicinity of the plastic limit reflects the potential to shrink or swell upon changes in the in-situ moisture content of this clay. The weathered Yazoo clay usually has a liquid limit higher than 70% to 100% and plastic limits from 20% to 30%, results in a plasticity index greater than 50%. (Douglas and Dunlap, 2000). According to Holtz et al. 2010, a soil with a plasticity index greater than 35 may have a very high degree of expansion (shrink/swell potential) where the probable expansion could be more than 30% when the water content is changing from dry to a wet condition. Based on the plasticity index values reported for Yazoo Clay, a very high shrink/swell potential exists. As a result, moisture changes cause swelling, shrinkage, and otherwise destructive behavior, which in turn cause detrimental effects to the roads, foundations, and related infrastructure in the central Mississippi region (Douglas and Dunlap, 2000; Lee 2012). The change in volume of the Yazoo clay between the liquid limit and completely dry state ranges from 100 to 235 percent. On the other hand, swell pressures have been measured as high as 25,000 psf (Johnson 1973).

Moderate (3:1) to steeper slopes constructed on high plasticity clay is susceptible to the softening behavior within the upper topsoil zones due to seasonal wet-dry cycles. Skempton (1977) first proposed the concept of fully softened strength for natural and excavated slopes in London Clays. Skempton (1977) reported that over time, the slopes in the highly plastic London clay lost strength, eventually reaching what Skempton termed as “fully-softened” strength, which lies between peak and residual strength, as presented in Figure 1.2. Skempton (1977) indicated that the fully softened strength is comparable to the peak shear strength of the soil in a normally consolidated state. Fully softened shear strength values corresponding to the shear strengths of high plastic clay reported by Skempton (1977) seems to develop for the Yazoo clay during Mississippi seasonal wetting and drying rainfall cycles (Wright, 2005).

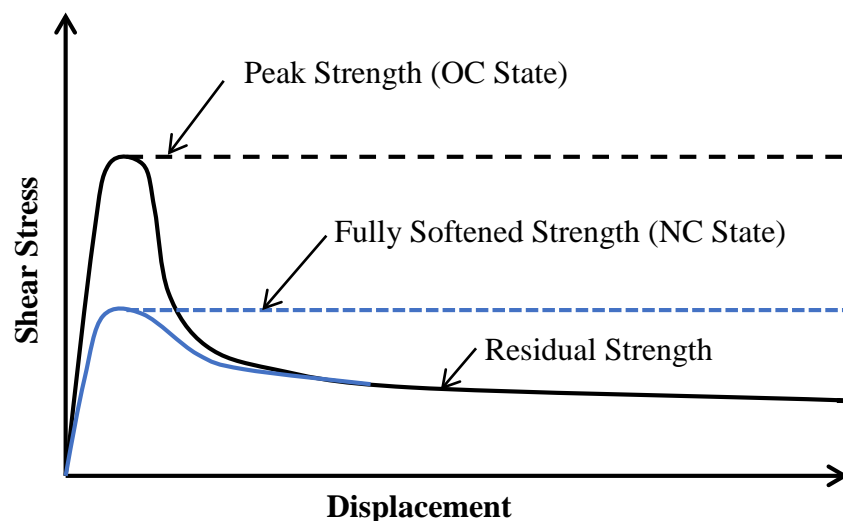


Figure 1.2 Comparisons of peak, residual and fully softened shear strength (redrawn after Skempton, 1977)

Rainfall-induced slope failure is a common problem in areas with slopes constructed on highly plastic clay. Usually, in an unsaturated state, soils have high matric suction with a low moisture content, which usually provides a slope with a higher factor of safety against landslide conditions developing.

However, during a moderate to heavy rainfall event, water infiltrates the slope, which saturates the slope and may reduce the matric suction capacity of the soil enough to result in the slope becoming unstable and lead to slope failure. Most of these failure types involve shallow surface slides with depths less than 3 m (10 ft.), which often leading to required periodic maintenance (Duncan and Wright, 2005). All to often earth fills or cut embankments are constructed on unsaturated soils. For unsaturated soils the existing magnitude of negative pore water pressure or matric suction plays a vital role in the additional shear strength of the soil (Melinda et al., 2004). Previous studies have investigated the effect of rainfall infiltration on the stability of slopes in field-scale which indicated a drop in the matric suction and shear strength of soil due to water infiltration during rainfall (Lim et al., 1996; Kim et al., 2010; Gan et al., 1998; Fredlund et al., 1996, Jotsankasa, and Mairaing, 2010). The extent of reduction in shear strength depends on the rate of water infiltration, which in turn depends on rainfall duration and intensity. Highly plastic clay often experienced a significant number of cracks and fissures in the upper soil layer due to seasonal rainfall moisture variation. This crack-rich, highly plastic clay often results in a complex process of rainfall infiltration and volume change (Zhan et al. 2007). Hossain et al. 2016 conducted a field investigation at a highway slope over the expansive soil in Texas to investigate the effect of rainfall on the change in the moisture content and matric suction. During the study, the crests of the slopes were instrumented using moisture sensor and water potential probes and were monitored in real-time, to investigate the effect of the rainfall. Results from the study, as presented in Figure 1.3, indicated that the initial moisture content was relatively low (4%), and matric suction was high (-600 kPa) at the time of installation of the sensors at the 1.2 m (4 ft.) depth. Afterward, total precipitation of 181.9 mm (7 in.) was observed in one month between April and May 2011, which increased the moisture content to a maximum of 37% and decreased the matric suction to -10 kPa (-1.45 psi). Based on the field study, a variation of moisture content at 1.2 m (4 ft.) depth due to rainfall is evident.

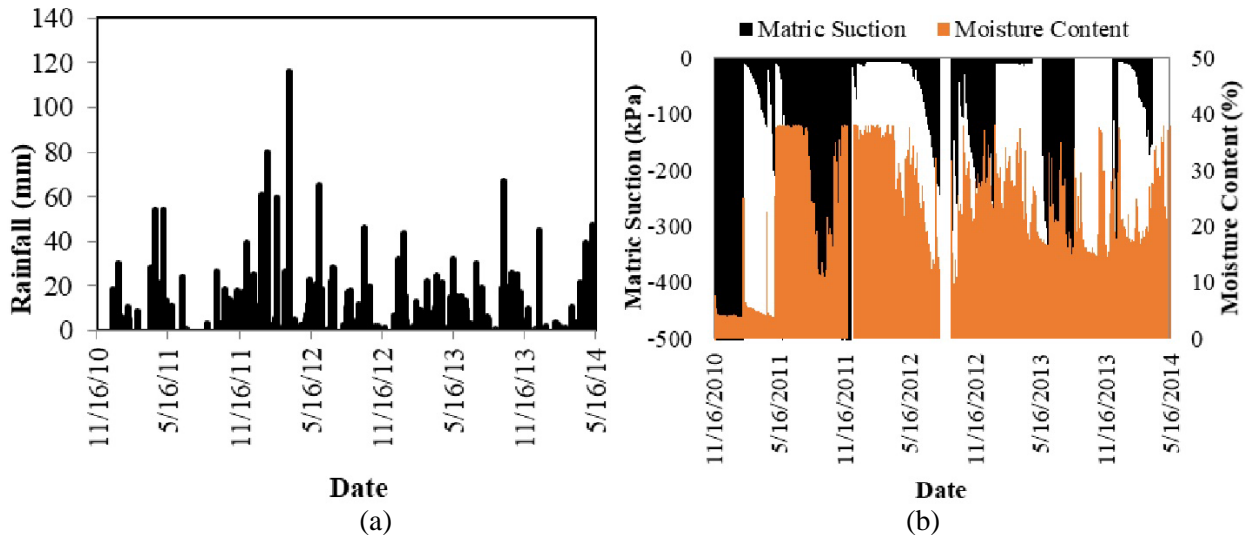


Figure 1.3 Instrumentation results at the crest of the slope (a) daily rainfall data (b) Moisture content and matric suction at 1.2 m depth (Hossain et al., 2016)

The factor of safety of the slope is higher at low moisture content and high matric suction. Due to the infiltration of the rainwater, soil near the surface gets saturated, and the matric suction of slope decreases, which eventually reduces the factor of safety of the slope and may cause slope failure. Khan et al., 2016 conducted a flow analysis using finite element analysis to evaluate the effect of rainfall on a slope constructed using highly plastic clay soil in Texas. The flow analysis results are presented in Figure 1.4, which indicated a drop in matric suction due to rainfall after 2 days of rainfall.

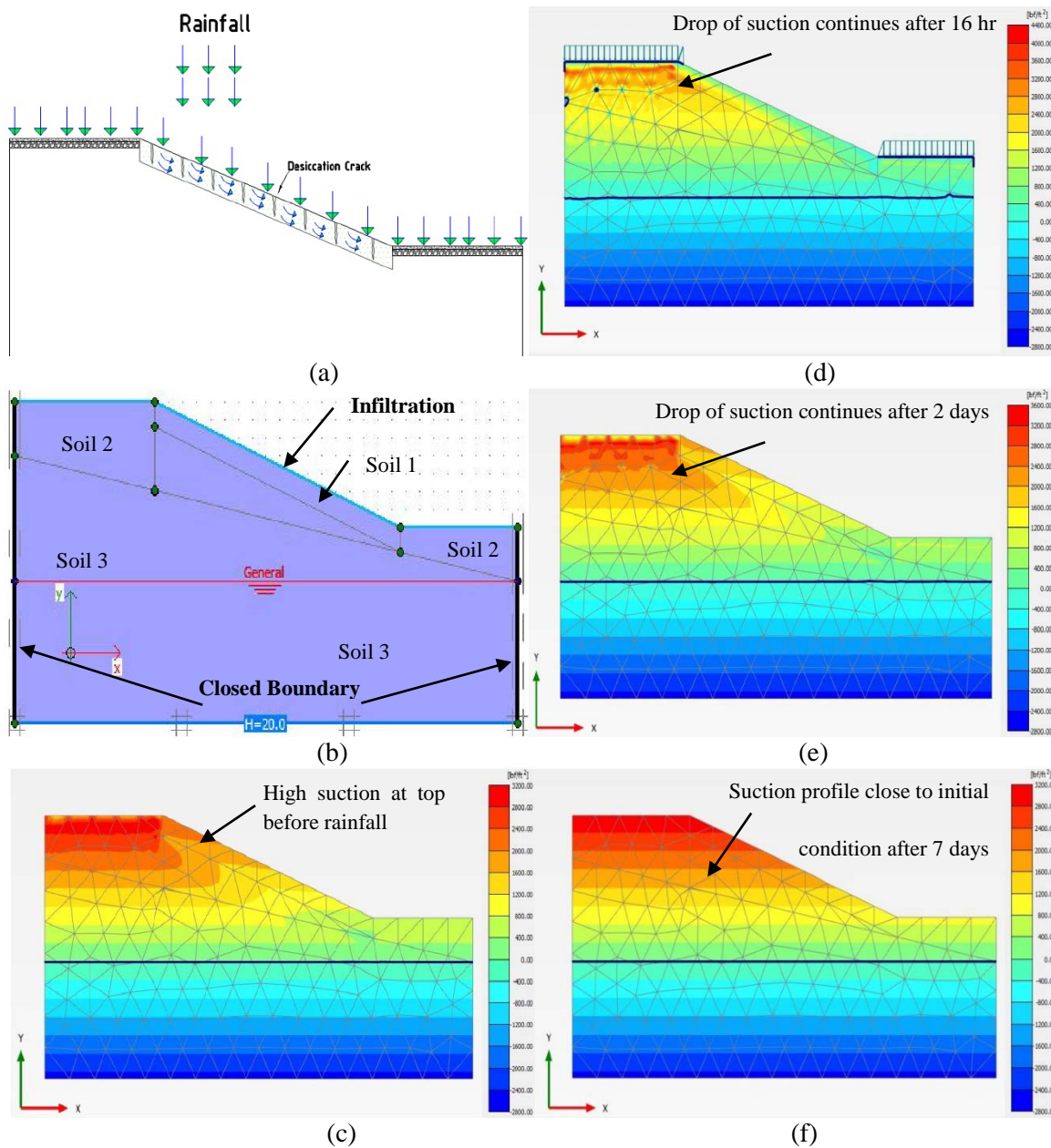


Figure 1.4 (a) Schematic of rainfall intrusion through desiccation crack (b) Boundary conditions for the flow model (c) Suction profile of slope before rainfall (d) Suction profile 16 hours after rainfall (e) Suction profile 2 days after rainfall (f) Suction profile 7 days after rainfall (Khan et al., 2016)

In many locations, near the metropolitan Jackson area, the highway slope is constructed at a steeper angle (around 3H: 1V). As a result, the conventional design practice of widening the highway slopes to 5H: 1V to 6H: 1V cannot be undertaken by MDOT. Moreover, many of these highway slopes containing HVC clay, such as Yazoo clay, experience shallow to deep-seated failure taking place only after a few years following construction and after the slopes have experienced several wet-dry cycles due to seasonal moisture variation. To improve the design standard and reduce the detrimental effect of the volume change behavior of the expansive clay, it is vital to understand the behavior with seasonal moisture variation and rainfall on the slope stability of HVC clays such as the Yazoo clay.

The performance of the highway slopes on HVC expansive Yazoo clay is a complex phenomenon that depends on the local climate factors, such as rainfall, temperature variation, and evapotranspiration, as well as the shear strength properties of soil. Real-time instrumentation data on the slopes constructed by expansive Yazoo clay is minimal at the field scale. Moreover, the conventional slope stability analysis using the limit equilibrium method fails to explain the deformation behavior of the slope. An advanced numerical analysis using the Finite Element Method, considering the effect of wet-dry cycles and the amount of rainfall, will substantially improve the understanding of the performance of these slopes in Mississippi, which will help to improve design practice and reduce the frequency of slope failures in the area.

1.3 Research Objective and Major Tasks

The State Study 286 was conducted to understand the performance of highway slope containing Yazoo clay. *The objective of the study is to investigate the infiltration behavior of the slope on expansive Yazoo clay during rainfall using field monitoring and evaluate its impact on the performance and safety of the slope.*

Slope failure is widespread on highway slopes containing HVC highly plastic soils such as the Yazoo clay, which have caused damage to many Mississippi roadway shoulders and pavement structures, as well as bridge abutment spill-thru slopes; all of which cause unpredictable routine maintenance and often require costly slide remediation construction projects. The local climatic variation is one of the major factors that trigger the slope movement and if unchecked, can eventually lead to slope failure. The current report documents the work performed under state study 286 through the following tasks:

- Select and investigate highway slopes containing Yazoo Clay in the Jackson Metroplex
- Instrument and monitor selected slopes to investigate moisture, temperature, and matric suction variation as well as slope deformation during seasonal rainfall events.
- Investigate the effect of rainfall using advanced Finite Element Method. This analysis is conducted to investigate the infiltration behavior and its effect on the changes in the performance and safety of the selected slope, as well as duration and amounts of rainfall.
- Conduct data analysis to determine the mechanism of landslides at highway slopes made of expansive Yazoo clay.

Chapter 2: LITERATURE REVIEW

2.1 Expansive Soil

The behavior of expansive soil is highly dependent on moisture content changes. It undergoes volumetric deformation that gradually damages essential infrastructure such as foundation slabs, bridges, roadways, and residential homes. Present in both humid and arid/semi-arid environments, expansive soils cover nearly a quarter of the area of the United States (Nelson and Miller 1992). Annually, expansive soils alone incur more financial losses to US property owners than earthquakes, floods, hurricanes, and tornadoes combined (Jones and Jefferson 2012). In a typical year, the associated financial losses caused by expansive soil can be as high as 15 billion dollars (Jones and Jefferson 2012). The current chapter summarizes the different physical and mechanical properties of Expansive soil that are available in the literature.

2.2 Identification of Expansive Clay

The identification of potential shrink-swell problems in the subsoil is essential for selecting the appropriate design and method of construction (Van Der Merwe, 1964; Hamilton, 1966). Despite the lack of a standard definition of swell potential, there exist various geotechnical methods to identify the swelling potential of soil (Nelson and Miller, 1992). Surface examination, as well as geological and geomorphological description, can indicate expansive soils (Lucian, C. 2008). Identification is not just restricted to the present visual precursors of expansive soil, but also the careful review of the formation history of the grains. Generally, the soils fabric is the result of geological history, soil mineral and composition, climatic and hydrological conditions, precipitation, and pH levels.

The morphological description includes a series of factors, such as the location of a groundwater table, soil consistency, texture, structure and even the color of the soil (Charles L. 2008). Most of the relevant physical and mechanical property indicators of swell potential are obtained by performing geotechnical index property tests such as moisture content, Atterberg limits, and grain size distribution. Other tests to determine the swell potential include the volume change test such as the free swell test or the swell in odometer test, the coefficient of linear extensibility (COLE) test, mineralogical compositions by x-ray diffraction (XRD) test, and total suction test.

Lucian, C. (2008) stated that geotechnical methods for identifying expansive soils can be broadly divided into direct and indirect methods. The direct method consists of laboratory swell tests. In contrast, indirect methods are based on the correlation of measured soil properties, relying on the empirical correlations of geotechnical properties like moisture content, Atterberg's limits, and free swell index.

2.2.1 Identification by Atterberg Limits

The Atterberg limits represent the water holding capacity at different states of consistency and are the most popular techniques for getting information on the expansive nature, mechanistic and swelling behavior of clay soils. The most useful for classifying and identifying the relative swell potential of subsoil are liquid limits (LL) and plasticity index (PI).

The liquid limit is the water content at which a subsoil changes from the plastic state to a liquid state, while the plastic limit is the water content at which a subsoil changes from the plastic state to a semisolid state (Figure 2.1). The plasticity index is calculated by subtracting the plastic limit (PL) from the liquid limit (LL). i.e., $PI = LL - PL$. This number indicates the range over which the soil remains plastic. Soils that possess no clay minerals do not exhibit plasticity, and they pass directly from their liquid to a semi-solid state when their moisture content is reduced.

The physical and mechanistic behavior of clay soils are controlled by their mineral structure. Clayey soils that are rich in smectite (a mineral group), such as montmorillonite, tend to absorb more water and thus exhibit much greater swelling capacity of water than non-expansive clays like chlorite, illite, and kaolinite. Generally, finer soils with particle size diameters less than 0.075 mm, such as silts and clays, have a higher capacity to hold water due to their greater specific surface area. Clayey soils rich in smectite tend to retain their plasticity even at lower moisture contents.

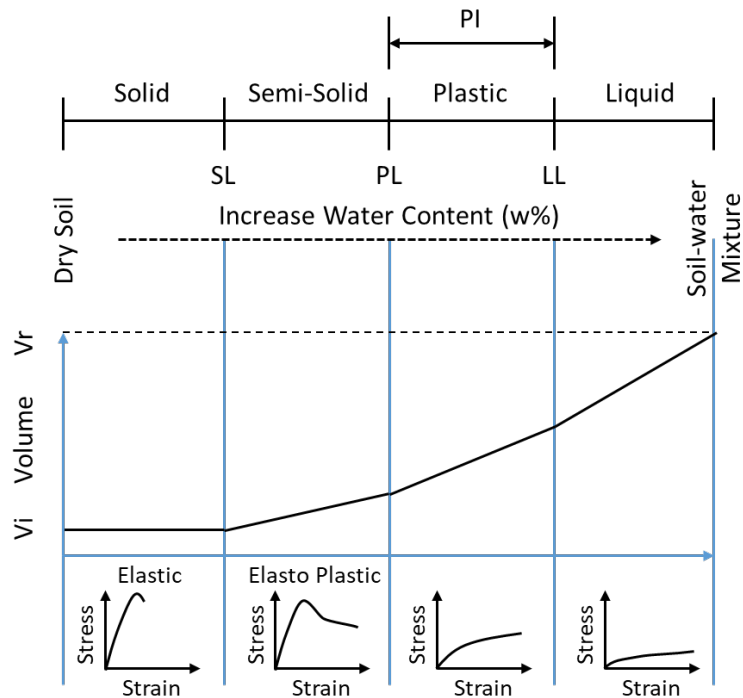


Figure 2.1 Atterberg limits description, volume change and generalized stress-strain response of expansive soils (redrawn After Holtz and Kovacs (1981))

2.2.2 Clay Minerals and Its Effect on the plasticity

Clay minerals consist of two or three layers of gibbsite and silica sheets, as presented in Figure 2.2 (Das, 2013). These are negatively charged aluminosilicate layers with the ability to absorb water between the layers (Hensen et al., 2002). Due to the presence of exchangeable ions on the surface of clay particles, dipolar water molecules are attracted to clay minerals, resulting in a double layer of water. The plastic behavior of clay is directly attributed to the presence of this double layer. The surface area of clay particles per unit mass is generally referred to as a specific surface. The specific surfaces of kaolinite, illite, and montmorillonite are about 15, 90, and 800 m²/g, respectively, as presented in Figure 2.34 (Das, 2013). Clay minerals that have less surface area attract less water (such as illite and kaolinite) and are characterized as low plastic clay.

On the other hand, montmorillonite has a significantly larger surface area, which attracts a high volume of water, and is characterized as a high plasticity clay. The thickness of the double layer of water is highest for montmorillonite (Das, 2013). Due to the affinity of a high volume of water, high plastic clay exhibits expansive behavior: it swells when it absorbs water and shrinks when water is dissipated. Chabrilat et al. (2002) reported an abundance of montmorillonite in clays in the mid-zone of the United States.

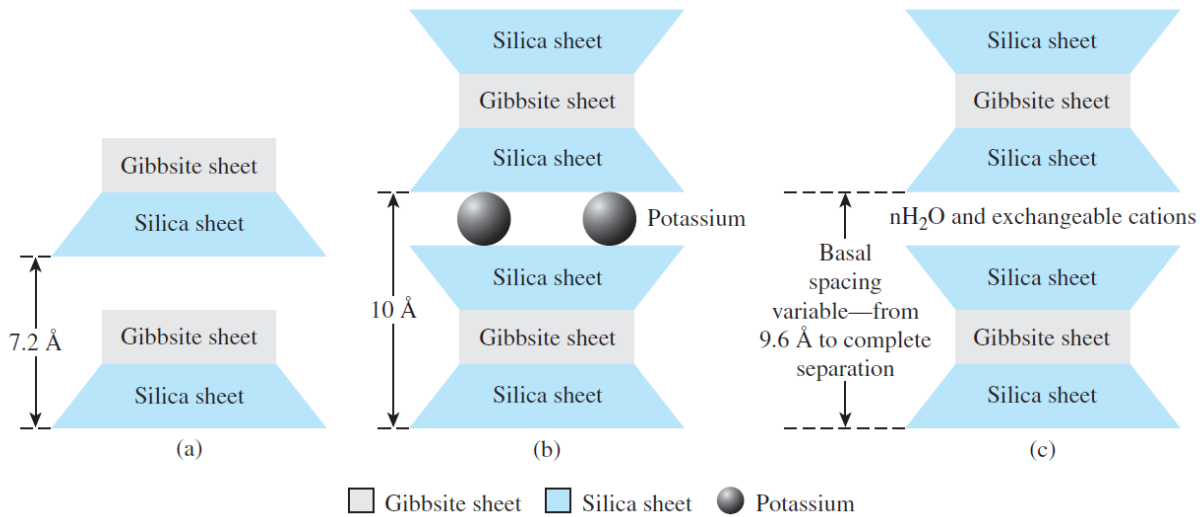


Figure 2.2 Diagram of the structures of (a) Kaolinite, (b) Illite, and (c) montmorillonite (Das, 2010)

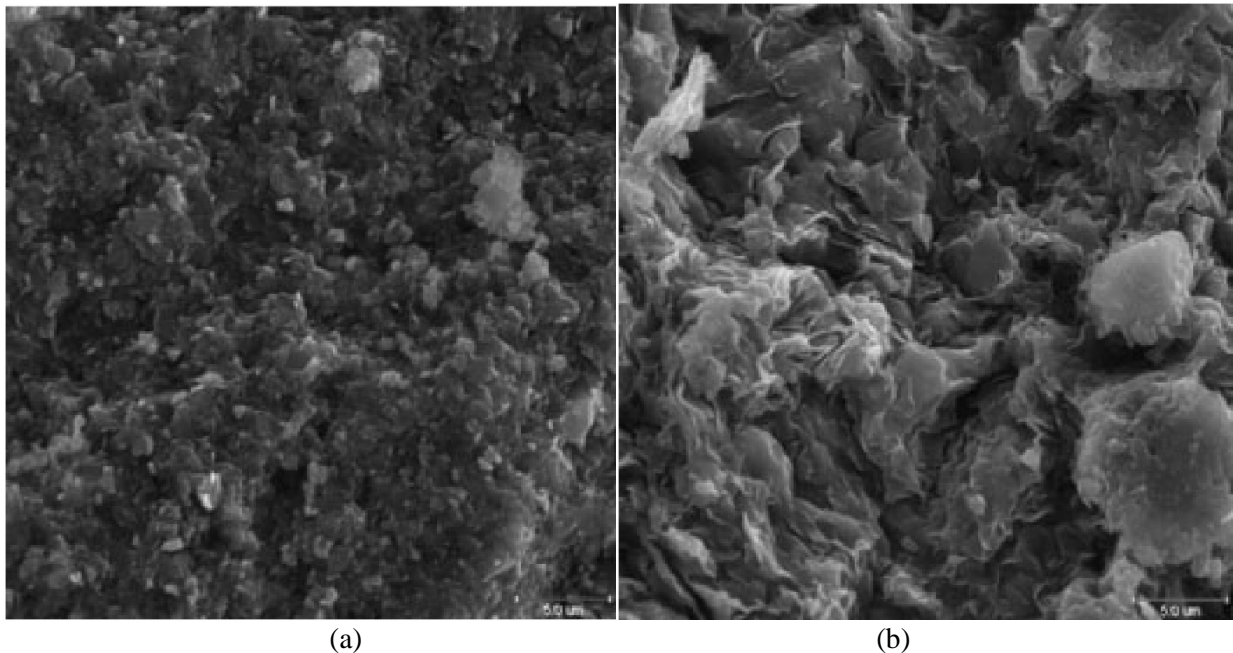


Figure 2.3 Scanning Electron Microscope Image (a) Kaolinite, and (b) Illite (Das, 2010)

2.2.3 Indirect Measurement of Potential Swell

2.2.3.1 Classification of potential swell based on Casagrande's plasticity chart

The plot of PL vs. LL is used to detect the swelling potential of soil using Casagrande's plasticity chart (Figure 2.4). For example, a soil sample with a LL of 40% and PI of 25% plots on the chart typical for smectites (montmorillonite), which implies that it has a high potential for swelling as indicated in Table 2.1. Soils that plot above the A-line are plastic clays, and the soils that plot below are organic soils and silts. The U-line in the plasticity chart indicates the upper boundary for natural soils.

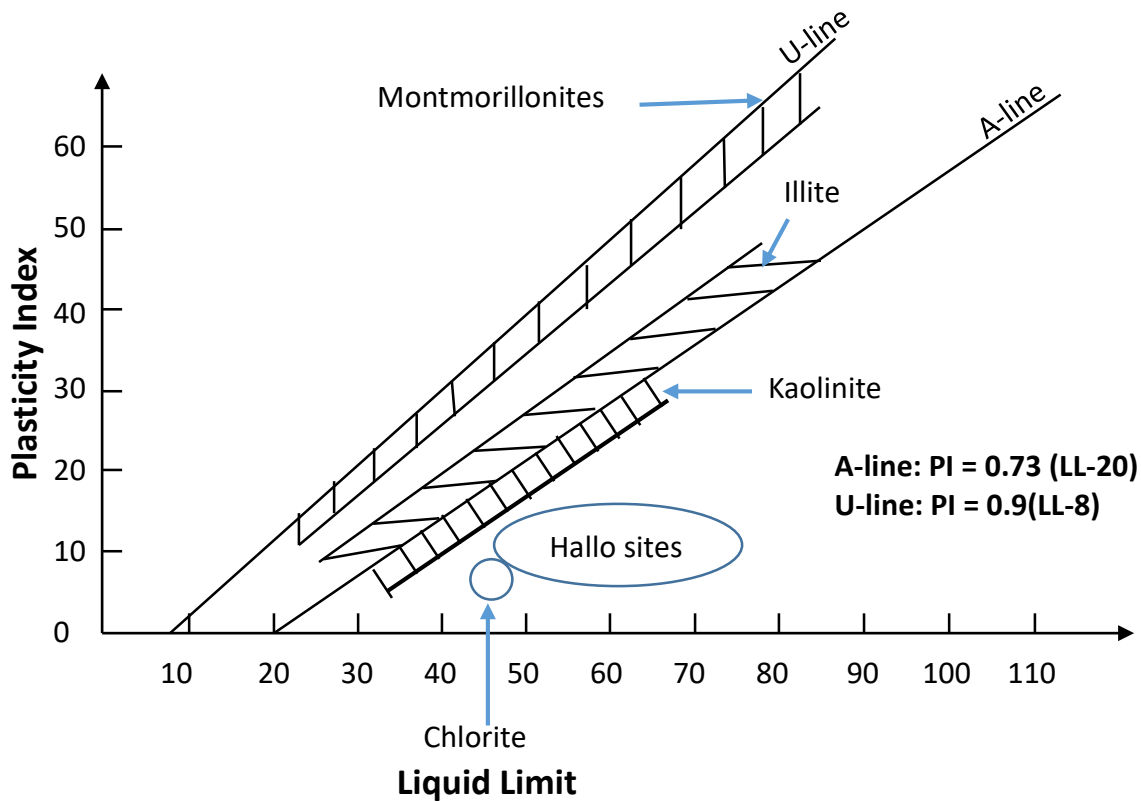


Figure 2.4 The plot of clay minerals on Casagrande's chart (redrawn after Chleborad et al. (2008))

2.2.3.2 Classification of Potential Swell Based on Plasticity Table

The change in Atterberg limits of a soil sample can be used to indicate the degree for potential swell, as presented in Table 2.1 and Table 2.2. For example, a soil sample with LL exceeding 70% and PI greater than 35% is judged to have a very high swell potential. Presumably, the overlapping intervals in Table 2.2 account for the variations in the chemical properties of soils and their environment.

Table 2.1 Potential swell based on plasticity (Holtz and Gibbs (1956))

Classification of potential swell	Liquid limit (LL)	Plasticity index (PI)	Shrinkage limit (SL)
	%	%	%
Low	20-35	<18	>15
Medium	35-50	15-28	10-15
High	50-70	25-41	7-12
Very high	>70	>30	<11

Table 2.2 Identification of potential swell based on plasticity (Carter and Bentley (1991))

Classification of Potential Swell	Plasticity Index (%)	Plasticity Index (%)
Low (0-1.5%)	0-15	0-15
Medium (1.5-5%)	10-30	15-24
High (5-25%)	20-55	25-46
Very high (>25%)	>40	>46

2.2.3.3 Classification of Potential Swell Based on Physical Properties of Soils

Skempton (1964);, Seed et al. (1960), and Van der Merwe (1964) developed a useful empirical relationship between the expansion potential and physical properties of soils like clay contents, soil activity, plasticity index, as presented in Figure 2.3. A preliminary classification based on percent clay fraction (soil particles < 0.002 mm or $2 \mu\text{m}$ in diameter, usually determined in a hydrometer test) and PI can be used to categorize probable potential swell.

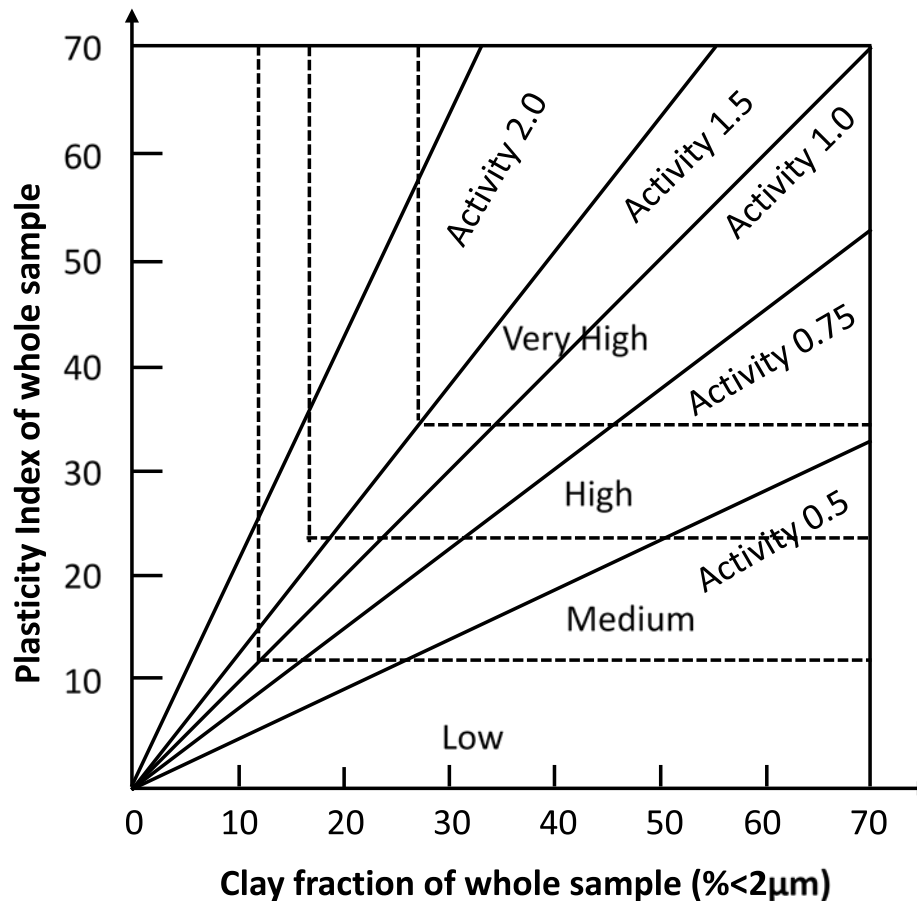


Figure 2.5 Chart for evaluation of potential expansiveness (Seed et al. (1960))

Generally, a soil having clay content higher than 30 percent and a plasticity index greater than 35 percent is considered to denote a very high potential for shrinkage or swelling (typically referred to as an “active soil”). In contrast, soil with clay content lower than 30% and a plasticity index between 10% to 20% can experience slight swelling or shrinking in response to moisture variation (Lucian, C. (2008)). The “Activity” in Figure 2.6 is a dimensionless ratio of % PI to % Clay Fraction, as presented in Equation 2.1.

$$\text{Activity (Ac)} = \text{plasticity index (PI) in \%} / \text{clay fraction finer than } 2 \mu\text{m in \%} \quad (2.1)$$

For example a soil with activity less than 0.75 is inactive, indicates a low potential for volume change, while a soil with activity between 0.75 and 1.0 is actively signifying a high potential for volume change. Anything above 1.0 is very active, demonstrating a very high potential for volume change.

Another way of identifying the expansive soil is to use the activity method quoted by Carter and Bentley (1991). The proposed classification chart is shown in Figure 2.4. The activity term in Figure 2.6 is defined in Equation 2.2, which is a bit different than Equation 2.1, as follows:

$$A_c = PI/(C - 5) \quad (2.2)$$

where PI is the plasticity index, and C is clay content.

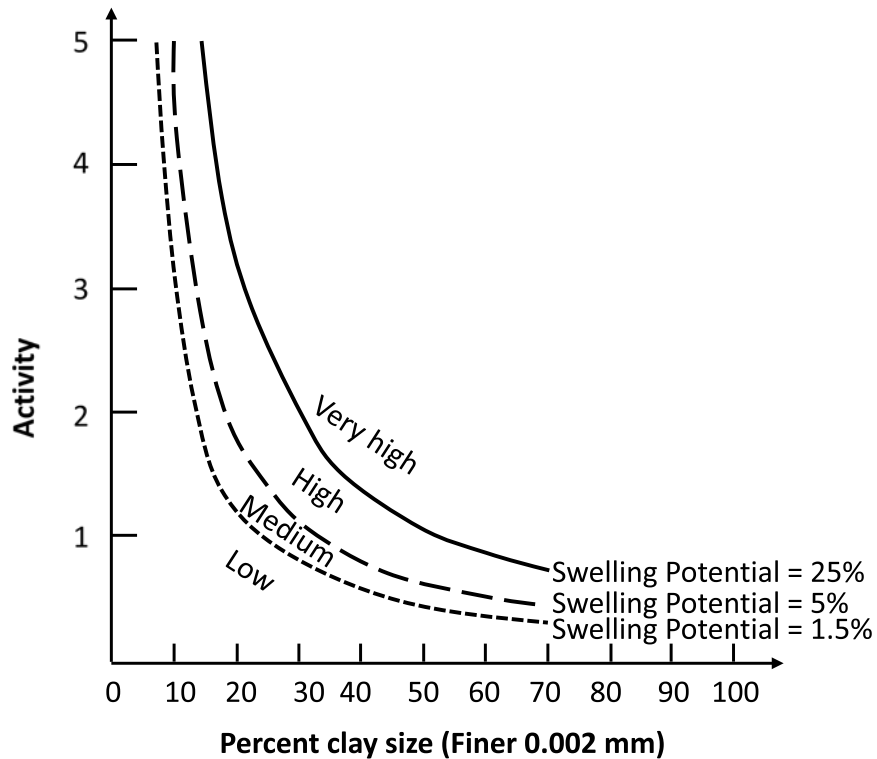


Figure 2.6 Classification chart for swelling potential proposed by Carter and Bentley (1991)

Several researchers have proposed empirical relationships to predict the swelling pressure of soils using soil characteristics like clay content, activity, and plastic limit. Carter and Bentley (1991) proposed an empirical Equation 2.3.1 to calculate the potential swell (as presented in Table 2.2) as follows:

$$\text{Swell (\%)} = 60\kappa (PI)^{2.44} \quad (2.3.1)$$

where PI is the plasticity index, and κ is a constant equal to 3.6×10^{-5}

Seed et al. (1962) suggested that the swelling potential of clay soil is related to its activity and clay content by the following formula as equation 2.3.2:

$$\text{Swell (\%)} = \kappa (A_c^{2.44})(C^{3.44}) c \quad (2.3.2)$$

Where A_c is the soil activity, and C is the clay content.

2.2.4 Variation of Shear Strength of Highly Plastic Clay soil

Moderate to steep slope constructed on high plasticity clay is susceptible to softening behavior within the slope active zone (upper 12 to 15 feet) during seasonal wet-dry cycles. When highway embankments are constructed the shear strength of the soil is usually placed at the soils Peak Strength value determined in any laboratory test. However, after the soil is exposed to seasonal wetting and drying cycles the peak shear strength value reduces to the fully softened shear strength over time (Wright, 2005). Skempton (1977) reported that over time during wet-dry cycles the strength of slopes in the highly plastic London clay lost shear strength capacity. Skempton termed this lost in shear strength as “fully-softened” strength, which he discovered lies between peak and residual strength, as presented in Figure 2.7. Skempton (1977) indicated that the fully softened strength is comparable to the peak shear strength of the soil in a normally consolidated state.

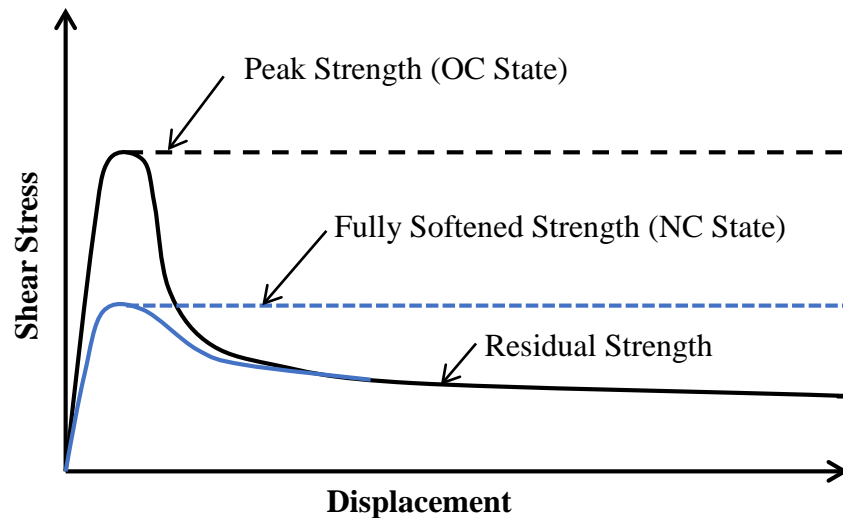


Figure 2.2 Comparisons of peak, residual and fully softened shear strength (Skempton (1970))

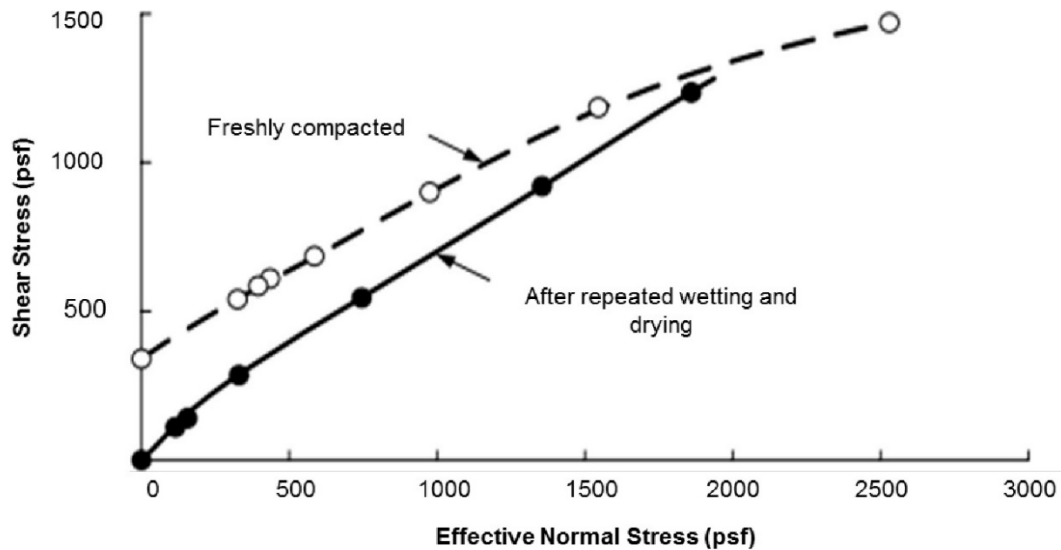
Rogers and Wright (1986) conducted a study to investigate the failure of slopes constructed over highly plastic clay soil in Texas. The author reported that the high plasticity of the clays experienced shrink-swell characteristics due to repeated wetting and drying cycles in the field, which is a cause of the softening behavior. Rogers and Wright (1986) performed direct shear tests on specimens that were subjected to repeated cycles of wetting and drying. These tests were all performed on clay soil collected from the Scott Street and I. H. 610 site in Houston, Texas, identified as the red clay. Four series of drained direct shear tests were performed on collected specimens that were subjected to 1, 3, 9, and 30 cycles of wetting and drying. Shear strength parameters obtained from the study are summarized below in Table 2.3.

Table 2.3 Summary of Shear Strength Parameters from drained direct shear tests on specimens subjected to wetting and drying cycles (Rogers and Wright (1986))

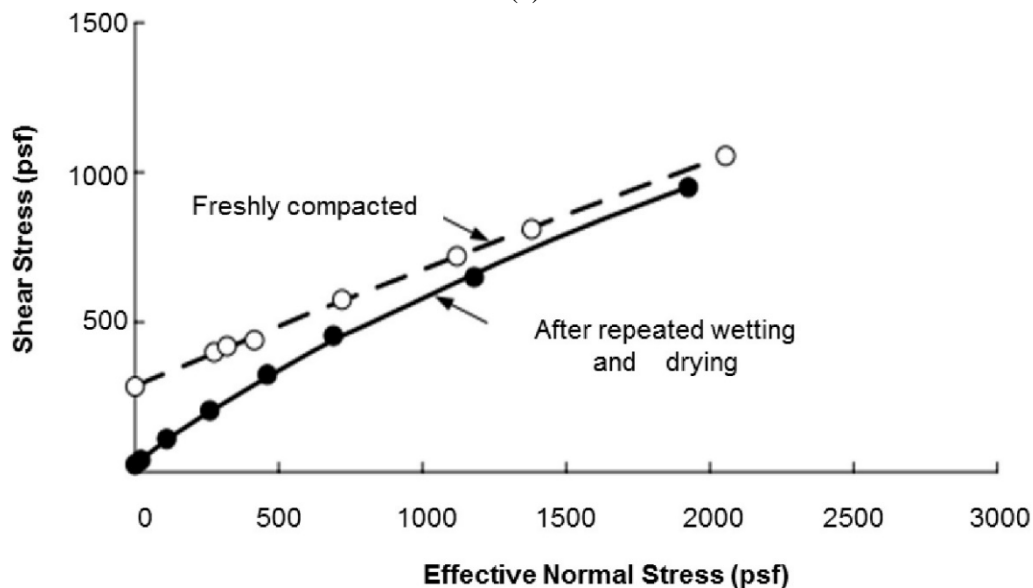
Number of Wet-Dry Cycles	Cohesion, c' (psf)	Friction Angle, Φ
1	29	23°
3	77	26°
9	33	25°
30	0	27°

Rogers and Wright (1986) reported that cyclic wetting and drying of the soil produces a significant shear strength loss, particularly regarding effective cohesion intercept, c' . The direct shear test also indicated that the loss in cohesion occurs within a relatively few numbers of cycles of wetting and drying. Most of the loss in strength occurred in the first cycles. Rogers and Wright (1986) suggested that the effect of wetting and drying in the laboratory was much severe compared to what is expected to occur in the field. Even so, the effects of wetting and drying in the laboratory and the field are believed to be similar.

Kayyal and Wright (1991) developed a new procedure for triaxial specimens subjected to repeated cycles of wetting and drying. The procedure allowed the specimens greater access to moisture and exposure for drying. Also, the procedure allowed substantial lateral expansion and volume change to occur in the soil during drying. Two soils were tested during the study, which included Red clay or Beaumont clay from Houston, Texas, and Highly plastic clay soil from Paris, Texas. Kayyal and Wright (1991) conducted several series of consolidated undrained compression tests with pore pressure measurement. Tests were performed on specimens subjected to repeated wetting and drying as well as on freshly compacted samples. Based on the study, the shear strength envelopes for specimens of Beaumont clay and Paris clay tested in the as compacted and after wetting and drying are presented in Figure 2.8. The results presented that both envelopes were distinctly nonlinear. Also, the strength envelope for the specimens subjected to wetting and drying cycles lied significantly below the envelope for the specimens tested in the as-compacted condition at lower values of normal stress. Moreover, the intercept of the strength envelope for specimens subjected to wetting and drying is small and could be considered negligible.



(a)



(b)

Figure 2.3 Shear strength envelopes regarding effective stress (a) Beaumont clay (b) Paris clay (Kayyal and Wright (1991))

2.2.5 Climate and hydrological condition

Climate, hydrological conditions, environmental conditions, topography, and geology govern the formation and behavior of soils. The climate, in particular, is one of the essential factors in soil profile development. It helps to change parent material into the soil. Climatic factors, such as precipitation, wind, sunlight, and temperature, accelerate the formation of the basic material of soil. The soil is a mixture of rock fragments, minerals, air, water, and organic materials. Soils vary due to the different ingredients they contain, and climate contributes to those differences. For example, the climatic and topographical conditions under which smectite is formed is entirely different from that of kaolinite. The formation of smectite requires low relief, low permeability, low rainfall, and low temperature. In these conditions, the environment offers extreme disintegration, intense hydration, and restrained leaching appropriate for the

formation of smectite rich, expansive soils (Tourtelot, 1973 and Azam et al., 1998). In contrast, high temperature, strong hydrolysis by high permeability, and high rainfall intensities favor the formation of kaolinite (Tourtelot, 1973 and Weaver, 1989). Therefore, while expansive clays such as montmorillonite are more prevalent in drier environments, non-expansive clays, like kaolinite, are more common in warm, humid environments.

2.3 Yazoo Clay

Yazoo clay soil is highly expansive and extends over central Mississippi, Alabama, and Southern Louisiana (Figure 2.9). Most of the structures are constructed on expansive Yazoo clay in Mississippi. The average composition of the Yazoo clay is 28% smectite (probably montmorillonite), 24% kaolinite, 22% quartz, 15% calcite, 8% illite, 2% feldspar, and 1% gypsum based on recent x-ray diffraction results (Taylor 2005). Yazoo clay is highly plastic with high shrink-swell potential which experiences high volume change (Douglas et al., 2000; Lee et al., 2012).

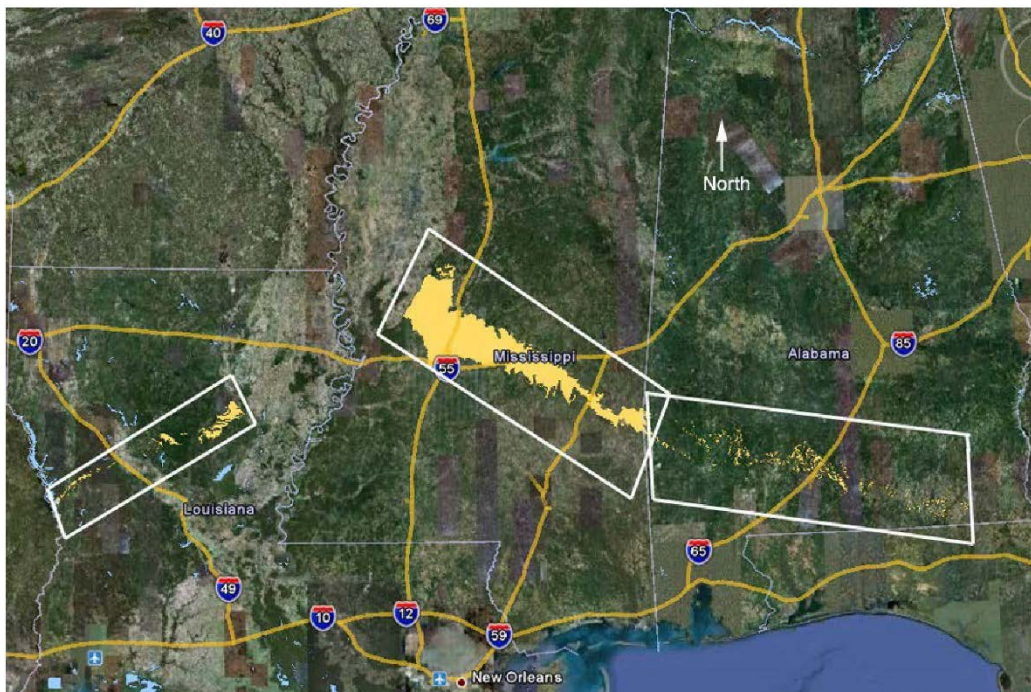


Figure 2.4 Boundary boxes of the Jackson Formation, including Yazoo clay and its geological equivalents, in Mississippi, Alabama, and Louisiana (after USGS 2010)

The Yazoo clay in the Jackson area consists of a weathered upper zone overlying unweathered clays. The weathered portion of the Yazoo clay varies in depth; however, it mostly extends to a depth of around 30 feet (Taylor, 2005). The weathered Yazoo clay usually has a liquid limit greater than 70% to 100%, and a plastic limit from 20% to 30%, results in a plasticity index greater than 50% (Douglas et al., 2000). The change in volume of the Yazoo clay between the liquid limit and oven-dry moisture contents ranged from 100 to 235 percent (Lee, 2012). Over time, it has been shown that the top few feet of highway slopes containing weathered yazoo clay can experience a significant strength loss during seasonal wet-dry cycles.

2.3.1 Engineering Aspects of Yazoo Clay

2.3.1.1 Weathered versus Unweathered Clay

Local geologists and engineers describe Yazoo clay as being either “unweathered” or “weathered.” Unweathered clay has a visually distinct blue color that grades into a gray-blue and gray, or it may have a green to grayish-green color. Cycles of exposure to air, wetting, and drying tend to cause oxidation and acceleration of clay weathering. Exposure to drying is accompanied by shrinkage and weathering, causing mineralogical changes, which in turn change the structural and strength characteristics of clay. Many types of clay lose their stability due to drying and tend to “slake” during rewetting (Mitchell, 1993). When air-dried Yazoo clay is wetted, it quickly slakes but is affected very little by exposure to additional water if already at its natural water content. Detrimental swelling can be expected when Yazoo clay is allowed to dry below the optimum gravimetric water content (~15%) and is then wetted (Redus, 1962). As shown later in this report, Yazoo clay can appreciably swell when inundated from its natural water content state. The unweathered Yazoo clay has structural breaks with slickenside (joints and fissures) features. These slickenside breaks are probably due to unloading after pre-consolidation or from shrinkage cracking during drying. Fissures have been found in normally consolidated clays at water contents well above their shrinkage limit (Lee, 2012).

Yazoo clay is similar to another sedimentary expansive soil, known as London Clay, assumed to originate during the same Eocene era (De Freitas and Mannion 2007). London Clay’s weathered upper consistency is soft to firm, with ochre staining due to oxidation of iron compounds. The upper 4 ft (1.21 m) or so is the active zone. The lower-depth unweathered clay has blue-gray color and is firm to very stiff. London clay, similar to Yazoo clay is also problematic as a shrink-swell material (Kovacevic et al. 2007; Hight et al. 2007; Jones and Terrington 2011).

The Mississippi weathered Yazoo clay formation is generally found in a zone between the ground surface and the deeper unweathered clay. It has a visually distinct color ranging from a limonite-stained orange to yellow. Near the surface, its consistency is usually soft and gummy, but it becomes firmer with depth. At the surface, caliche and gypsum crystals are common weathering features, and the clay may or may not be calcareous. Near the surface, the fractured nature of the soft clay allows mixing with the surface material, which can include loess silt, alluvial sands, and gravel. Thus, the near-surface weathered zone can have a significantly altered structural composition. Weathered Yazoo clay is marked by numerous fractures and these fractures allow water to penetrate the otherwise low-permeability clay and enhance weathering at depth (Lee 2012). Martin’s (2007) conducted a Scanning Electron Microscope (SEM) study which concluded that highly fractured weathered Yazoo clay has surface coatings and vein fillings of secondary calcite, gypsum, manganese oxides, and iron oxides. Figure 2.10 indicates that the weathered Yazoo clay generally lies above the unweathered Yazoo clay (Lee, 2012).

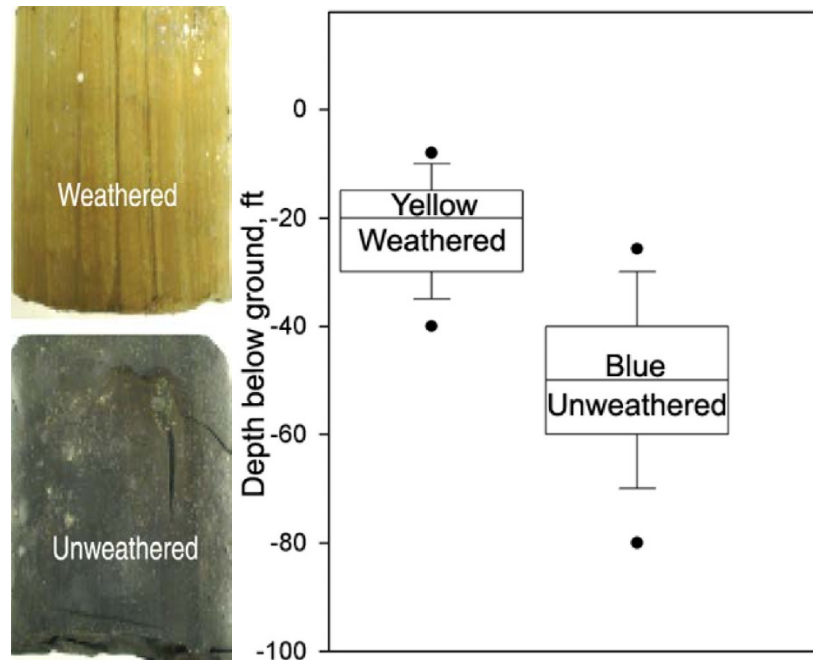


Figure 2.5 Box plots showing a range of depths for visually-classified samples (Lee (2012))

2.3.1.2 Geotechnical Index Properties

Lee (2012) performed an MDOT funded state study to investigate the properties and characteristics of Yazoo clay soil in Mississippi. During the study, Yazoo clay soil samples from different locations were investigated and presented an average index property value. Table 2.4 lists the mean values for all the Yazoo clay soil data visually separated by sample color from that study. The ‘weathered’ samples were yellowish, and the ‘unweathered’ samples had a blue color. Weathered clay was visually identified in samples from the surface to 40 ft. (12.19 m) depths. The study visually identified unweathered clay, which was sampled and tested between depths of 25 ft. and 80 ft. below ground surface.

Table 2.4 Yazoo clay average index property values (Lee (2012))

Parameter	Weathered (yellow)		Unweathered (blue)		All	
	Mean	Stan Dev	Mean	Stan Dev	Mean	Stan Dev
γ dry, lbs/cu ft	82	9	82	9	82	9
γ wet, lbs/cu ft	112	10	114	9	113	10
Moisture Content %	38	9	39	9	39	9
Field Void Ratio	0.99	0.21	1.03	0.22	1.02	0.22
LL %	94	19	95	16	94	17
PI %	35	8	37	8	36	8
PI %	59	16	58	13	59	14
VC %	140	39	138	38	138	39
*Clay %	53	21	65	14	60	18
* Calcite %	13	16	18	14	16	15
*Smectite %	45	18	48	13	46	15
*Illite %	16	17	11	10	13	14
*Kaolinite %	39	11	42	8	41	10

*XRD data

Lee (2012) also analyzed the correlations between geotechnical properties and available mineralogy data. The study indicated that the Yazoo clay includes quartz, clay, calcite, smectite, illite, and kaolinite. There was little correlation between sample depth (or elevation above mean sea level, as shown in Figure 2.11) and regional volume change (VC). There also appeared to be little correlation between regional VC and visual color identification of weathering as a function of depth (or elevation) (Lee (2012)). The study indicated that using visual color identification (yellow or blue) as the primary method to discriminate between weathered and unweathered clay may not be a reliable indicator for regional VC. Regression analysis, performed by Lee (2012), indicated almost no correlation between the averaged VC values as a function of depth. Averaged VC values exhibited an observable pattern when grouped by depth intervals (Lee (2012)).

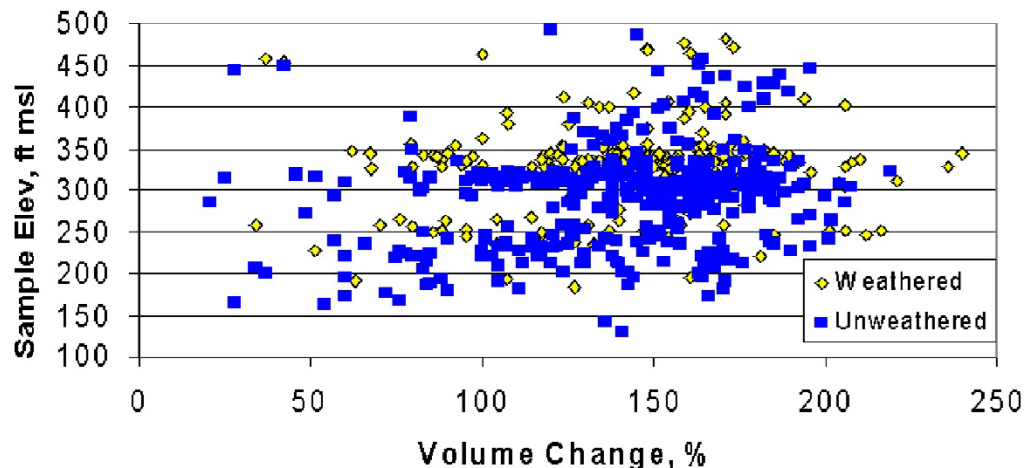


Figure 2.6 Volume change percent (VC%) values for all Yazoo clay data in the 5-county area of central Mississippi, plotted by elevation above mean sea level (MSL) (Lee (2012))

Based on the study performed and summarized by Lee (2012), Figure 2.12 shows that the plastic limit (PL) values did not change much by depth, but the liquid limit (LL) and thus the plasticity index (PI) values varied in concert with the VC% values. Although these data are regional, the study noted the following trends:

- Average VC% and LL values were lowest above 10 ft (3.048m) and around 50 ft (15.24m).
- Average VC% and LL values were highest around 10 ft (3.048m), 25 ft (7.62m), and 55 ft (16.76m).
- These regional data indicated the non-uniformity of Atterberg limits and expansive behavior patterns with depth.

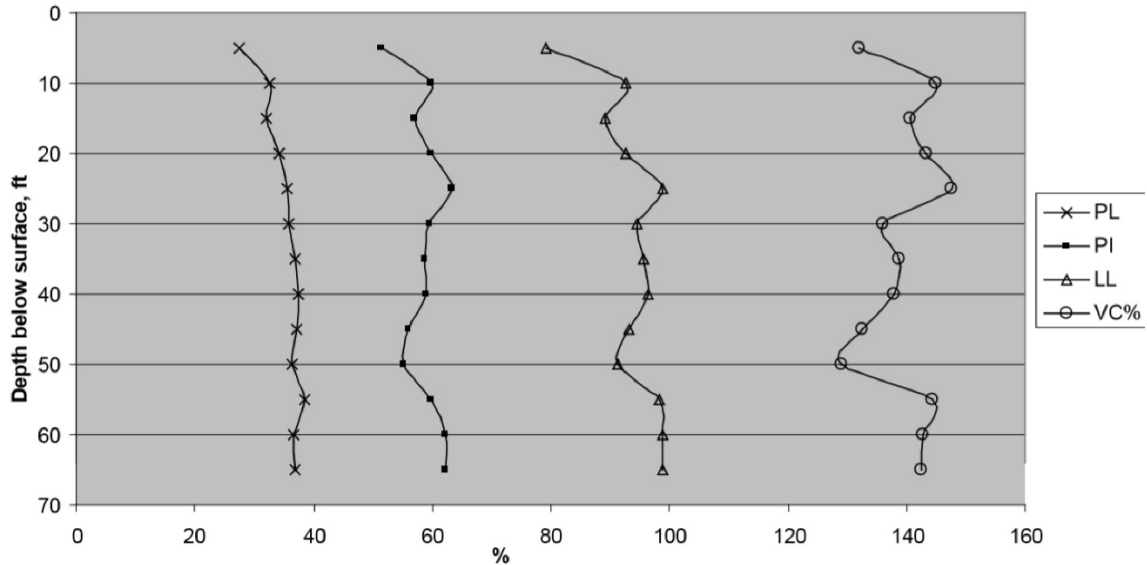


Figure 2.7 Regional weathered plus un-weathered Yazoo clay VC % and Atterberg limit values, averaged by 5-ft (1.524m) depth intervals (Lee (2012))

Lee (2012) indicated that the only significant geotechnical index property correlation was between dry density and natural water content (correlation coefficient $R^2 = 0.94$), whether the sample is weathered Yazoo clay or unweathered Yazoo clay was irrelevant for this correlation. The high correlation was noted regardless of the degree of weathering. The best-fit non-linear regression equation is presented as Equation 2.4 (Figure 2.13):

$$Dry_{density}, (pcf) = 142.2e^{-0.0143w(\%)} \quad (2.4)$$

Where e = natural log base = 2.178 and $w\%$ = water content.

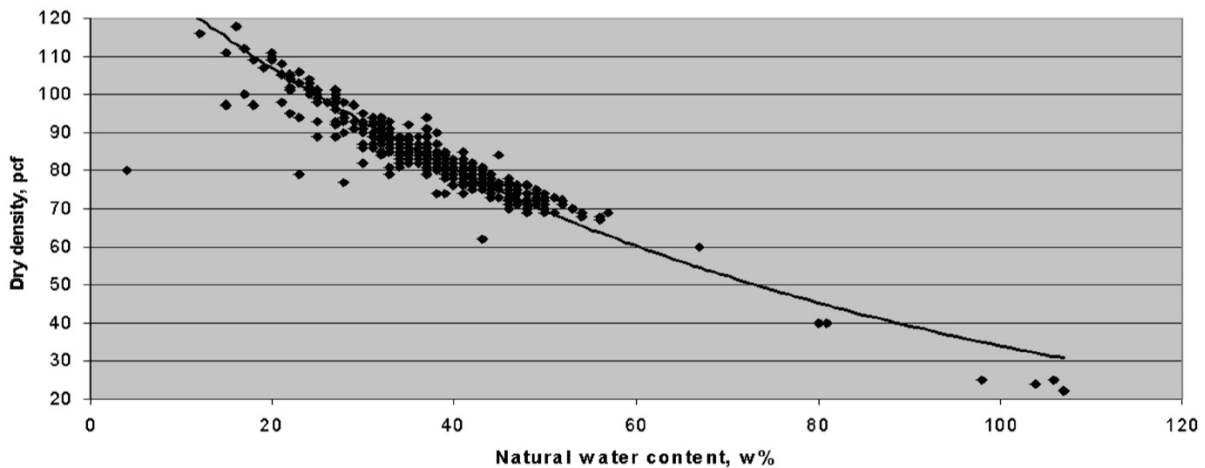


Figure 2.8 Dry density versus natural water content for all Yazoo clay data in the 5-county area of central Mississippi (Lee (2012))

2.3.2 Synopsis of Regional Observations

Lee (2012) has performed rigorous analyses on the Yazoo clay soil samples and developed several correlations between different soil parameters. Based on the study, some of the useful correlations for the weathered, unweathered, and visually non-discriminated Yazoo clay samples are presented in this chapter.

Strong relationships existed between average natural water content, LL, PL, and dry density. For example, knowing the natural water content averaged over any 5-ft (1.524m) depth interval for a Yazoo clay sample retrieved from less than 45 ft (13.72 m) below ground surface enabled estimates in equation 2.5 to equation 2.8 such that:

$$LL\% = 15.17(w\%)^{0.49} \quad (R = 0.90) \quad (2.5)$$

$$PL\% = 1.36(w\%)^{0.89} \quad (R = 0.91) \quad (2.6)$$

$$\text{Dry density, pcf} = 296.6(w\%)^{-0.35} \quad (R = 0.95) \quad (2.7)$$

$$\text{Wet density, pcf} = 188.1(w\%)^{-0.14} \quad (R = 0.80) \quad (2.8)$$

Lee (2012) indicated that for non-discriminated samples (i.e., those not separated by visual degree of-weathering), averaged PL and clay content percent were strongly related to depth. They were also strongly related to averaged smectite, illite, and kaolinite percentages. For example, knowing the Yazoo clay sample depth (less than 45 ft (13.72m) below ground surface) enabled estimates of interval averaged values in equation 2.9 to equation 2.11 such as:

$$PL\% = 24.63(\text{Depth, ft})^{0.11} \quad (R = 0.94) \quad (2.9)$$

$$\text{Clay}\% = -33.5 + 0.31(\text{Depth, ft}) + 2.33(PL\%) \quad (R = 0.97) \quad (2.10)$$

$$\text{Smectite}\% = -21.94 - 0.21(\text{Depth, ft}) + 2.18(PL\%) \quad (R = 0.91) \quad (2.11)$$

Lee (2012) indicated that VC was poorly related to any of the index or mineralogy properties. The regional data yielded poor correlations for Yazoo clay behavior (i.e., volume change percent) to geotechnical index or mineralogical properties, with the one exception being the dry density-natural water content relationship previously shown. The regional data yielded poor correlations between the geotechnical index and mineralogical properties related to a depth below the ground surface unless those values were depth-averaged in 5-ft (1.524m) intervals. Poor regional correlations to an elevation above MSL were also noted (Lee, 2012).

2.3.2.1 Useful Equations Site-specific data

Lee (2012) has performed rigorous analyses on the Yazoo clay soil samples and develop several correlations between different soil parameters. The following useful equations were derived from the lab data from the study site:

- If the natural water content % (in the range 25% to 50%) is known as presented in equation 2.12 to equation 2.14. It should be noted that *Iss* in equation (2.14) represents the shrink-swell index with a consolidation cell load of 144 psf.

$$\text{Dry density, pcf} = 137.19e^{-0.012w\%}, e = 2.718(R^2 = 0.85) \quad (2.12)$$

$$\text{Free Swell \%} = 0.9212w\%^{1.2737} \text{ for } (25\% < w\% < 50\%); (R^2 = 0.90) \quad (2.13)$$

$$\text{Iss 144} = 0.251w\% - 4 \quad (R^2 = 0.83) \quad (2.14)$$

The average total suction below the active zone depth is presented in equation 2.15.

$$\log \text{ suction, psf} = -0.079w\% + 6.47 \quad (2.15)$$

- If the average total suction below the active zone depth is known as presented in equation 2.16,

$$\text{Potential combined shrink – swell vertical movement (strain) \%} = 51(\log \text{ suction, psf}) - 222 \quad (2.16)$$

- If the dry density γ_d , pcf is known as presented in equation 2.17.

$$\text{Free Swell \%} = 1636.4e^{-0.034\gamma_d} \quad (R^2 = 0.88) \quad (2.17)$$

- If the Free swell % is known as presented in equation 2.18,

$$LL\% = 6.6168FS\%^{0.5741} \quad (R^2 = 0.90) \text{ for } (70\% < FS\% < 140\%) \quad (2.18)$$

If LL is known as presented in equation 2.19 to equation 2.21,

$$VC \% = 0.5665LL^{1.2368} \quad (R^2 = 0.88) \text{ for } (80 < LL < 120) \quad (2.19)$$

$$\text{Free Swell \%} = 0.08LL^{1.5754} \quad (R^2 = 0.90) \quad (2.20)$$

$$w_{24hr}\% = 2.5559LL^{0.8571} \quad (R^2 = 0.92) \quad (2.21)$$

• If the water content after 24 hours ($w_{24hr}\%$) is known as presented in equation 2.22,

$$LL = 0.5344w_{24hr}\%^{1.0708} \quad (R^2 = 0.92) \quad \text{for } (100\% < w_{24hr}\% < 150\%) \quad (2.22)$$

2.3.3 Extended Mohr-Coulomb failure envelope

Slopes constructed in the arid and semi-arid regions remain in the unsaturated condition above the groundwater table. To accurately predict the mechanical behavior of unsaturated soil, two stress state variables are required, of which the most widely used, is the combination of net normal stress ($\sigma - u_a$) and matric suction ($u_a - u_w$). Based on these two stress state variables, Fredlund et al. (1978) proposed the following equation 2.23, which is an extension of the M-C theory to describe the shear strength of unsaturated soil:

$$\tau = c' + (\sigma - u_a)\tan\phi' + (u_a - u_w)\tan\phi^b \quad (2.23)$$

Where,

$(\sigma - u_a)$ = net normal stress

$(u_a - u_w)$ = matric suction

ϕ' = angle of internal friction associated with the change in net normal stress

ϕ^b = angle representing the rate of change in shear strength relative to matric suction change

The first two terms on the right-hand side in equation 2.23 describes the conventional MC theory to determine the strength of saturated soil. The third term indicates the change in shear strength due to a change in matric suction in unsaturated soil. The corresponding failure envelope for the extended M-C criterion is presented in three-dimensional stress space in Figure 2.14.

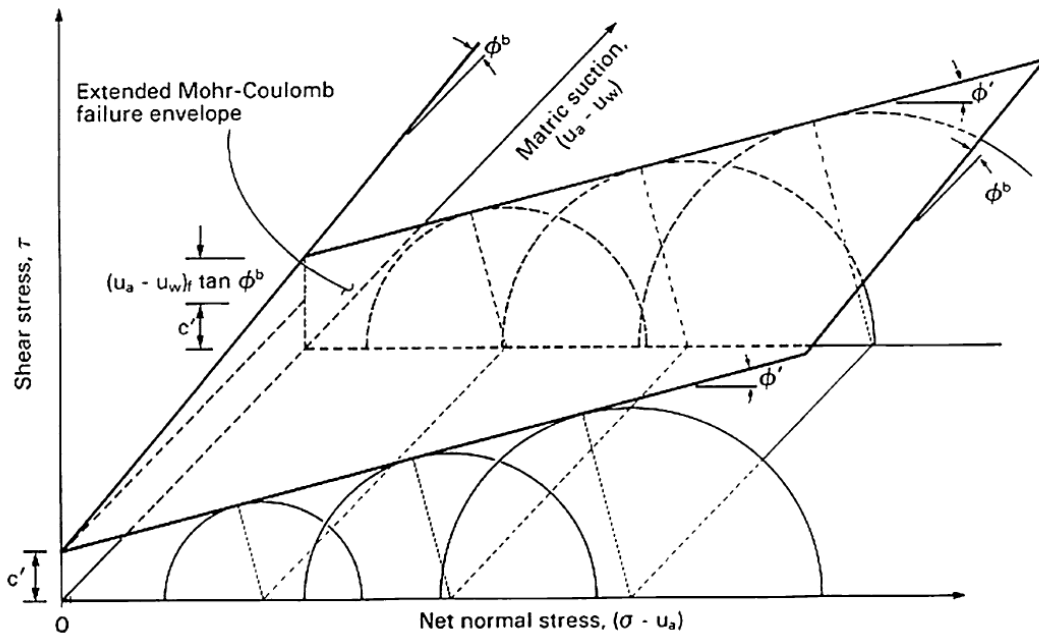


Figure 2.9 Extended Mohr-Coulomb failure envelope for unsaturated soils (Fredlund and Rajardjo, 1993)

2.3.3.1 Soil Water Retention Curve for Yazoo Clay

Nobahar et al. (2019) developed the Soil Water Retention Curve (SWRC) curve for the Yazoo clay soil in Mississippi. The Van Genuchten (1980) model is presented in equation 2.24 and equation 2.25:

$$\theta = \theta_r + (\theta_s - \theta_r) / [1 + (\alpha h)^n]^m \quad (2.24)$$

$$m = 1 - (1/n) \quad (2.25)$$

Where h is the pressure head, α , m and n are the Van Genuchten fitting parameters, and θ_s and θ_r are the saturated and residual water content, respectively. The SWRC curve of Yazoo clay soil is presented in Figure 2.15. The fitting curve was developed through different trials considering the Van Genuchen (1980) model. A simple spreadsheet was developed that plots the SWRC curved with the value of the fitting parameters (α , m , and n) and compared with tested results. After several trials, the best fitted SWRC curve with the tested results was considered, and the final fitting parameters were set. The spreadsheet is available with the paper.

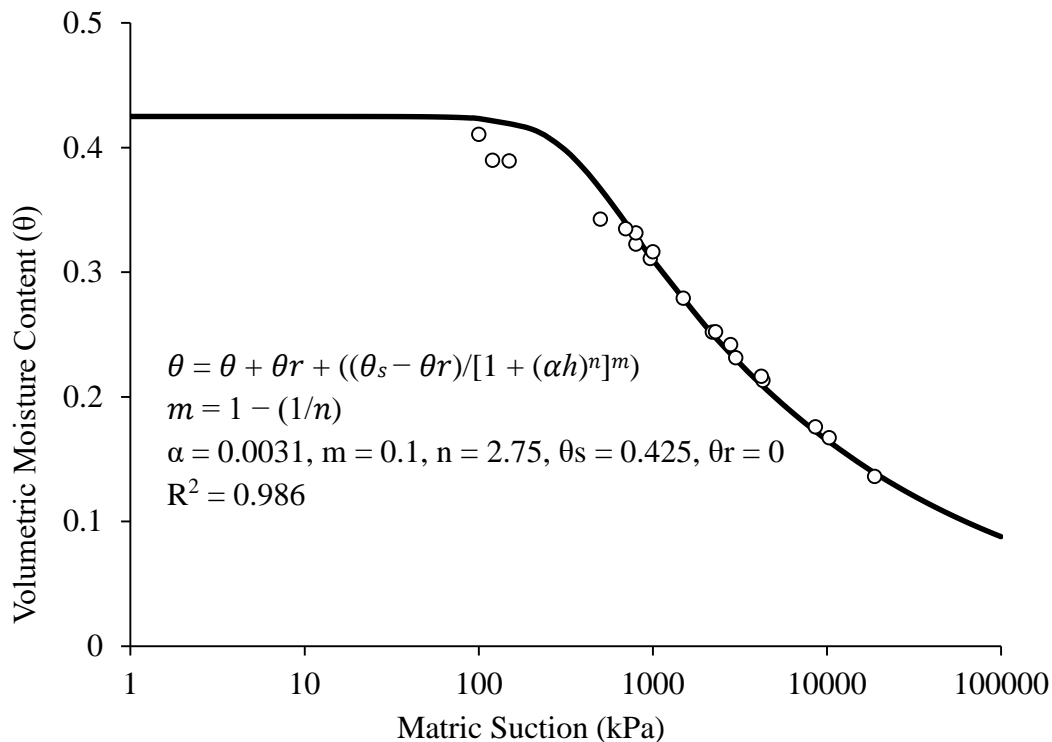


Figure 2.10 Soil water retention curve of Yazoo clay (Nobahar et al., 2019)

2.3.4 Effect of the wet-dry cycle of Yazoo clay

Khan et al. (2019) have conducted several tests to investigate the effect of the wet-dry cycles on the changes in the shear strength of Yazoo clay. During this study, tests were conducted on the representative Yazoo clay samples, which were collected from a borehole in a highway slope site in Jackson, Mississippi. The collected samples were investigated and classified as highly plastic clay (CH) from a grain size distribution analysis according to ASTM D422 and ASTM D7928. A liquid limit and plasticity index of 108% and 84% (Table 2.5) were determined according to ASTM D4318.

Table 2.5 Yazoo clay soil properties

Physical Properties	Values
Unified Classification	CH
Liquid Limit	108%
Plasticity Index	84%
Dry unit weight	12.88 kN/m ³
Specific Gravity	2.68
Natural Moisture Content	35%

Khan et al., 2019 reconstituted Yazoo clay soil samples with a height of 25.4 mm and a diameter of 76.2 mm to investigate the effect of wet-dry cycles in a controlled environment in the laboratory. During this study, the Yazoo clay samples were subjected to 3, 5, and 7 numbers of wet-dry cycles and then tested for the void ratio, microstructure, volumetric deformation, and shear strength. The laboratory program is tabulated in Table 2.6. The direct shear test was conducted following ASTM D3080 to determine the shear strength of the samples subjected to different wet-dry cycles. A 63.5 mm diameter shear box was used for testing with a maximum possible shear displacement of 20 mm. The rate of shearing is 0.0025 mm/min to maintain a drained condition. Direct shear tests were conducted for compacted specimens that underwent 3, 5, and 7 wet-dry cycles with three different normal stresses of 25, 50, and 100 kPa. The shear strength parameters (cohesion and friction angle) of the drying-wetting cycle specimens were determined using a Mohr-Coulomb (M-C) failure envelop.

Table 2.6 Laboratory study of the effect of the wet-dry cycle on Yazoo clay

Number of Samples	No of Wet-Dry Cycles	Investigative Parameters
	1	
3	3	Void Ratio,
	5	Drained Shear Strength
	7	

Based on the study conducted by Khan et al., 2019, the axial deformation of Yazoo clay soil under different wet-dry cycles is presented in Figure 2.16. The axial deformation of the samples is the difference between the height of the sample after deformation vs. the original height of the samples before any wet-dry cycle. The change in height is relative to the initial height of the sample. The study indicated that at three wet-dry cycles, the axial deformations at shrinkage are greater than deformations during swelling. However, the swelling is lower for 5 and 7 wet-dry cycles compared to the swelling of three wet-dry cycles. Thus, the swelling potential of Yazoo clay is higher at low wet-dry cycles and decreases with the increasing number of wet-dry cycles. These findings are consistent with the results that were reported by Alonso et al. (2005), Rosenbalm and Zapata (2017), and Tripathy et al. (2002).

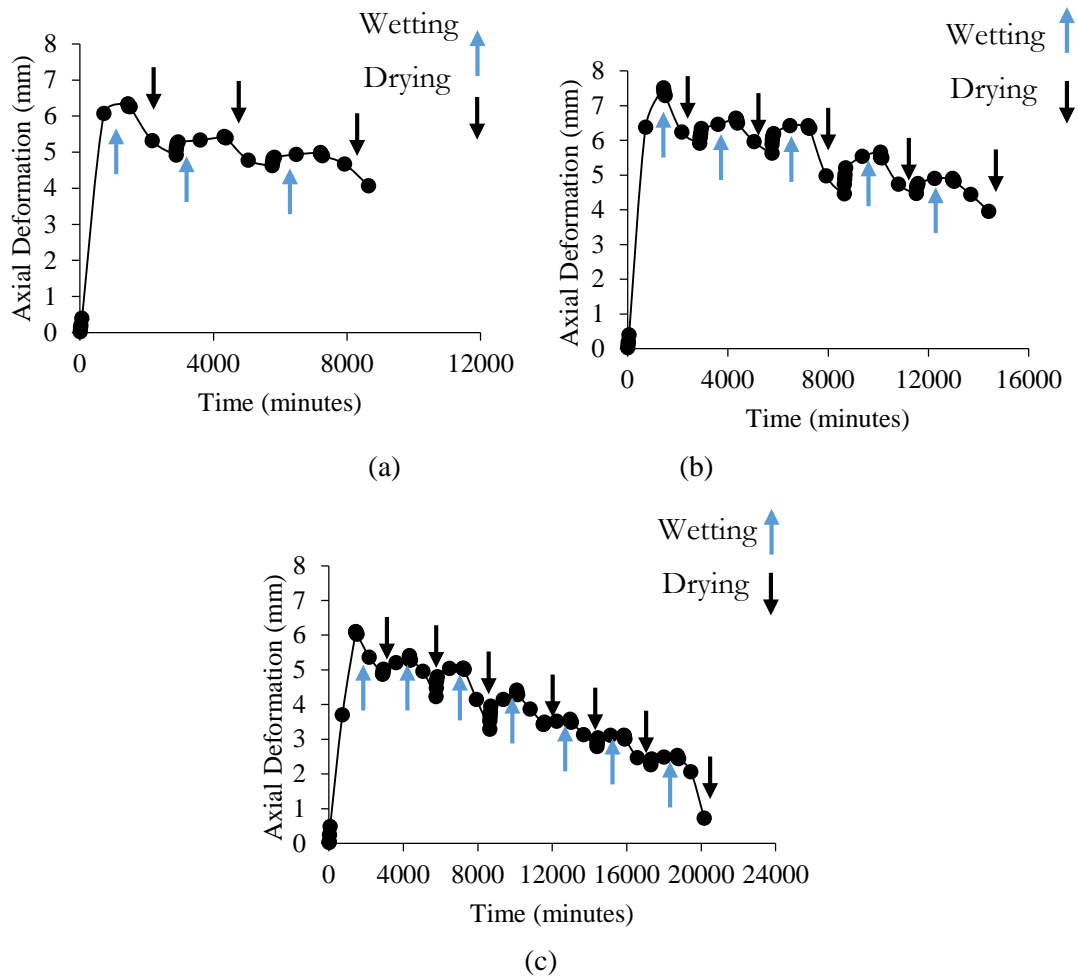


Figure 2.11 Vertical deformation curve of Yazoo clay sample at (a) 3 wet-dry cycles (b) 5 wet-dry cycles (c) 7 wet-dry cycles

Khan et al., 2019 indicated that with the increase in the number of drying-wetting cycles, the compaction segment of the curve grows significantly, mainly because the sample grain skeleton structure under the action of a cycle is changing. Microcracks evolve, which continuously increases the voids. As indicated in Figure 2.17, the initial void ratio of the Yazoo clay was 0.94, which increases to 1.2 after the end of the third wet-dry cycle, which further increased to 1.4 after the end of the seventh wet-dry cycle. These values agree with an initial to the final void ratio of 0.75 to 1.12 for three wet-dry cycles reported by Rogers and Wright (1986), while investigating the effect of wetting and drying for long-term shear parameters for compacted Beaumont clay. It should be mentioned that at the end of each wetting and drying phase, the void ratio increases, and porosity increases which will make the samples softer over time.

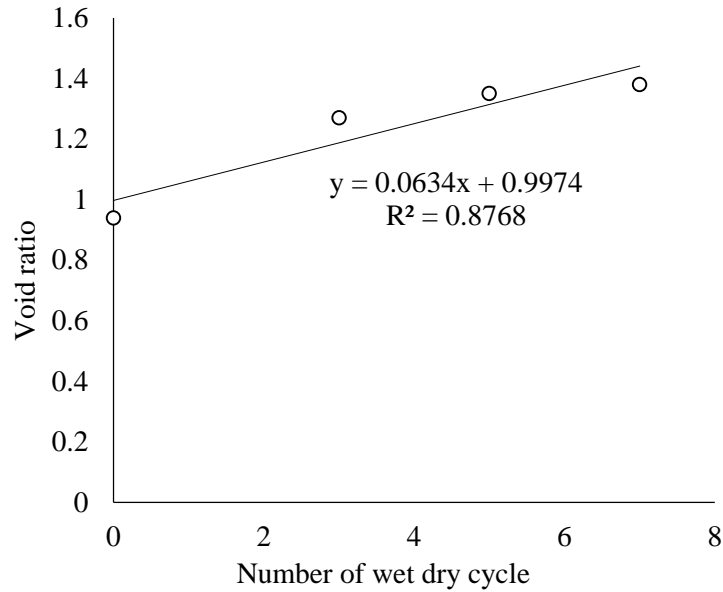


Figure 2.12 Change in void ratio with different wet-dry cycles

Khan et al., 2019 further extended the study to examine the chemical composition of the Yazoo clay sample (Table 2.7) and changes in pores (voids) using Scanning Electron Microscopy (SEM). As indicated in Table 2.7, Yazoo clay has a high percentage of oxygen (54.14%), silicon (25.21%) and aluminum (10.90%), which indicates that most of Yazoo clay is montmorillonite (Barton, 2002).

Table 2.7 Yazoo clay sample chemical composition based on SEM data

Mineral Composition of Yazoo Clay Sample	Weight (%)	Weight % Error (+/-1 Sigma)	Normalized Weight (%)	Normalized Weight % Error (+/- Sigma)	Atom %
Carbon	1.36	±0.11	1.36	±0.11	2.26
Oxygen	54.14	±0.40	54.14	±0.40	67.67
Fluorine	0.00	---	0.00	---	0.00
Magnesium	1.22	±0.08	1.22	±0.08	1.00
Aluminum	10.90	±0.13	10.90	±0.13	8.08
Silicon	25.21	±0.18	25.21	±0.18	17.95
Potassium	1.44	±0.08	1.44	±0.08	0.74
Calcium	1.53	±0.09	1.53	±0.09	0.77
Titanium	0.46	±0.05	0.46	±0.05	0.19
Iron	3.74	±0.21	3.74	±0.21	1.34

Figure 2.18 shows the changes of Yazoo clay voids/porosity after the 3rd, 5th, and 7th wet-dry cycles. The ultimate available resolution with SEM is of the order of 0.2 μm (0.66 μft). This order was used during the examination of Yazoo clay because of the sample's high cohesion and very tiny particles compared to silt or sand that can be examined on the order of 0.5 μm (1.64 μft). Conclusively, from the SEM image shown below, the increase in the void ratio will reduce to fully soften shear strength.

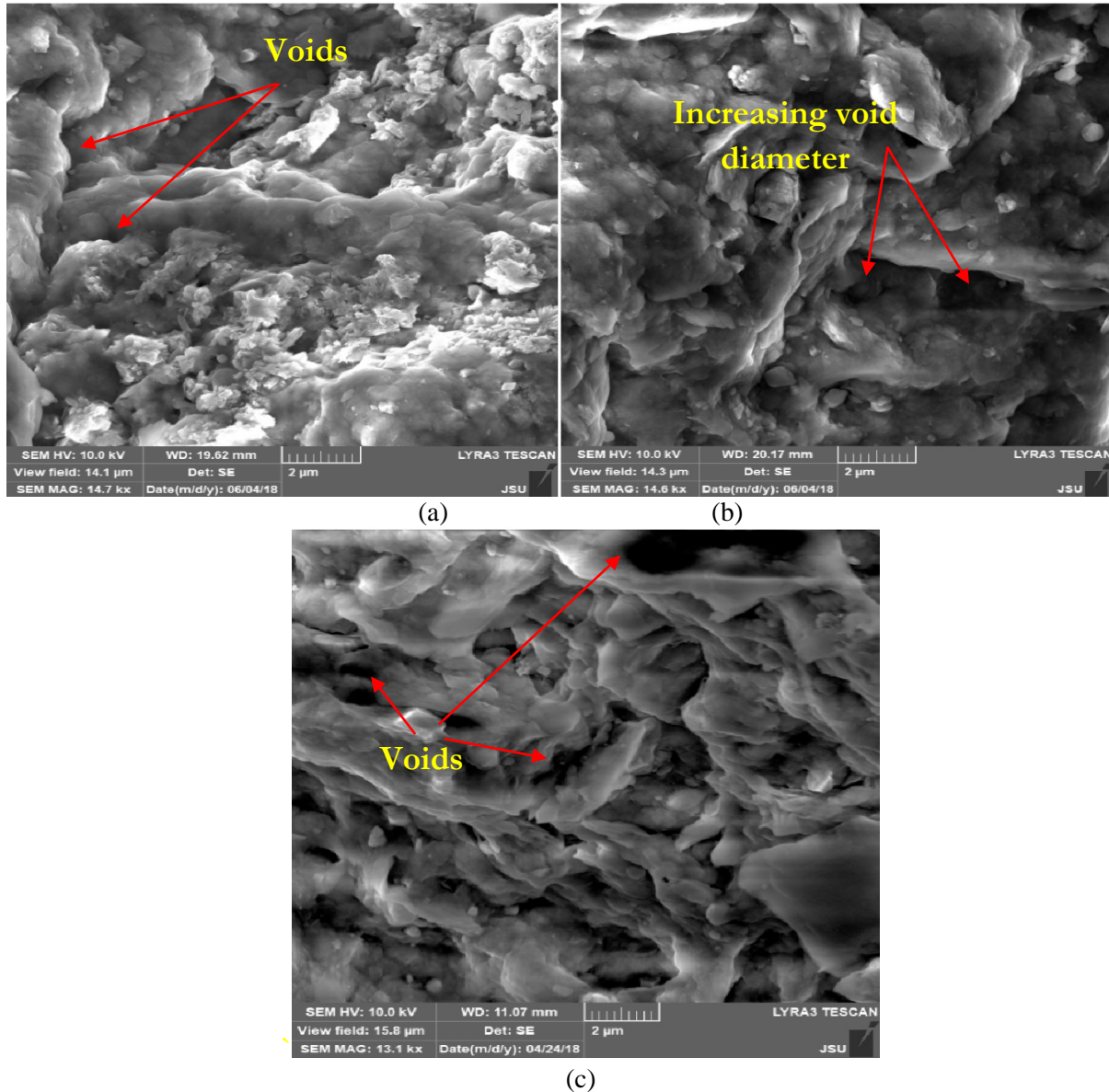


Figure 2.13 Change in pore space of Yazoo clay using SEM imaging after the sample subjected to (a) 3 wet-dry cycles (b) 5 wet-dry cycles (c) 7 wet-dry cycles

Results obtained from the direct shear tests on wet-dry samples, as conducted by Khan et al., 2019, are presented in Figure 2.19. As the soil strength parameters decrease with the increasing number of wet-dry cycles, the position of the M-C failure surface also shifts downward. It indicates the dependency of the failure envelope with the changes in the void ratio. An increase in some wet-dry cycles increases the void ratio and reduces the shear strength envelope.

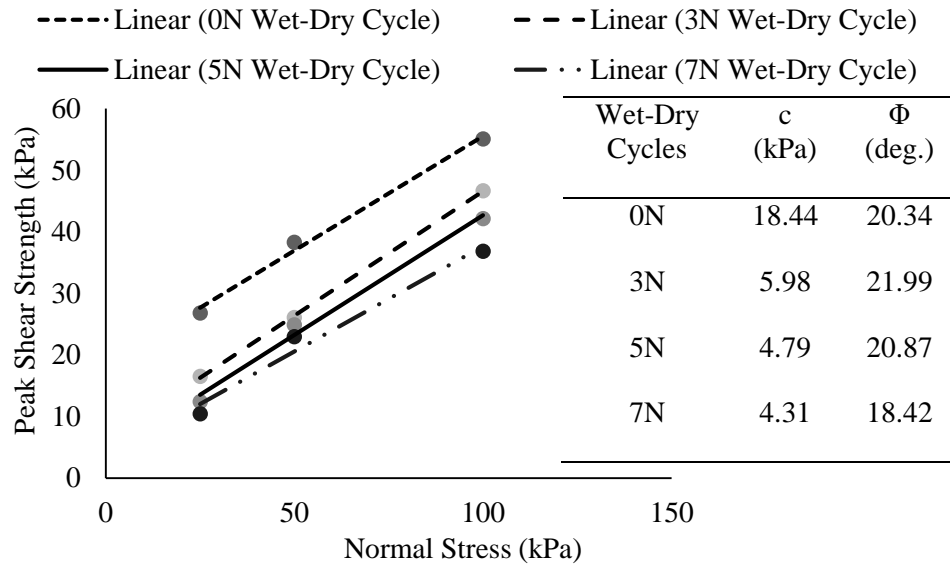


Figure 2.14 Mohr-coulomb failure envelopes of the samples subjected to different wet-dry cycles

Based on the direct shear test of results of the Yazoo clay soil samples reported by Khan et al., 2019, the variation in cohesion and the friction angle was calculated based on the test results of wetting and drying cycles of 0, 3, 5, and 7 times respectively. The results indicated that with the increase of drying-wetting cycles, the cohesive force is significantly reduced. In the 7th number of wetting and drying cycles, the cohesive force was reduced to a minimum of 4.31 kPa from 18.44 kPa for zero wetting and drying cycle, which is a 77% drop in cohesion. On the other hand, there is a drop in the friction angles as observed; however, this drop is not as significant as observed in the cohesion. For example, the frictional angle for 0 wet-dry cycles is 20.34, which dropped to 18.42 deg — with 7 numbers of wet-dry cycles, resulting in only a drop of 10%. This result is in good agreement with the observation made by Rogers and Wright 1986 and Zornberg et al., 2007.

2.3.5 Progressive change on Shear Strength

Nobahar et al., 2020 investigated the progressive changes in the shear strength of Yazoo clay. During this study, representative Yazoo clay soil samples from a highway slope in Mississippi were collected and tested. The physical properties of the soil sample utilized by Nobahar et al., 2020 is presented in Table 2.8. The variation of shear strength of the Yazoo clay samples was determined using the direct shear test. The test apparatus used in these investigations had a pneumatic loading piston for applying the vertical load to the sample and an automated data collection system. A 63.5 mm diameter shear box was used for testing with a maximum possible shear displacement of 20 mm. The rate of shearing is 0.0025 mm/min to maintain drained condition.

Table 2.8 Soil Properties

Physical Properties	Values
Unified Classification	CH
Liquid Limit	108%
Plasticity Index	84%
Dry Unit weight	12.8 kN/m ³
Specific Gravity	2.68

2.3.5.1 Peak drained shear strength

Nobahar et al., 2020 collected undisturbed specimens from the Shelby tube to determine the peak drained shear test. The peak drained shear strength represents the highest shear strength possible that develops as the soil dissipates excess pore water pressure after construction. The extruded sample was trimmed to a height of 38 mm to fit in the shear box of 63.5 mm diameter. The shear box is then assembled with the top and the bottom halves of the box screwed (or otherwise rigidly attached) together. The inside of the shear box is typically lightly greased to minimize side friction. The lower porous stone is placed in the shear box. After placing the samples in the shear box, the undisturbed sample is soaked underwater. Since the permeability of the Yazoo clay is very low, the undisturbed sample is submerged underwater for a week, to ensure the sample is fully saturated. The sample is consolidated under the normal stress of 25 kPa (522 psf), 50 kPa (1044 psf), and 100 kPa (2088 psf), respectively. The direct shear test results are presented in Figure 2.20. The peak shear stress is utilized to determine the peak shear strength of the Yazoo clay.

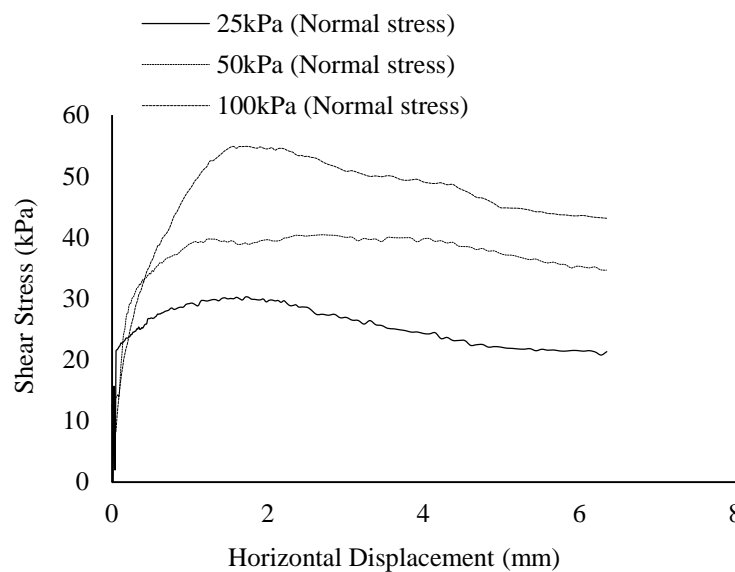


Figure 2.15 Peak drained shear strength curves for three applied normal stresses

2.3.5.2 Fully Soften Shear Strength

Stephens and Branch (2013) have developed a sample preparation procedure to determine the fully softened shear strength of the expansive soil at the US Army Corps of Engineers – Engineer Research and Development Center. Nobahar et al., 2020 followed this procedure to determine the fully softened shear strength. Yazoo clay samples were shaved or shredded at their natural water content. The shredded material was dried for at least 48 hours at a temperature of less than 50 °C and relative humidity below 30%. The sample was then soaked in distilled water for at least 48 hours. The resulting slurry of soaked material had a moisture content more than double the estimated liquid limit. About 500 ml of the slurry was placed in a mechanical blender. The soil water slurry was then mixed without interruption for 10 minutes. After mixing, it was washed through a No. 40 sieve into several plaster of Paris dishes lined with filter paper. These filter paper lined dishes helped wick out excess water from the slurry. A combination of draining and air drying was used to bring the water content of the soil near the liquid limit. The resulting material was then combined into one homogenous sample by working with a steel spatula on a glass plate to make sure that no clay clumps, extraneous nodules, or other 'coarse,' non-clay particles remained. The sample was placed in the shear box, which was assembled with filter paper and a porous stone on top and bottom and placed in the shearing device. The sample preparation photos are presented in Figure 2.21. The ASTM D3080-11

procedure was followed for the remainder of the process except where indicated otherwise. The soil sample was incrementally consolidated to the required normal stress.



Figure 2.16 Sample preparation from the slurry mix to fully soften shear strength, (a) Shredding (b) Slaking (c) Blending and (d) Sieving

Figure 2.22 shows a reduction in strength with accumulated displacement beyond the peak strength. Moreover, the amount of horizontal displacement used in the direct shear testing was sufficient to mobilize post-peak shear strengths.

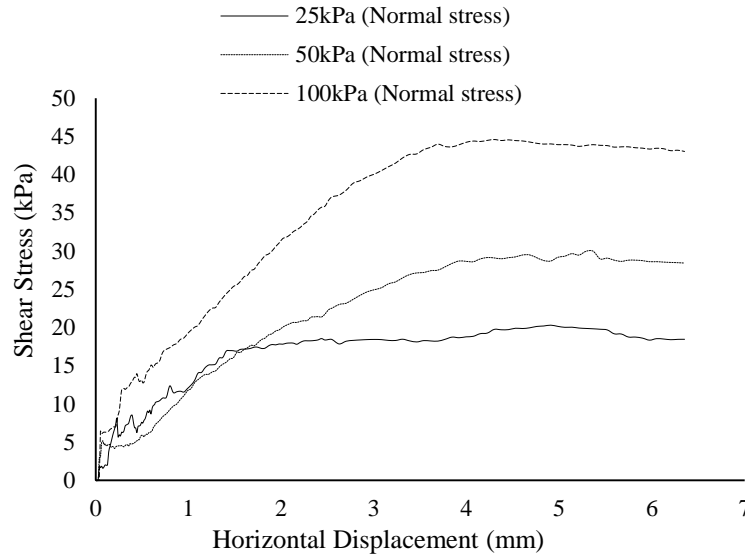


Figure 2.17 Fully softened shear strength curves for three applied normal stresses

2.3.5.3 Residual Shear Strength

The most commonly used method for determining the drained residual shear strength of stiff clays, shales, and mudstones is by drained multiple reversal direct shear tests or by drained ring shear tests, using either undisturbed or reconstituted specimens (e.g., Bishop et al. 1971; Bromhead and Dixon 1986). For direct shear tests, the best procedure is to start with precut specimens, sometimes cut from intact, undisturbed samples, but more often prepared from reconstituted samples (Mesri and Cepeda-Diaz 1986).

Nobahar et al., 2020 determined the residual shear strength of Undisturbed Yazoo clay soil samples. The undisturbed soil from the Shelby tube is shredded and placed in the direct shear test box and then soaked underwater for saturation. Once the sample is fully saturated, the specimen was consolidated for 24 hours. To determine residual shear strength, the device was modified to enable the reversing of the upper one-half of the shear box to its original position after each run. Therefore, the test is conducted with the desired amount of accumulated one-directional displacement for each value of effective normal stress (or normal stress increment).

Nobahar et al., 2020 conducted the cyclic direct shear test under normal stresses of 25 kPa (522 psf), 50 kPa (1044 psf), and 100 kPa (2088 psf) applied at a displacement rate of 0.00254mm/min for 30 number of cycles respectively. The variation of shear stress against the elapsed time of the sample is presented in Figure 2.23.

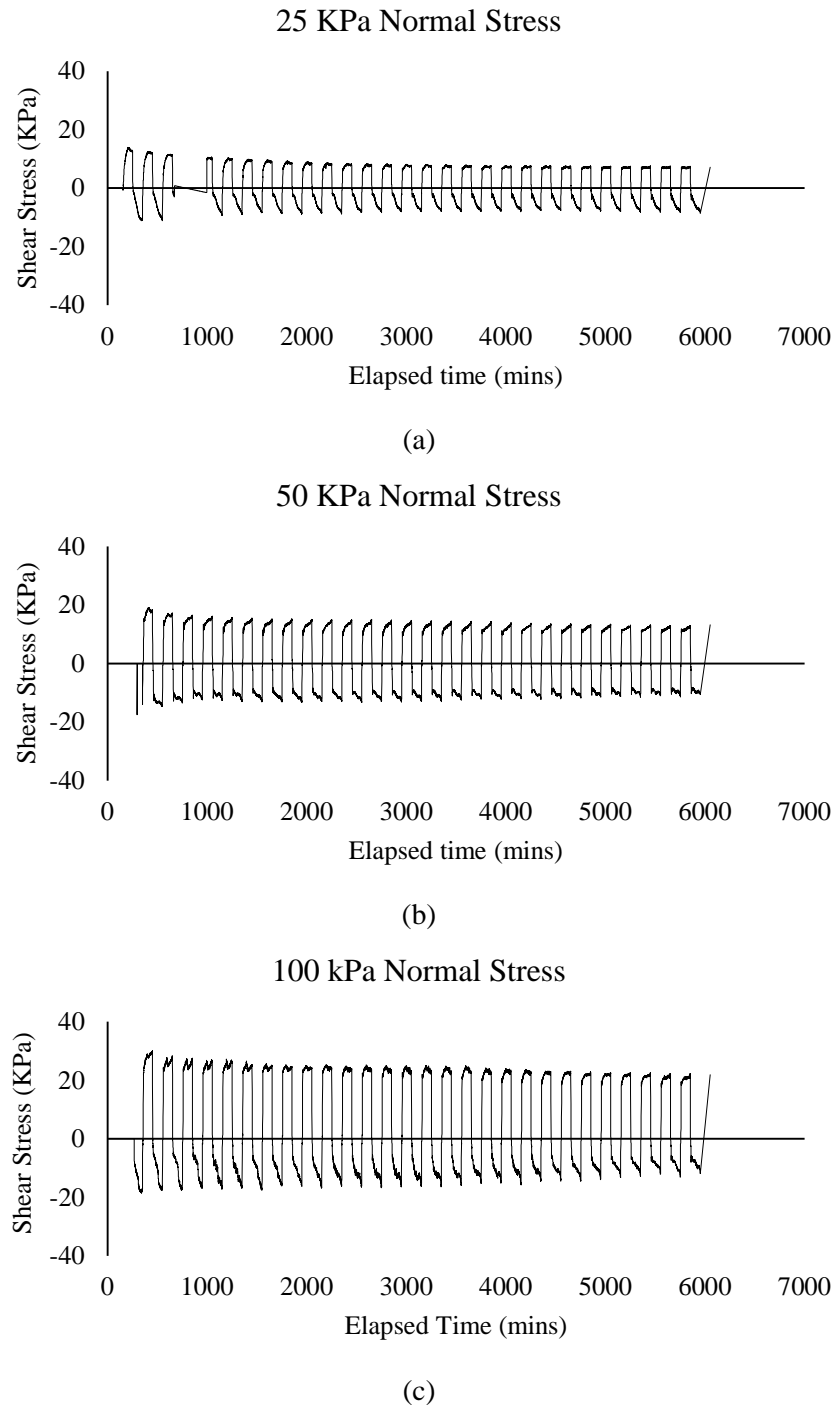


Figure 2.18 Shear Stress variations with time for residual shear strength test (a) Normal Stress of 25kPa (b) Normal Stress of 50kPa and (c) Normal Stress of 100kPa

It was observed that the residual strength of the soil decreases as the number of cycles increases until it gets to the point of constant strength. It is called the zone of constant residual strength, as shown in Figure 2.24. According to Mesri and Huvaj-Shahien (2003), drained residual shear strength represents the face-to-face alignment and interaction of plate-shaped clay particles that are predominantly oriented parallel to the direction of shearing to the maximum extent possible for that composition. The residual friction angle depends on the nature of the particles and effective normal stress because the latter determines the

arrangement of particles during consolidation and shear. Based on Figure 2.23, the residual shear stress is considered when the shear-stress displacement curve becomes almost flat.

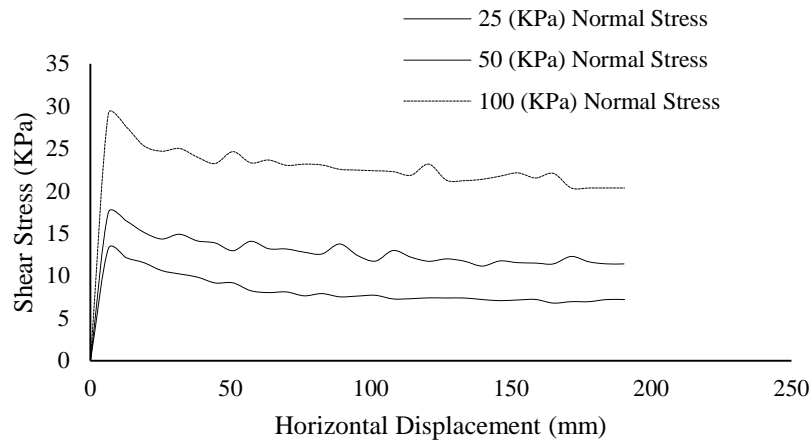


Figure 2.19 Residual shear strength curves for three applied normal stresses

2.3.5.4 Variation of the Shear Strength

Based on the study conducted by Nobahar et al., 2020, the Mohr-Coulomb failure envelop from the peak, fully softened, and the residual tests are presented in Figure 2.25. The highest shear strength was determined with the peak shear strength test ($c = 18.4$ kPa, 384 psf, and $\phi = 20.2$ deg.), whereas the residual test ($c = 5.45$ kPa, 113 psf, and $\phi = 10.52$ deg.) generated the lowest strength. It is worth mentioning that the fully softened shear strength test results were $c = 10.8$ kPa (225 psf) and $\phi = 18.6$ deg.

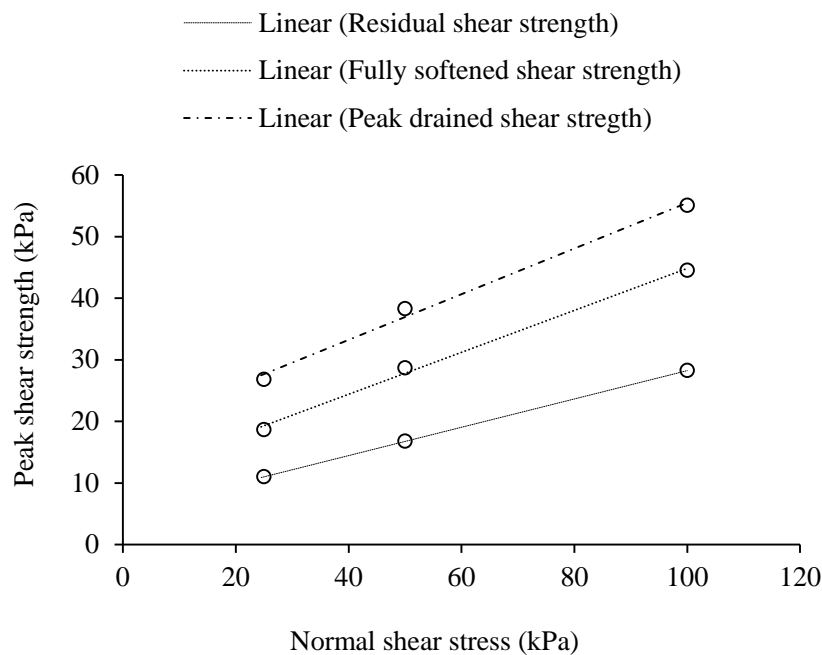


Figure 2.20 Mohr-coulomb failure envelopes of the samples subjected to different wet-dry cycles

Table 2.9 Peak, fully soften and Residual Shear Strength of Yazoo clay

Tests	Cohesion	Friction angle (deg.)
Peak Shear Strength	18.4 kPa 384 psf	20.2
Fully Softened Shear Strength	10.8 kPa 225 psf	18.6
Residual Shear Strength	5.45 kPa 113 psf	10.52

2.3.6 Permeability

The Yazoo clay when subjected to different wet-dry cycles will have different shrinkage cracks (Figure 2.26). With different wet-dry cycles, the void ratio of soil is going to change, which affects the hydraulic behavior. Khan et al., 2020 has conducted a study on the effect of the wet-dry cycles on the changes in the hydraulic conductivity of Yazoo clay. The study was conducted using two methods, 1. Using Mini Disk Infiltrometer and 2. Using instantaneous profile method, as presented in the subsequent section.

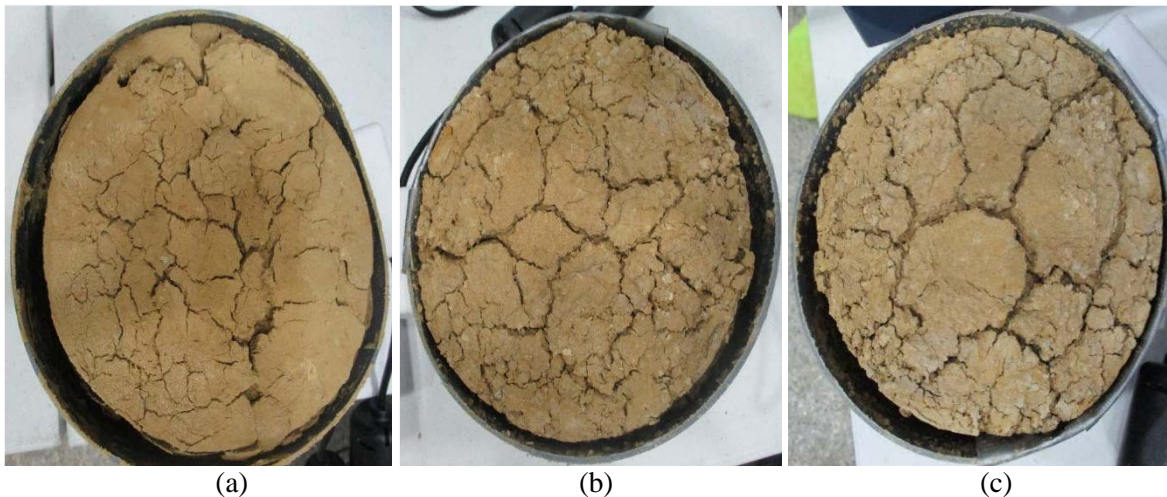


Figure 2.21 Propagation of desiccation at different wet-dry cycle (a) 1N (b) 2N (3N)

2.3.6.1 Unsaturated Hydraulic Conductivity Testing using Mini Disk Infiltrometer

The Mini Disk Infiltrometer measures the hydraulic conductivity of the soil. Khan et al., 2020 utilized the Mini Disk Infiltrometer to investigate the changes in hydraulic conductivity under different wet-dry cycles. For this task of the study soil samples were prepared under different initial moisture content and then subjected to different wet-dry cycles. A mini disk test set up is presented in Figure 2.27.

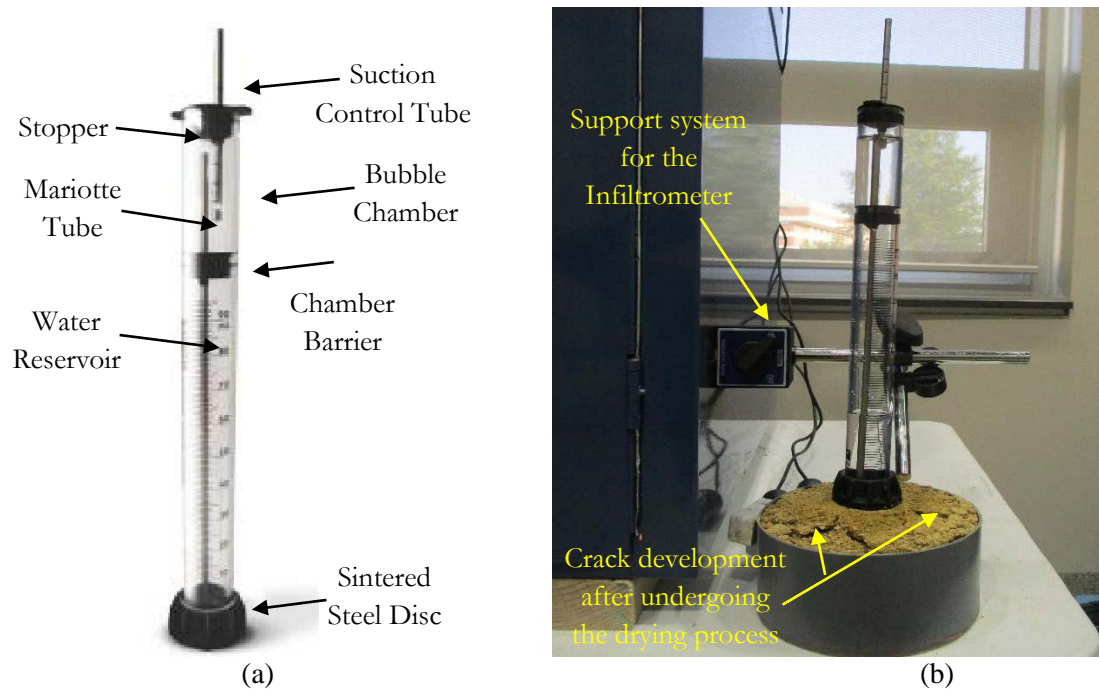


Figure 2.22 Laboratory hydraulic conductivity set up (a) Mini disk Infiltrometer (b) Testing of the samples using Mini Disk Infiltrometer

Based on the study conducted by Khan et al., 2020, the variation of the hydraulic conductivity values with different wet-dry cycles is presented in Table 2.10 and Figure 2.28. The study indicated an increment of the hydraulic conductivity (k_v) with the increase of the number of wet-dry cycles.

Table 2.10 Laboratory Hydraulic Conductivity values at different wet-dry cycles

Initial Moisture Content (%)	Calculated Hydraulic conductivity (k_v) at different wet-dry cycles (N) (cm/sec)		
	1N	2N	3N
0	$2.3E^{-2}$	$1.64E^{-1}$	$1.56E^{-1}$
10	$3.91E^{-2}$	$1.98E^{-1}$	$1.67E^{-1}$
15	$4.85E^{-2}$	$7.82E^{-2}$	$2.06E^{-1}$
20	$1.52E^{-2}$	$6.98E^{-2}$	$4.39E^{-2}$
25	$9.1E^{-3}$	$8.50E^{-3}$	$3.59E^{-1}$
35	$7.25E^{-4}$	$1.17E^{-1}$	$4.03E^{-1}$

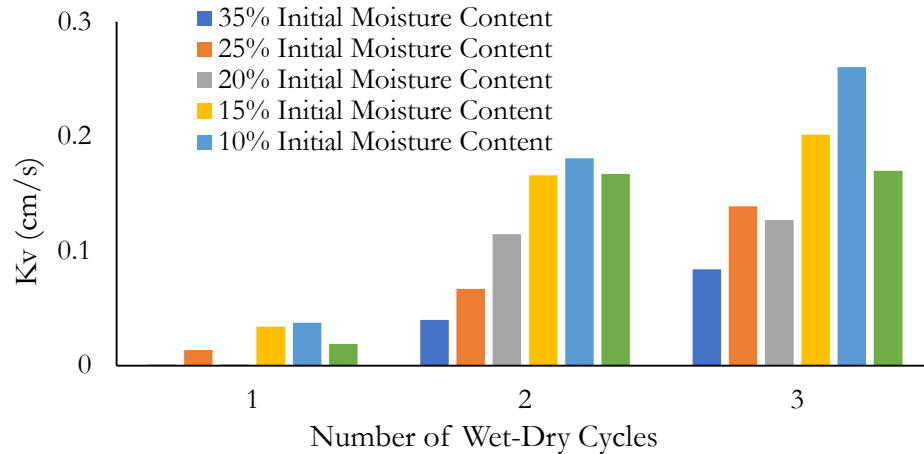


Figure 2.23 Change in Hydraulic conductivity of different initial moisture contents at different wet-dry cycle

2.3.6.2 Unsaturated Hydraulic Conductivity Testing using Moisture Sensors

Khan et al., 2020 also used the instantaneous profile method to determine the variation of the vertical hydraulic conductivity change. During this study, a 3-inch (7.62 cm) diameter PVC pipe section, 6 inches (15.24 cm) in length was utilized to compact Yazoo clay soil samples at different initial moisture content. Two moisture sensors were installed at 2 inches (5.08 cm) spacing along the height of the samples. Each test sample at a compacted state was subjected to 0, 3, and 5, wet-dry cycles, as presented in Figure 2.29. The samples inside the test devices were wetted to a fully saturated state and then dried by controlling the incandescent bulb attached to the box, to simulate the most extreme case.

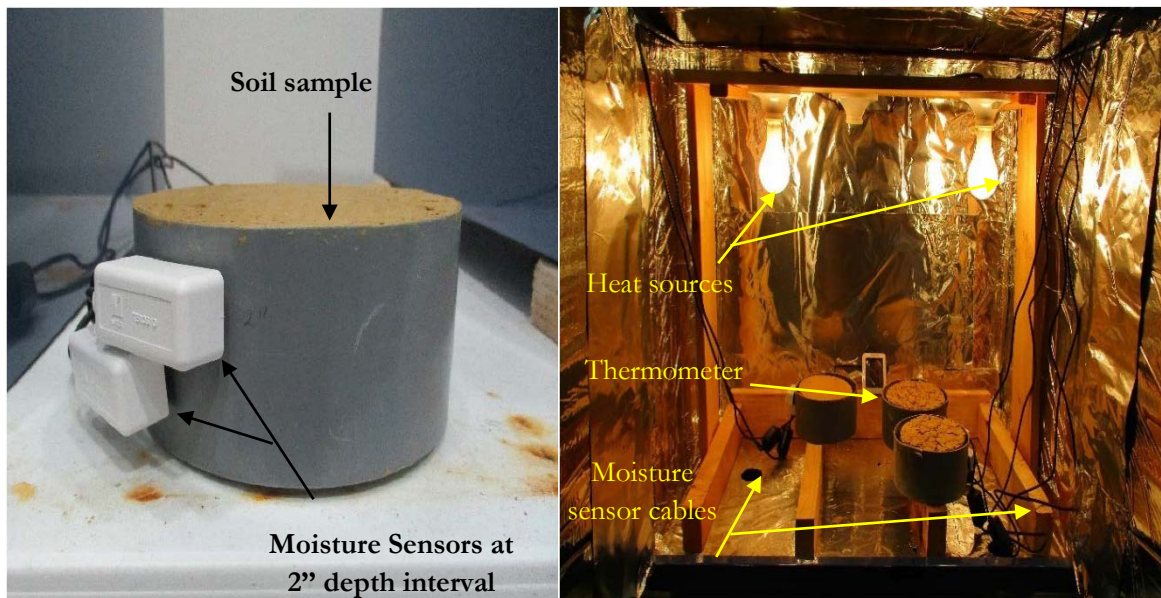
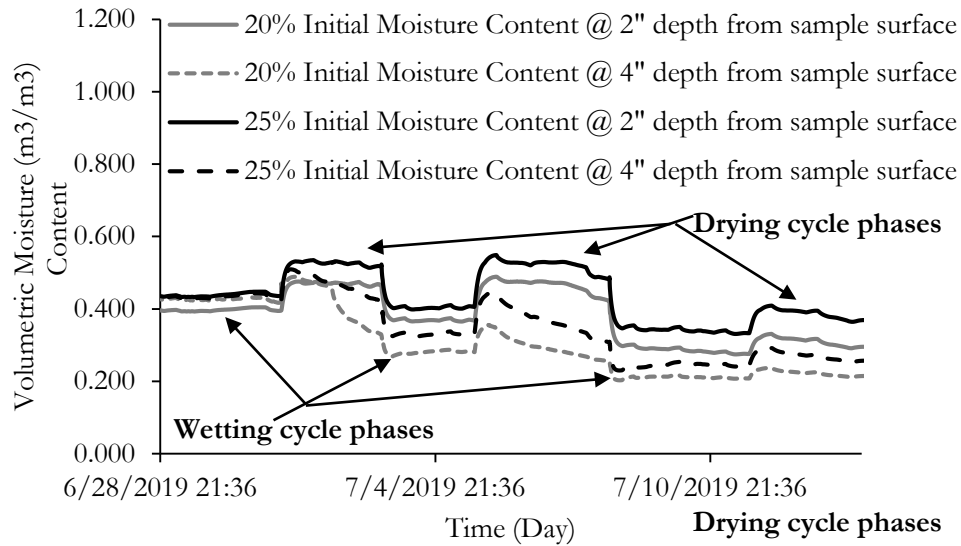
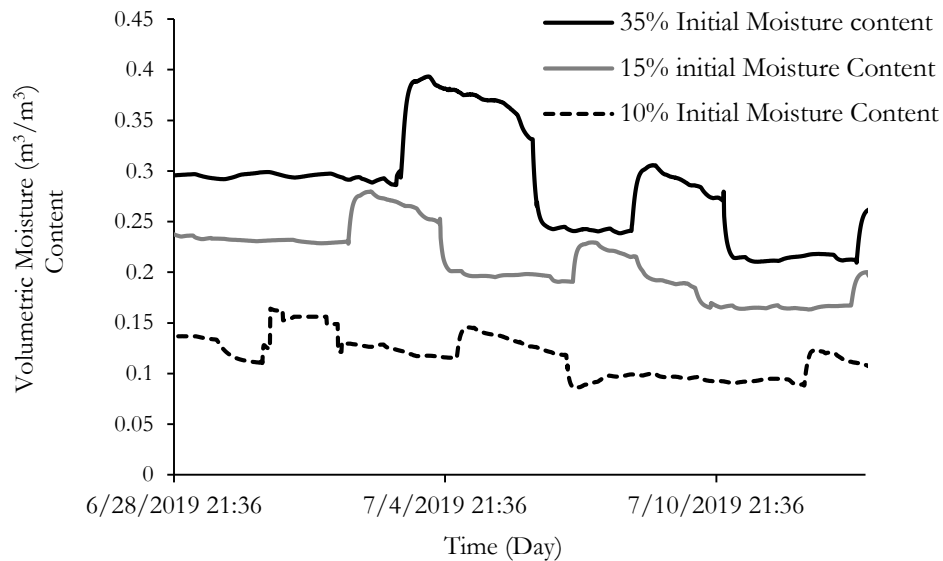


Figure 2.24 Laboratory hydraulic conductivity set up (a) Yazoo clay soil sample with instrumented moisture sensors (b) Drying cycle simulation process with the instrumented samples

Based on the study conducted by Khan et al., 2020, a variation of volumetric moisture content up to the 3 number of wet-dry cycle is shown in Figure 2.30.



(a)



(b)

Figure 2.25 Variation of volumetric moisture content overtime at 3N wet-dry cycle (a) change in volumetric moisture content for 20% and 25% initial moisture contents at different sample depth (b) change in volumetric moisture content for 10%, 15% and 35% initial moisture contents

According to the study conducted by Khan et al., 2020, the vertical permeability was determined by finding the ratio between the vertical distance traveled by the water and the time required to travel that distance, as presented in Table 2.11 and Table 2.12. The study indicated that the hydraulic conductivity of soil increases with the number of wet-dry cycles. Moreover, the largest increases in vertical hydraulic conductivity occurred during the first wet-dry cycle.

Table 2.11 Variation of VMC and hydraulic conductivity in response to water infiltration and number of wet-dry cycles respectively with 20% initial moisture content

<i>Sensor Depth</i> (Inch)	<i>1N</i>			<i>2N</i>			<i>3N</i>		
	<i>Peak Sensor Reading</i>	<i>Time (hr)</i>	<i>Kv (cm/sec)</i>	<i>Peak Sensor Reading</i>	<i>Time (hr)</i>	<i>Kv (cm/sec)</i>	<i>Peak Sensor Reading</i>	<i>Time (hr)</i>	<i>Kv (cm/sec)</i>
2	0.432	21:45	1.47E ⁻⁴	0.37	06:50	1.41E ⁻³	0.298	06:30	1.69E ⁻²
4	0.405	03:30		0.334	17:50		0.247	09:40	

Table 2.12 Variation of VMC and hydraulic conductivity in response to water infiltration and number of wet-dry cycles respectively with 25% initial moisture content



<i>Sensor Depth</i> (Inch)	<i>1N</i>			<i>2N</i>			<i>3N</i>		
	<i>Peak Sensor Reading</i>	<i>Time (hr)</i>	<i>Kv (cm/sec)</i>	<i>Peak Sensor Reading</i>	<i>Time (hr)</i>	<i>Kv (cm/sec)</i>	<i>Peak Sensor Reading</i>	<i>Time (hr)</i>	<i>Kv (cm/sec)</i>
2	0.448	03:30	8.65E ⁻⁵	0.408	06:20	1.22E ⁻⁴	0.349	06:40	4.7E ⁻⁴
4	0.442	20:00		0.334	17:50		0.247	09:40	

Chapter 3: SITE LOCATION AND SITE INVESTIGATION

3.1 Site Selection

The major objective of State Study 286 is evaluating the performance of the repaired slopes as well as understanding the failure mechanism. Six highway slopes in Jackson Metroplex have been selected in State Study 286. The location of each of the slopes is presented in Table 3.1. The selected slopes have already shown an early sign of movement or have a record of failure and previous repair. Each of the slopes was investigated using the Cone Penetration Test (CPT) before field instrumentation. MDOT hired Thompson Engineering to perform the CPT. The JSU research team was present during the CPT and monitored the operation. JSU team utilized the results from the CPT and conducted engineering analysis.

Table 3.1 Selected highway site slopes locations

Site No	Site Location	Site Coordinate	Aerial view
Slope 1	I220N Ramp Toward I55N	32°24'46.60"N, 90° 8'57.32"W	
Slope 2	Metro Center	32°17'58.85"N, 90°14'47.00"W	
Slope 3	Terry Road	32°16'48.92"N, 90°12'44.03"W	
Slope 4	Highland Drive	32°17'21.22"N, 90°14'17.58"W	
Slope 5	Sowell Road	32°32'30.11"N, 90° 5'50.49"W	
Slope 6	McRaven Road	32°17'45.71"N, 90°16'17.17"W	

3.2 Slope 1: I220N Ramp Toward I55N Highway Slope

The Slope 1 is located in the I220N ramp toward I55N. The slope has shown movement, which was repaired using H-piles. During this study, the repaired area and the as-built section of the slope was considered. The as-built section was used as a control section to compare the performance of the repaired section. Figure 3.1 shows the location and photo of Slope 1.

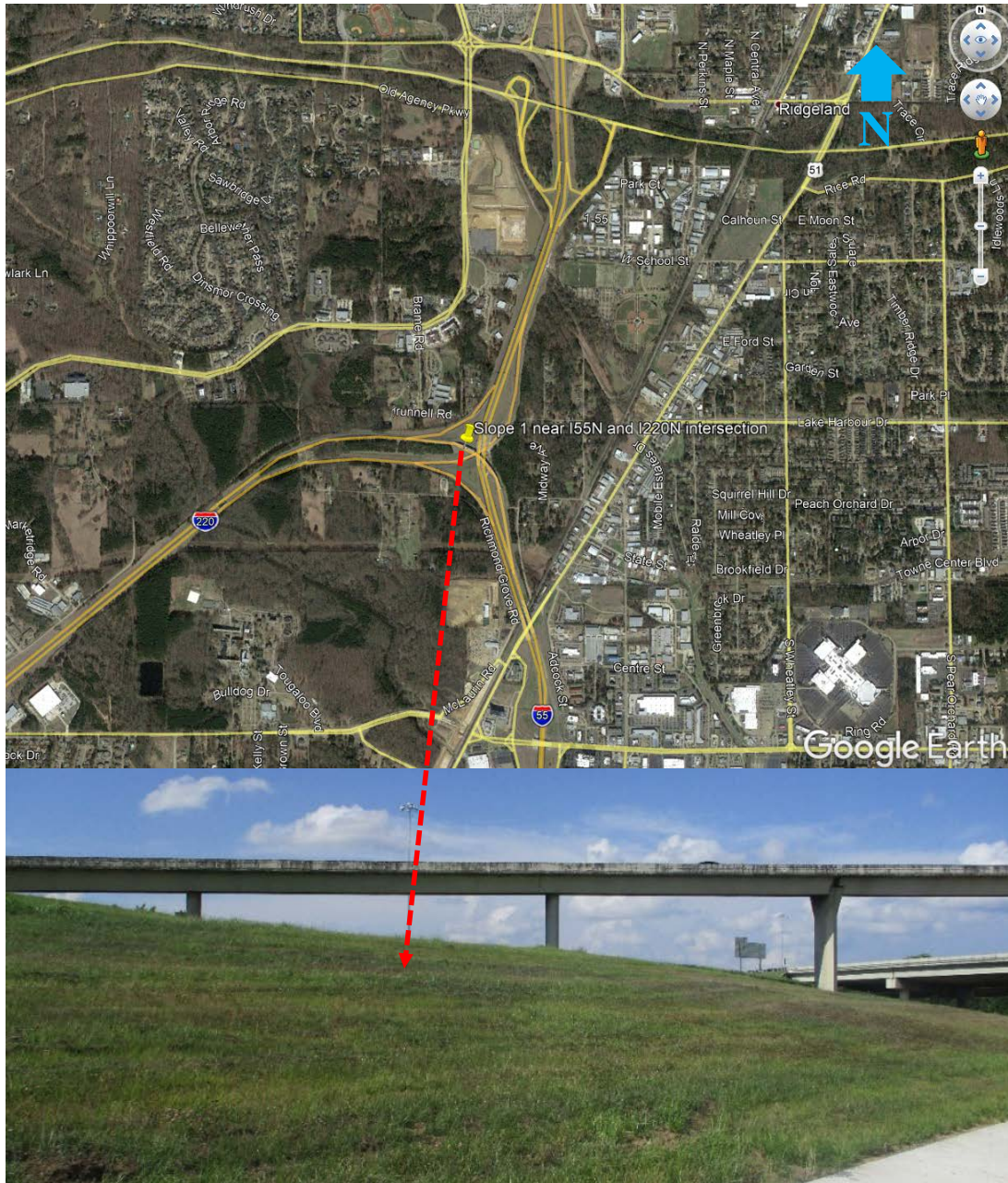


Figure 3.1 Location of Slope 1

3.2.1 Investigation of CPT Testing

Table 3.2 presents the details of the site investigation plan of Slope 1. Beside the site investigation, Thompson Engineering performed the drilling operations to install instrumentations. Two slope inclinometers with 30 ft. depth was considered to monitor the performance of the slope, at the repaired and as built section. In addition, three 15 ft. boreholes were drilled at the crest, middle, and toe of the slope at both sections. The borehole locations are BH1, BH2, and BH3 at the as-built and repaired areas, as presented in Figure 3.2.

Table 3.2 Site investigation details for Slope 1

Borehole/Test Designation	Borehole Depth (ft.)	Slope Area	Purpose of the Boring
Inclinometer 1	30	As-built slope	Continuous Shelby tube sampling and Install Inclinometer
Inclinometer 2	30	Repaired slope	Continuous Shelby tube sampling and Install Inclinometer
BH-1	15	As-built slope	Instrumentation
BH-2	15	As-built slope	Instrumentation
BH-3	15	Repaired slope	Instrumentation
CPT 1	30	As-built slope	CPT Test
CPT 2	30	Repaired slope	
CPT 3	25	As-built slope	
CPT 4	25	Repaired slope	
CPT 5	20	As-built slope	
CPT 6	20	Repaired slope	

Six CPT tests were conducted at both repaired and the as-built section of the slope at the crest, middle, and toe of the slope. The depth of CPT at the crest, middle, and toe of the slope was 30 ft., 25 ft., and 20 ft., respectively. The layout of the CPT's are presented in Figure 3.2. The CPT was performed using standard 15 cm² Piezocone by Thompson Engineering. The JSU team analyzed the CPT results using applicable correlations to determine the required physical and mechanical properties of soil. These derived parameters were further used in the Finite Element Analysis.

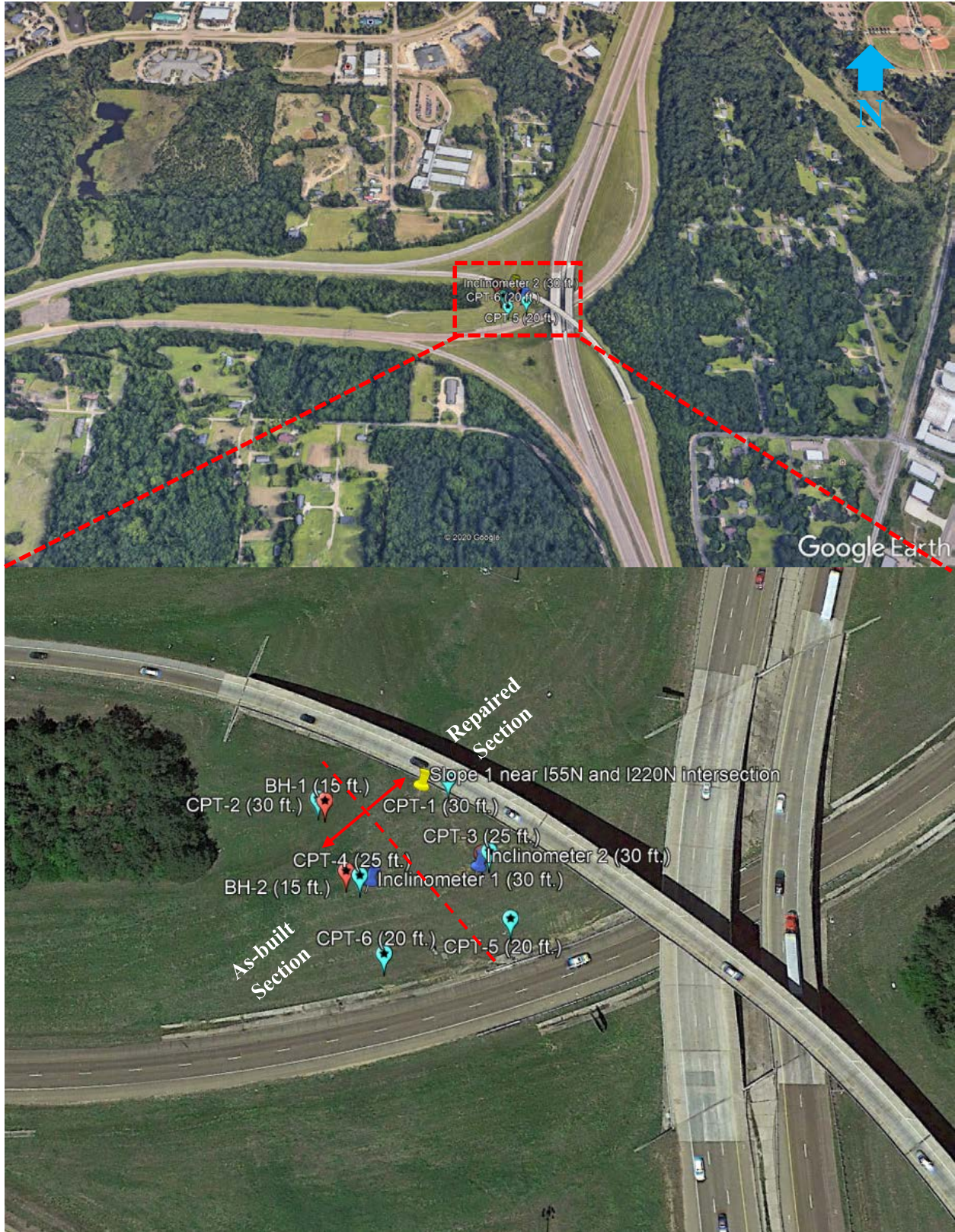


Figure 3.2 Location of Boreholes and CPT at Slope 1

Figure 3.3 shows the site investigation photo using CPT testing at Slope 1. Figure 3.4 shows the CPT results at the crest of the slope at the failed section. Figure 3.4 presents the tip resistance (q_t), sleeve friction (f_s), pore pressure (u_2 & u_0), and friction ratio (R_f). The complete CPT results are available in Appendix A.



Figure 3.3 Conducting CPT test at Slope 1

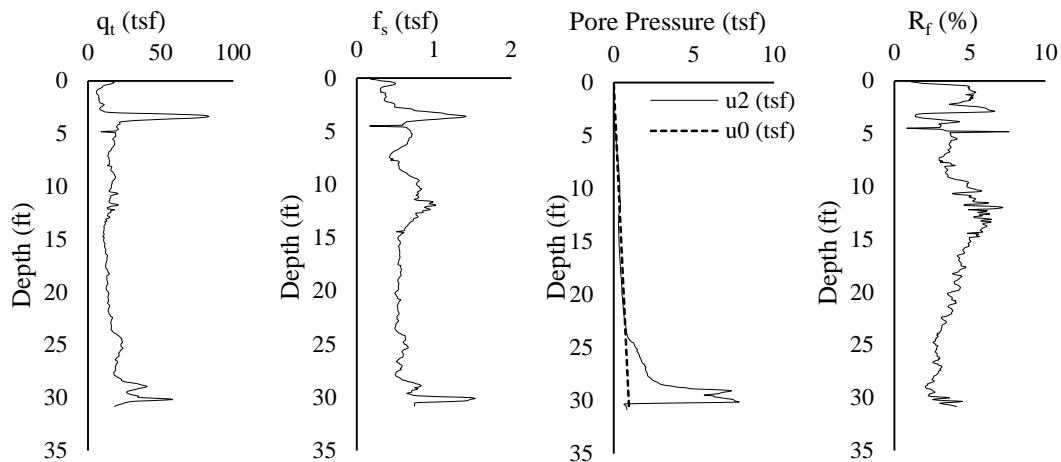


Figure 3.4 Piezo Cone Penetration Test (CPT) results at the crest of Slope 1 at CPT 1

The tip resistance, sleeve friction, pore pressure, friction ratio from the CPT test were utilized to determine friction angle, dry unit weight, undrained shear strength, and Young's modulus using Equation 3.1 to Equation 3.8 based on Robertson et al., 2015 and NASEM 2007.

- Peak Friction Angle, ϕ'

$$\tan \phi' = \frac{1}{2.68} \left[\log \left(\frac{q_c}{\sigma'_{v0}} \right) + 0.29 \right] \quad (3.1)$$

$$3.27 < I_c < 4, \quad K = 10^{(-4.52 - 1.37I_c)} \quad (3.2)$$

- Soil Unit Weight, γ (after Robertson 2010)

$$\frac{\gamma}{\gamma_w} = 0.27 (\log R_f) + \left(0.36 \log \left(\frac{q_t}{P_a} \right) \right) + 1.236 \quad (3.3)$$

$$R_f = F_R = \left(\frac{f_s}{q_t} \right) 100\% \quad (3.4)$$

- Young's Modulus, E

$$E = \alpha_E (q_t - \sigma_{v0}) \quad (3.5)$$

$$\alpha_E = 0.015 \left(10^{(0.55 I_c + 1.68)} \right) \quad (3.6)$$

- Undrained Shear Strength, S_u

$$S_u = \frac{q_t - \sigma_v}{N_{Kt}} \quad (3.7)$$

$$N_{Kt} = 10 \sim 18 \text{ (theories)} \quad (3.8)$$

3.2.2 Soil Parameters from CPT

The peak friction angle for three areas of Slope 1 (crest, middle, and toe) is presented in Figure 3.5, where C1 and C2 represent CPT locations at the crest of the slope for both repaired and as-built sections, respectively. C3 and C4 represent the CPT locations in the middle of the slope for both sections. Similarly, C5 and C6 also represent the CPT locations at the toe of the slope for both sections. The Undrained Shear Strength, dry unit weight, and Young's modulus for both sections are presented in Figure 3.6, Figure 3.7 and Figure 3.8, respectively. The derived parameters from the CPT testing were further utilized in Finite Element Analysis.

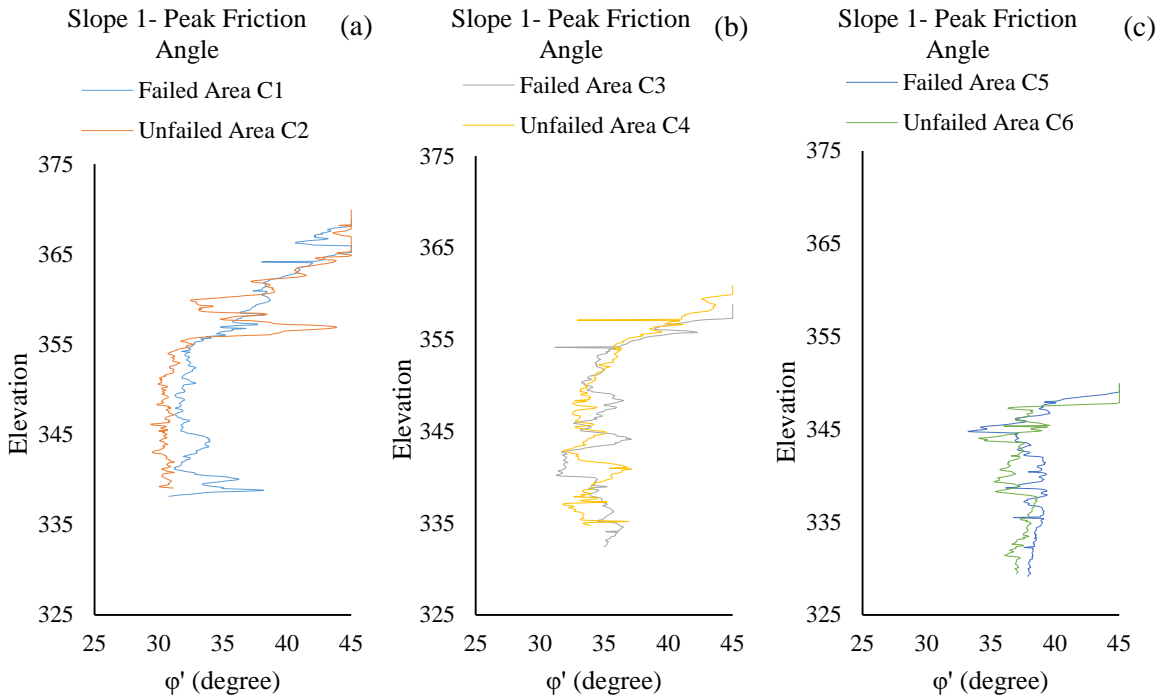


Figure 3.5 Variation of peak friction angle at Slope 1 (a) crest of the slope (b) middle of the slope (c) toe of the slope

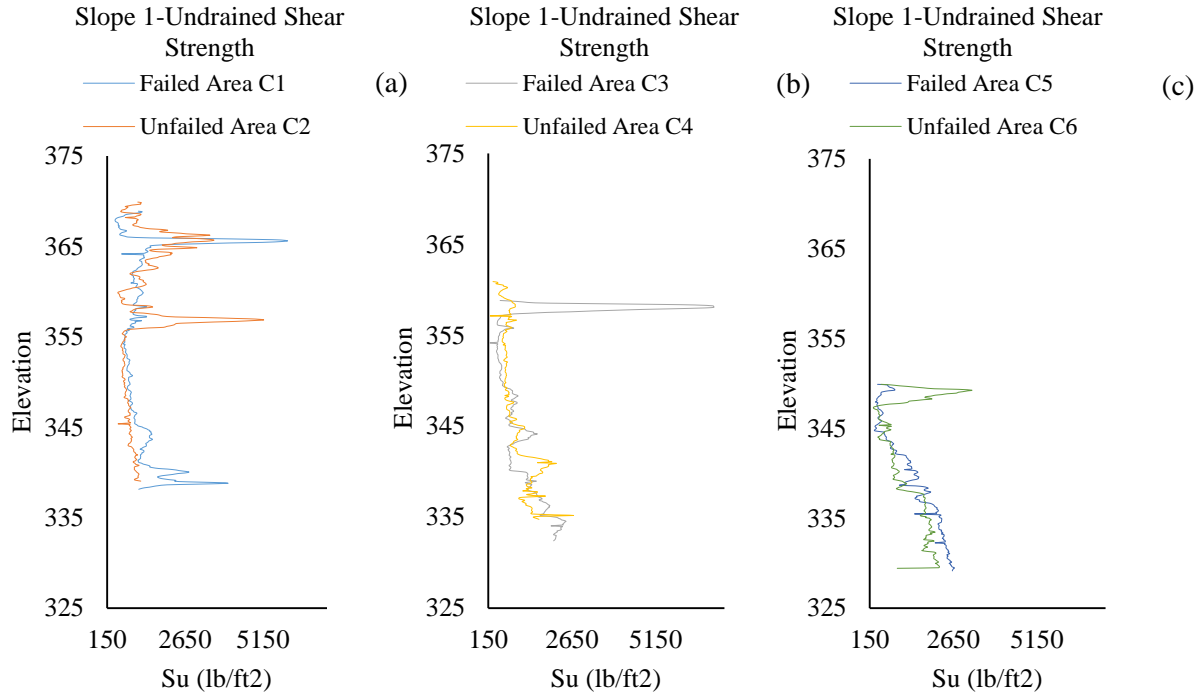


Figure 3.6 Variation of undrained shear strength at Slope 1 (a) crest of the slope (b) middle of the slope (c) toe of the slope

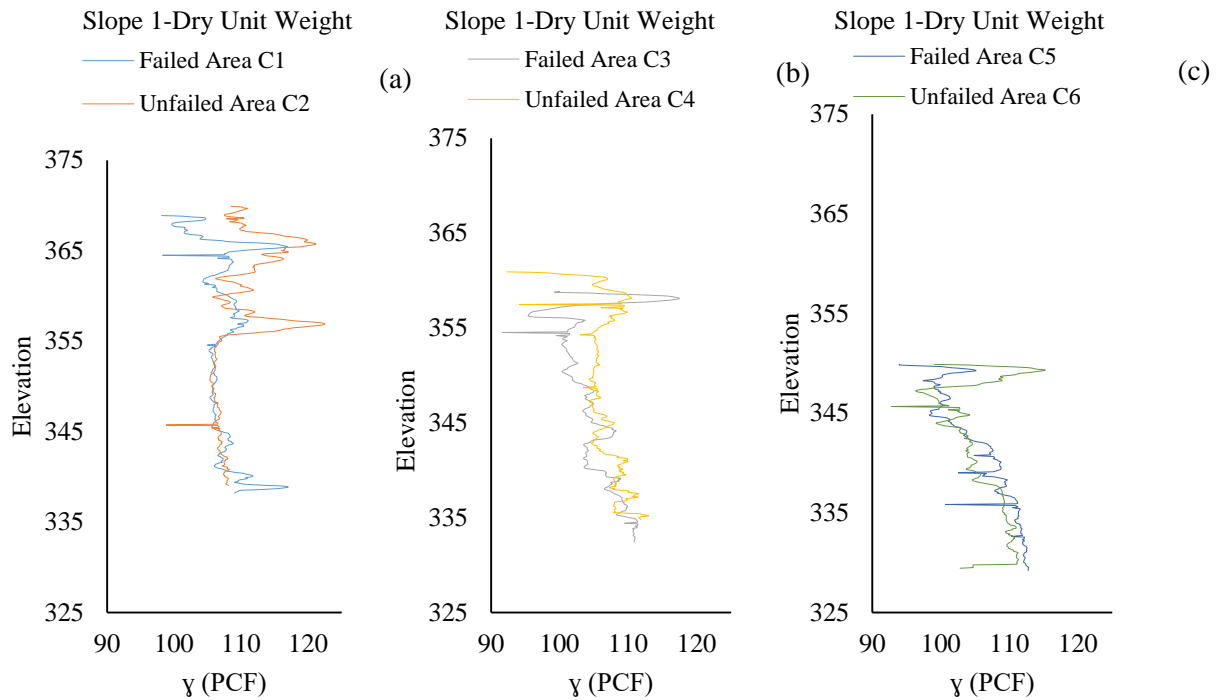


Figure 3.7 Variation of dry unit weight at Slope 1 (a) crest of the slope (b) middle of the slope (c) toe of the slope

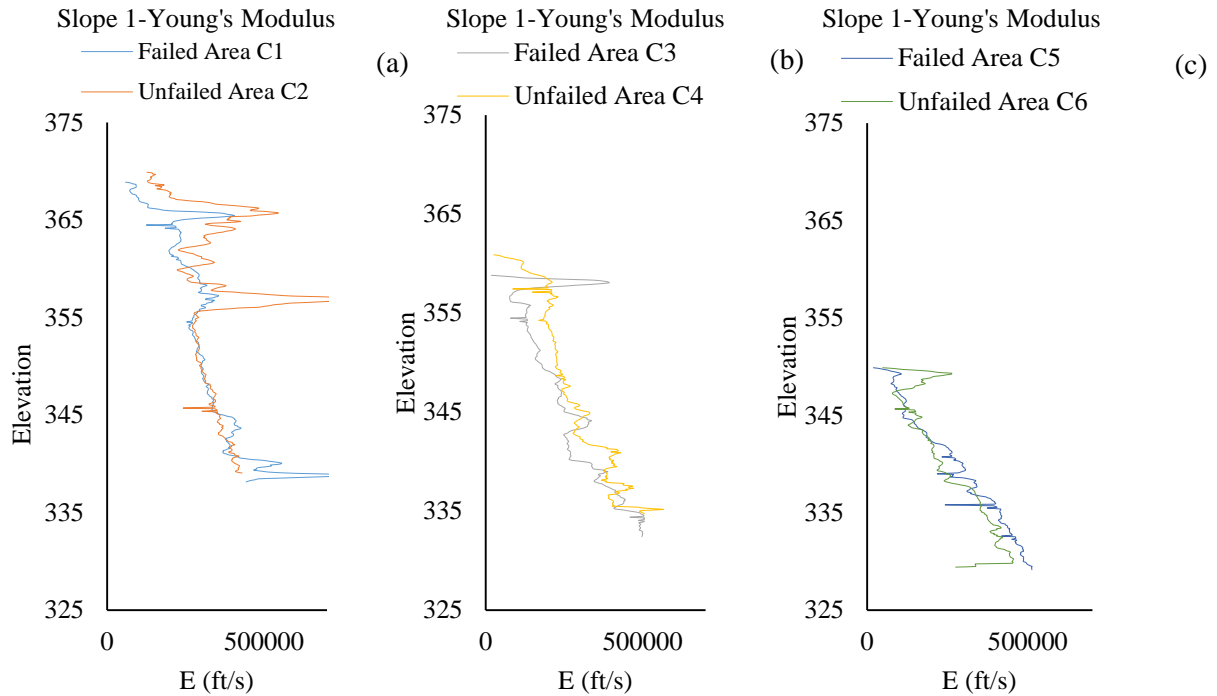


Figure 3.8 Variation of Young's modulus at Slope 1 (a) crest of the slope (b) middle of the slope (c) toe of the slope

3.3 Slope 2: Metro Center Highway Slope

Slope 2 is located along I220 N over the ramp from US 80E, close to the Metro center, as presented in Figure 3.9. It is a 3H: 1V slope with a height of 23 ft. For this slope, the repaired area and the as-built slope section were selected for monitoring. The slope has failed near the bridge along I-220N, which is repaired using H-piles installed at the crest of the slope.

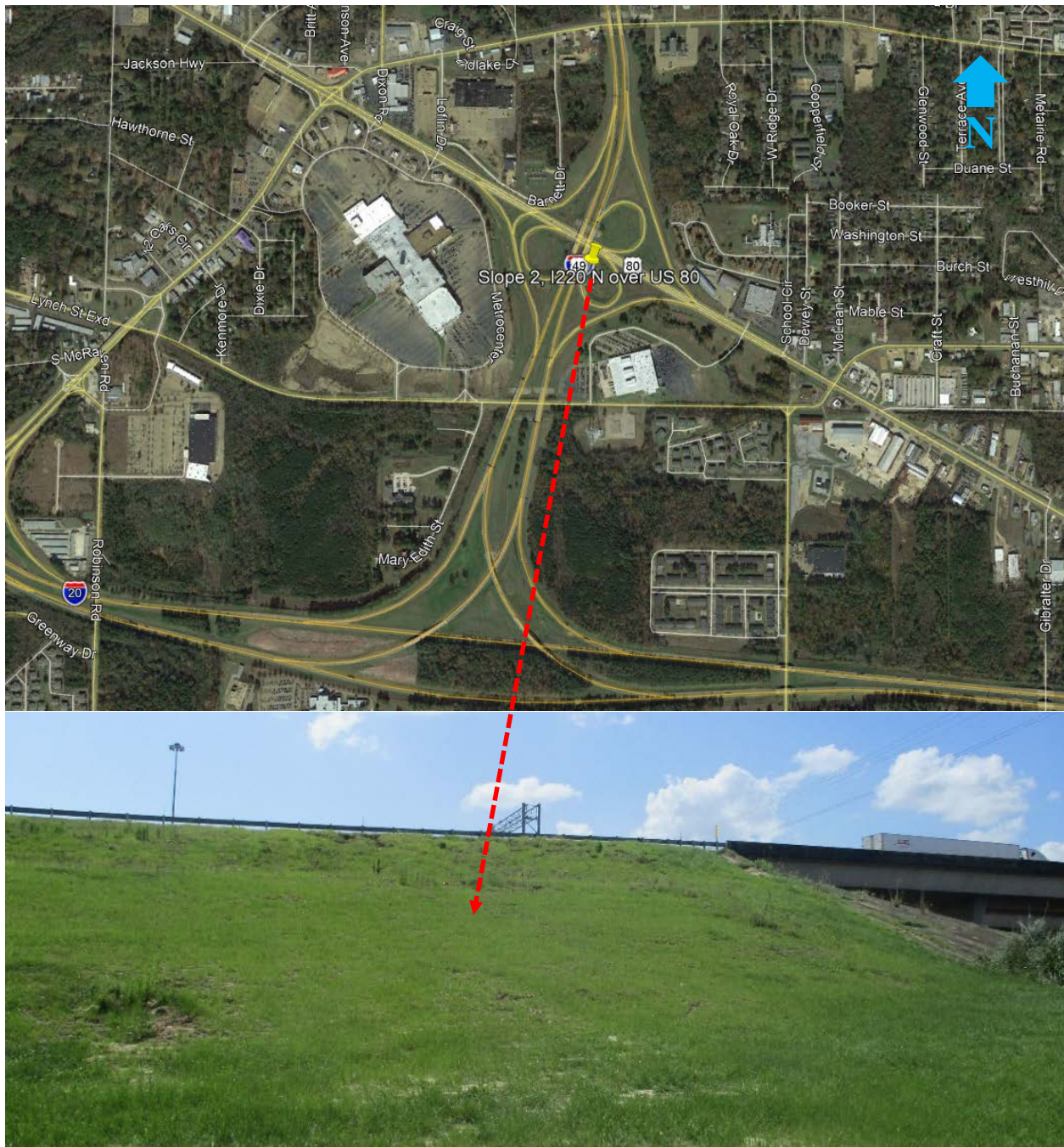


Figure 3.9 Location of Slope 2

Table 3.3 presents the details of the site investigation program of Slope 2. The location of the boring and CPT tests are presented in Figure 3.10. As a part of the site investigation, two slope inclinometers with 30 ft. depth at the repaired and as-built section of the slope site was installed. For field instrumentation at this site, three boreholes were drilled at the crest, middle, and toe of the slope with 15 ft depth.

Table 3.3 Site investigation details at Slope 3

Borehole/Test Designation	Borehole Depth (ft.)	Slope Area	Boring/Test type
Inclinometer 1	30	Repaired slope	Continuous Shelby tube sampling and Install Inclinometer
Inclinometer 2	30	As-built slope	Continuous Shelby tube sampling and Install Inclinometer
BH-1	15	Repaired slope	Instrumentation
BH-2	15	Repaired slope	Instrumentation
BH-3	15	As-built slope	Instrumentation
CPT 1	30	Repaired slope	CPT Test
CPT 2	30	As-built slope	
CPT 3	25	Repaired slope	
CPT 4	25	As-built slope	
CPT 5	20	Repaired slope	
CPT 6	20	As-built slope	

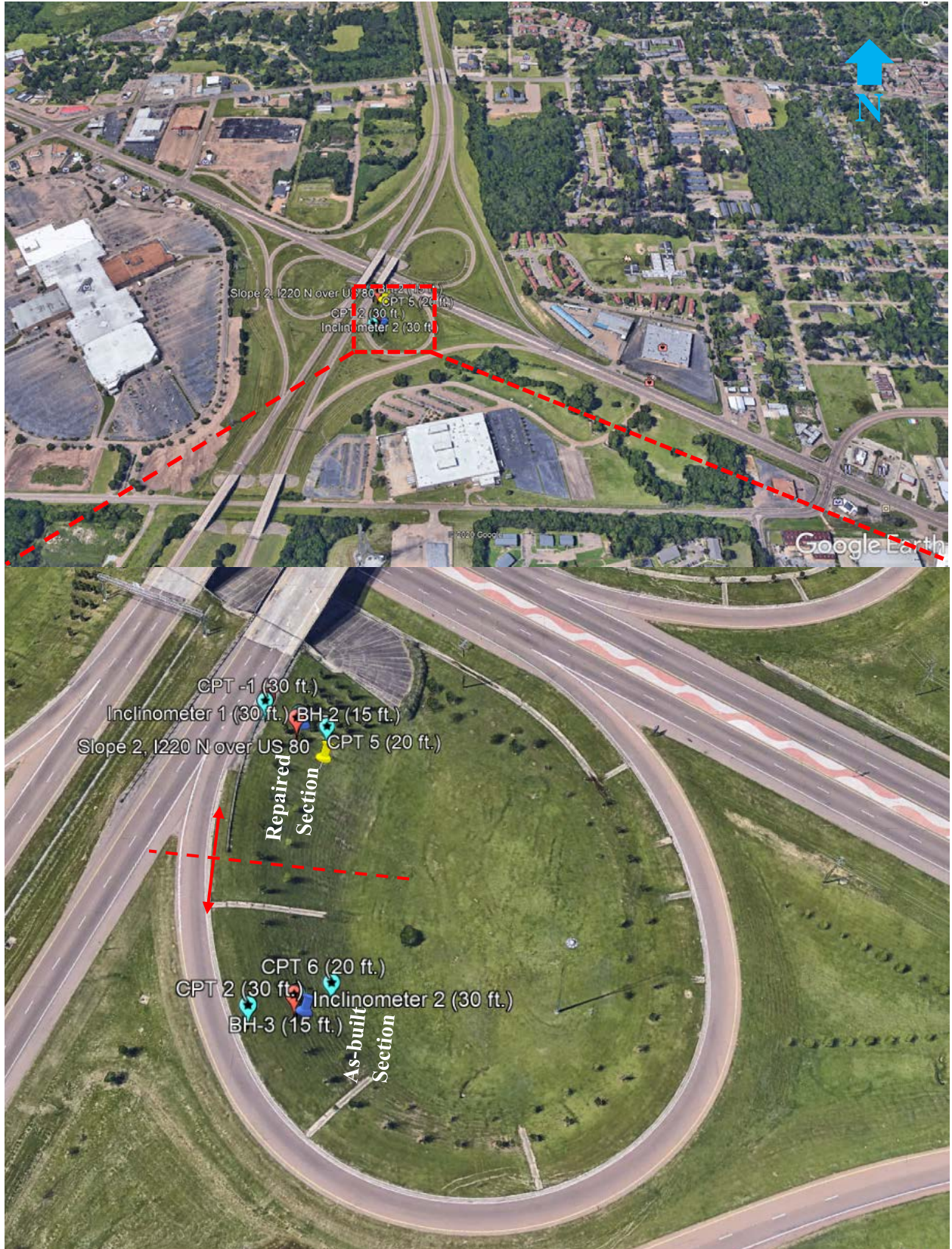


Figure 3.10 CPT and Boring Locations at Slope 2

3.3.1 Investigation of CPT Testing

Six CPT tests were conducted at both repaired and at as-built sections of the slope at the crest, middle, and toe of the slope. The depth of the CPT test at the crest, middle, and toe of the slope was 30 ft., 25 ft., and 20 ft., respectively. Thompson Engineering conducted the CPT testing at the slope. The CPT was performed using standard 10 cm² piezocone at the specified project locations, as presented in Figure 3.10. The CPT test photo at Slope 2 is presented in Figure 3.11. The tip resistance (q_t), sleeve friction (f_s), pore pressure (u_2 & u_0), and friction ratio (R_f) of the test location CPT 1 at the repaired area of the crest of the slope is presented in Figure 3.12. Other CPT test results from this slope are available in Appendix A.



Figure 3.11 Field Activity of CPT test at Slope 2

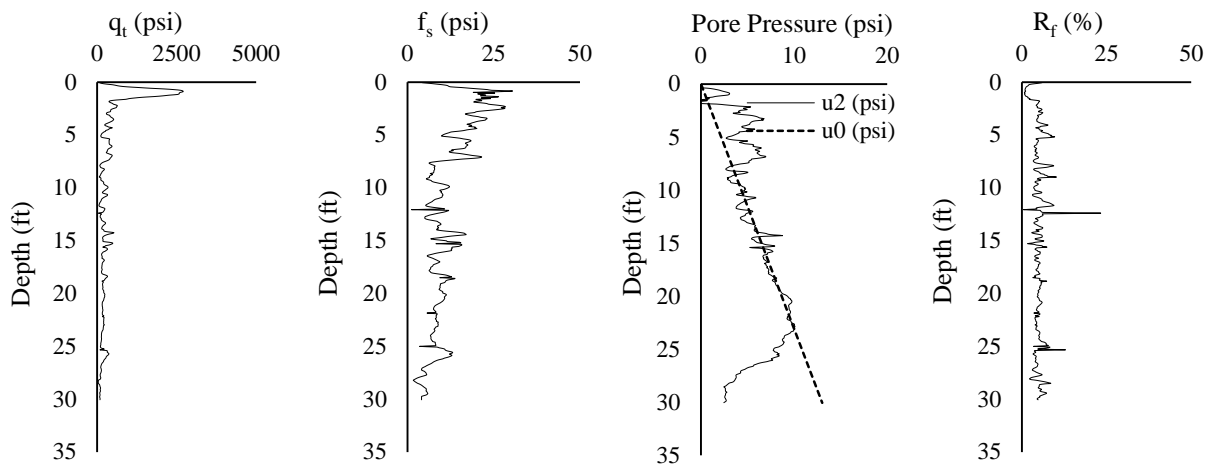


Figure 3.12 Cone Penetration Test (CPT) results at the crest of Slope 2

3.3.2 Soil Parameters from CPT

Using applicable correlations for CPT results, as presented in Equation 3.1 to Equation 3.8, the physical and mechanical properties of soil for Slope 2 are presented in Figure 3.13 to Figure 3.16. Figure 3.13 presents the CPT results for friction angle for repaired and as-built area at the crest, middle, and toe of the slope. The CPT locations at the repaired section of slope 2 are C1, C3, and C5 for the crest, middle, and the toe of the slope.

Similarly, the CPT locations at the as-built section of slope 2 are C2, C4, and C6 for the crest, middle, and the toe of the slope. In Slope 2, the CPT testing was not conducted at C1 and C3 as there was

limited site access. Figure 3.14, Figure 3.15, and Figure 3.16 present the undrained shear strength, dry unit weight, and Young’s modulus from the CPT results for repaired and as-built sections. It should be noted that the derived shear strength parameter from CPT was high at higher elevation. Thus, only applicable and realistic parameters from CPT test was utilized in FEM analysis. More details are presented in Chapter 5.

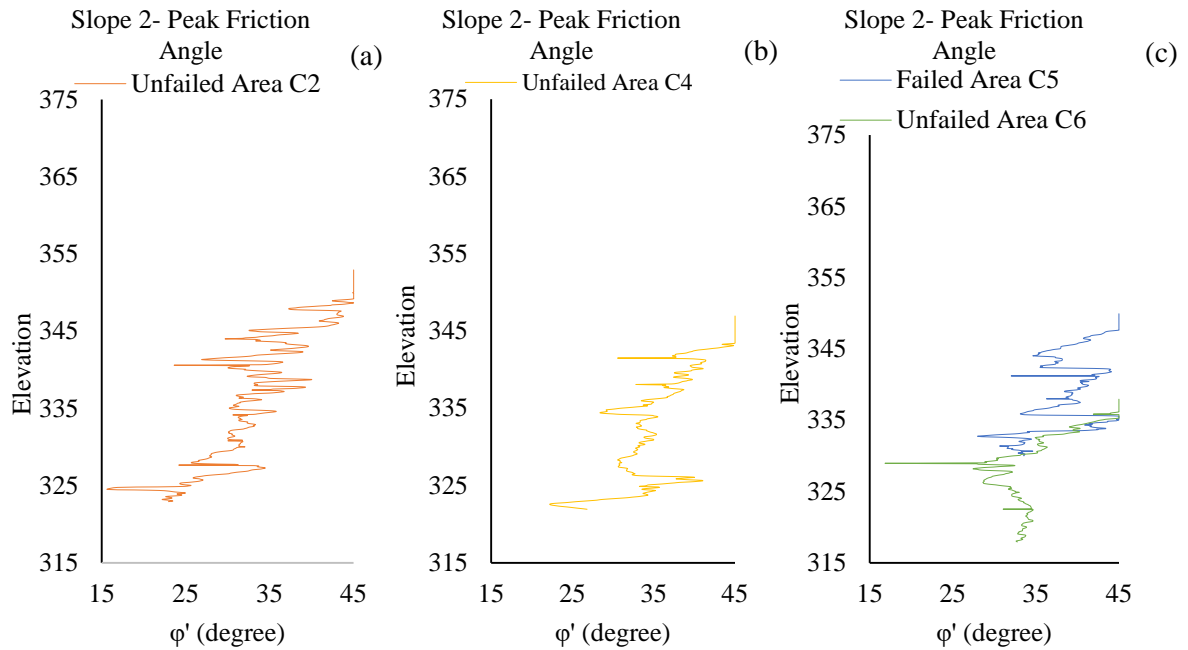


Figure 3.13 Variation of Peak friction angle at Slope 2 (a) crest of the slope (b) middle of the slope (c) toe of the slope

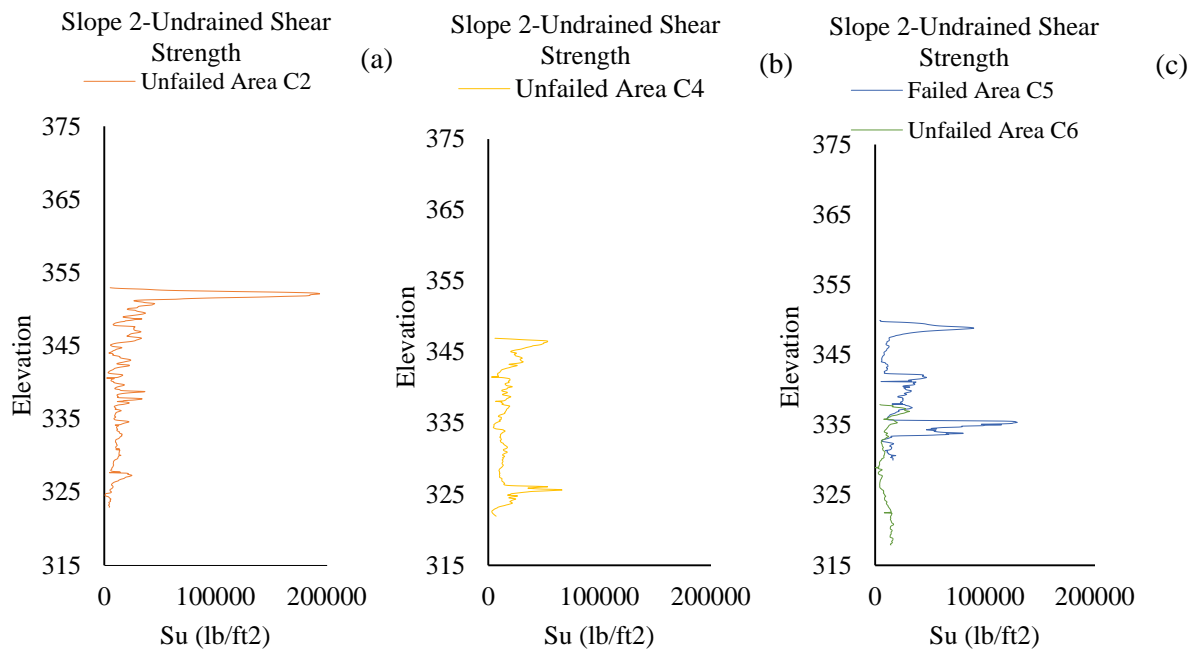


Figure 3.14 Variation of Undrained shear strength at Slope 2 (a) crest of the slope (b) middle of the slope (c) toe of the slope

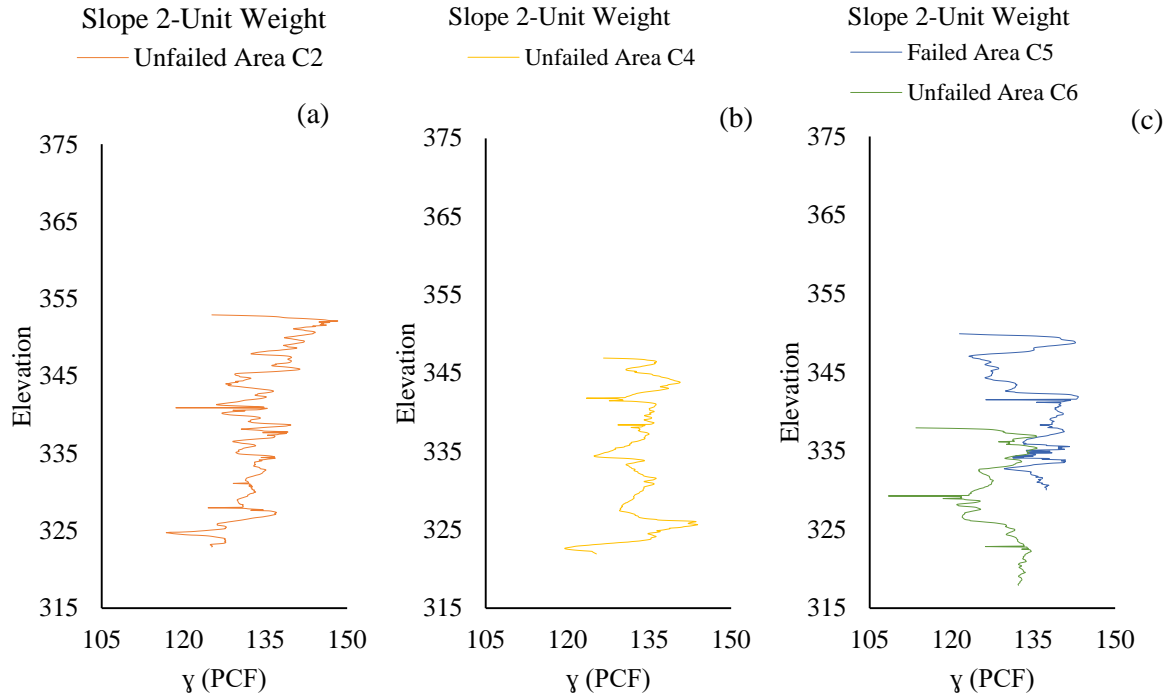


Figure 3.15 Variation of dry unit weight at Slope 2 (a) crest of the slope (b) middle of the slope (c) toe of the slope

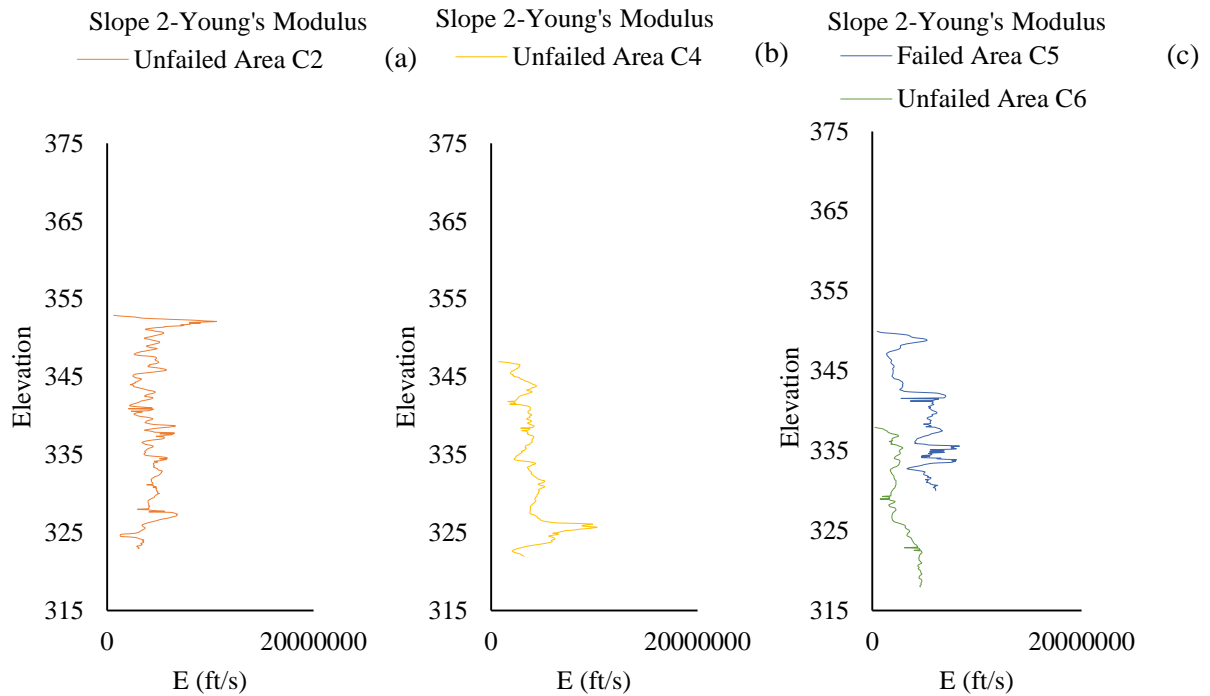


Figure 3.16 Variation of Young's modulus at Slope 2 (a) crest of the slope (b) middle of the slope (c) toe of the slope

3.4 Slope 3: Terry Road Site Highway Slope

The Slope 3 is located along I20E exit toward Terry road. It is a 3.5 H: 1V to 4H: 1V slope with a height of 15 ft. The location and site photo of the slope is presented in Figure 3.17. The slope near the bridge has experienced shallow landslides, which was repaired using H-piles.



Figure 3.17 Location of Slope 3

Similar to other slopes, the Slope 3 was investigated using CPT during the field instrumentation. The CPT test was conducted by Thompson Engineering. The CPT was performed using standard 10 cm² Piezocone by Thompson Engineering. The depth and location of the each of the CPT is presented in Table

3.4. Besides site investigation, two slope inclinometers with 30 ft depth were installed at the repaired and as-built section of the slope. The as-built section served as the control section to evaluate the performance of the repaired section. For field instrumentation at this slope, three boreholes were drilled at the crest, middle, and toe of the slope with 15 ft depth at both sections. The layout of the boreholes and CPT are presented in Figure 3.18.

Table 3.4 Site investigation details at Slope 3

Borehole/Test Designation	Borehole Depth (ft.)	Slope Area	Boring/Test type
Inclinometer 1	30	As-built slope	Continuous Shelby tube sampling and Install Inclinometer
Inclinometer 2	30	Repaired slope	Continuous Shelby tube sampling and Install Inclinometer
BH-1	15	As-built slope	Instrumentation
BH-2	15	As-built slope	Instrumentation
BH-3	15	Repaired slope	Instrumentation
CPT 1	30	As-built slope	CPT Test
CPT 2	30	Repaired slope	
CPT 3	25	As-built slope	
CPT 4	25	Repaired slope	
CPT 5	20	As-built slope	
CPT 6	20	Repaired slope	

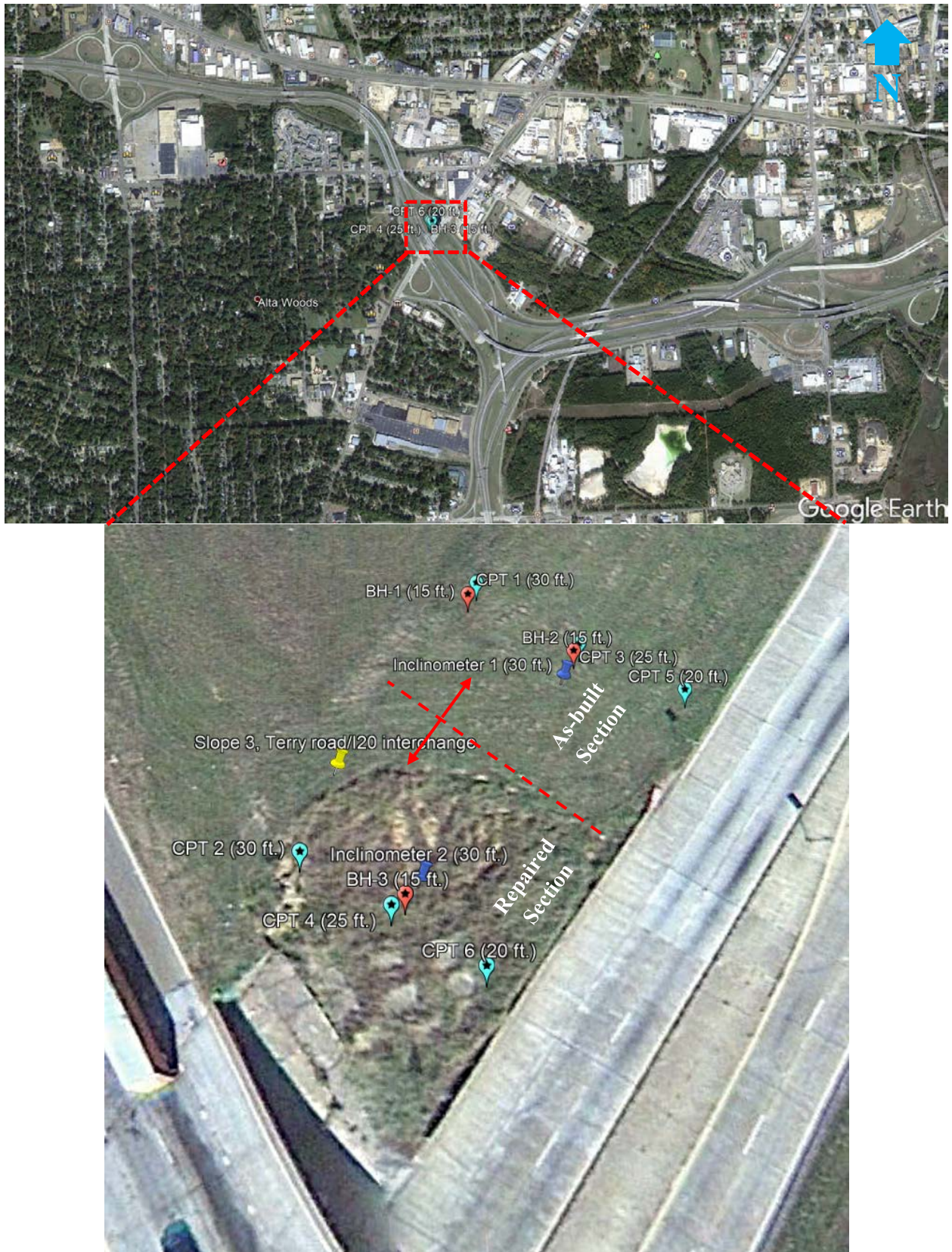


Figure 3.18 CPT and Borehole locations at Slope 3

3.4.1 Investigation of CPT Testing

Thompson Engineering conducted six CPT tests at both repaired and an as-built section of the slope. The depth of CPT at the crest, middle, and toe of the slope was 30 ft., 25ft., and 20 ft.; respectively. The CPT was performed using standard 10 cm² 1Piezocone. The CPT results at location C1 is presented in Figure 3.19. All other CPT results are included in Appendix A.

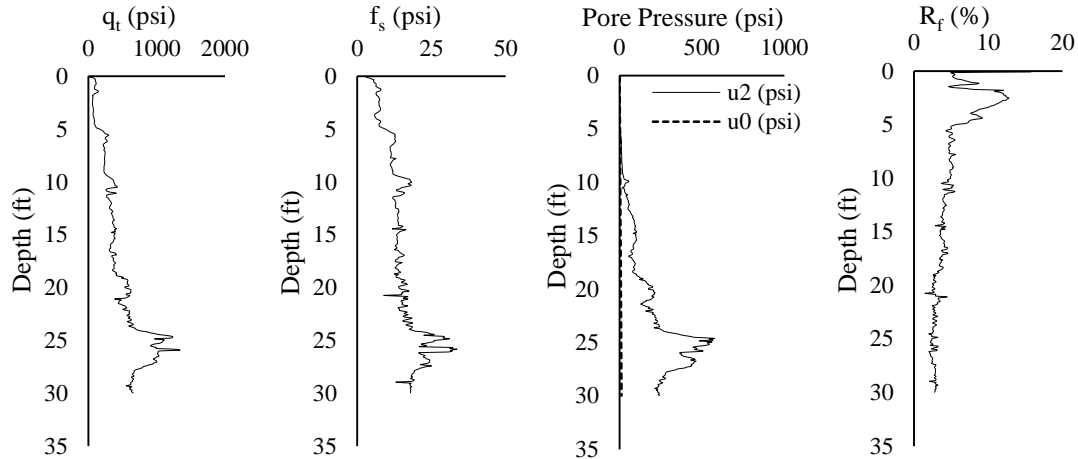


Figure 3.19 CPT results at the crest of Slope 3

3.4.2 Soil Parameters from CPT

Using applicable correlations as presented in Equation 3.1 to Equation 3.8, the friction angle, undrained shear strength, dry unit weight, and Youngs Modulus at Slope 3 was determined from each CPT location, as presented in Figure 3.20 to Figure 3.23, respectively. The CPT locations at the repaired section of slope 3 are C1, C3, and C5 for the crest, middle, and the toe of the slope. Similarly, the CPT locations at the as-built section of slope 3 are C2, C4, and C6 for the crest, middle, and the toe of the slope. It should be noted that some of the soil parameters derived in Slope 3 is misleading, which was adjusted with laboratory test parameters in Finite Element Analysis. The details parameters are presented in Chapter 5.

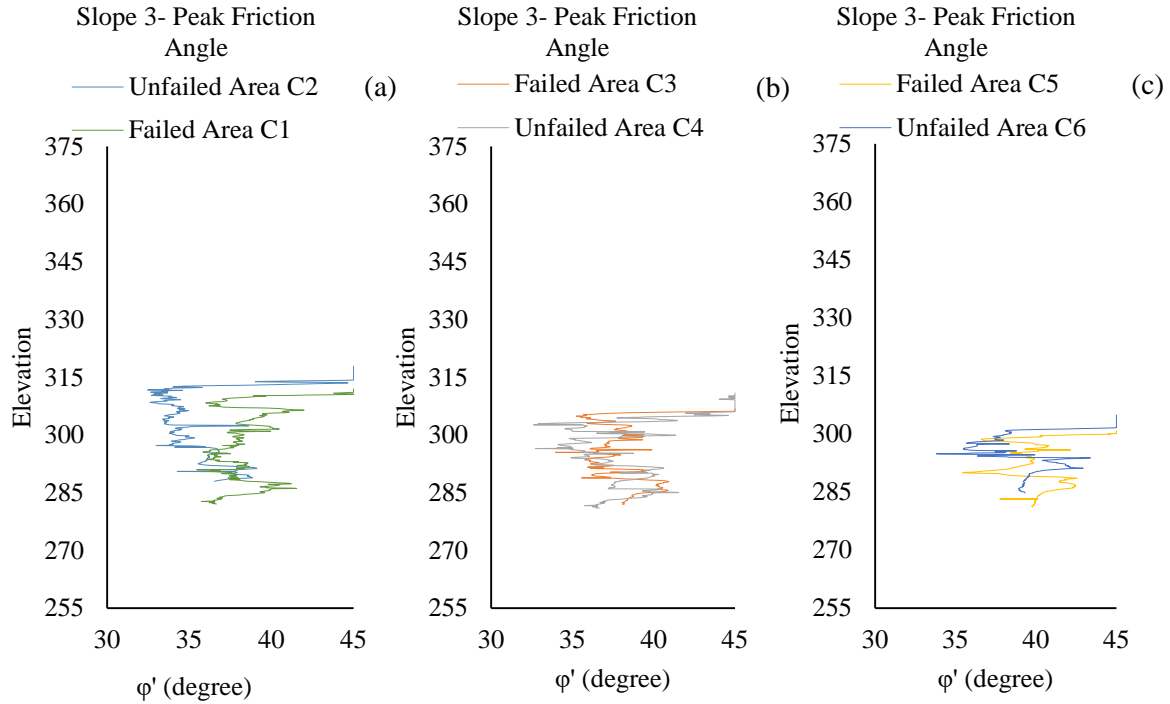


Figure 3.20 Variation of friction angle at Slope 3 (a) crest of the slope (b) middle of the slope (c) toe of the slope

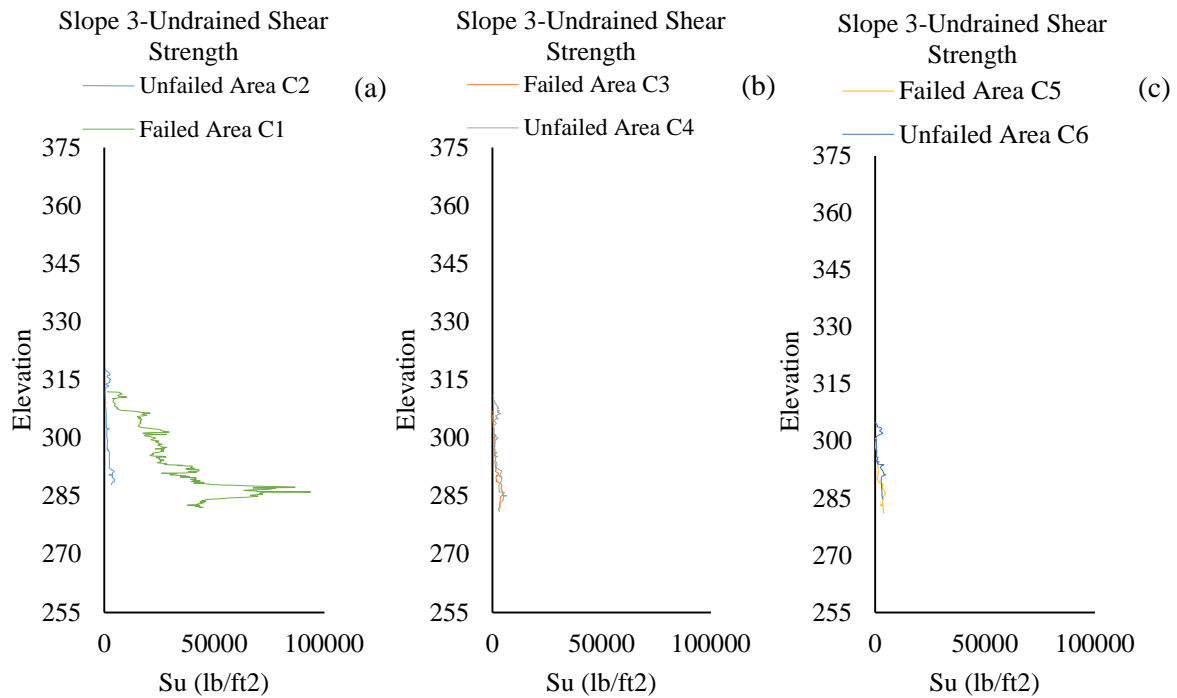


Figure 3.21 Variation of Undrained shear strength at Slope 3 (a) crest of the slope (b) middle of the slope (c) toe of the slope

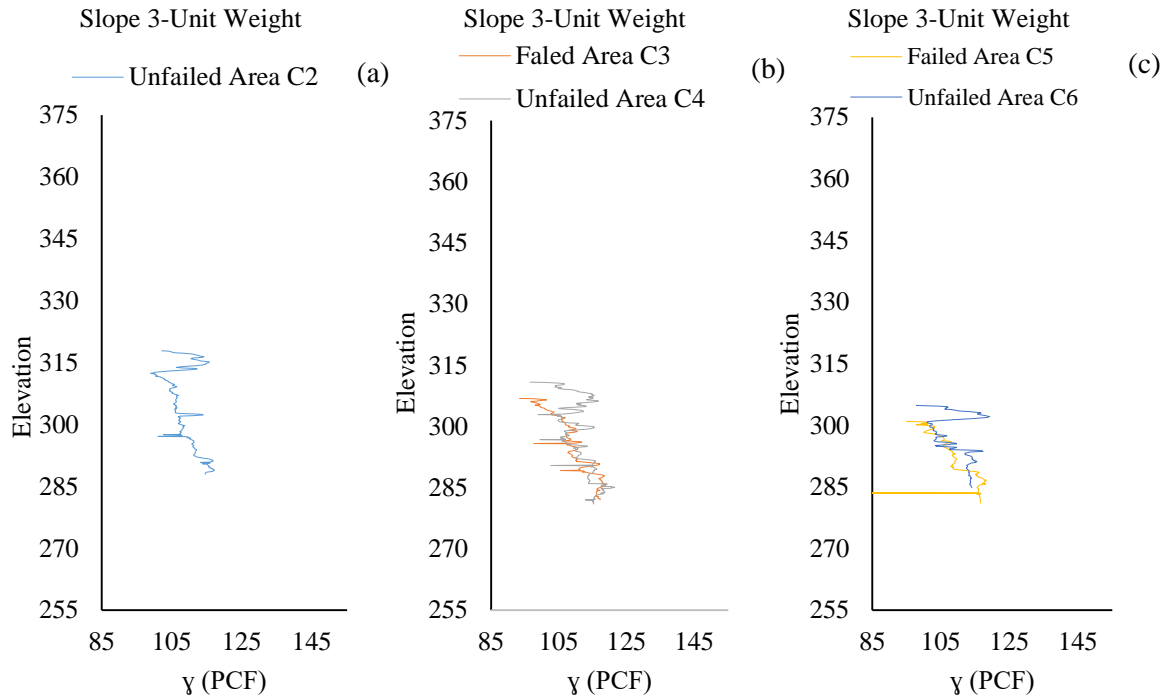


Figure 3.22 Variation of dry unit weight at Slope 3 (a) crest of the slope (b) middle of the slope (c) toe of the slope

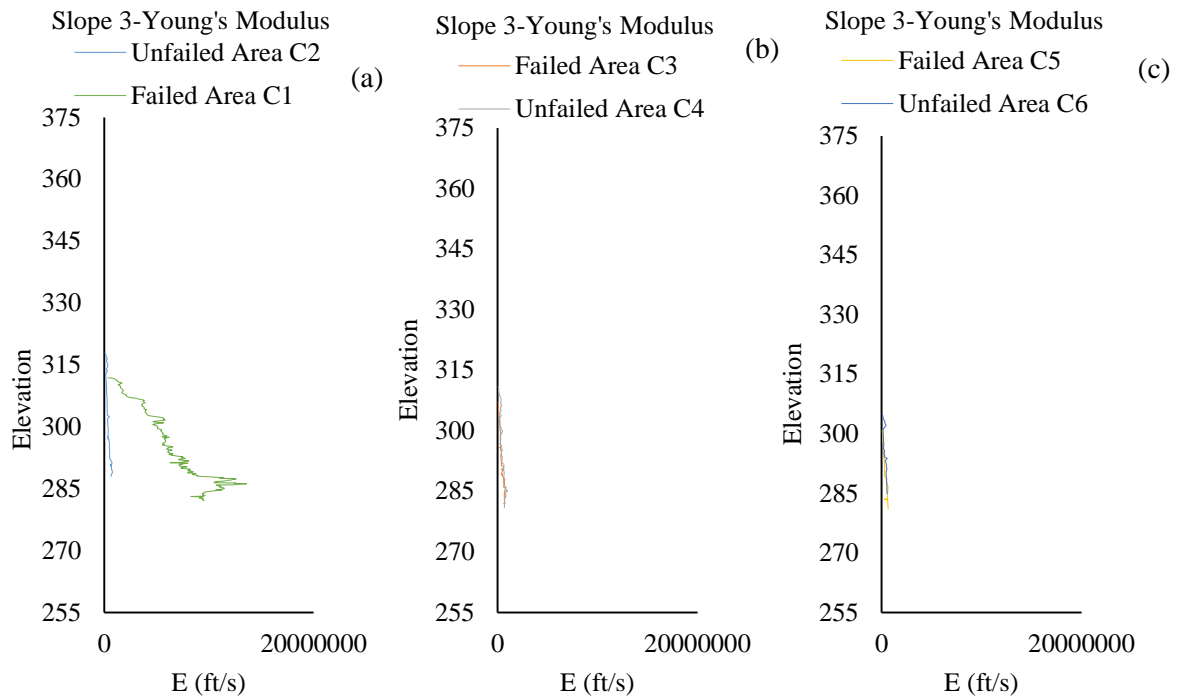


Figure 3.23 Variation of Young's modulus at Slope 3 (a) crest of the slope (b) middle of the slope (c) toe of the slope

3.5 Slope 4: Highland Drive Highway Slope

The Slope 4 is located along with I20 E near Highland drive. The location of the slope and site photos are presented in Figure 3.24. For this slope no pre-existed failure area was reported and therefore only the as-built section of the slope was investigated. It is a 3.5H:1V slope with a height of 20 ft.

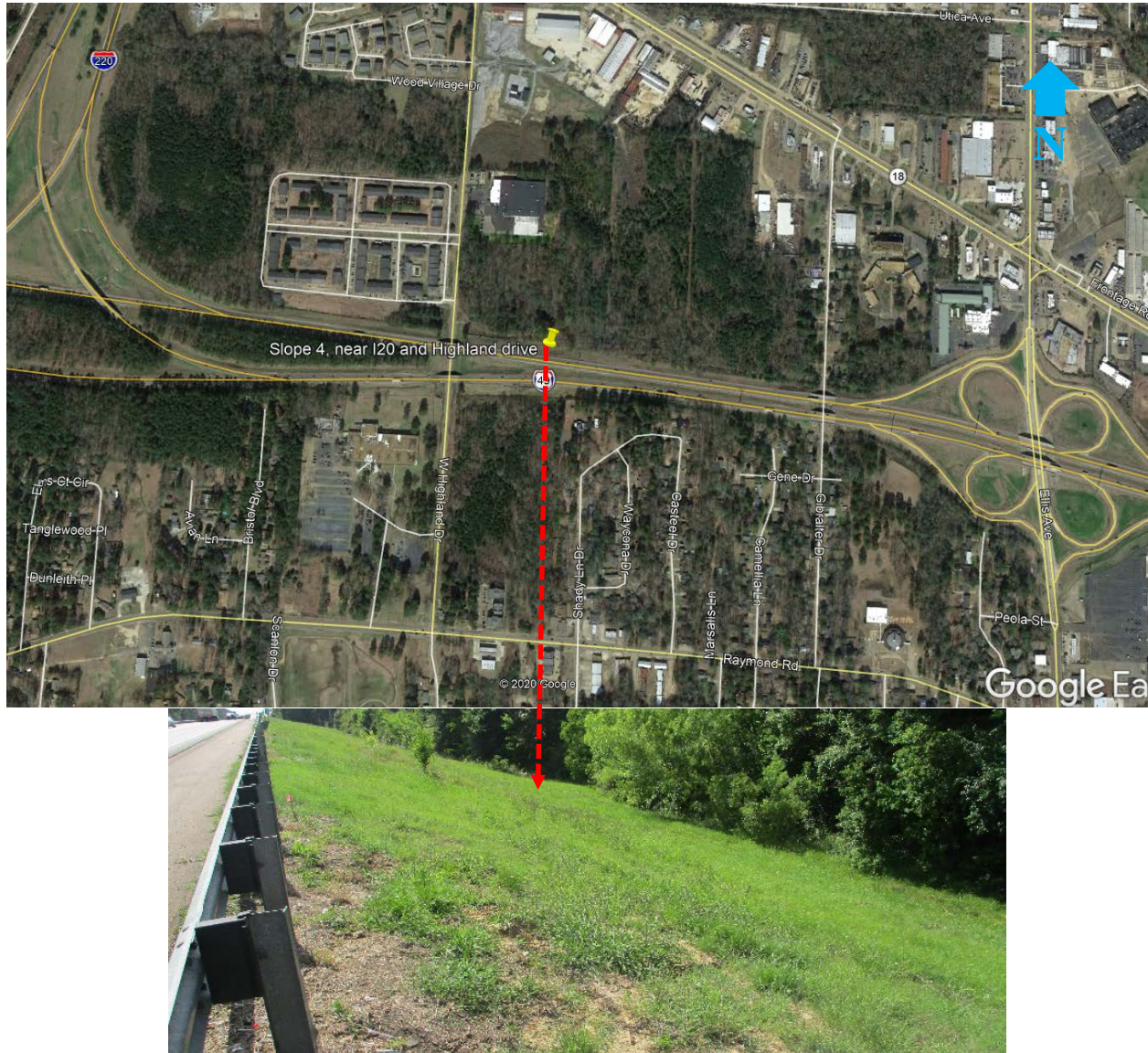


Figure 3.24 Location of Slope 4

Table 3.5 presents the details of the site investigation for Slope 4. The layout of the CPT and boreholes are presented in Figure 3.25. As no previous failure plane was located, only one slope inclinometer with 30 ft depth was installed at Slope 4. For field instrumentation, three boreholes were drilled at the crest, middle, and toe of the slope with 15 ft depth. Additionally, three CPT tests were conducted in the slope at the crest, middle, and toe of the slope.

Table 3.5 Site investigation details at Slope 4

Borehole/Test Designation	Borehole Depth (ft.)	Slope Area	Purpose of the Boring
Inclinometer 1	30	As-built slope	Continuous Shelby tube sampling and Install Inclinometer
BH-1	15	As-built slope	Instrumentation
BH-2	15	As-built slope	Instrumentation
BH-3	15	As-built slope	Instrumentation
BH-4	30	As-built slope	Additional sampling
CPT 1	30	As-built slope	CPU Test
CPT 2	30	As-built slope	
CPT 3	25	As-built slope	
CPT 4	25	As-built slope	
CPT 5	20	As-built slope	
CPT 6	20	As-built slope	

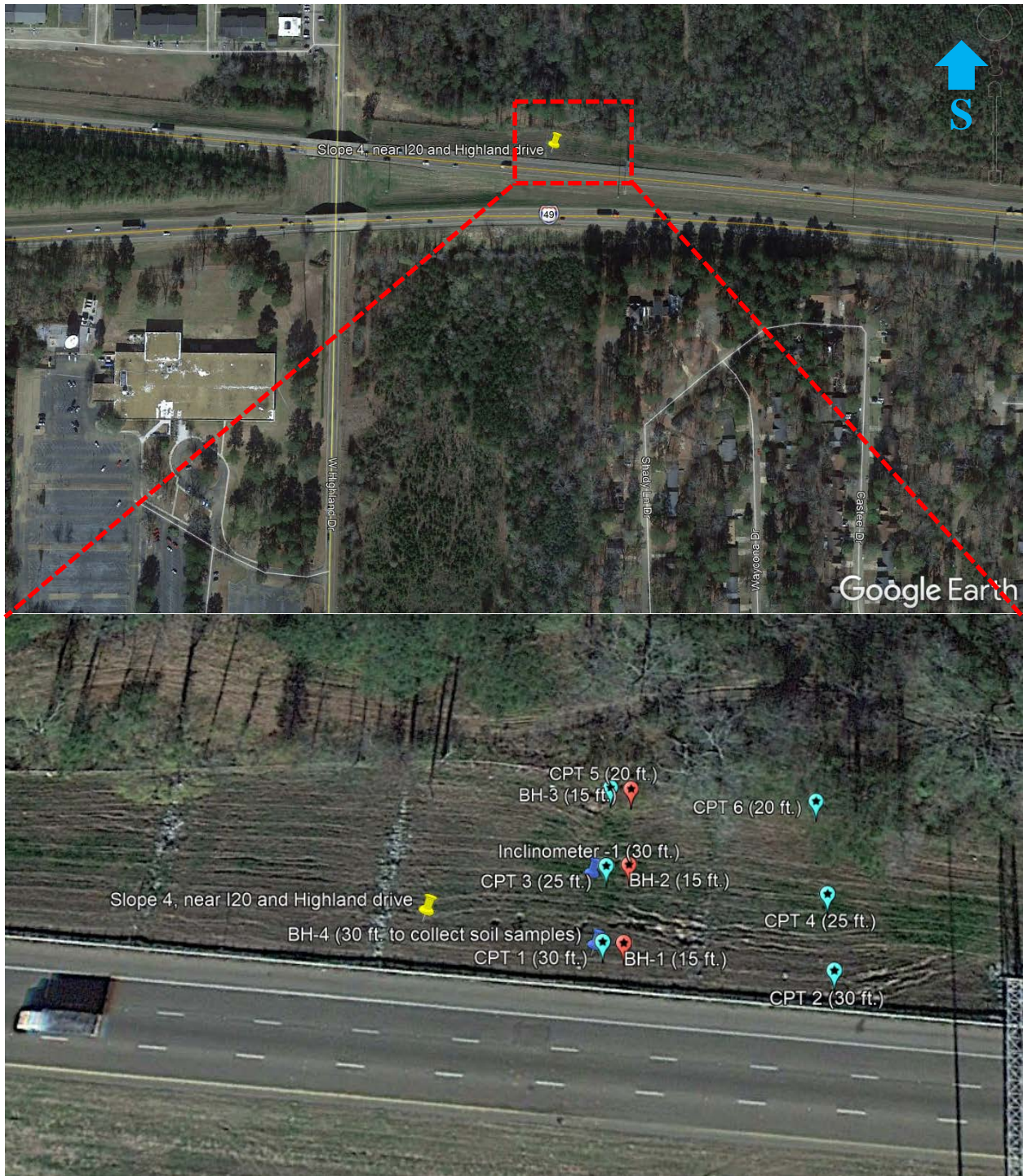


Figure 3.25 CPT location at Slope 4

3.5.1 Investigation of CPT Testing

Thompson Engineering conducted six CPT tests at the highland drive slope at the crest, middle, and toe of the slope. The depth of CPT at the crest, middle, and toe of the slope was 30 ft., 25 ft., and 20 ft.; respectively. The field activity of the CPT at the site is presented in Figure 3.26. The CPT was performed

using standard 10 cm² Type 1 Piezocone. The CPT results of location C1, which was located at the crest of the slope is presented in Figure 3.27. All other CPT results are included in Appendix A.



Figure 3.26 Field activity of CPT at Slope 4

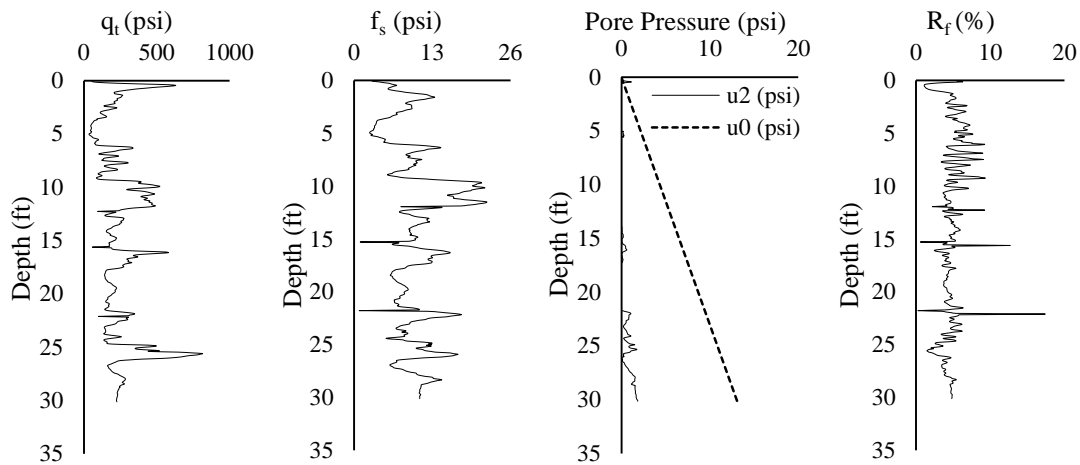


Figure 3.27 CPT results at the crest of Slope 4.

3.5.2 Soil Parameters from CPT

Using applicable correlations as presented in Equation 3.1 to Equation 3.8 for the CPT results, the friction angle, undrained shear strength, dry unit weight, and Young's Modulus of soil for Slope 4 are determined and presented in Figure 3.28 to Figure 3.31, respectively. It should be noted that only realistic values of the soil parameters were used in the Finite Element Modeling, which is discussed in Chapter 5.

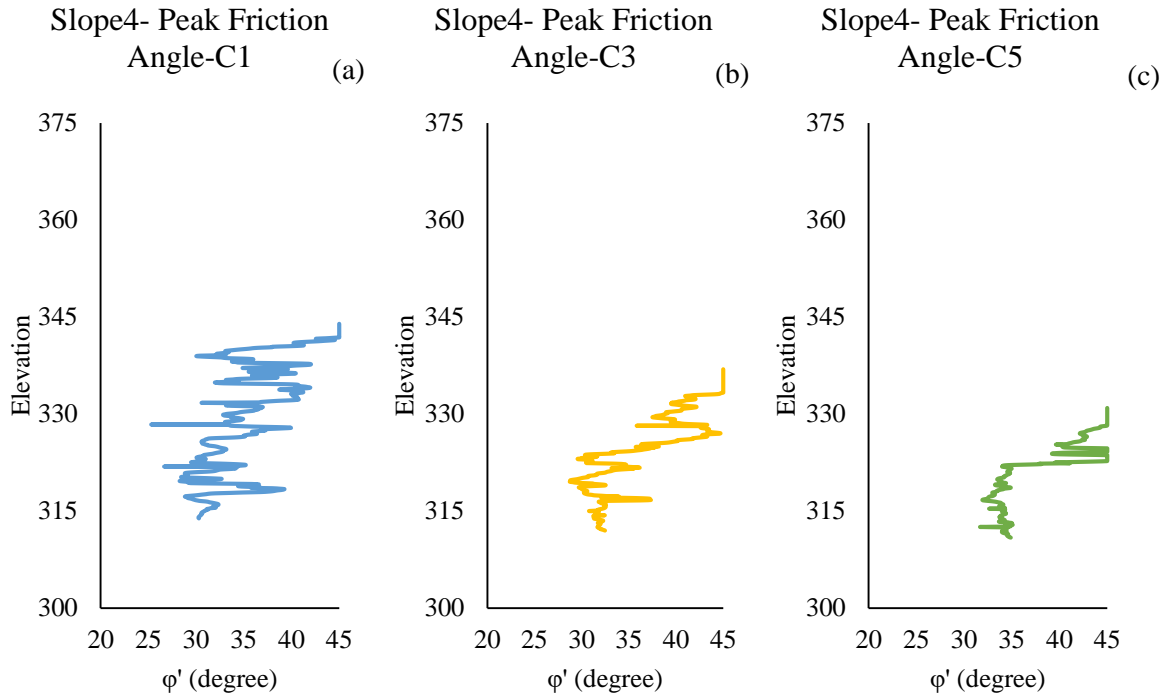


Figure 3.28 Variation of friction angle at Slope 4 (a) crest of the slope (b) middle of the slope (c) toe of the slope

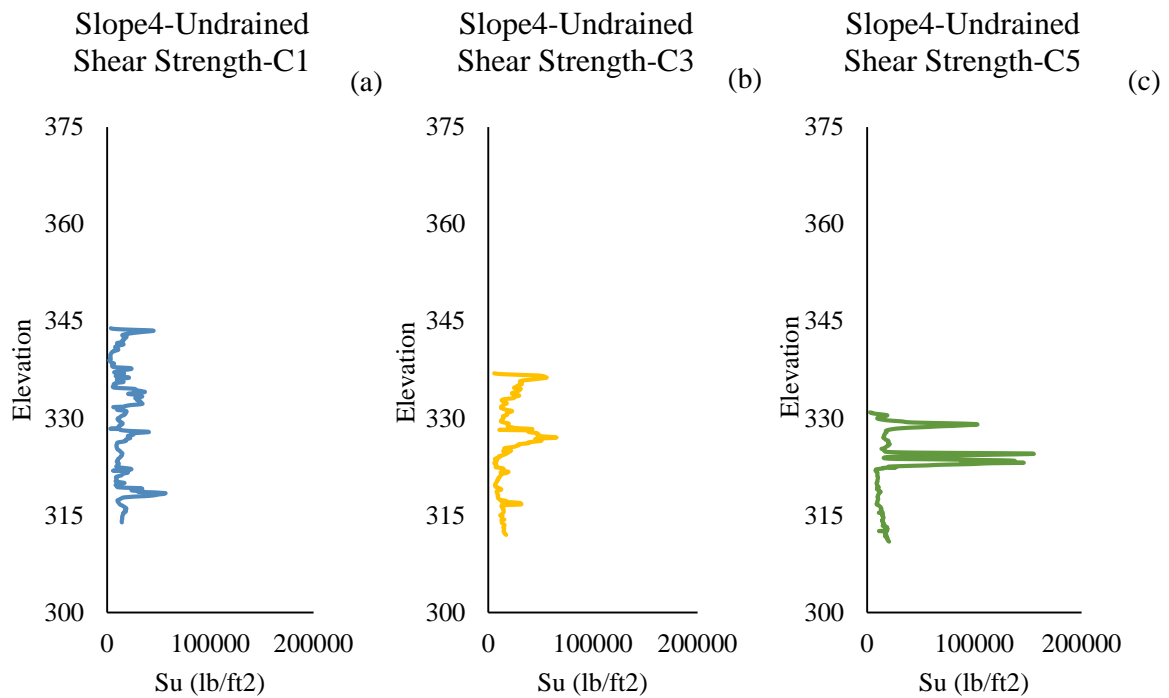


Figure 3.29 Variation of Undrained Shear Strength at Slope 4 (a) crest of the slope (b) middle of the slope (c) toe of the slope

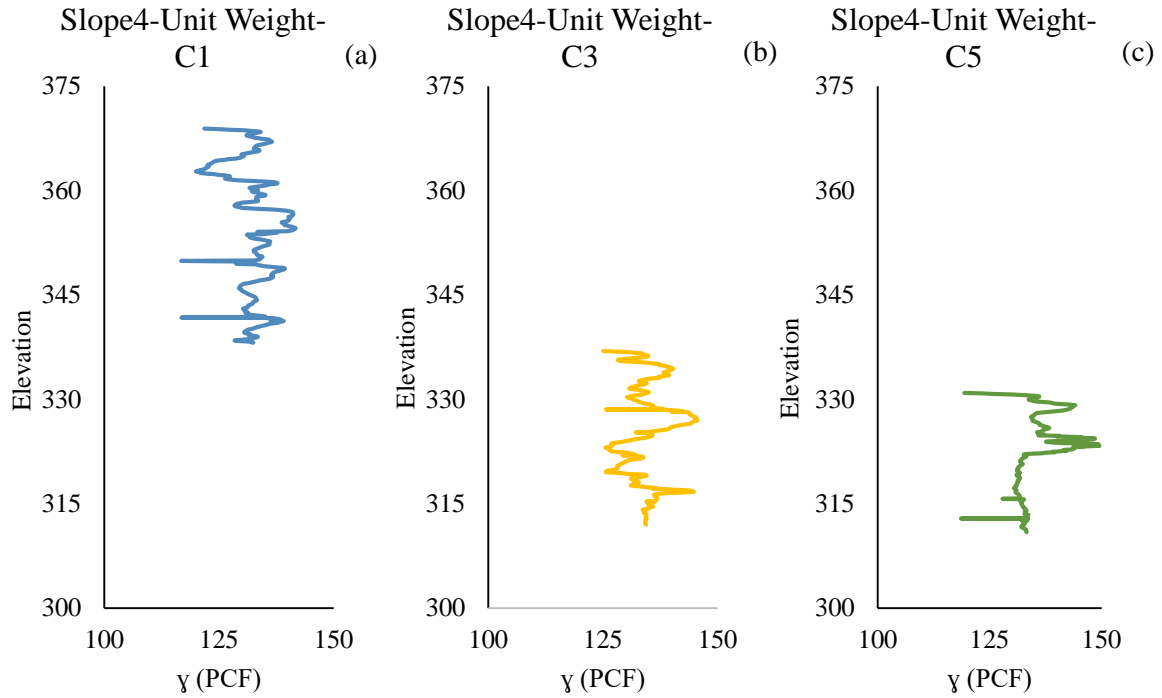


Figure 3.30 Variation of dry unit weight at Slope 4 (a) crest of the slope (b) middle of the slope (c) toe of the slope

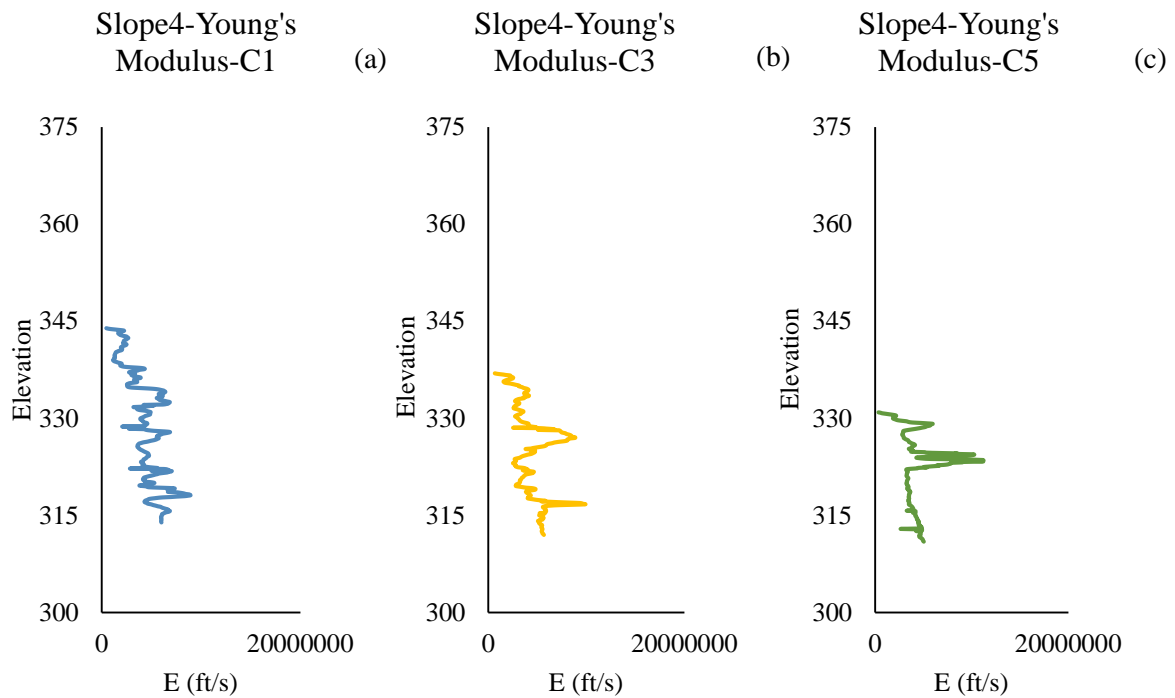


Figure 3.31 Variation of Young's modulus at Slope 4 (a) crest of the slope (b) middle of the slope (c) toe of the slope

3.6 Slope 5: Sowell Road Highway Slope

Slope 5 is located along the exit of I55 South toward Sowell road. The slope has experienced a slide with a failure depth of 15 ft., which was rebuilt and repaired using 30 ft. long HP 14x73 at the middle of the slope. In addition, two layers of uniaxial Geogrid was installed from the middle to toe of the slope. For this slope, both the repaired section and the as-built section were considered as a study area. The site location and photo of the site is presented in Figure 3.32.

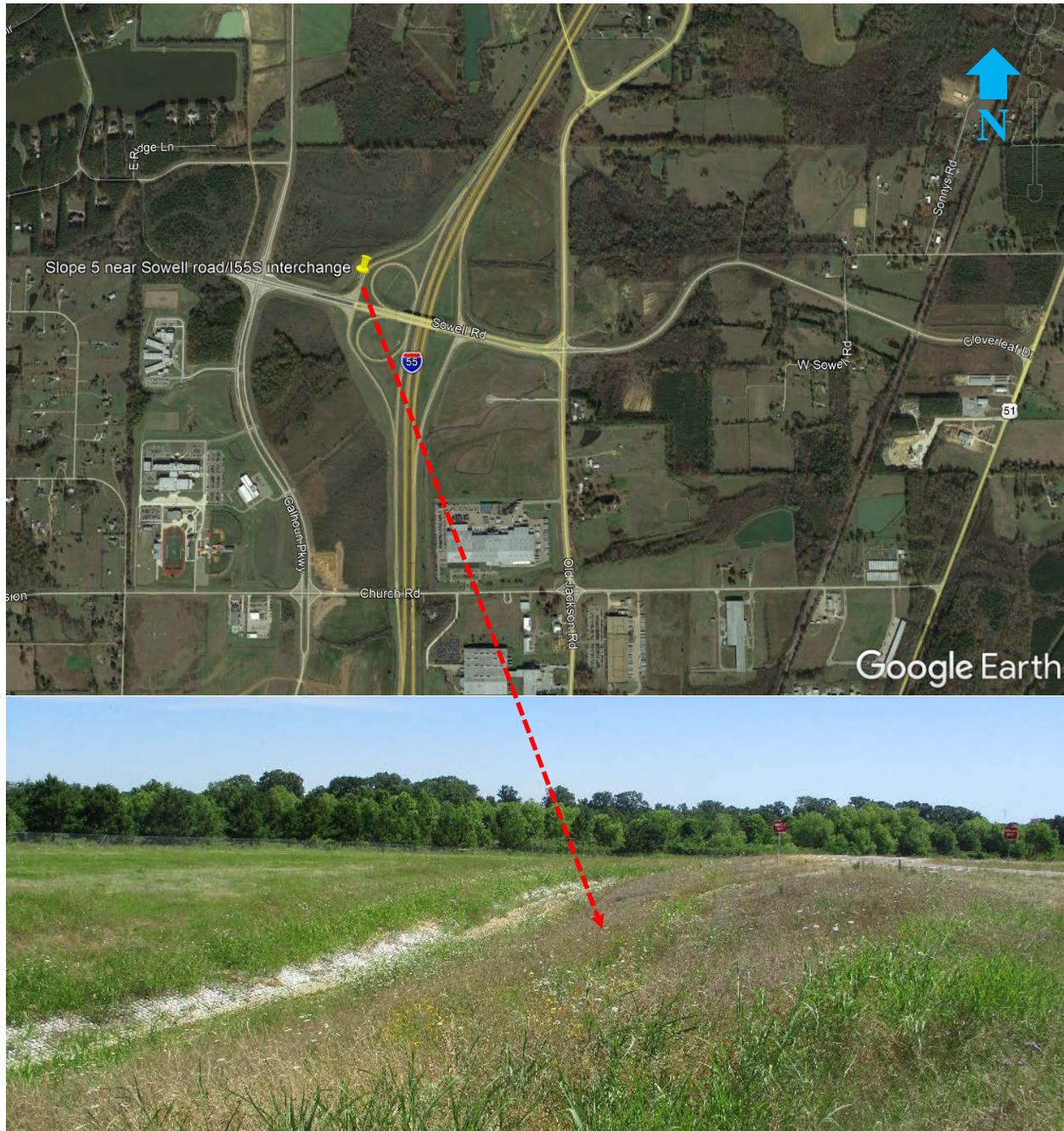


Figure 3.32 Location of Slope 5

Table 3.6 presents the details of the site investigation for Slope 5. The layout of the CPT and borehole locations are presented in Figure 3.33. As part of the site investigation, two slope inclinometer

with 30 ft depth was installed at the as-built section and the repaired section of the slope. For field instrumentation at this site, three boreholes were drilled at the crest, middle, and toe of the slope with 15 ft depth. In addition, six CPT tests were conducted at both repaired and as-built sections of the slope.

Table 3.6 Site investigation details at Slope 5

Borehole/Test Designation	Borehole Depth (ft.)	Slope Area	Purpose of the Boring
Inclinometer 1	30	As-built slope	Continuous Shelby tube sampling and Install Inclinometer
Inclinometer 2	30	Repaired slope	Continuous Shelby tube sampling and Install Inclinometer
BH-1	15	As-built slope	Instrumentation
BH-2	15	As-built slope	Instrumentation
BH-3	15	Repaired slope	Instrumentation
CPT 1	30	As-built slope	CPT Test
CPT 2	30	Repaired slope	
CPT 3	25	As-built slope	
CPT 4	25	Repaired slope	
CPT 5	20	As-built slope	
CPT 6	20	Repaired slope	

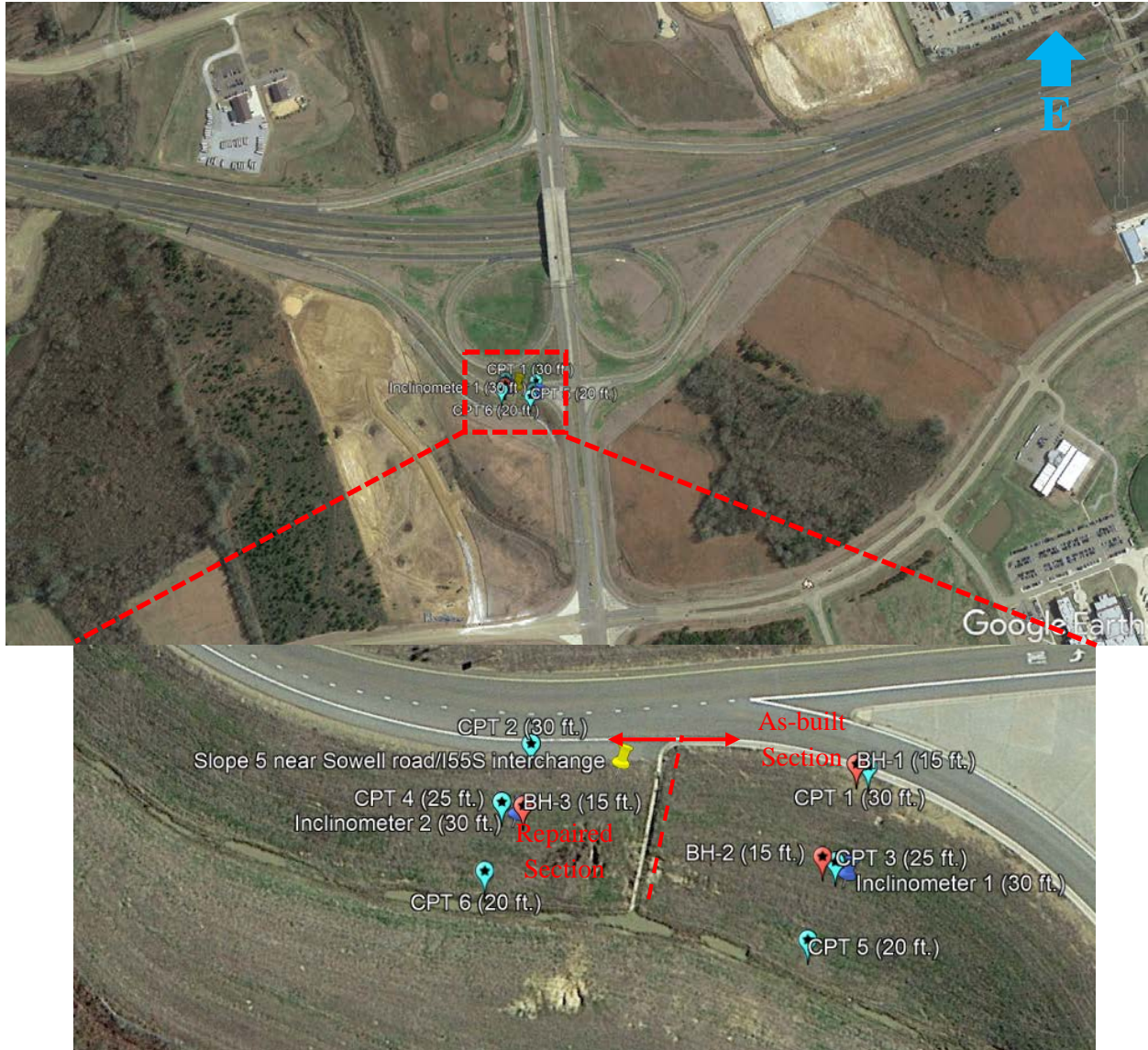


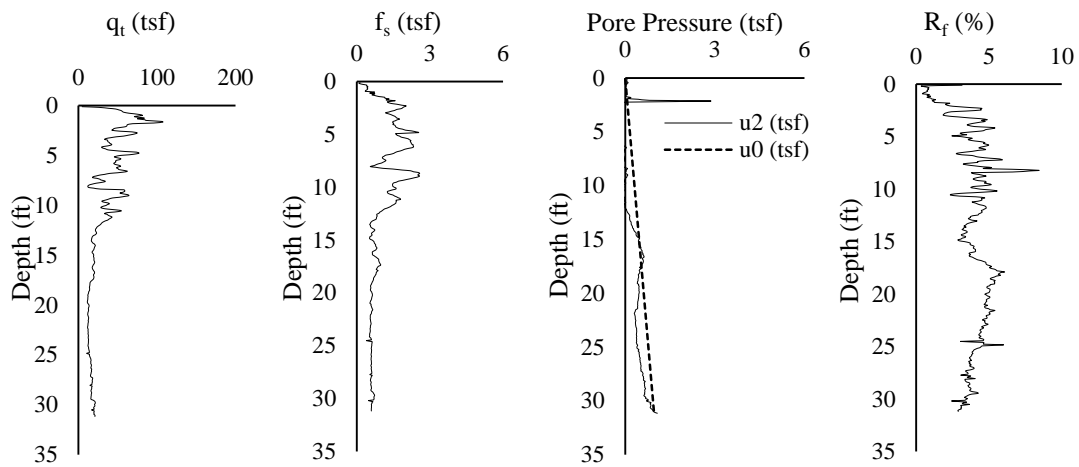
Figure 3.33 CPT location at Slope 5

3.6.1 Investigation of CPT Testing

Thompson Engineering conducted six CPT tests at the crest, middle, and toe of the slope. The depth of the CPT at the crest, middle, and toe of the slope was 30 ft., 25 ft., and 20 ft.; respectively. A field activity photo of the CPT at Slope 5 and CPT test results at location C1 is presented in Figure 3.34. The CPT performed using standard 10 cm² Type 1 Piezocone, suitable for this location. The CPT results at other locations of Slope 5 are included in Appendix A.



(a)



(b)

Figure 3.34 (a) Field Activities, (b) CPT results at the crest of Slope 5

3.6.2 Soil Parameters from CPT

Using applicable correlations as presented in Equation 3.1 to Equation 3.8 for CPT results, the friction angle, undrained shear strength, dry unit weight, and Youngs Modulus at Slope 5 were determined and presented in Figure 3.35 to Figure 3.38, respectively. Similar to other slopes, some of the parameters determined from CPT test results were observed unrealistic and misleading, which was adjusted based on the laboratory test results and back calculated soil parameters.

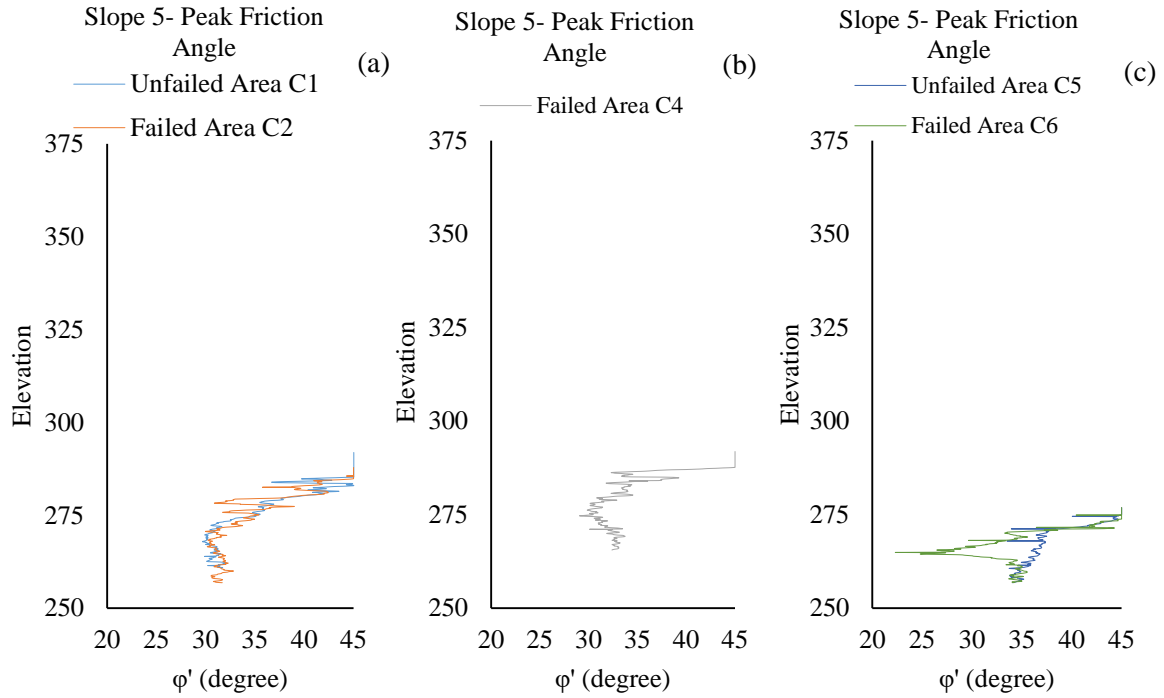


Figure 3.35 Variation of friction angle at Slope 5 (a) crest of the slope (b) middle of the slope (c) toe of the slope

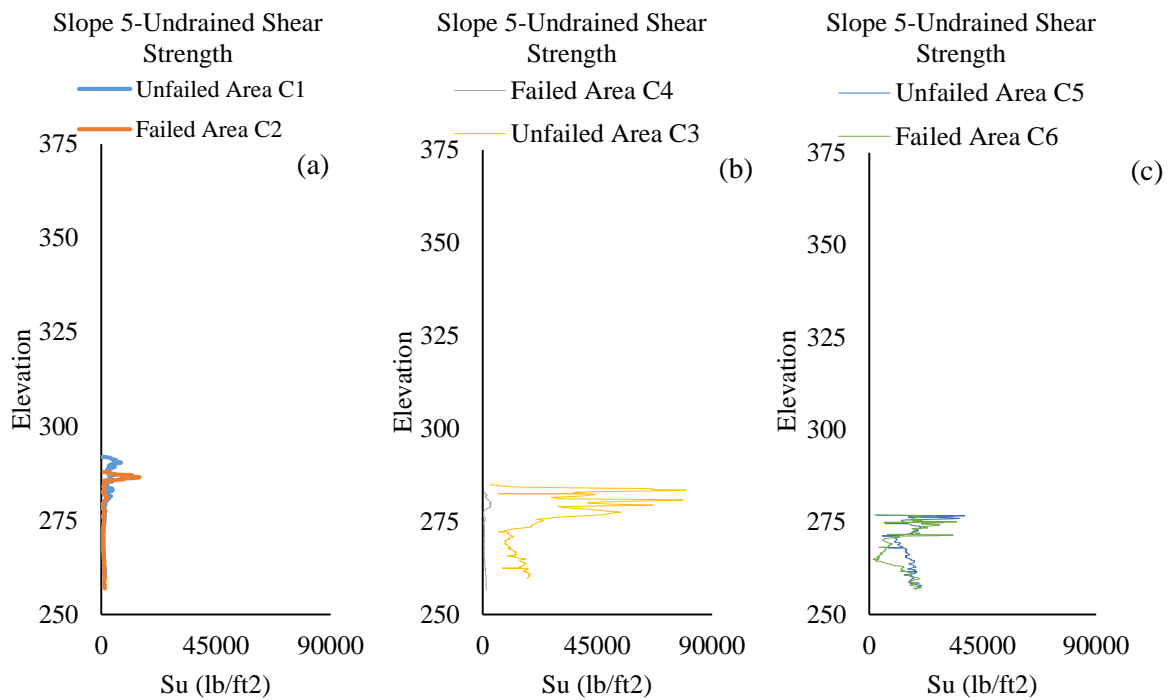


Figure 3.36 Variation of Undrained Shear Strength at Slope 5 (a) crest of the slope (b) middle of the slope (c) toe of the slope

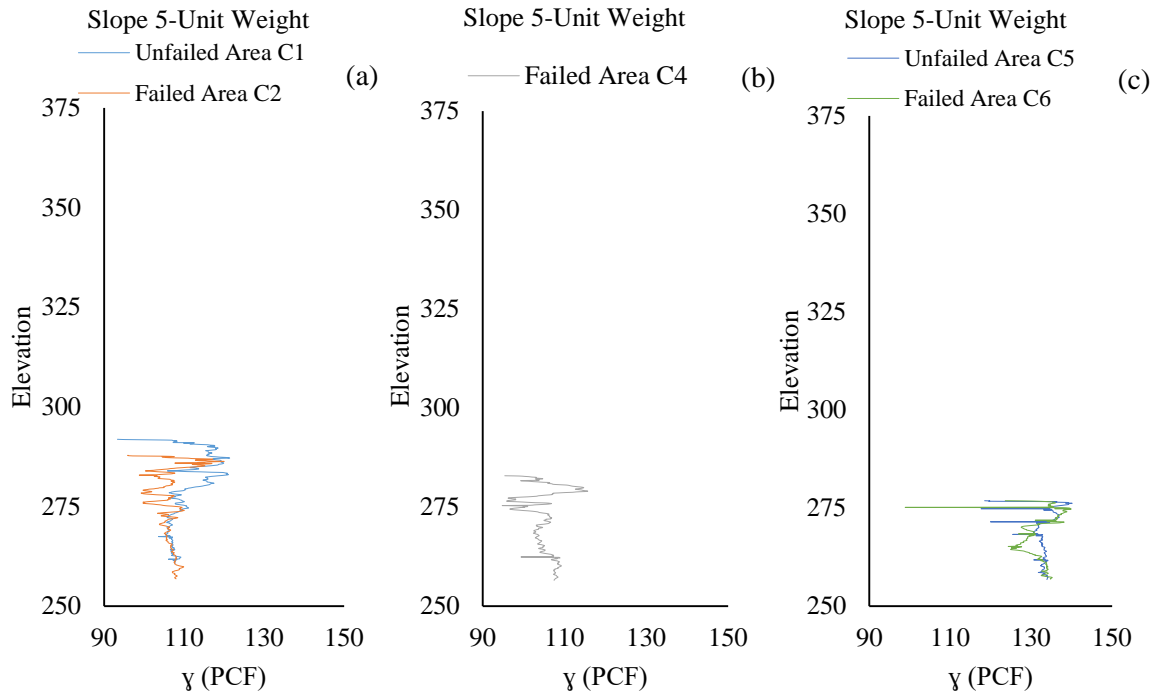


Figure 3.37 Variation of dry unit weight at Slope 5 (a) crest of the slope (b) middle of the slope (c) toe of the slope

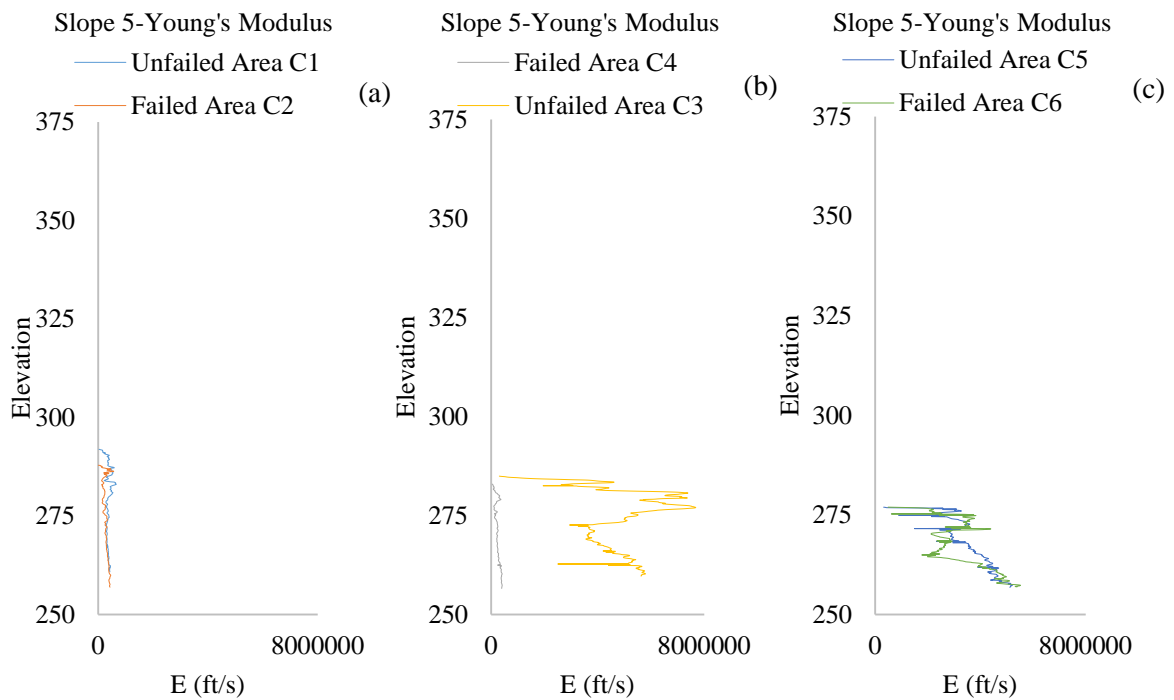


Figure 3.38 Variation of Young's modulus at Slope 5 (a) crest of the slope (b) middle of the slope (c) toe of the slope

3.7 Slope 6: McRaven Road Highway Slope

Slope 6 is located on along I20E near McRaven road. The location of the slope and site photo is presented in Figure 3.39. It is a 4H: 1V slope with a height of 15 ft. Some part of the slope has shown prior movement, which was re-built, re-graded and the drainage structure of the slope was reestablished. Both the repaired section and the as-built section were considered for this study.



Figure 3.39 Location of Slope 6

Table 3.7 presents the details of the site investigation of Slope 6. The location of the boreholes is presented in Figure 3.40. During the site investigation, two slope inclinometers with 30 ft depth at both sections were installed. For field instrumentation at this site, three boreholes were drilled at the crest, middle, and toe of the slope with 15 ft depth. In addition, six CPT tests were conducted at both of the sections at the crest, middle, and toe of the slope.

Table 3.7 Site investigation details at Slope 6

Borehole/Test Designation	Borehole Depth (ft.)	Slope Area	Purpose of the Boring
Inclinometer 1	30	Repaired slope	Continuous Shelby tube sampling and Install Inclinometer
Inclinometer 2	30	As-built slope	Continuous Shelby tube sampling and Install Inclinometer
BH-1	15	Repaired slope	Instrumentation
BH-2	15	Repaired slope	Instrumentation
BH-3	15	As-built slope	Instrumentation
CPT 1	30	As-built slope	CPT Test
CPT 2	30	Repaired slope	
CPT 3	25	As-built slope	
CPT 4	25	Repaired slope	
CPT 5	20	As-built slope	
CPT 6	20	Repaired slope	



Figure 3.40 Location of CPT at Slope 6

3.7.1 Investigation of CPT Testing

Thompson Engineering conducted six CPT tests at slope 6. A field activity photo of the CPT at Slope 6 e is presented in Figure 3.41. The depth of the CPT at the crest, middle, and toe of the slope was 30 ft., 25 ft., and 20 ft.; respectively. The CPT performed using standard 15 cm² Type 1 Piezocone. The CPT results at location C1 is presented in Figure 3.42. The other CPT results are included in Appendix A.



Figure 3.41 CPT test at Slope 6

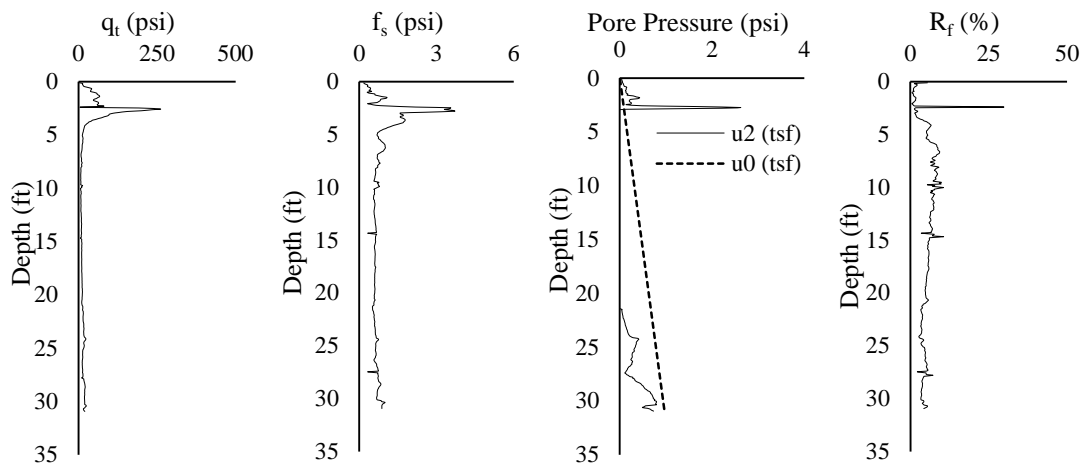


Figure 3.42 CPT results at the crest of Slope 6

3.7.2 Soil Parameters from CPT

Using applicable correlations as presented in Equation 3.1 to Equation 3.8 for CPT results, the friction angle, undrained shear strength, dry unit weight, and Youngs Modulus at the crest, middle, and toe of soil for Slope 6 are presented in Figure 3.43 to Figure 3.46, respectively. The soil parameters were used for numerical analysis, which is discussed in Chapter 5.

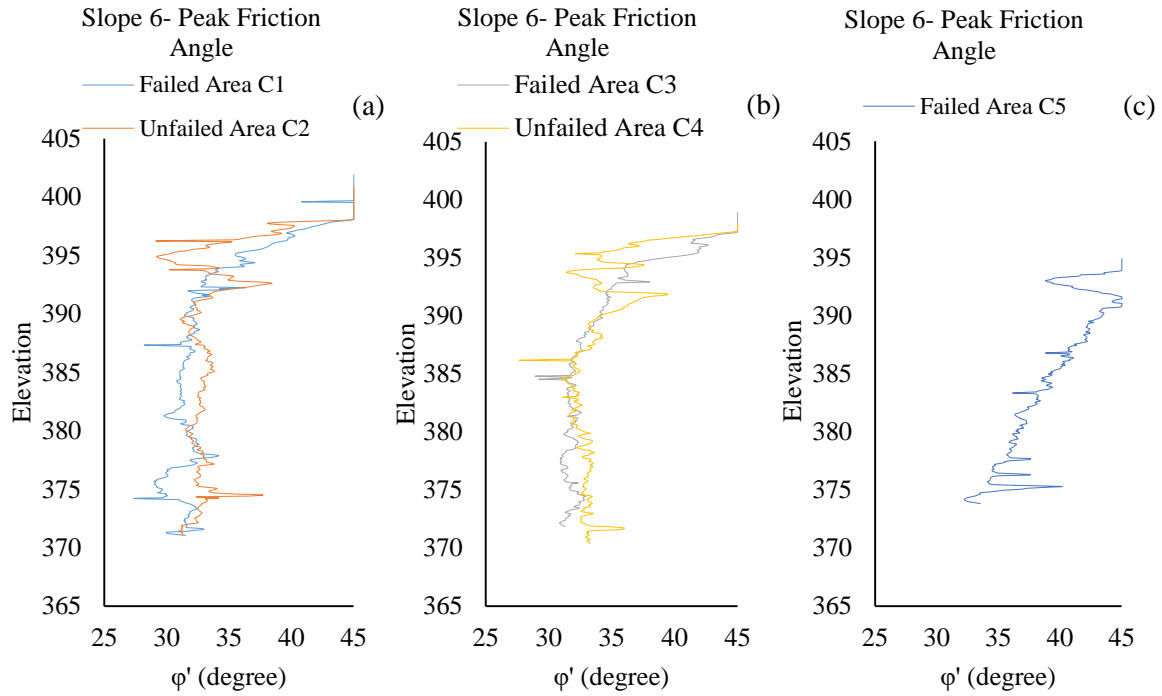


Figure 3.43 Variation of Friction Angle at Slope 6 (a) crest of the slope (b) middle of the slope (c) toe of the slope

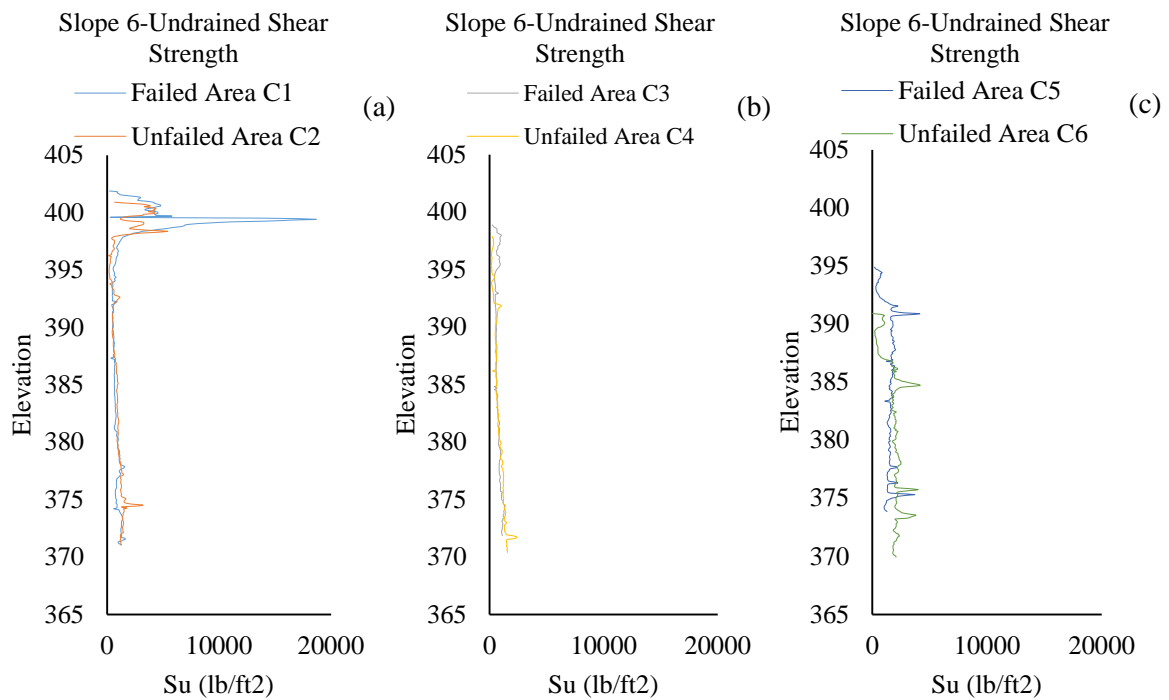


Figure 3.44 Variation of Undrained Shear Strength at Slope 6 (a) crest of the slope (b) middle of the slope (c) toe of the slope

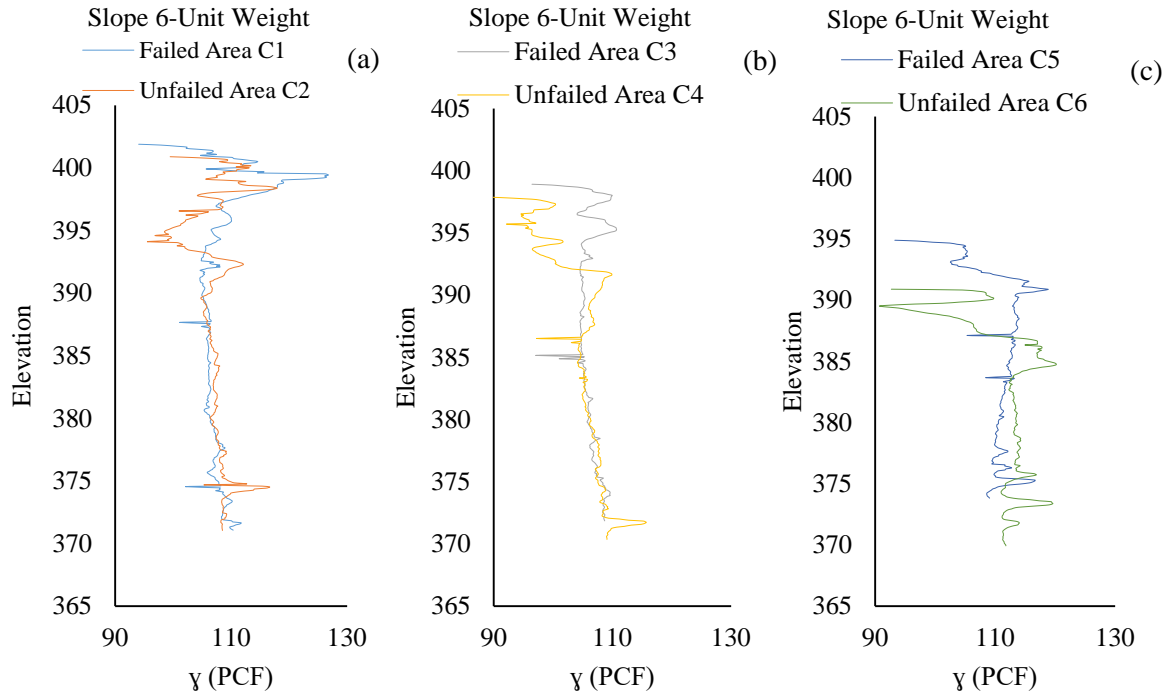


Figure 3.45 Variation dry unit weight at Slope 6 (a) crest of the slope (b) middle of the slope (c) toe of the slope

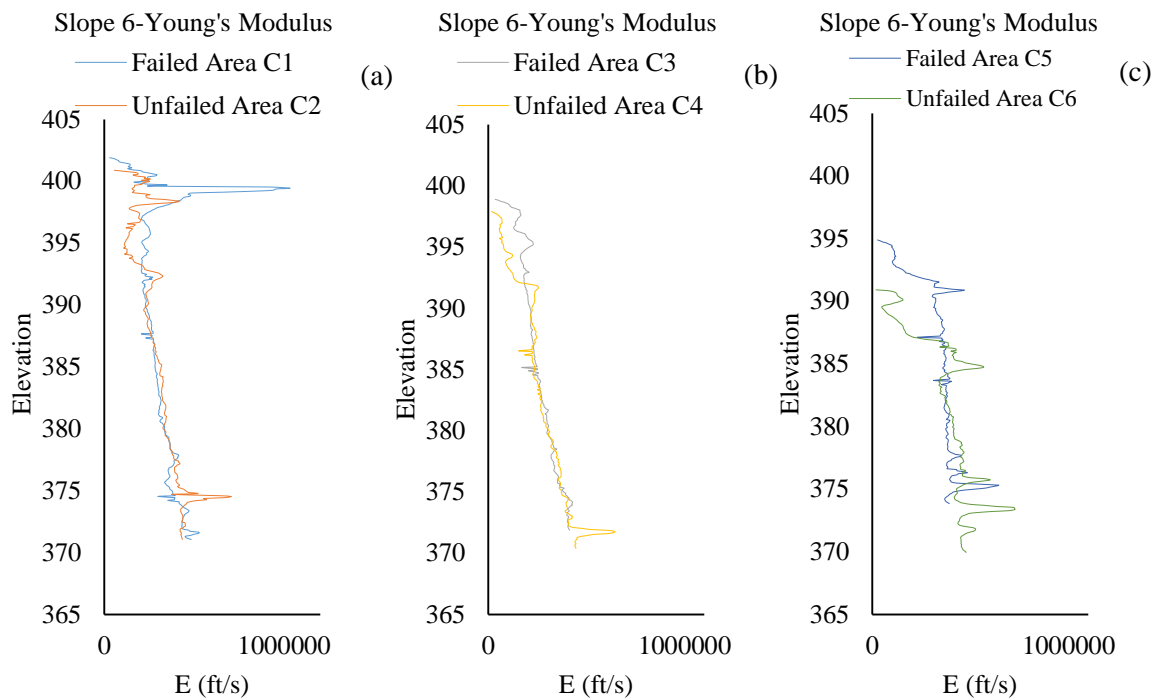


Figure 3.46 Variation of Young's modulus at Slope 6 (a) crest of the slope (b) middle of the slope (c) toe of the slope

Chapter 4: FIELD INSTRUMENTATION AND MONITORING

4.1 Field Instrumentation

Comprehensive field instrumentation was executed at the six slopes to monitor the moisture content, matric suction, soil temperature, air temperature, and rainfall intensity. Industrial grade sensors, such as GS-1 moisture sensors, Meter Teros 21 soil water potential sensors, ECRN-50 tipping-bucket rain gauge, EM50 data logger, and RT-1 air temperature sensor were installed at each slope. In addition, two 30 ft. long inclinometer casing pipes were installed to monitor the slope movement. The field instrumentation layout is illustrated in Figure 4.1. The sensors are installed at the crest, middle, and toe of the slope. The moisture sensors and water potential sensors located at 5 ft. (1.5 m), 10 ft. (3 m), and 15 ft. (5 m) depths, were installed at three 15 ft. deep boreholes. The location and number of sensors are also presented in Table 4.1

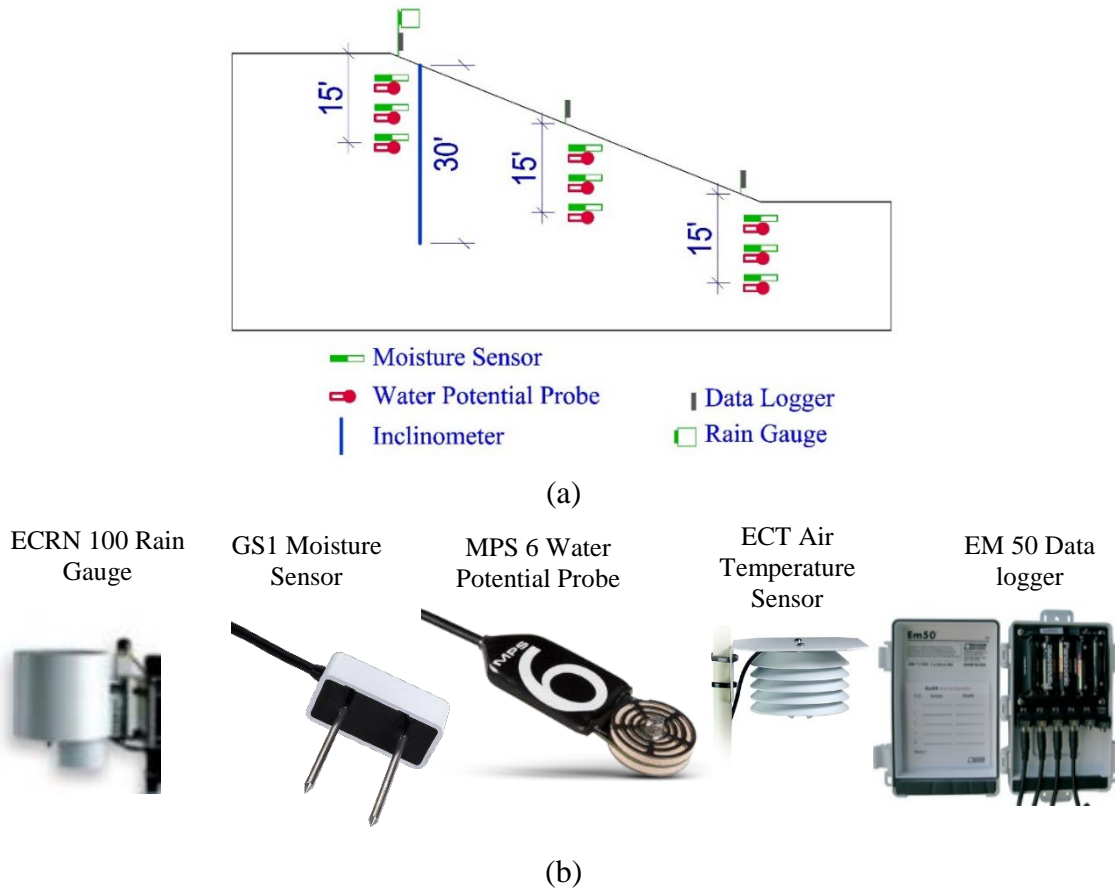


Figure 4.1 (a) Instrumentation layout at each slope (b) image of individual sensors

Table 4.1 Field Instrumentation for Data Collection

Sensor Name	Purpose	Location	Depth (ft.)	Number of Sensors
ECRN 100 Rain Gauge	Collect Precipitation Data	At the middle of the slope	Atmosphere	1
GS1 Moisture Sensor	Collect Volumetric Moisture Content	Crest, middle, toe	5, 10, 15	9
MPS 6 Water Potential Probe	Collect Matric Suction and Soil Temperature Data	Crest, middle, toe	5, 10, 15	9
ECT Air Temperature	Collect Precipitation Data	At the middle of the slope	Atmosphere	1
EM 50 Data Logger	Data Collection and Storage	At the middle of the slope	At the top of the slope	4

In each of the slopes investigated, twenty sensors and two inclinometer castings were installed. Figure 4.2 and Figure 4.3 present the process of sensors assemblage and color-coding. About 150 ft. long cables were used for the installation of the sensors. Each of the sensors is connected with a 3.5 mm stereo audio extension cable with the data loggers to record a continuous reading of in situ measurements.



Figure 4.2 Field sensor preparation



Figure 4.3 Field sensor color-coding set up

The instrumentation at each site was conducted during the time of site investigation, as discussed in Chapter 3. The schedule of field instrumentation is presented in Table 4.2. The installation process took about one month.

Table 4.2 Schedule of sites instrumentation

Sites	Field Instrumentation		
	Starting Date	Ending Date	
Slope 1	I220N Ramp toward I55N	8/14/2018	8/15/2018
Slope 2	Metro Center	8/29/2018	8/30/2018
Slope 3	Terry Road	8/16/2018	8/17/2018
Slope 4	Highland Drive	8/23/2018	8/27/2018
Slope 5	Sowell Road	8/9/2018	8/11/2018
Slope 6	McRaven Road	8/26/2018	8/29/2018

After installation, the data loggers were programmed to collect data from the moisture sensor, water potential probe, soil temperature, rain gauge, and air temperature sensors on an hourly basis from the field instrumentation. Table 4.3 presents the schedule of all six site slopes of the monitoring program. Furthermore, the JSU team visited each site bi-weekly to obtain inclinometer readings.

Table 4.3 Schedule of the site monitoring program

Instrumentation Type	Monitoring Type and Frequency	Data Collection Frequency
Vertical Inclinometer	Bi-weekly	Bi-weekly
Moisture Sensor	continuous (every hour)	Bi-weekly
Water Potential Probe	continuous (every hour)	Bi-weekly
Air Temperature	continuous (every hour)	Bi-weekly
Rain Gauge	continuous (every hour)	Bi-weekly

4.2 Slope 1: I220N Ramp Toward I55N Highway Slope

Slope 1 is located along the I220N ramp toward I55N and has a reinforced and as-built section, as presented in Chapter 3. Two 15 ft. boreholes were drilled and then instrumented at the as-built section,

which are designated as Instrumentation 1 and Instrumentation 3, as presented in Figure 4.4. In addition, a third 15 ft. deep borehole was drilled and then instrumented in the repaired area, which is designated as Instrumentation 3. Instrumentation 1 is located at the crest whereas, Instrumentation 2 and Instrumentation 3 are located in the middle of the slope. In each of the Instrumentation locations, at 5 ft (1.5 m), 10 ft (3 m), and 15 ft (5 m) depths, a moisture sensor, and a potential water sensor were installed. Additionally, a rain gauge and air temperature were installed at Instrumentation 1 at Slope 1. The sensor installations photos are presented in Figure 4.5.

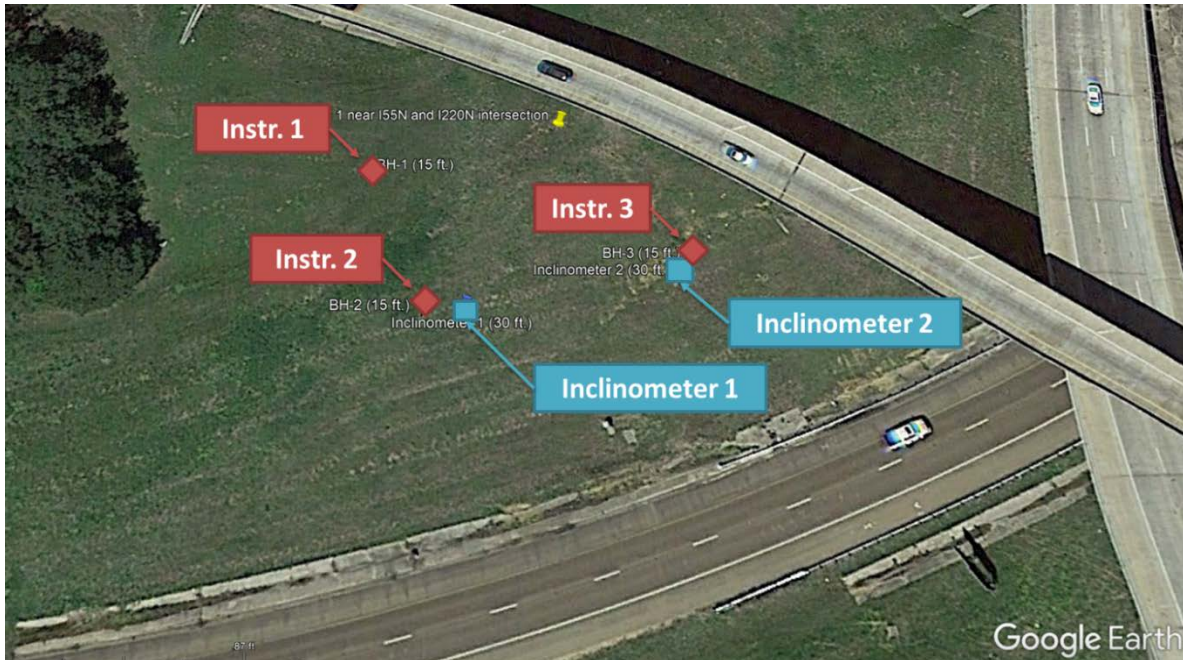


Figure 4.4 Layout of the instrumentation at Slope 1



Figure 4.5 Slope 1 sensor installation

The slope inclinometer installations photos are presented in Figure 4.6. The inclinometer 1 is installed at the as-built section, whereas the inclinometer 2 is installed at the repair sections. Both of the inclinometers were installed in the middle of the slopes.



Figure 4.6 Slope 1 slope inclinometer installation

4.2.1 Field Monitoring Results

JSU team visited the slope and collected data from the data loggers. Moreover, lateral deformation of the slope is monitored using slope inclinometer. The field monitoring results are discussed in the following section.

4.2.1.1 Slope Movement Data

The horizontal movement data from the slope was observed using slope inclinometer measurements collected at every 2 ft spacing along the slope inclinometer pipe. After data collection, the inclinometer data is downloaded and analyzed to determine the slope movement. The horizontal movement data from Inclinometer 1 at the as-built section and time-dependent movement along the crest of the slope is presented in Figure 4.7 and Figure 4.8, respectively. Similarly, the horizontal movement data from Inclinometer 2 at the repaired section and time-dependent movement along the crest of the slope is presented in Figure 4.9 and Figure 4.10. As indicated in Figure 4.7 to Figure 4.10, no significant movement is observed in both sections, and the performance of the slope is within the satisfactory level in both of the sections.

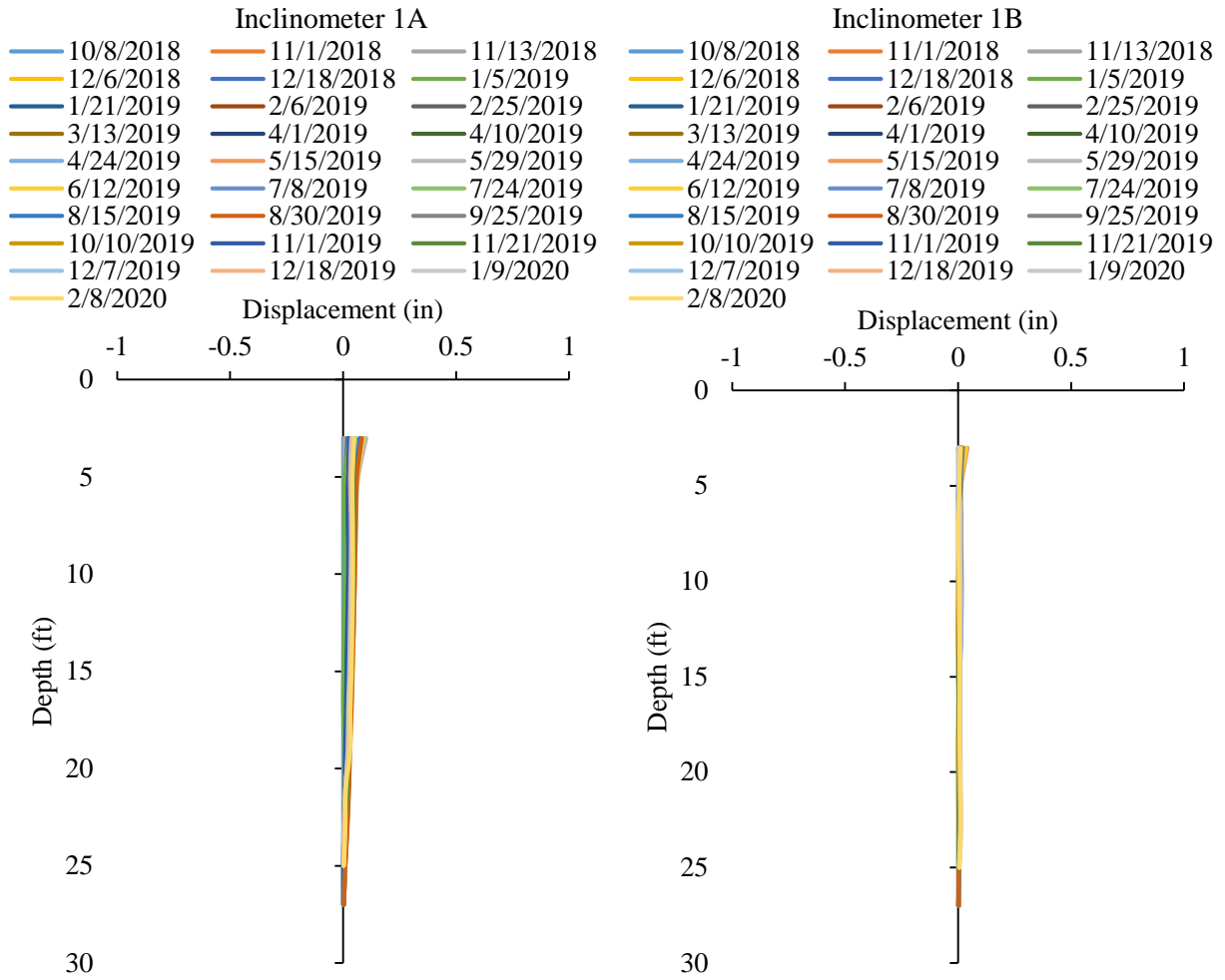


Figure 4.7 Horizontal displacements of the Inclinator 1 at Slope 1

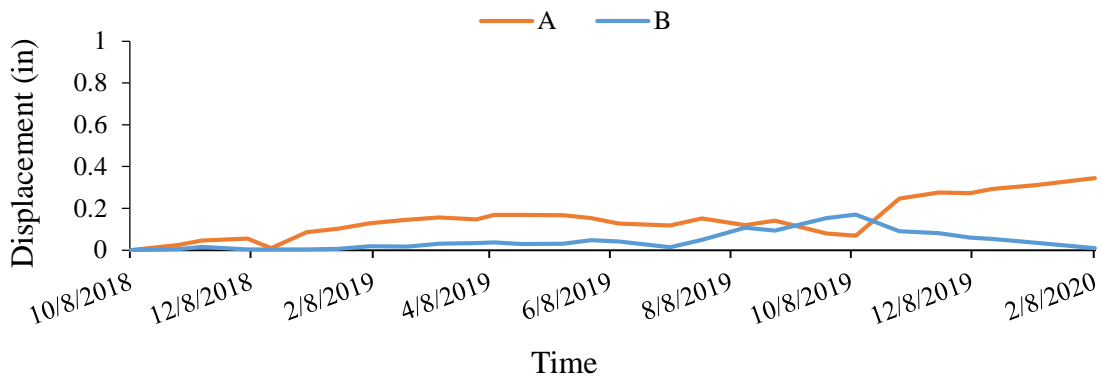


Figure 4.8 Variation of lateral deformation at the top of inclinometer at Slope 1 as-built section

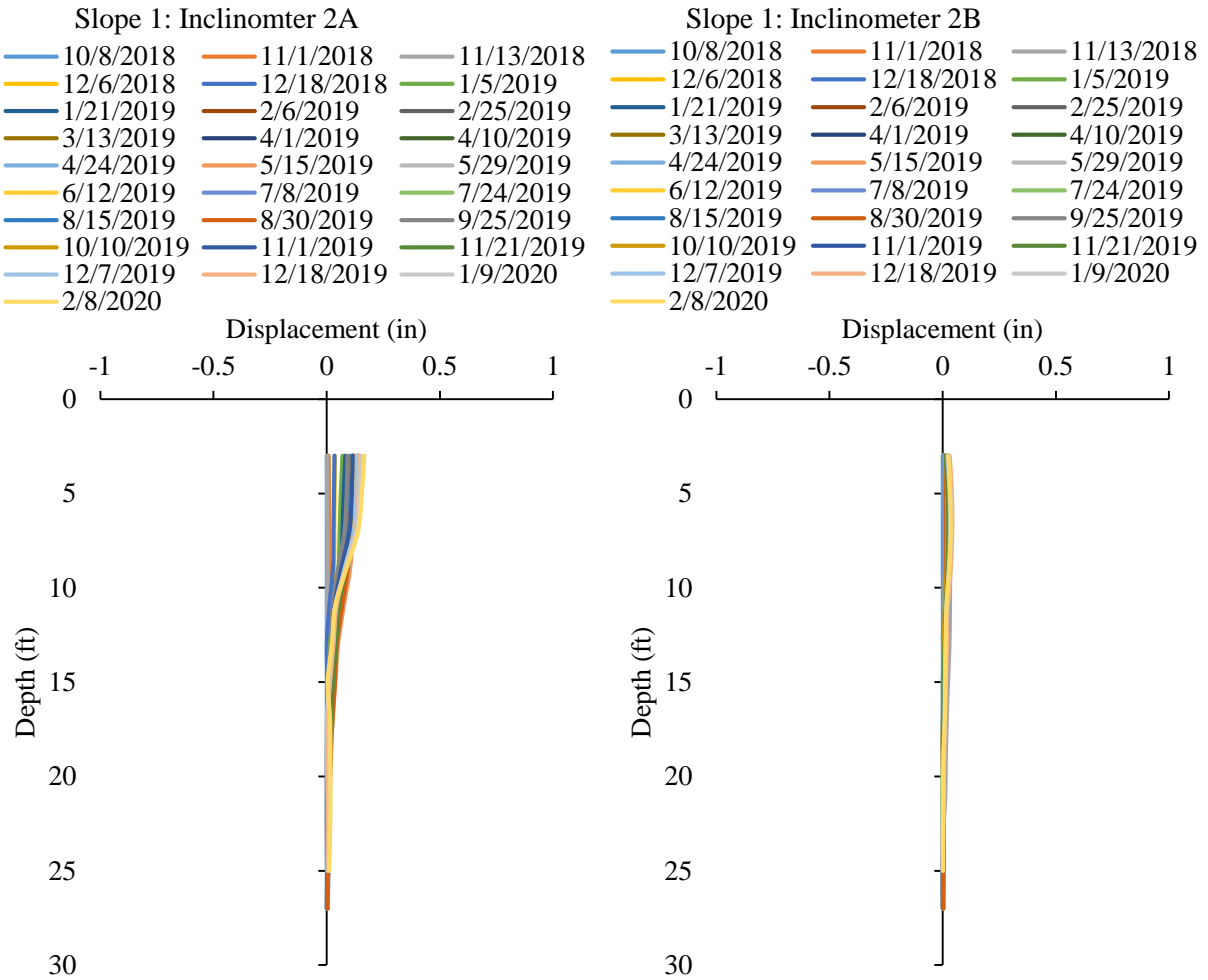


Figure 4.9 Horizontal displacements of the Inclinator 2 at Slope 1

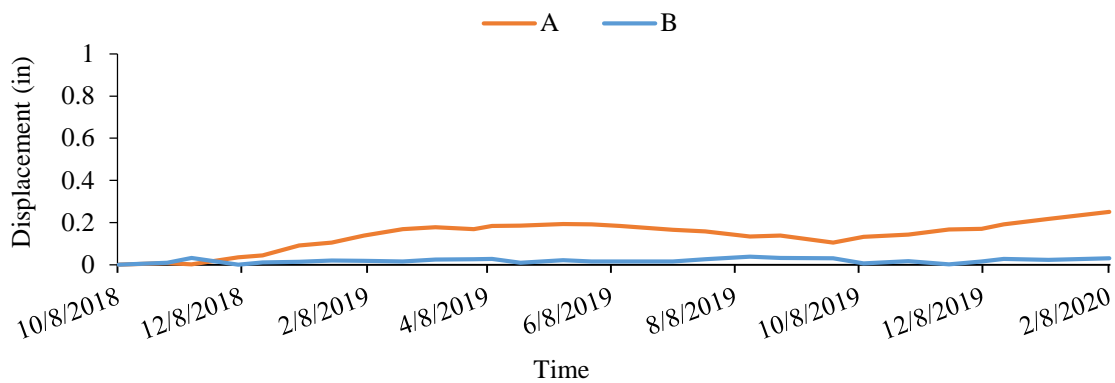


Figure 4.10 SI2 Variation of lateral deformation at Slope 1 repaired section

4.2.1.2 Field Instrumentation Data

Based on the field instrumentation results, variation of in situ matric suction profile, and moisture content at 5 ft. (1.5 m), 10 ft. (3 m), and 15 ft. (5 m) depths with rainfall are presented in Figures 4.11 to Figure 4.13. The sensor monitoring results collect the data at the crest, middle, and toe of the slope. The

moisture content and matric suction variations at Instrumentation 1, Instrumentation 2, and Instrumentation 3 are presented in Figure 4.11, Figure 4.12 and Figure 4.13, respectively. It is observed that the slope has shown few variations of moisture content value for all three depths. However, the matric suction have shown no variation. Within this 2-year data monitoring, the highest rainfall occurred in late December 2018. However, no significant changes in the moisture content and matric suction was observed.

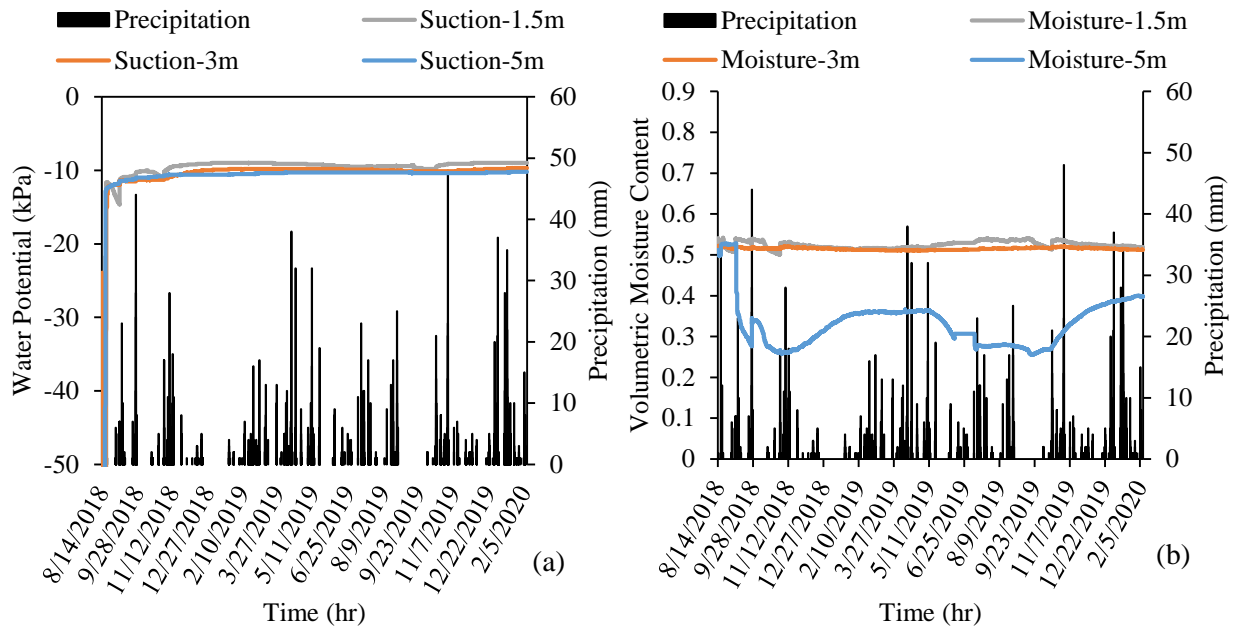


Figure 4.11 In situ variation of (a) matric suction (b) moisture content with rainfall across instrumentation 1 at Slope 1

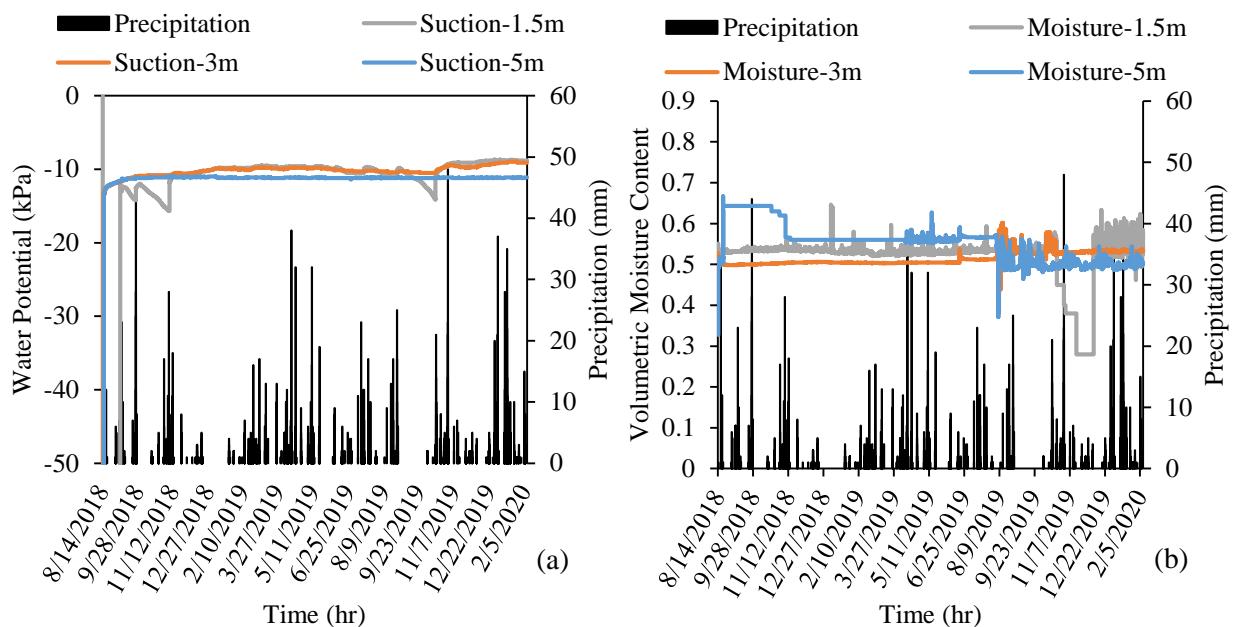


Figure 4.12 In situ variation of (a) matric suction (b) moisture content with rainfall across instrumentation 2 at Slope 1

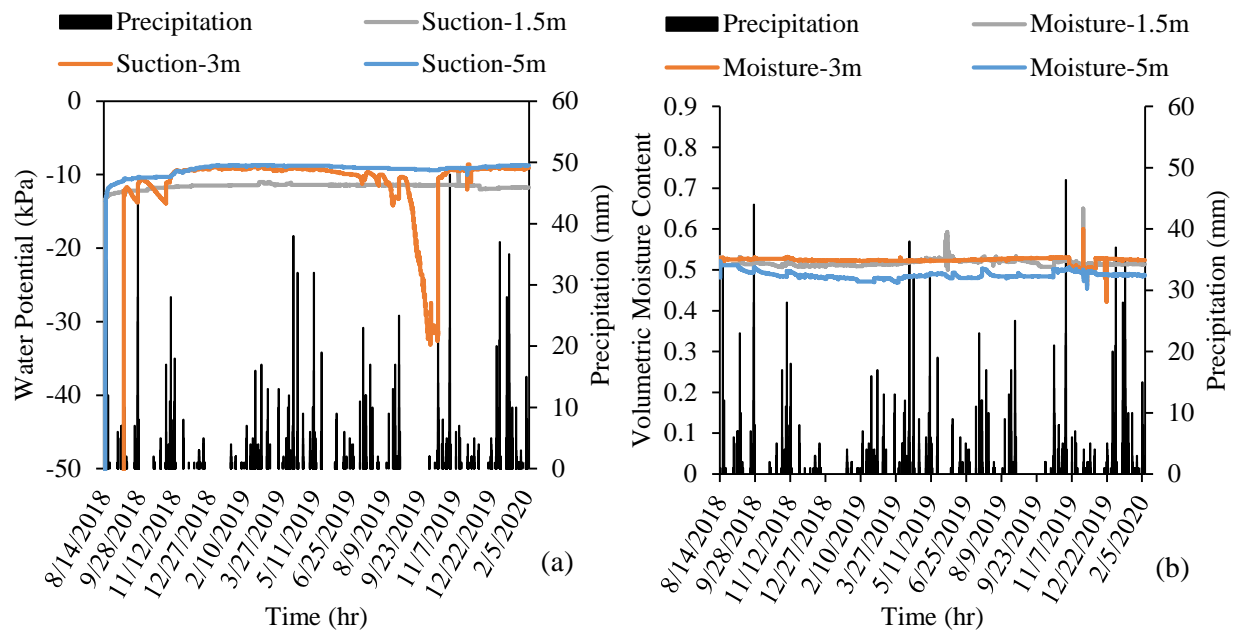


Figure 4.13 In situ variation of (a) matric suction (b) moisture content with rainfall across instrumentation 3 at Slope 1

Figure 4.11 to Figure 4.13 presents the variation of volumetric moisture content with time. The change in moisture content at the soil layers of the referenced site slopes is related to the rainfall infiltration affected by total daily rainfall events. In general, the variation of moisture content trend is related to the inverse variation in matric suction profile. In other words, the soil moisture content increases during total daily rainfall, whereas the matric suction decreases (Hossain et al., 2013). Yet, regarding the characteristic of Yazoo clay soil, it is observed that the change in the soil water content at deeper depth is mild. However, the change in the matric suction profile is steady and very low. The volumetric moisture content is between 0.5 to 0.7. Moisture content was saturated during the rainfall at all depths. Figure 4.11 to Figure 4.13 also shows the variation of matric suction at three different depths at the crest and middle of the slope with total daily rainfall. The change in matric suction is steady and very low before and after rainfall events. This is indicating that the soil is totally saturated below about 5 ft. (1.5 m) depth of the slope surface. Due to the high plasticity of Yazoo clay, traveling from shallower depth to deeper depth, the infiltration of rainwater is delayed, and it may take a long time. Moreover, at the crest of the slope, suction value increased from shallow to deep depth. However, this pattern changed in the middle of the slope at the location of Instrumentation 2 and Instrumentation 3.

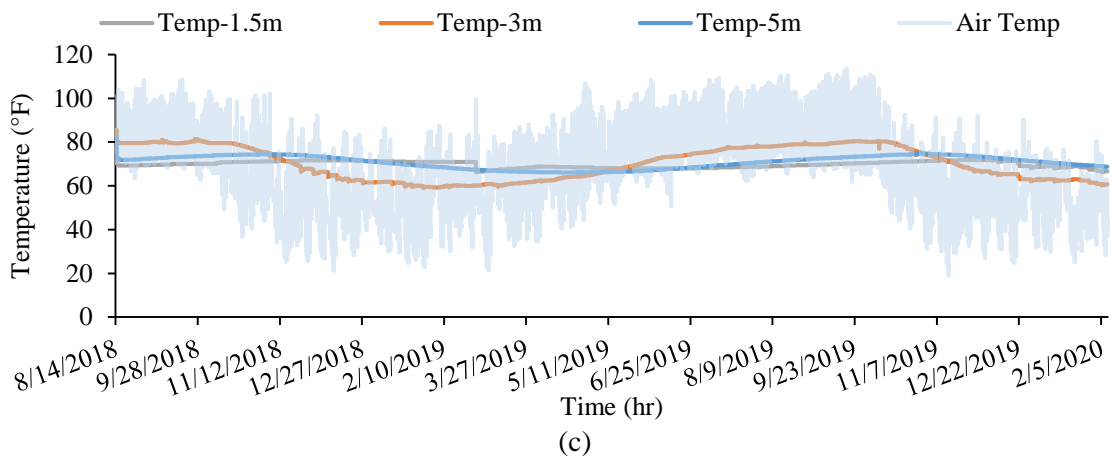
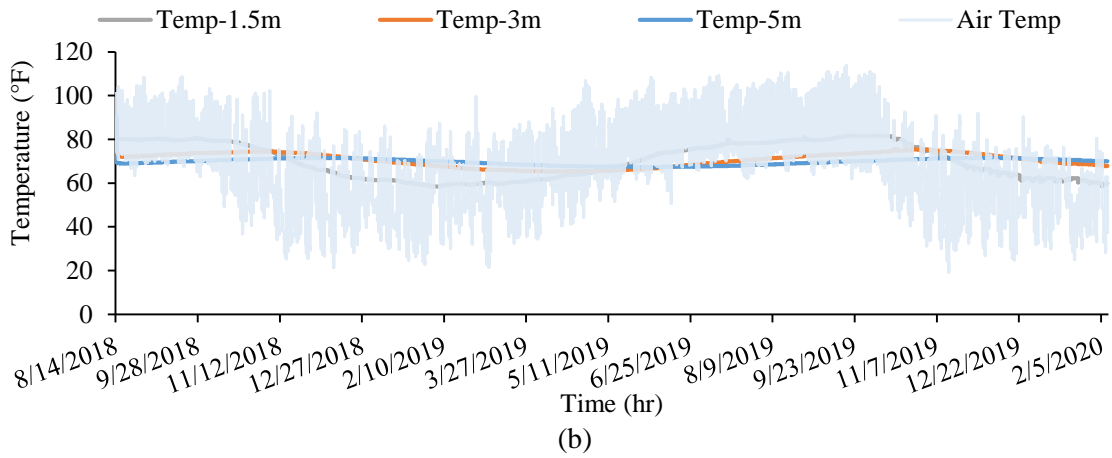
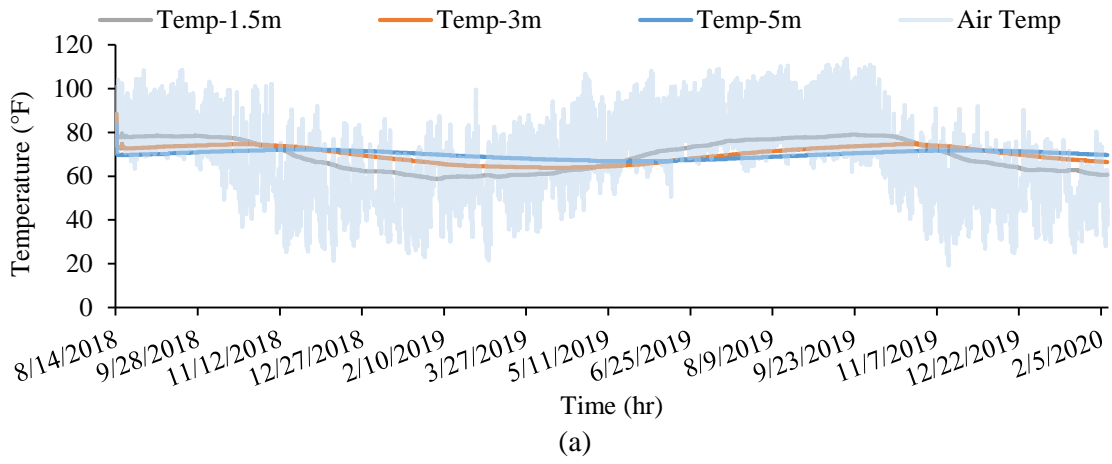


Figure 4.14 Combined air and soil temperature variation at Slope 1 at (a) Instrumentation 1 (b) Instrumentation 2 (c) Instrumentation 3

4.3 Slope 2: Metro Center Highway Slope

The Slope 2 is located along I220 N over the ramp from US 80E and has a reinforced and as-built section, as presented in Chapter 3. Three 15 ft. boreholes were drilled and then instrumented at the reinforced section at the crest, middle, and toe of the slope, which is designated as Instrumentation 1, Instrumentation 2, and Instrumentation 3, respectively. The location of the boreholes is presented in Figure 4.15.

In each of the Instrumentation locations, at 5 ft (1.5 m), 10 ft (3 m), and 15 ft (5 m) depths, a moisture sensor, and a water potential sensor were installed. Additionally, a rain gauge and air temperature were installed at instrumentation 1 at Slope 2. The sensor installations photos are presented in Figure 4.16.

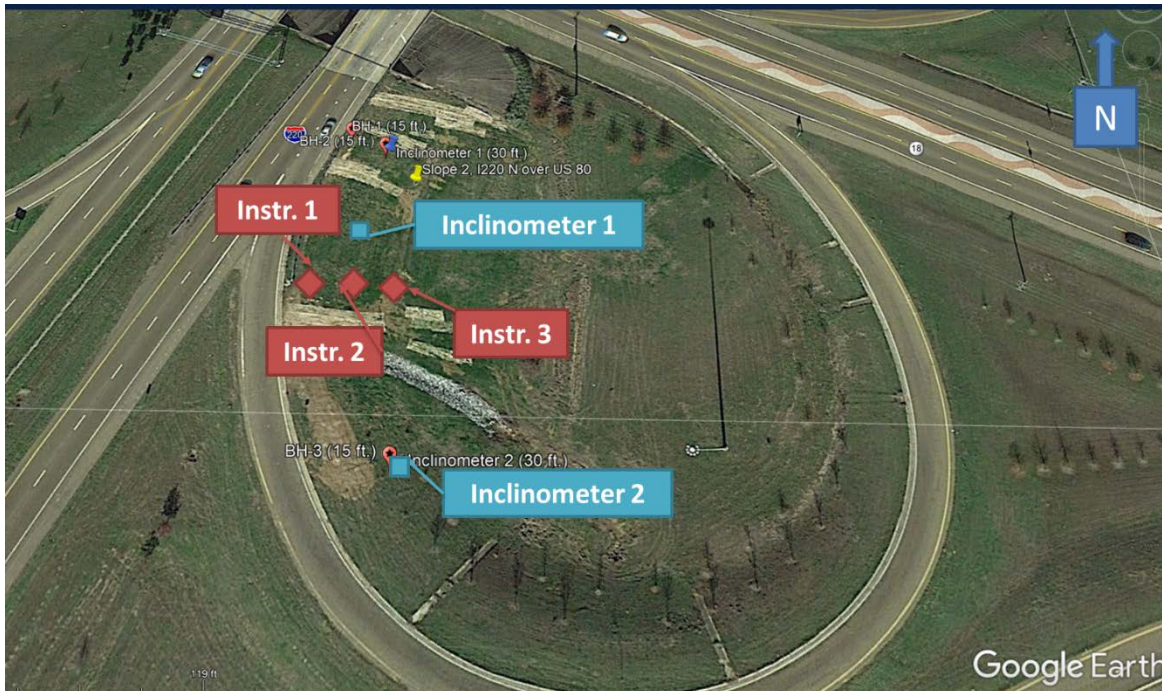


Figure 4.15 Instrumentation layout at Slope 2



Figure 4.16 Field Activities photo at Slope 2.

The slope inclinometer installation photos are presented in Figure 4.17. The inclinometer 1 is installed at the reinforced section, whereas the inclinometer 2 is installed at the as-built section. Each of the inclinometers were installed in the middle of the slopes.



Figure 4.17 Inclinometer casing at Slope 2

4.3.1 *Field Monitoring Results*

After completion of the instrumentation, the JSU team visited Slope 2 and collected data from the data loggers. Moreover, lateral deformation of the slope at Slope 2 is monitored using slope inclinometer. The field monitoring results for Slope 2 are discussed in the following section.

4.3.1.1 *Slope Movement Data*

The horizontal movement data from the slope was observed using slope inclinometer measurements collected at every 2 ft. spacing along the slope inclinometer pipe. The collected data were analyzed to determine the slope movement. The horizontal movement data from Inclinometer 1 at the reinforced section and time-dependent movement at the surface of the slope is presented in Figure 4.18 and Figure 4.19, respectively. Similarly, the horizontal movement data from Inclinometer 2 at the as-built section and time-dependent movement at the surface of the slope is presented in Figure 4.20 and Figure 4.21. As indicated in Figure 4.18 to Figure 4.21, no significant movement is observed in both of the sections, and the performance of the slope is within the satisfactory level in both of the sections.

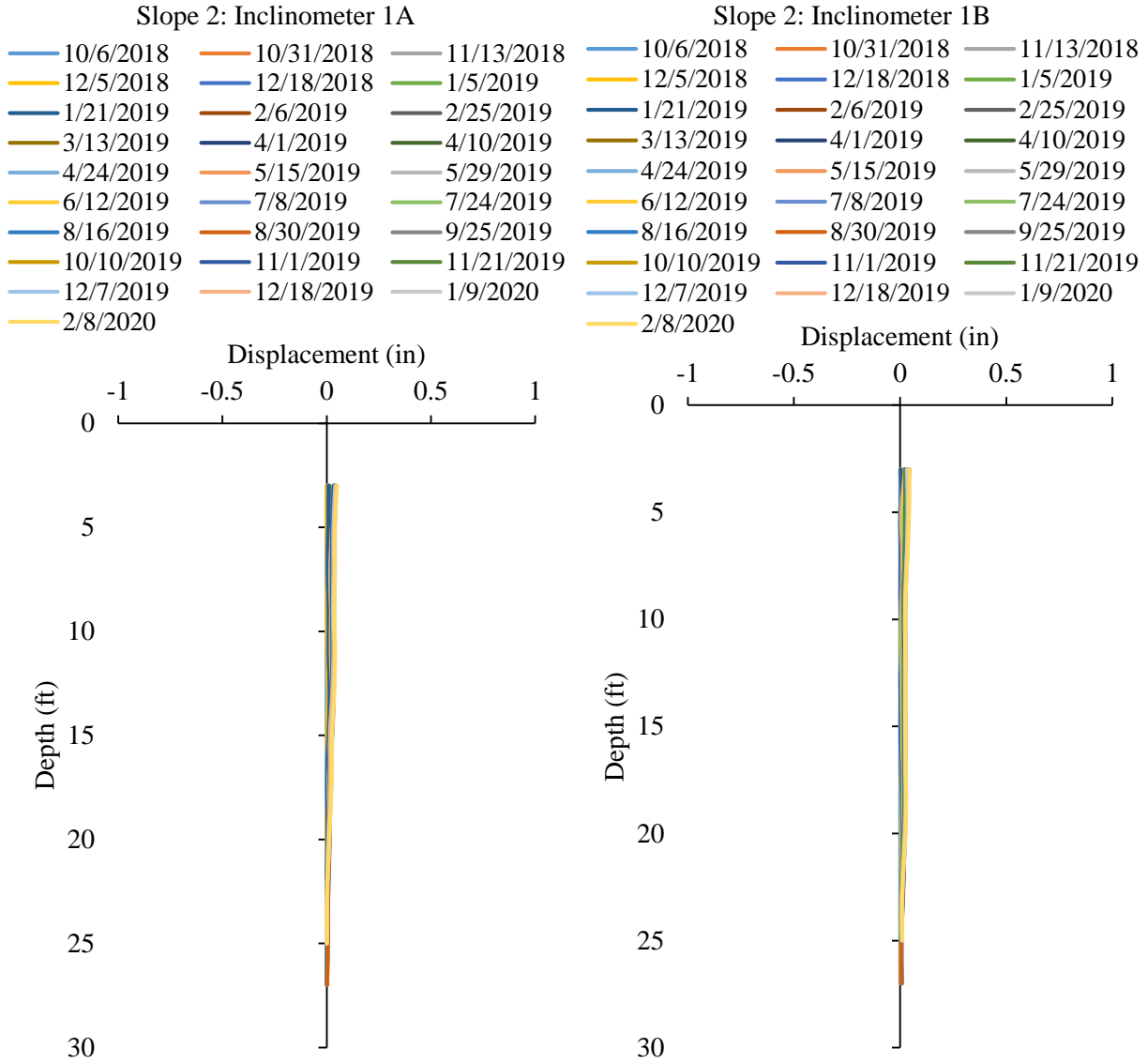


Figure 4.18 Horizontal displacements of the Inclinator 1 at Slope 2

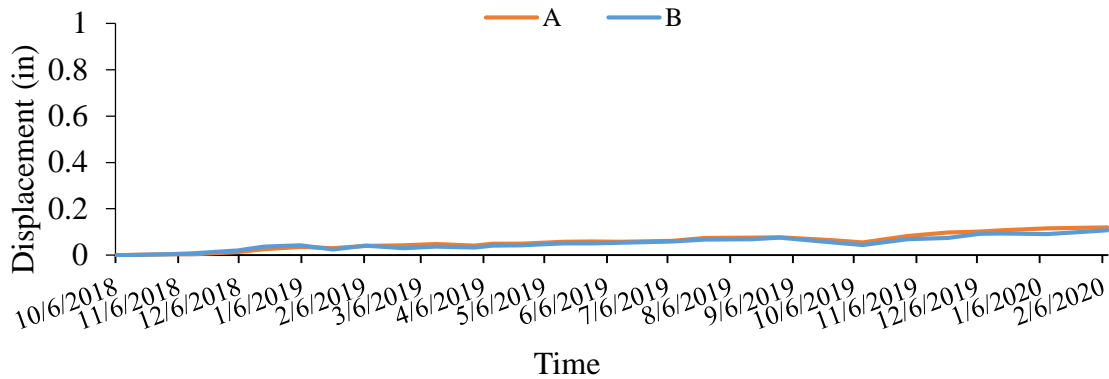


Figure 4.19 Variation of lateral deformation at the top of Inclinator 1 at Slope 2.

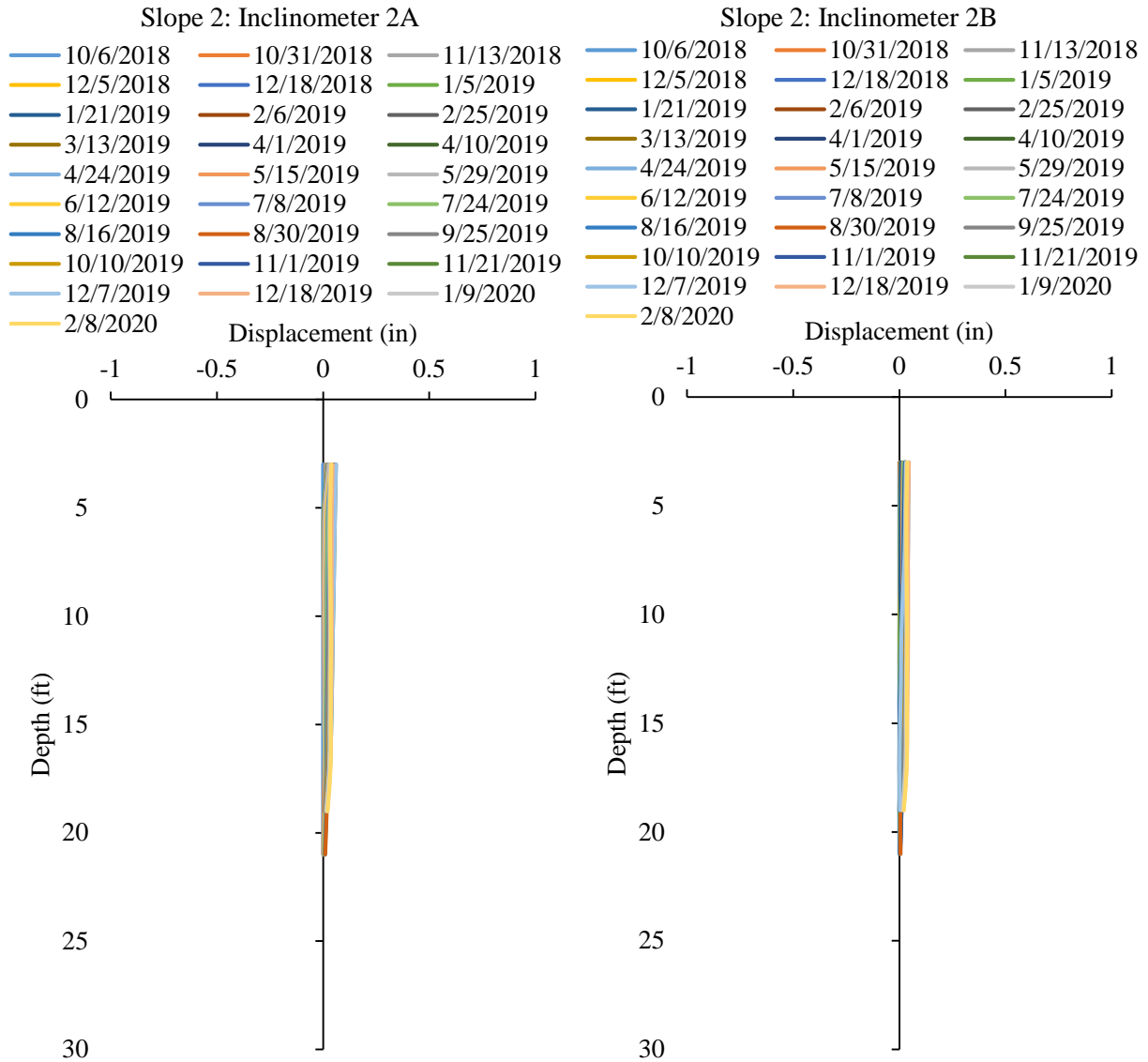


Figure 4.20 Horizontal displacements of the Inclinerometer 2 at Slope 2

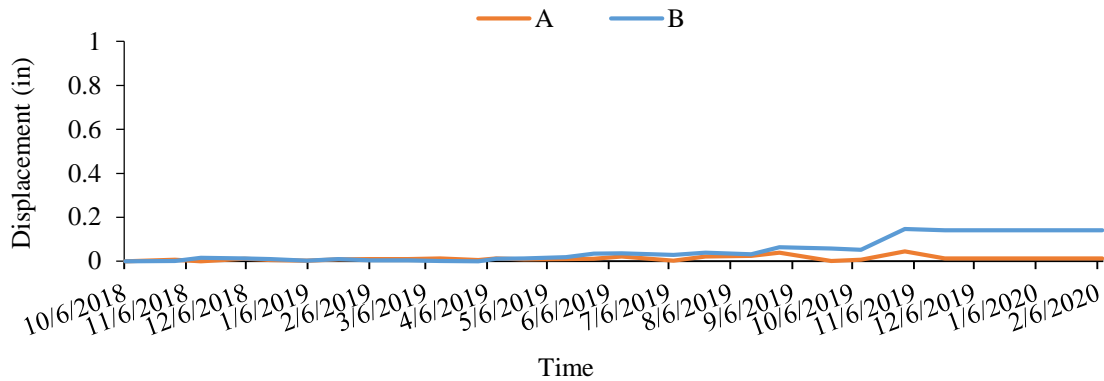


Figure 4.21 Variation of lateral deformation at the top of Inclinerometer 2 at Slope 2.

4.3.1.2 Field Instrumentation Data

Variation of in situ matric suction profile and moisture content at 5 ft. (1.5 m), 10 ft. (3 m), and 15 ft. (5 m) depths with rainfall are presented in Figure 4.22, Figure 4.23, and Figure 4.24, respectively. In Instrumentation 1 and Instrumentation 2, an initial moisture variation was observed within the first 3 months after instrumentation installation, which can be considered as the adjustment period of the moisture distribution. It should be noted that the matric suction at those locations did not present any changes. Within the 2-years of data monitoring, at the Instrumentation 1 in the crest, minimum moisture variation was observed. In the middle of the slope in Instrumentation 2, variation of the moisture content was observed during the summer of 2019 and late December, which indicated infiltration of rain water; however, near the toe, a significant variation of moisture content was observed at a different season. At slope 2, near the toe, surface cracks were observed within the slopes. The high variation of the moisture content indicated the infiltration of the rainwater into these surface cracks. It is unlikely, a perched water table exist at this slope and was not the reason for the moisture variations observed.

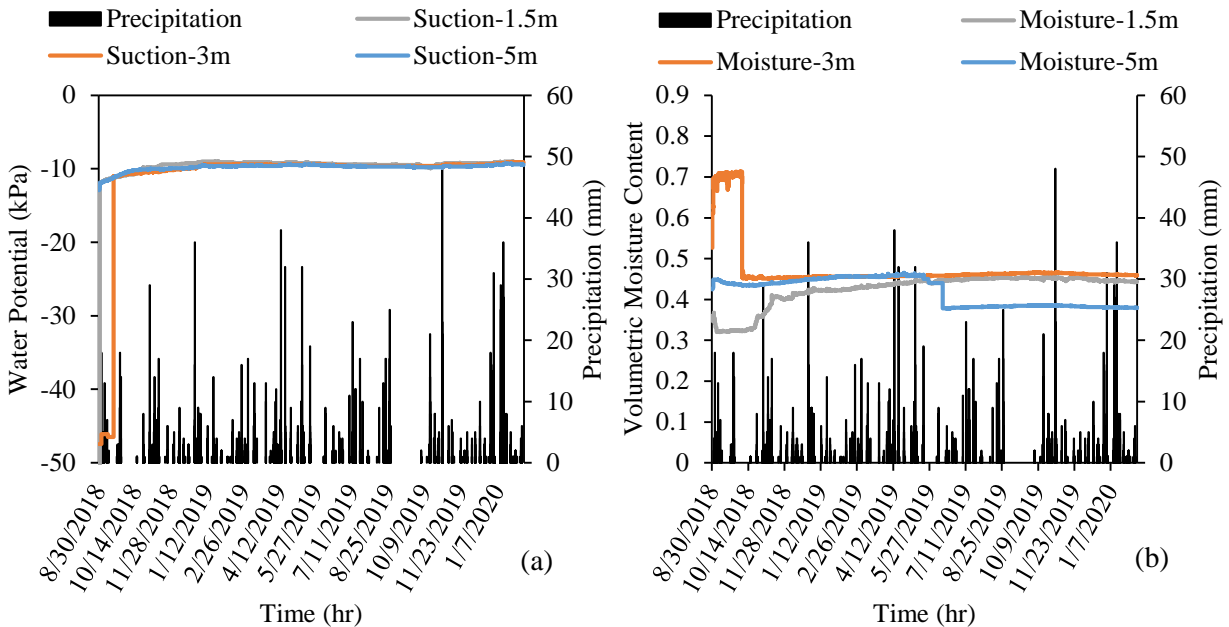


Figure 4.22 In situ variation of (a) matric suction (b) moisture content with rainfall across instrumentation 1 at Slope 2

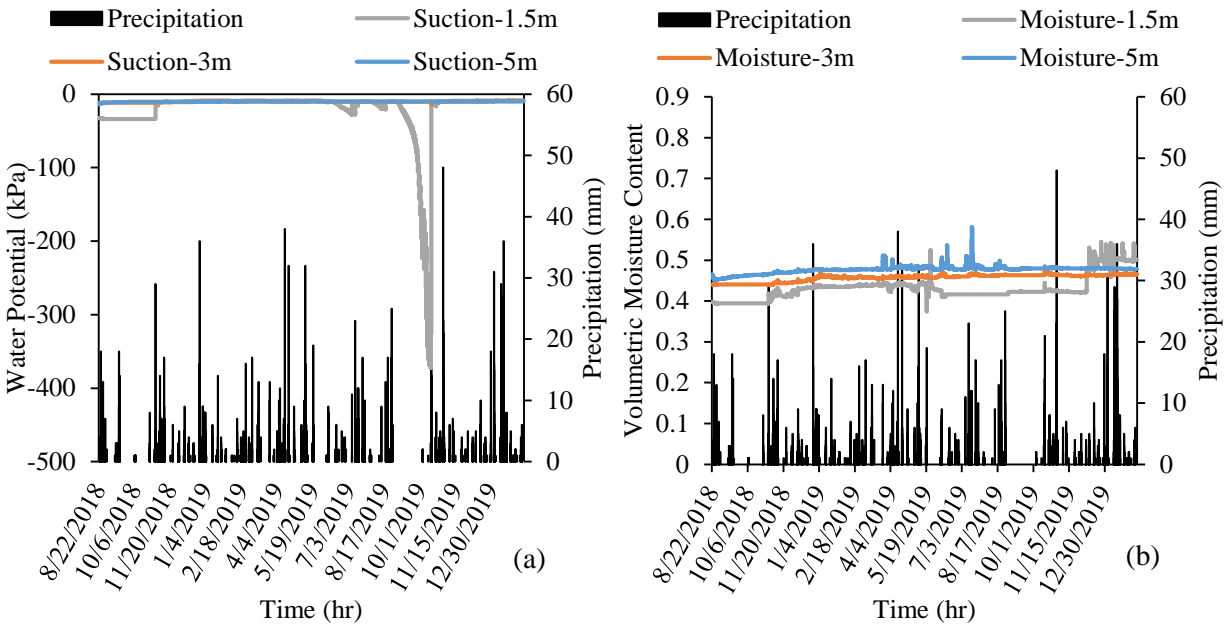


Figure 4.23 In situ variation of (a) matric suction (b) moisture content with rainfall across instrumentation 2 at Slope 2

Variation of in situ matric suction with daily rainfall data at the crest, middle, and toe of the slope at three different depths 5 ft. (1.5 m), 10 ft. (3 m), and 15 ft. (5 m) is also presented in Figure 4.22 to Figure 4.24. The slope experiences a low steady change in matric suction. Unlike the crest of the slope, it can be seen that there are some variations in matric suctions at the middle and toe of the slope.

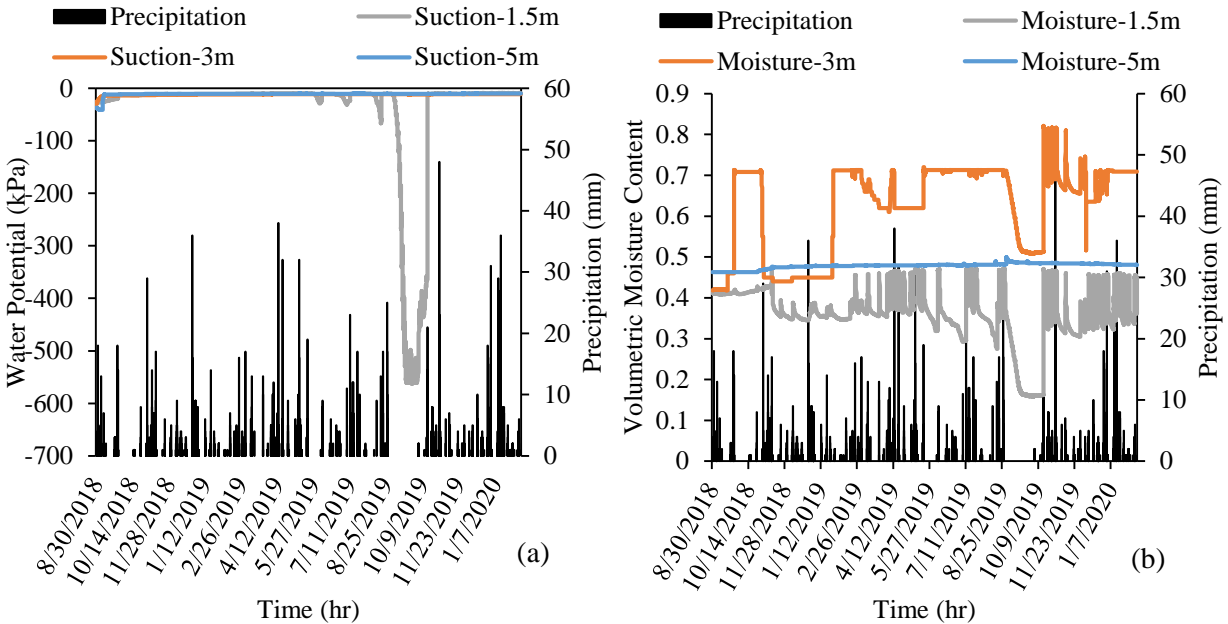


Figure 4.24 In situ variation of (a) matric suction (b) moisture content with rainfall across instrumentation 3 at Slope 2

Figure 4.25 presents the in situ variations of soil and air temperature at Instrumentation 1 to Instrumentation 3. It is observed that with the changes in the air temperature, the soil temperature at the shallow depth (5 ft. and 10 ft.) has experienced some variations. However, at the deeper depth (15 ft.), the soil temperature remains quite constant.

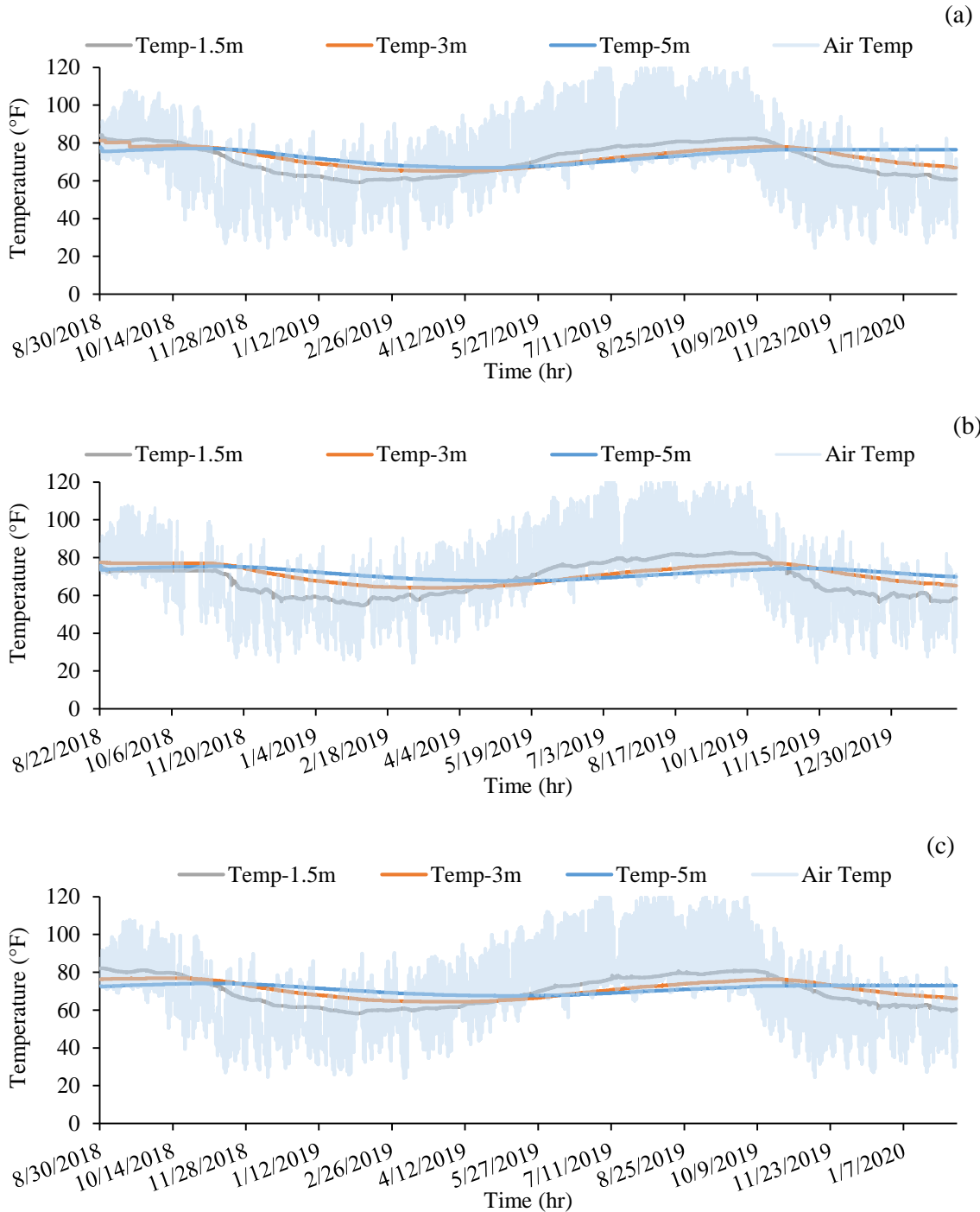


Figure 4.25 Combined air and soil temperature variation at Slope 2 at (a) Instrumentation 1 (b) Instrumentation 2 (c) Instrumentation 3

4.4 Slope 3: Terry Road Highway Slope

Slope 3 is located along in I20E exit toward Terry road and has a reinforced and as-built section, as presented in Chapter 3. Two 15 ft. boreholes were drilled and then instrumented at the repaired section. These two boreholes are designated as Instrumentation 1 and Instrumentation 2, as presented in Figure 4.26. In addition, a third 15 ft. deep borehole was drilled and then instrumented in the as-built section, which is designated as Instrumentation 3. Instrumentation 1 is located at the crest whereas, Instrumentation 2 and Instrumentation 3 are located in the middle of the slope. Two inclinometers were installed in the middle of the slopes as well in the reinforced section and as-built section.

In each of the Instrumentation locations, at 5 ft (1.5 m), 10 ft (3 m), and 15 ft (5 m) depths, a moisture sensor, and a water potential sensor were installed. Additionally, a rain gauge and air temperature were installed at instrumentation 1 at Slope 3. The sensor installations photos are presented in Figure 4.27.

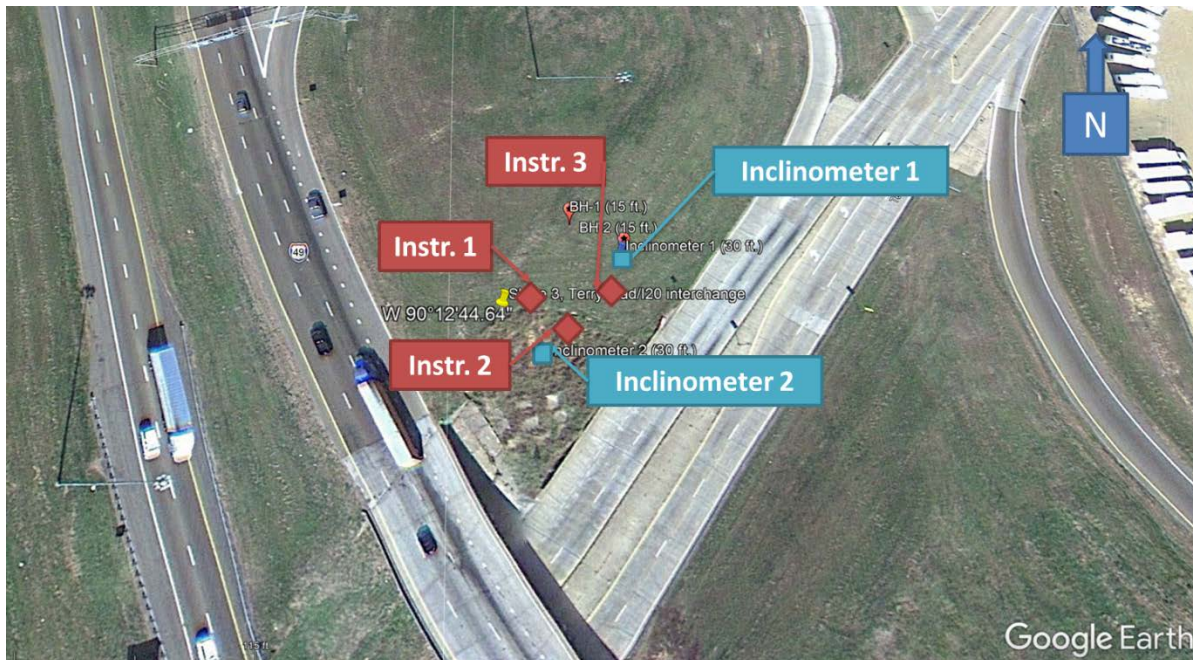


Figure 4.26 Instrumentation layout at Slope 3



Figure 4.27 Field Instrumentation Activities at Slope 3

The slope inclinometer installations are presented in Figure 4.28. The 30 ft slope inclinometer 1 was installed at the as-built section, whereas, Inclinometer 2 was installed at the repaired section of Slope 3.



Figure 4.28 Inclinometer casting at Slope 3

4.4.1 Field Monitoring Results

4.4.1.1 Slope Movement Data

The horizontal movement data from the slope was observed using slope inclinometer measurements collected at every 2 ft. spacing along the slope inclinometer pipe. After data collection, the slope movement data is downloaded and analyzed to determine the slope movement. The horizontal movement data from Inclinometer 1 at the reinforced section and time-dependent movement at the surface of the slope is presented in Figure 4.29 and Figure 4.30, respectively. As observed from the inclinometer data, the as-built

section of Slope 3 is experiencing a movement from January 2019 and has moved up to 1.6 inches at the slope surface, within a year. In addition, the depth of the slope movement is around 6 ft., which is shallow in nature. This section of the slope will require maintenance to repair the shallow slope failure.

The horizontal movement data from Inclinometer 2 at the reinforced section and time-dependent movement at the surface of the slope is presented in Figure 4.31 and Figure 4.32. No movement is observed in the reinforced section, and the performance of the slope is satisfactory.

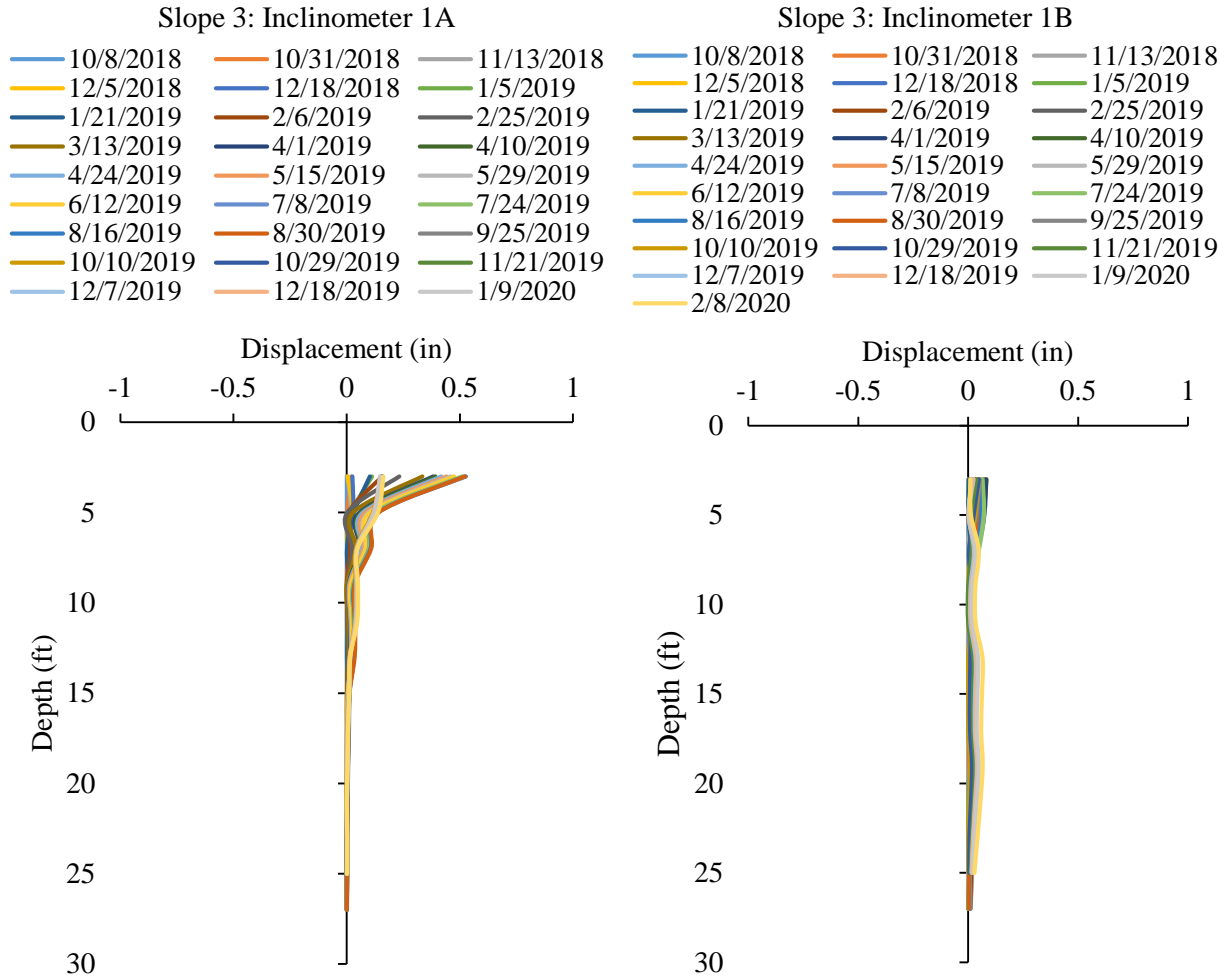


Figure 4.29 Horizontal displacements of the Inclinometer 1 (as built section) at Slope 3

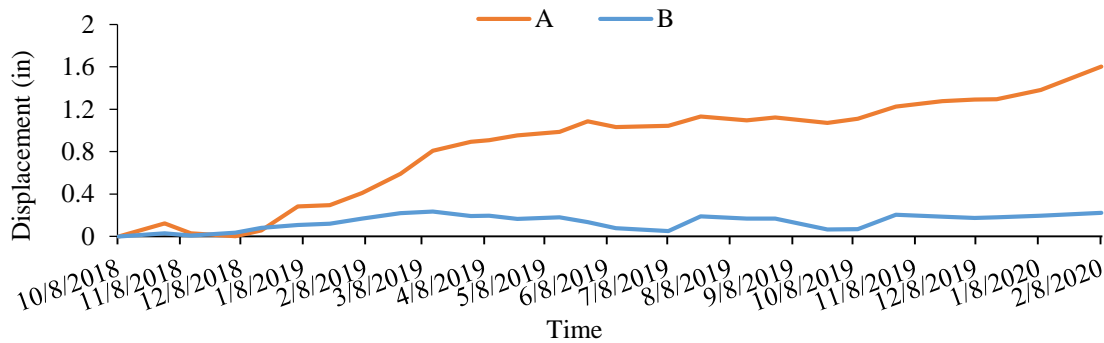


Figure 4.30 Variation of lateral deformation at the to of Inclinometer 1 (as built section) at Slope 3

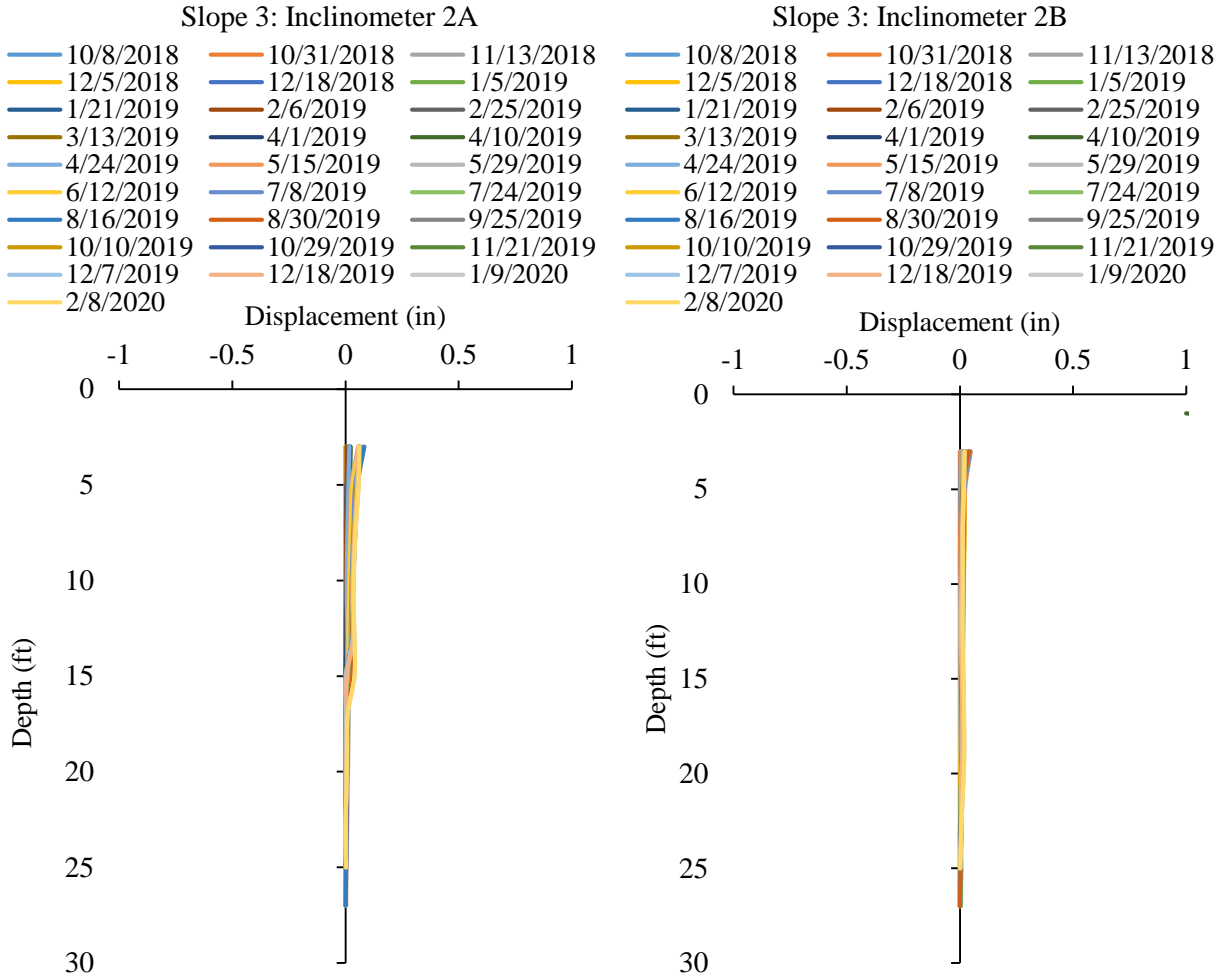


Figure 4.31 Horizontal displacements of the Inclinerometer 2 (repaired section) at Slope 3

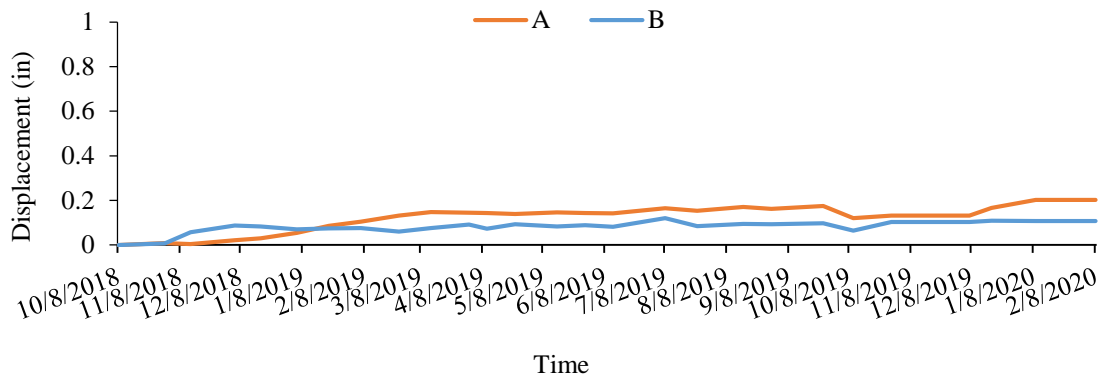


Figure 4.32 Variation of lateral movement at the top of Inclinerometer 2 (repaired section) at Slope 3.

4.4.1.2 Field Instrumentation Data

Variation of in situ matric suction profile and moisture content at 5 ft. (1.5 m), 10 ft. (3 m), and 15 ft. (5 m) depths with rainfall are presented in Figure 4.33, Figure 4.34, and Figure 4.35, respectively. Based on the field monitoring results presented in Figure 4.33 from instrumentation 1, the matric suction had a high number for around three months, and then reached an equilibrium condition, which presents a low

value (10 kPa, 209 psf), which also remain constant along the monitoring period. Similar to the matric suction variation, the volumetric moisture content remained constant over the last two years at instrumentation 1. The constant moisture content at the slope is highly possible if there is no moisture variation that has taken place, or the soil is in a fully saturated condition. The constant low value at the matric suction signifies that the soil is practically close to a fully saturated condition. This is likely possible, when there is a formation of perched water conditions at the slope.

Based on the instrumentation results presented in Figure 4.34 and Figure 4.35 in the middle of the slopes of both reinforced section and as-built section indicates a similar matric suction variation like Figure 4.33 for the crest of the slope. For the volumetric moisture content, few peaks and drops were observed during summer 2019, which indicates the intrusion of the rainwater; however, the overall moisture content remains constant throughout the monitoring period. The constant moisture content and matric suction at the instrumentation 2 and instrumentation 3 attribute to the existence of the perched water condition of the slope.

It should be noted that the as-built section of slope 3 has experienced shallow movement starting January 2019 (Figure 4.29 and Figure 4.30). In addition, it is evident from the instrumentation results that there is a presence of perched water conditions in Slope 3. Therefore, the movement at the as-built section of the slope is taking place due to the formation of perched water with the top part of the slope. It is important to mention that the slope at the reinforced section was stabilized using H-piles. As there is no movement at the reinforced section that was observed, the HP has provided adequate resistance against the slope movement. Therefore, the reinforced section is performing at a satisfactory level.

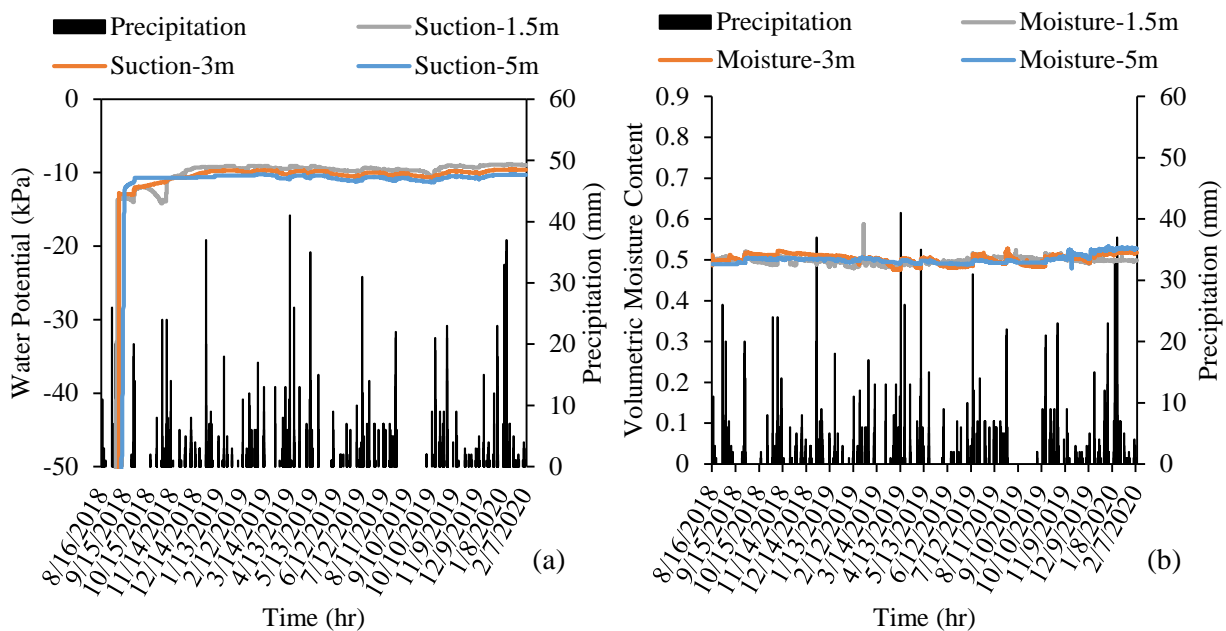


Figure 4.33 In situ variation of (a) matric suction (b) moisture content with rainfall across instrumentation 1 at Slope 3

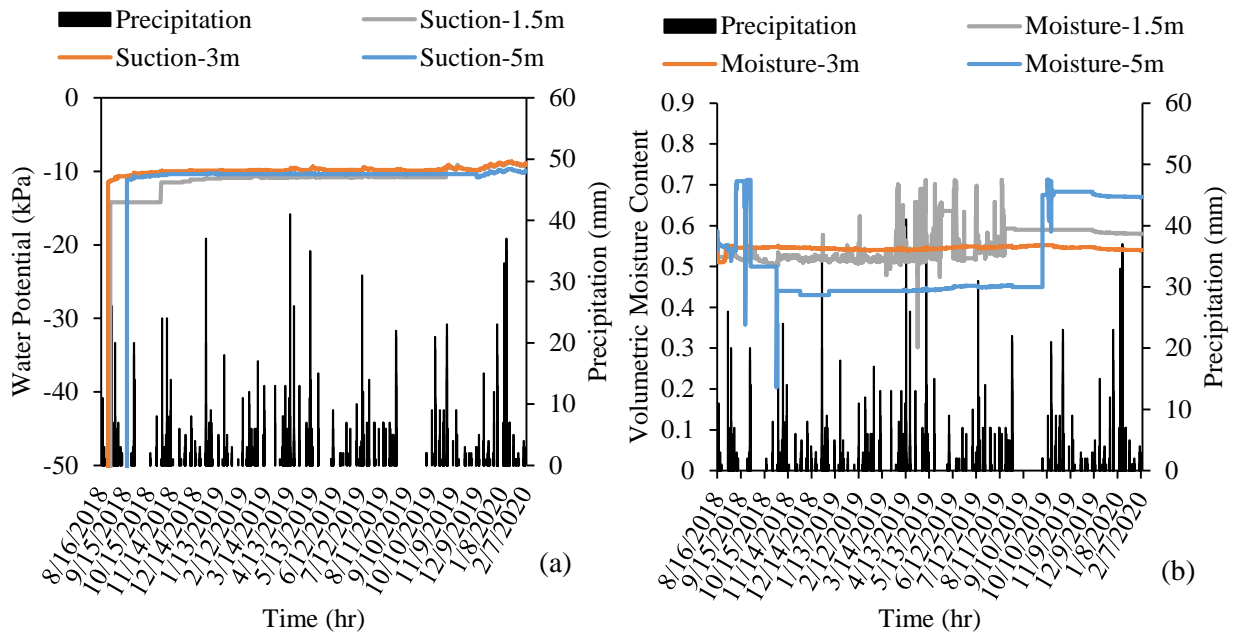


Figure 4.34 In situ variation of (a) matric suction (b) moisture content with rainfall across instrumentation 2 at Slope 3

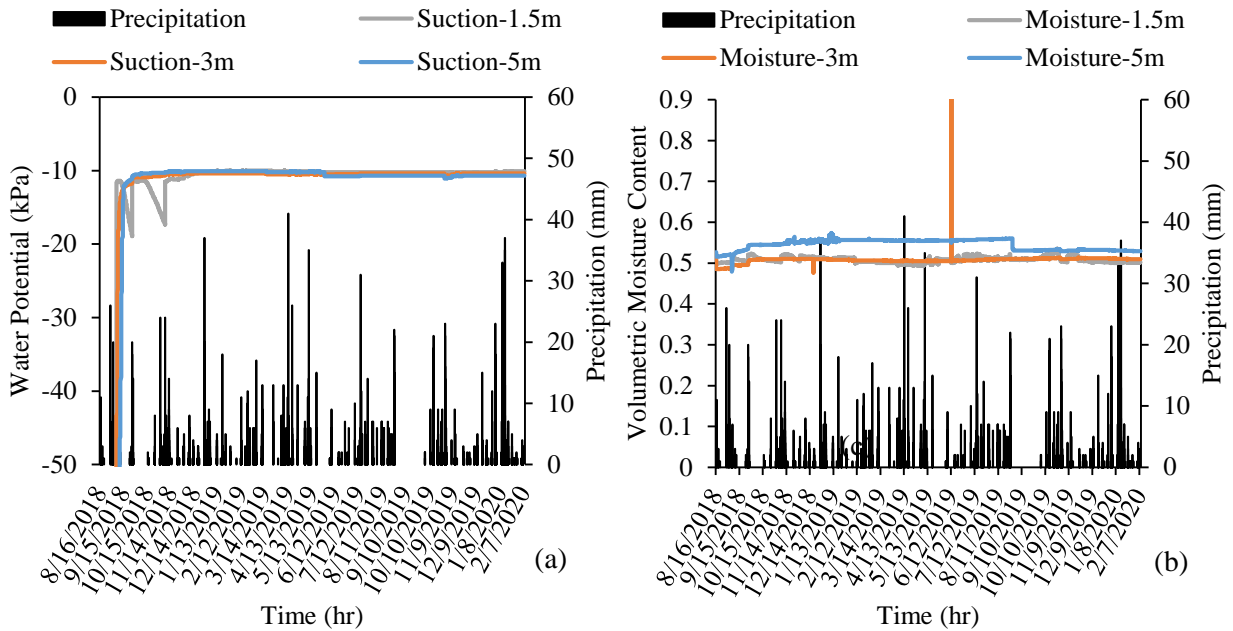


Figure 4.35 In situ variation of (a) matric suction (b) moisture content with rainfall across instrumentation 3 at Slope 3

Figure 4.36 presents the in situ variations of soil and air temperature at instrumentation 1 to instrumentation 3. It is observed that with the changes in the air temperature, the soil temperature at the shallow depth has experienced some variations. However, at the deeper depth, the soil temperature remains quite constant.

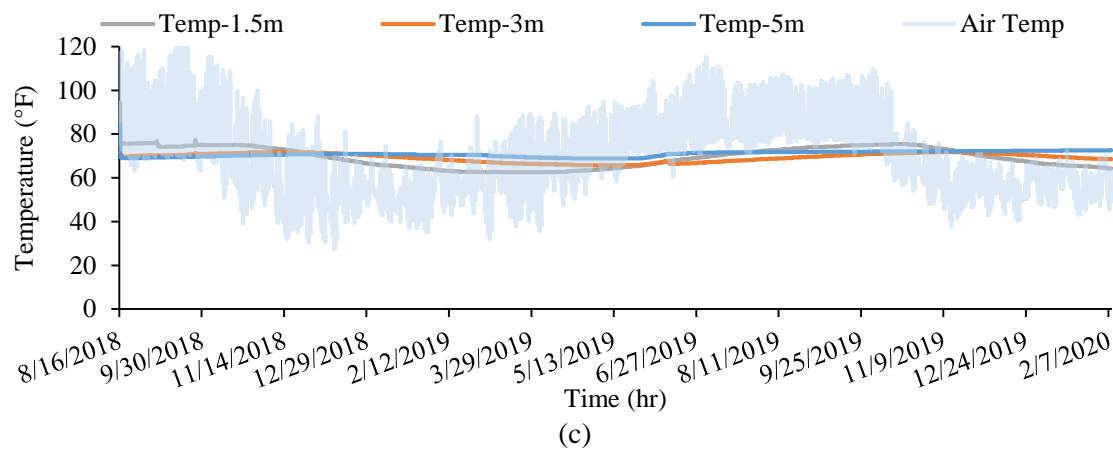
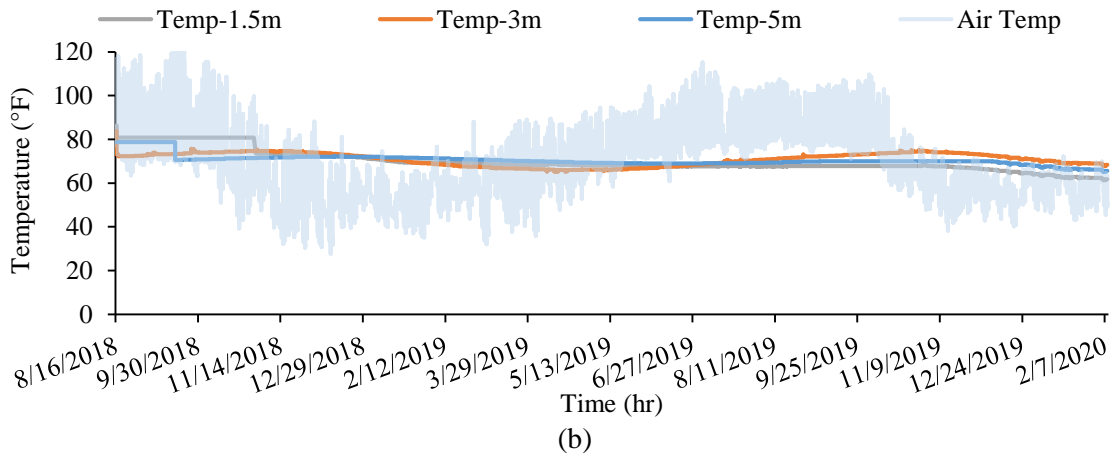
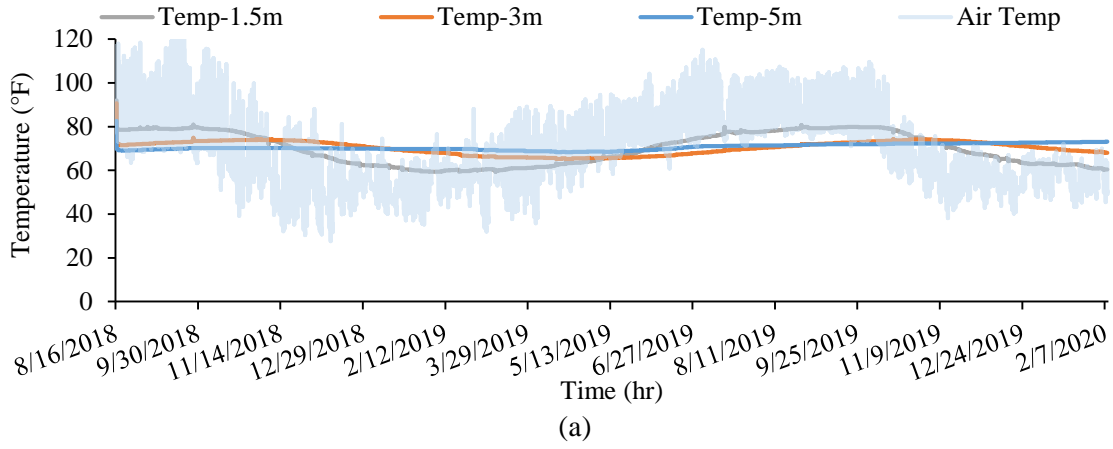


Figure 4.36 Combined air and soil temperature variation at Slope 3 at (a) Instrumentation 1 (b) Instrumentation 2 (c) Instrumentation 3

4.5 Slope 4: Highland Drive Highway Slope

The Slope 4 is located along I20E near Highland drive and has a repaired section, as presented in Chapter 3. During the repair of the slope, it was regraded and rebuilt with low plastic soil. Three 15 ft. boreholes was drilled and then instrumented at the reinforced section at the crest, middle, and toe of the slope, which is designated as Instrumentation 1, Instrumentation 2, and Instrumentation 3, respectively. The location of the boreholes is presented in Figure 4.37. A vertical inclinometer was installed in the middle of the slopes near instrumentation 2.

In each of the Instrumentation locations, at 5 ft (1.5 m), 10 ft (3 m), and 15 ft (5 m) depths, a moisture sensor, and a water potential sensor were installed. Additionally, a rain gauge and air temperature were installed near instrumentation 1 at Slope 4. The sensor installations photos are presented in Figure 4.38. The inclinometer installation photos are presented in Figure 4.39. An inclinometer 30 ft. deep was installed at the middle of the slope.

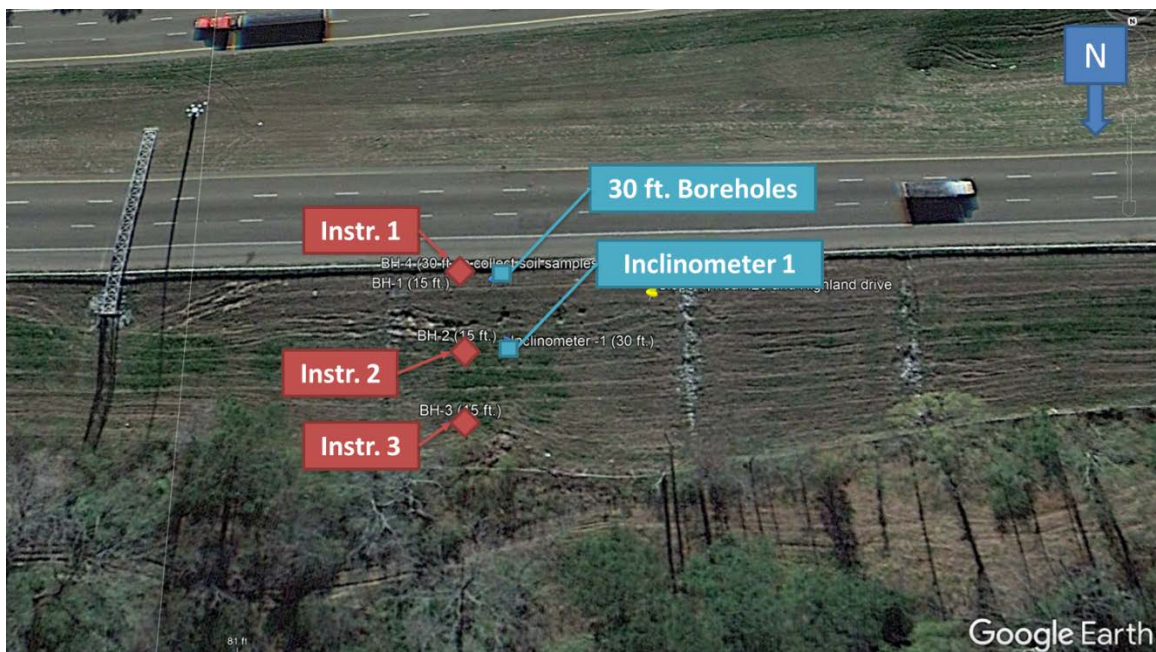


Figure 4.37 Instrumentation layout at Slope 4



Figure 4.38 Field installation of the sensors at Slope 4



Figure 4.39 Installation of vertical inclinometer at Slope 4

4.5.1 Field Monitoring Results

4.5.1.1 Slope Movement Data

The horizontal movement data from the slope was observed using slope inclinometer measurements collected at every 2 ft. spacing along the slope inclinometer pipe. The collected inclinometer data was analyzed to determine the slope movement. The horizontal movement data from Inclinometer 1 and time-dependent movement at the surface of the slope is presented in Figures 4.40 and Figure 4.41 respectively. No significant movement was observed that depicts any landslides. However, some movement was observed within the slope from 5 ft. to 10 ft. depth. During the field visit, formation of a void was observed near the inclinometer 1 due to erosion of the slope surface, as presented in Figure 4.42. Some measures are recommended, such as backfill the void with lean clay fill materials.

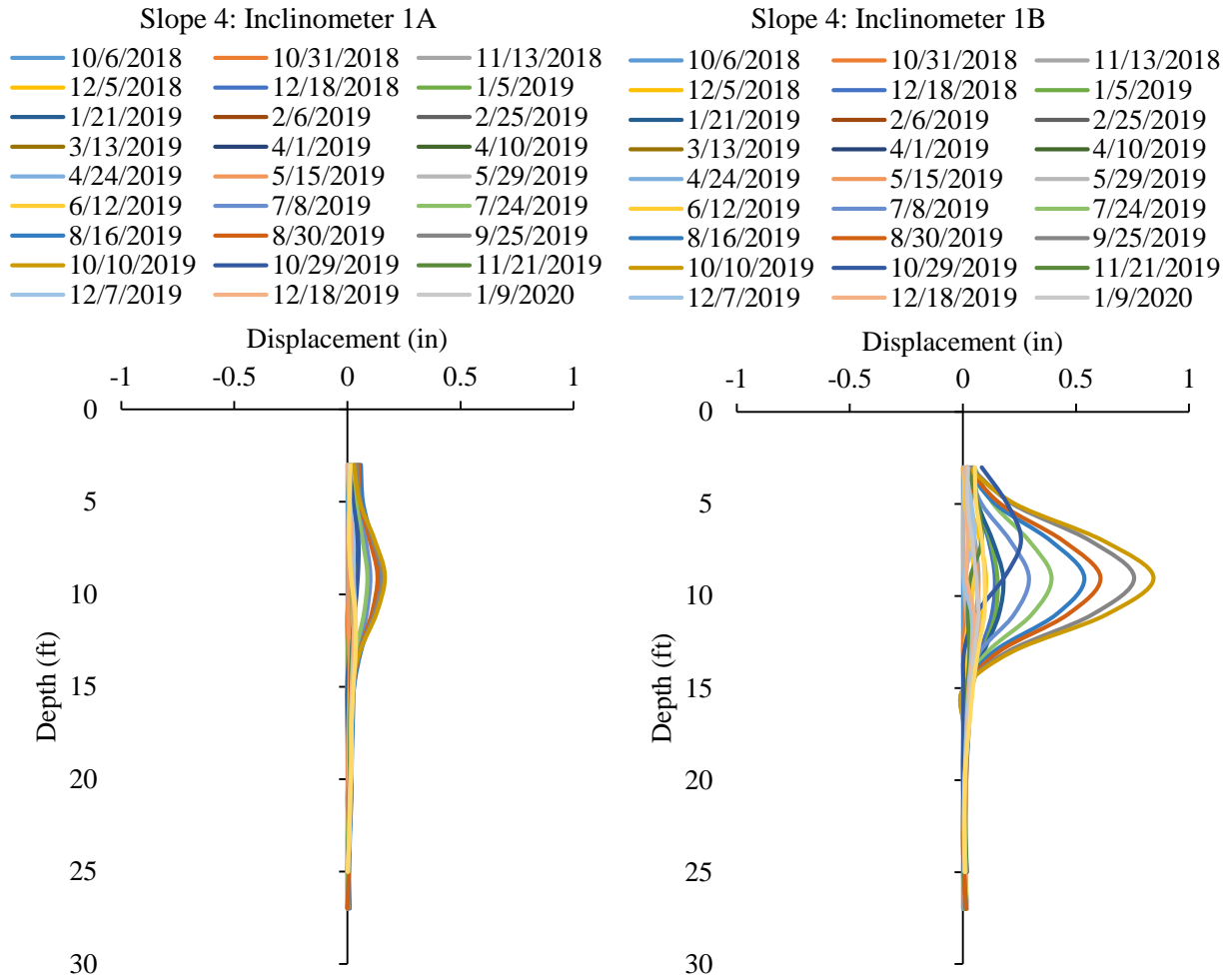


Figure 4.40 Horizontal displacements of the Inclinerometer 1 at Slope 4

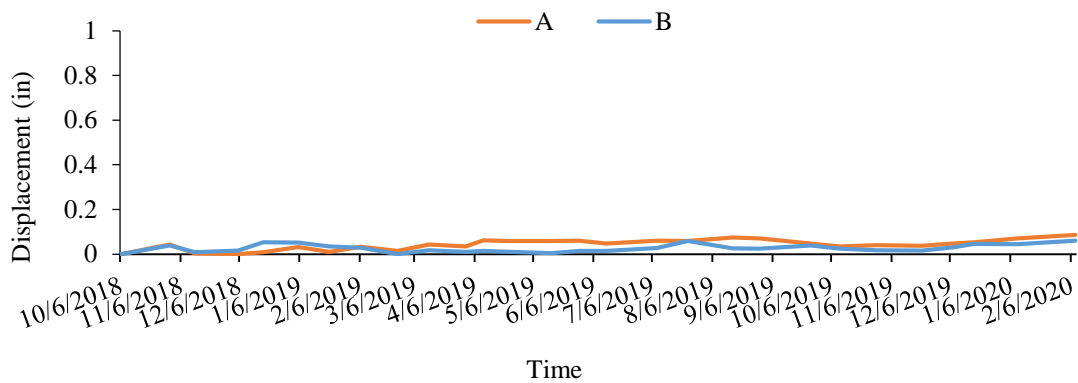


Figure 4.41 Variation of lateral deformation at the top of Inclinerometer 1 at Slope 4



Figure 4.42 Soil Erosion at the slope surface at Slope 4

4.5.1.2 Field Instrumentation Data

Variation of in situ matric suction profile and moisture content at 5 ft. (1.5 m), 10 ft. (3 m), and 15 ft. (5 m) depths with rainfall are presented in Figure 4.43, Figure 4.44, and Figure 4.45, respectively. Based on the field monitoring results presented in Figure 4.43 from instrumentation 1, the matric suction has a low value (10 kPa, 209 psf), which also remains constant along the monitoring period. Similar to the matric suction variation, the volumetric moisture content remained constant over the last two years at instrumentation 1. As discussed earlier for slope 3, the constant low value of the matric suction and constant moisture content signify that the soil is close to a fully saturated condition. This is highly possible, if there is a formation of perched water conditions at the slope.

Based on the instrumentation results presented in Figure 4.44 at the middle of the slope, a significant fluctuation of the moisture content was observed at all depths. In addition, the matric suction value at the 5 ft. (1.5 m) and 10 ft. (3 m) is lower than the matric suction value at 15 ft. (5 m) depth. This variation of the moisture content indicated the infiltration of rainwater in the middle of the slope. Similar moisture and matric suction variation were observed at the toe of the slope, as presented in Figure 4.45. It should be mentioned that during the rebuilding of the slope, the fill material has higher permeability, which allows consistent infiltration of the rainwater throughout the monitoring period. However, the fill material has underlying Yazoo clay, which has very low permeability ($<10^{-7}$ cm/s). As a result, the infiltration of rainwater has a ponding effect within the pore space of the fill soil and creates a perched water condition. The movement of the inclinometer 1 at 5 ft. (1.5 m) to 10 ft. (3 m) depth has taken place due to the presence of the perched water as well as the formation of the void due to soil erosion at the surface of the slope.

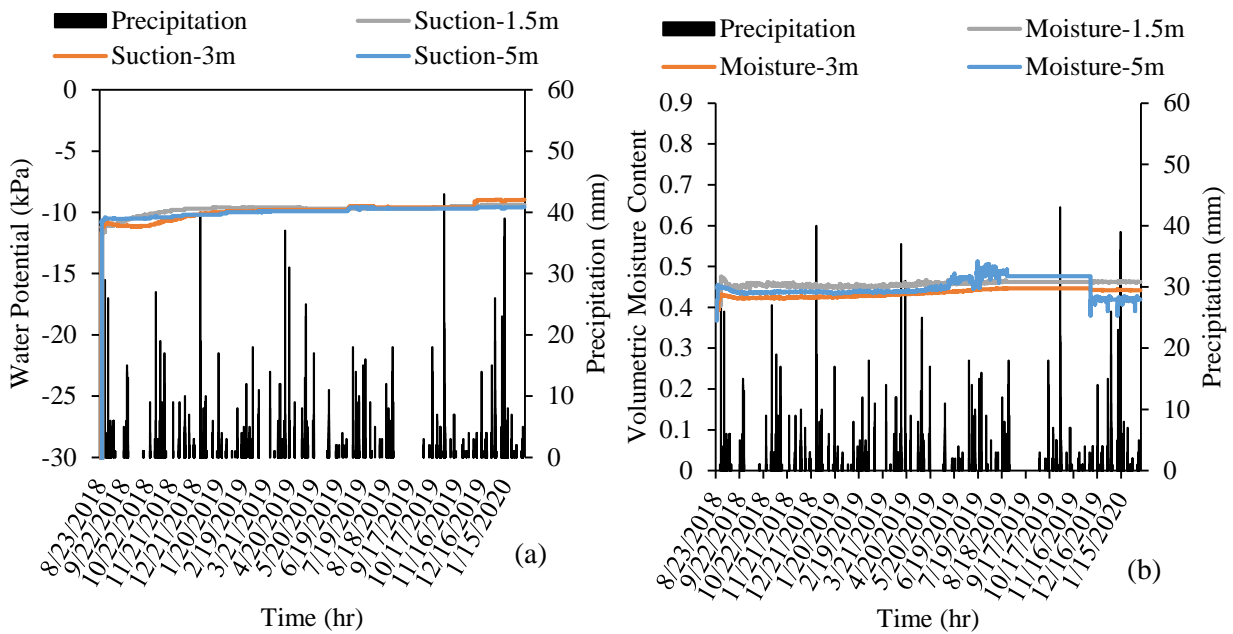


Figure 4.43 In situ variation of (a) matric suction (b) moisture content with rainfall across instrumentation 1 at Slope 4

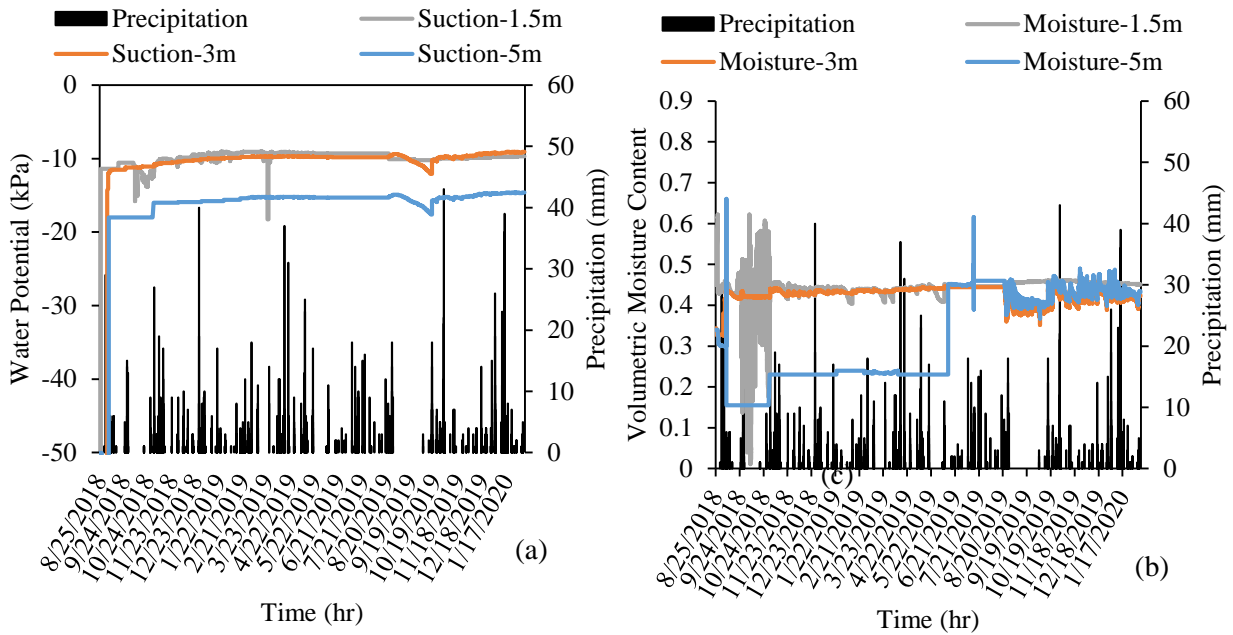


Figure 4.44 In situ variations of (a) matric suction (b) moisture content with rainfall across instrumentation 2 at Slope 4

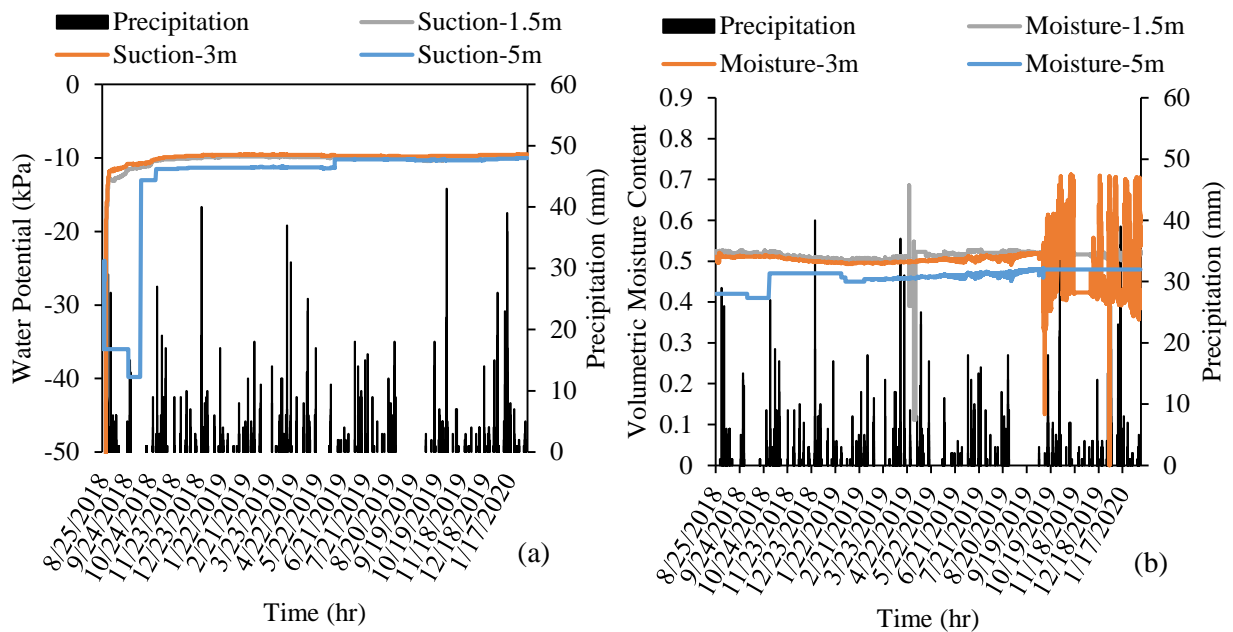
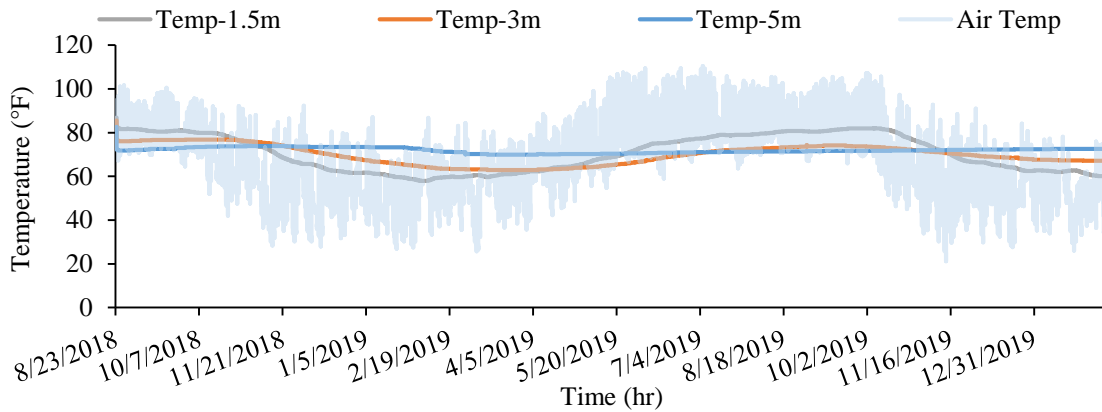
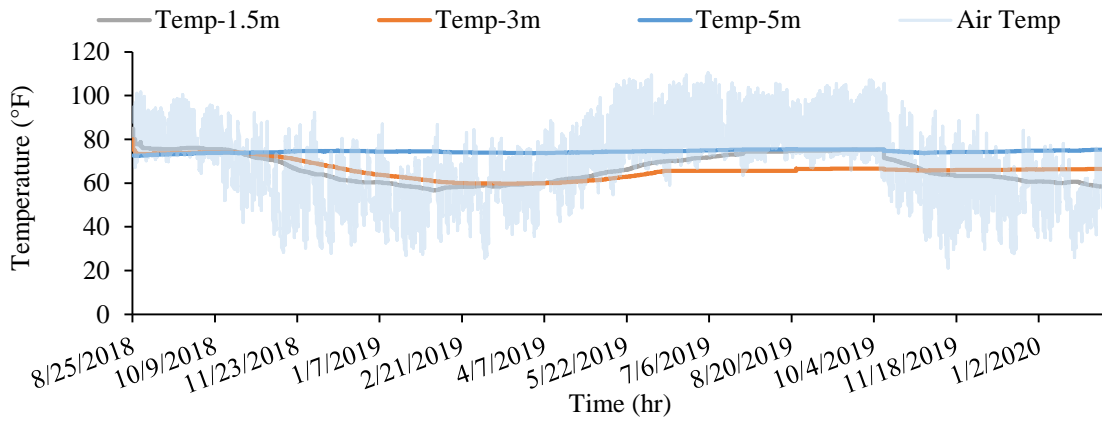


Figure 4.45 In situ variation of (a) matric suction (b) moisture content with rainfall across instrumentation 3 at Slope 4

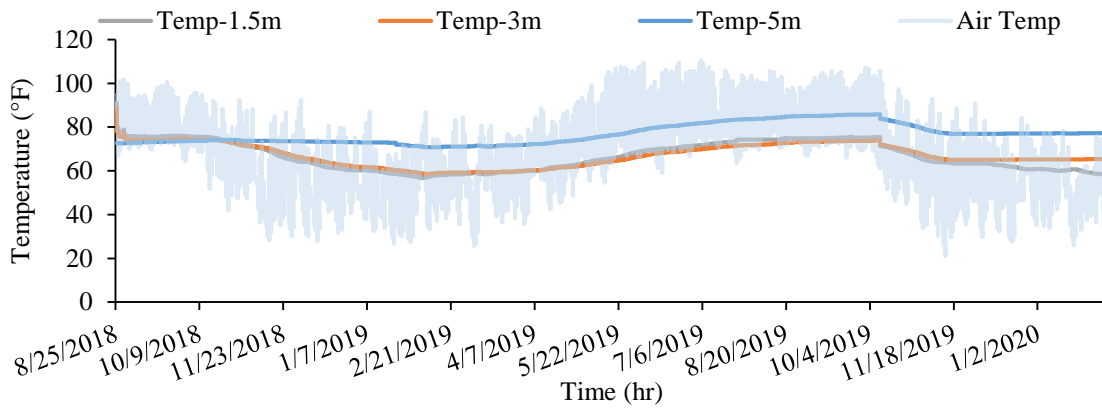
Figure 4.46 presents the in situ variations of soil and air temperature at Instrumentation 1 to Instrumentation 3. It is observed that with the changes in the air temperature, the soil temperature at the shallow depth has experienced some variations. At this location, the soil temperature at 15 ft. (5 m) experienced almost no variation.



(a)



(b)



(c)

Figure 4.46 Combined air and soil temperature variation at Slope 4 at (a) Instrumentation 1 (b) Instrumentation 2 (c) Instrumentation 3

4.6 Slope 5: Sowell Road Highway Slope

Slope 5 is located along I55 South and Sowell road and has a reinforced and as-built section, as presented in Chapter 3. Two 15 ft. bore holes were drilled at the as-built sections for instrumentation. These two boreholes are designated as Instrumentation 1 and Instrumentation 2, as presented in Figure 4.47. In addition, a third 15 ft. deep borehole was drilled and then instrumented in the reinforced section, which is designated as Instrumentation 3. Instrumentation 1 is located at the crest whereas, Instrumentation 2 and Instrumentation 3 are located in the middle of the slope. In each of the Instrumentation locations, at 5 ft (1.5 m), 10 ft (3 m), and 15 ft (5 m) depths, a moisture sensor, and a water potential sensor were installed. Additionally, a rain gauge and air temperature were installed at instrumentation 1 at Slope 5. The sensor installations photos are presented in Figure 4.48.

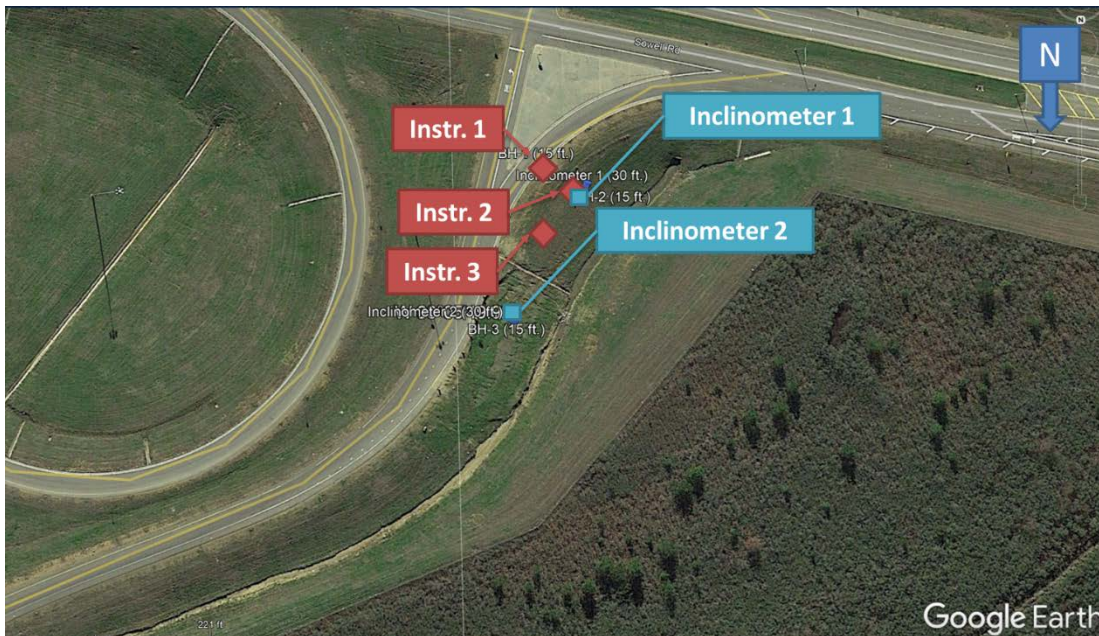


Figure 4.47 Instrumentation layout at Slope 5



Figure 4.48 Installation of sensors at Slope 5

The slope inclinometer installations are presented in Figure 4.49. The inclinometer 1 is installed at the as-built section, whereas the inclinometer 2 is installed at the repair sections. Each of the inclinometer is 30 ft. deep and installed at the middle of the slope.



Figure 4.49 Slope 5 slope inclinometer installation

4.6.1 Field Monitoring Result

4.6.1.1 Movement Data Slope

The horizontal movement data from the slope was collected using slope inclinometer at every 2 ft. spacing and then analyzed to determine the slope movement. The horizontal movement data from Inclinometer 1 at the reinforced section and time-dependent movement at the surface of the slope is presented in Figure 4.50 and Figure 4.51, respectively. As observed from the inclinometer data, the as-built section of Slope 5 has no sign of slope movement and landslides.

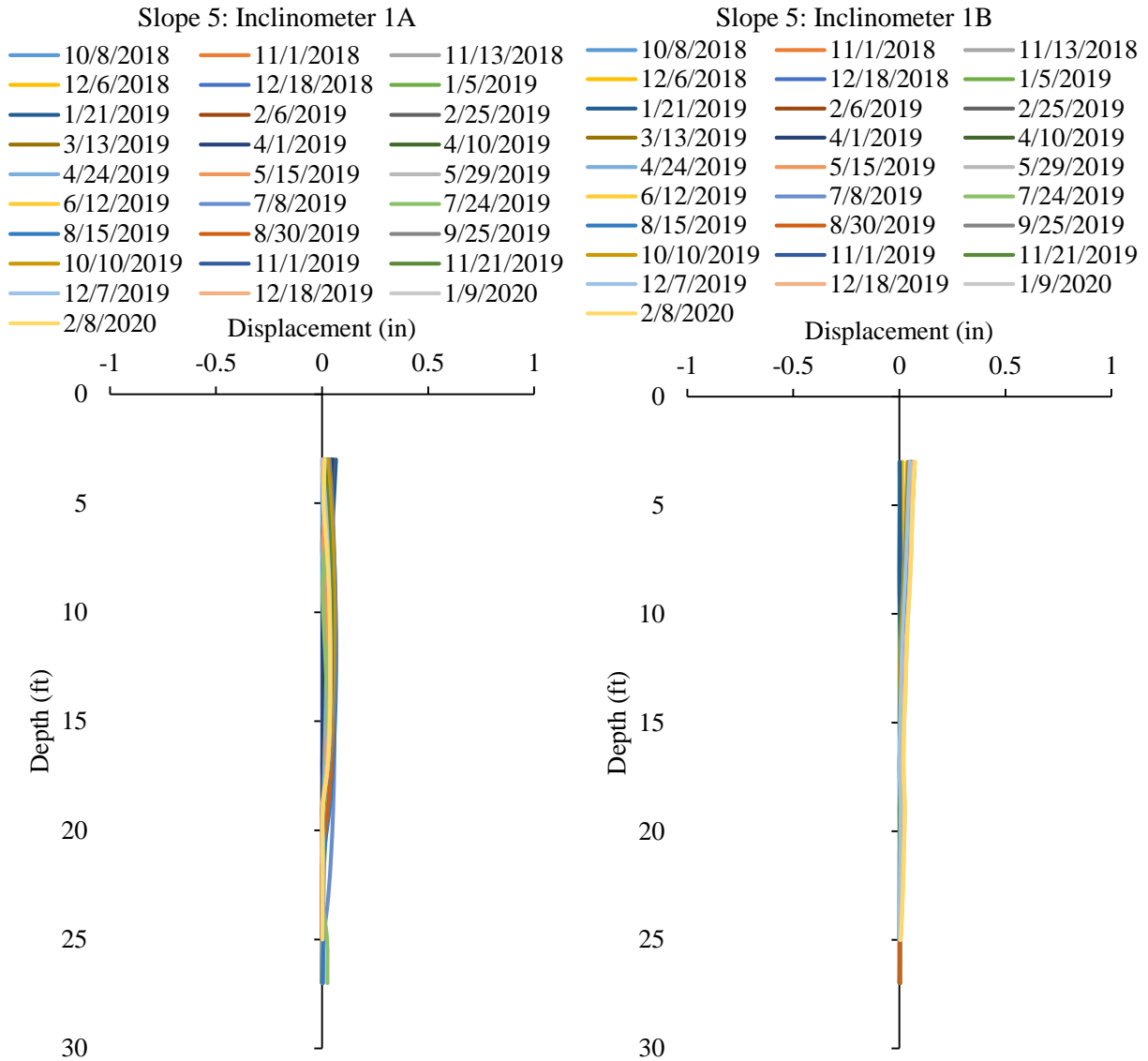


Figure 4.50 Horizontal displacements of the Inclinator 1 at Slope 5

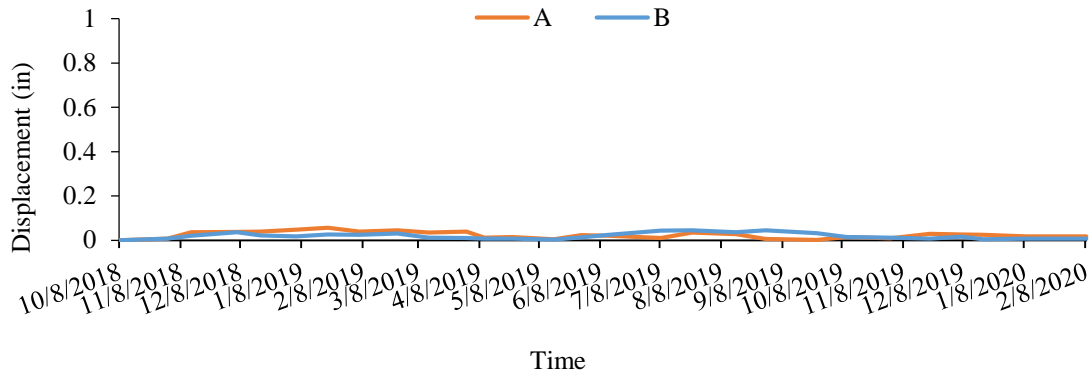


Figure 4.51 Variation of lateral deformation at the top of Inclinator 1 at Slope 5.

The horizontal displacement of inclinometer 2 at the repaired section is presented in Figure 4.52. Based on the inclinometer data, a 14 ft. (4.3 m) deep sliding movement was observed during November 2018. The failure photo of the slope is presented in Figure 4.53. It should be noted that the slope was repaired using 30 ft. long HP 14x73 at 3 ft. center to center spacing in the middle of the slope. The HP 14x73 has provided enough resistance at the active part of the slope and resisted any movement of the upper pavement ramp. However, the bottom part of the slope was unreinforced, which experienced the landslides. A detailed analysis of the slope failure was conducted in Finite Element Analysis, which is presented in Chapter 5.

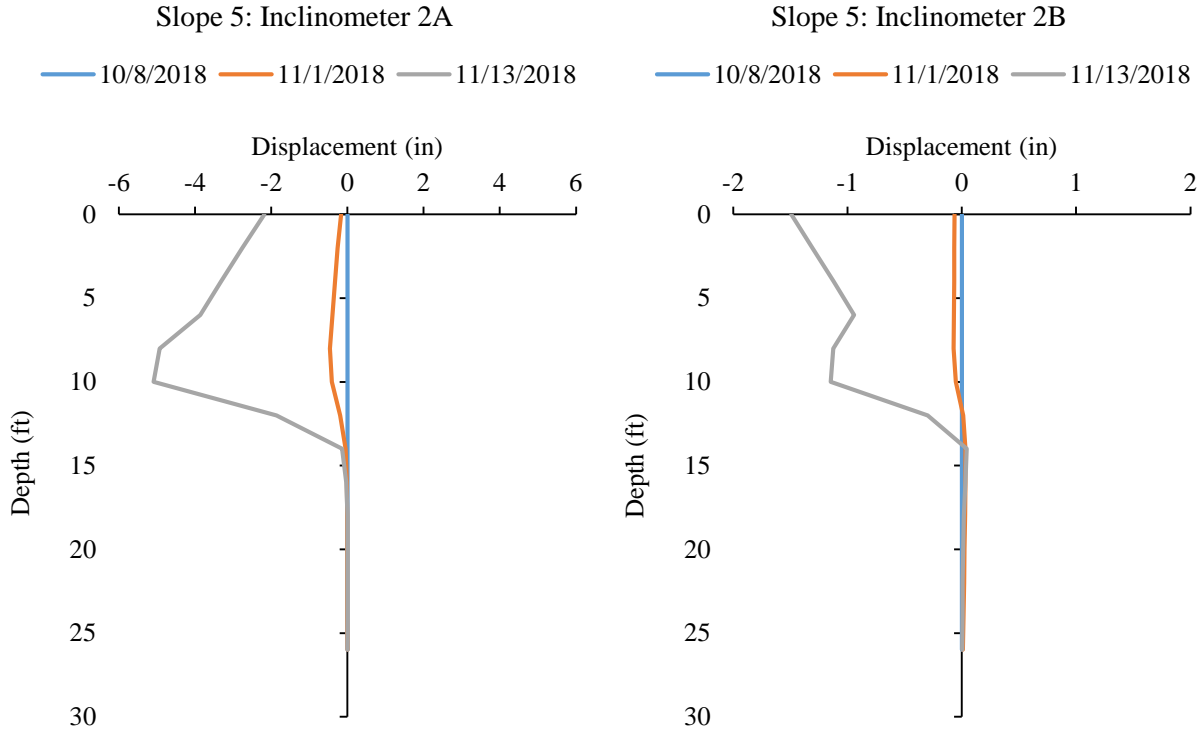


Figure 4.52 Horizontal displacements of the Inclinometer 2 at Slope 5



Figure 4.53 Landslides at Slope 5

4.6.1.2 Field Instrumentation Data

According to the obtained field instrumentation results, the change in moisture content and daily rainfall distribution at the crest, middle, and toe of the slope 5 at three different depths 5 ft. (1.5 m), 10 ft.

(3 m), and 15 ft. (5 m) at instrumentation 1, instrumentation 2, and instrumentation 3 for the time period of September 2018 to April 2019 are presented in Figures 4.54, Figure 4.55, and Figure 4.56, respectively. Since the slope has experienced a failure during the early part of this study, a special emphasis was given on the rainfall before the failure. Based on the instrumentation results, the matric suction of the slopes remains constant after the preliminary 2-3 months of the observation period. In addition, the lower suction value was present at the top part of the slope, which signifies low shear strength and high moisture content. The slope has experienced a significant moisture variation during the dry period, mostly at 5 ft. (1.5 m) and 10 ft. (3 m) depth. This significant variation of moisture indicated that the slope had desiccation/shrinkage cracks during the summer of 2019, which works as a preferential path for rainwater infiltration.

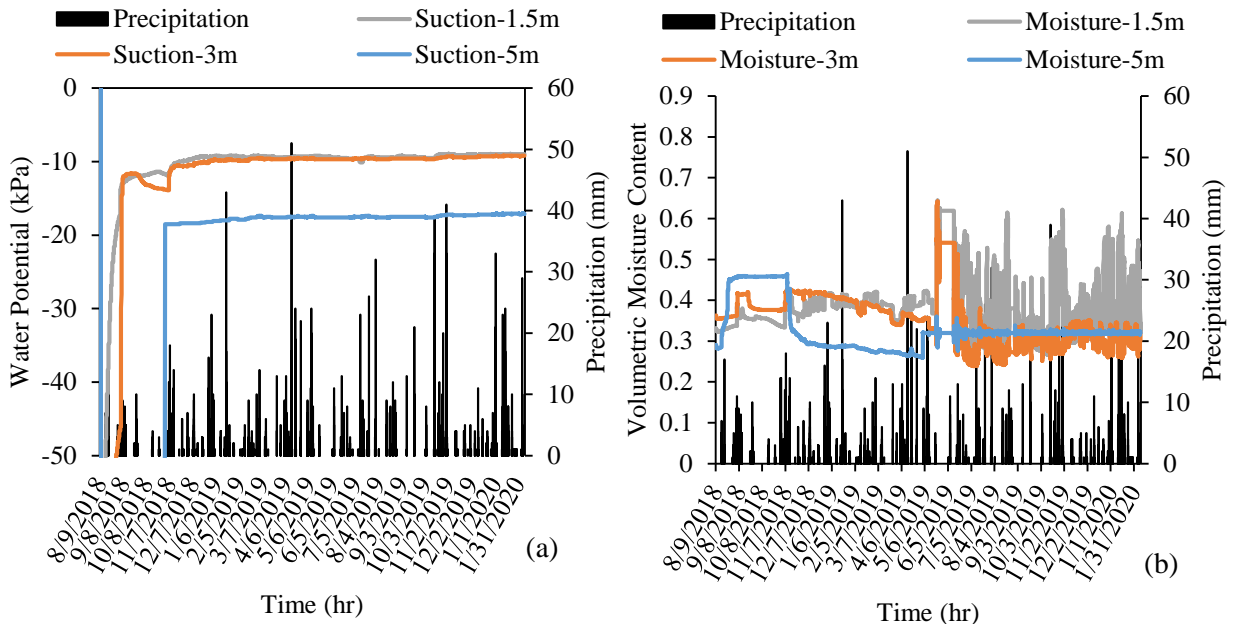


Figure 4.54 In situ variation of (a) matric suction (b) moisture content with rainfall across instrumentation 1 at Slope 5

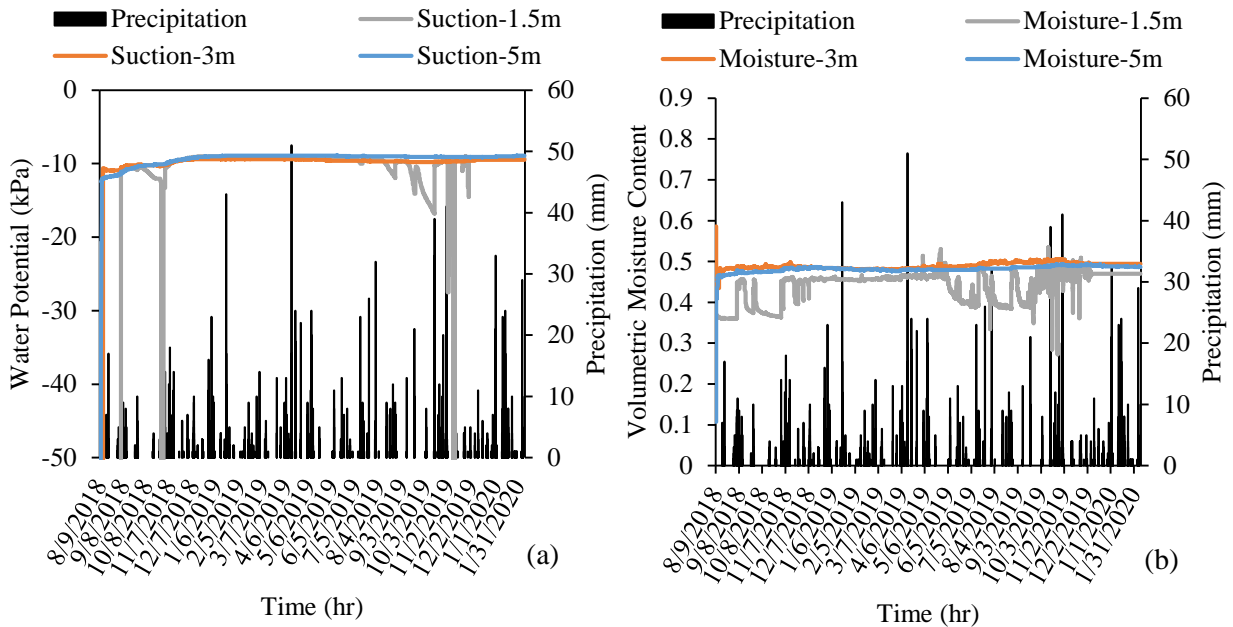


Figure 4.55 In situ variation of (a) matric suction (b) moisture content with rainfall across instrumentation 2 at Slope 5

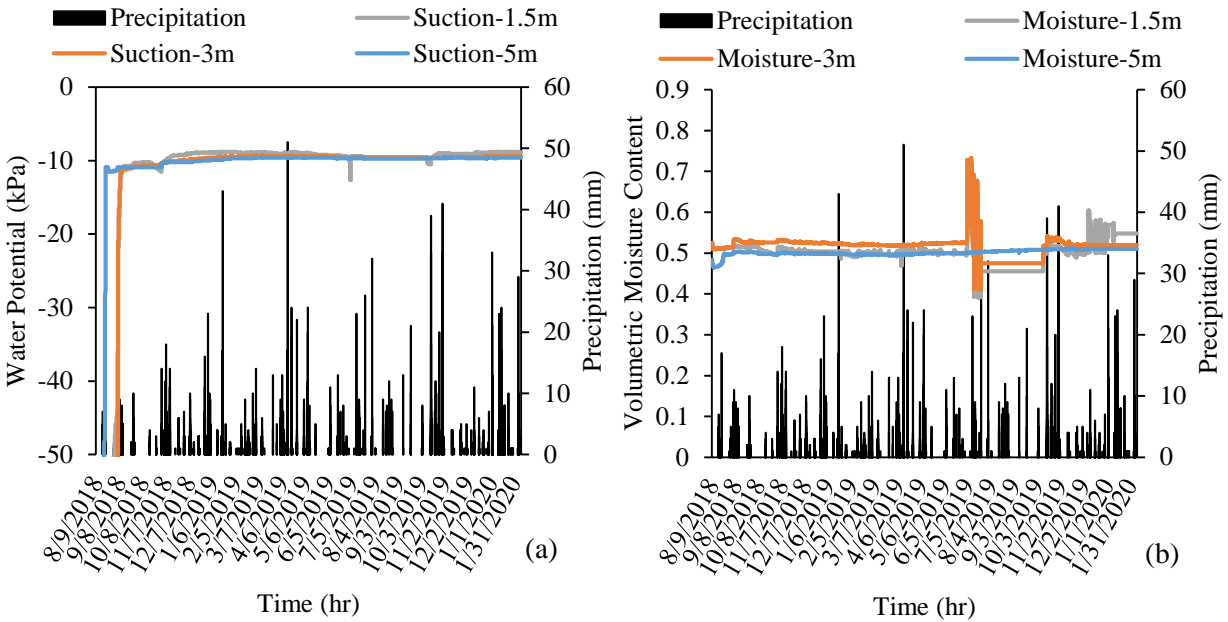
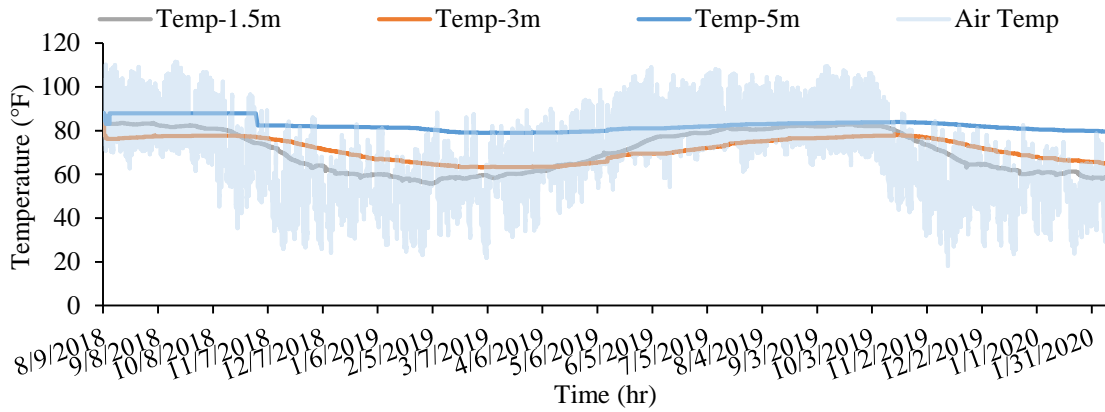
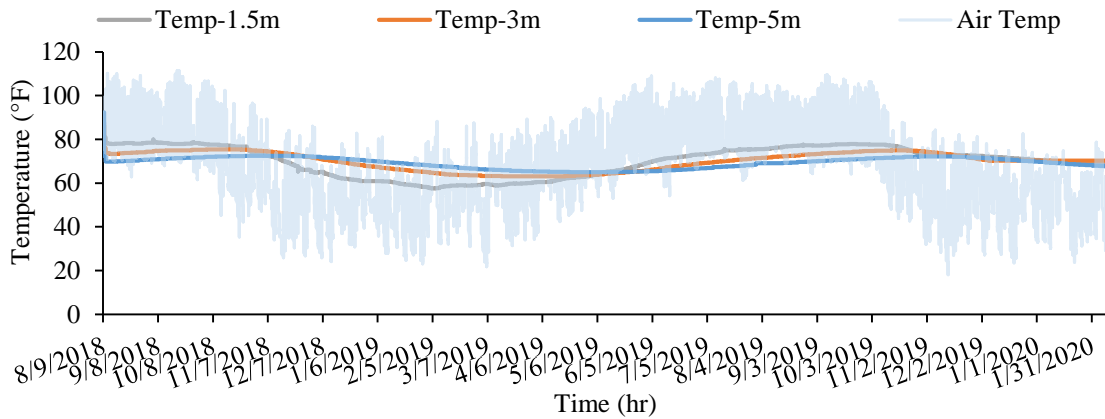


Figure 4.56 In situ variation of (a) matric suction (b) moisture content with rainfall across instrumentation 3 at Slope 5

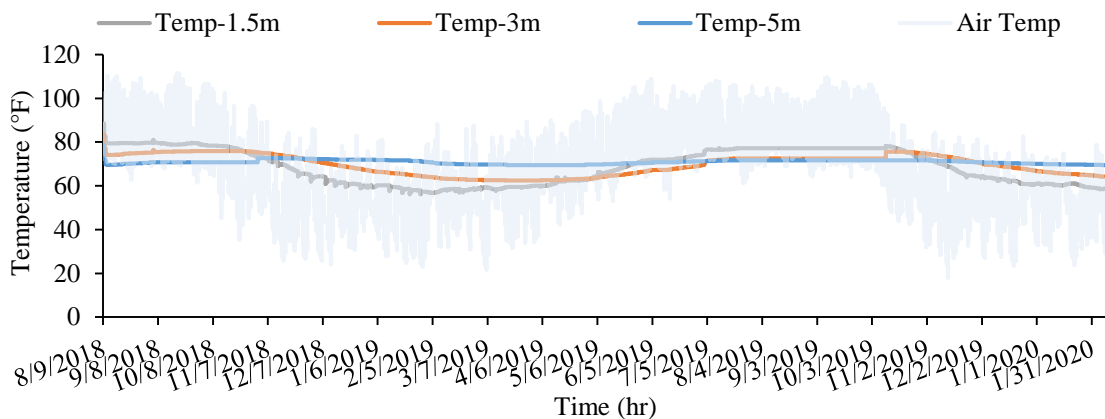
Figure 4.57 presents the in situ variations of soil and air temperature at instrumentation 1 to instrumentation 3 at Slope 5. Based on the temperature variation data, minor changes in the soil temperature at the deeper depth was observed. However, at a shallower depth, soil temperature varied with the changes in the air temperature. This behavior is consistent throughout all the slopes.



(a)



(b)



(c)

Figure 4.57 Combined air and soil temperature variation at Slope 5 at (a) Instrumentation 1 (b) Instrumentation 2 (c) Instrumentation 3

4.7 Slope 6: McRaven Road Highway Slope

Slope 6 is located along I20E near McRaven road and has a repaired and as-built section, as presented in Chapter 3. Two 15 ft. boreholes were drilled and then instrumented at the repaired section, as presented in Figure 4.58, which are designated as Instrumentation 1 and Instrumentation 2. In addition, a third 15 ft. deep borehole was drilled and then instrumented in the as-built section, which is designated as Instrumentation 3. Instrumentation 1 is located at the crest whereas, Instrumentation 2 and Instrumentation 3 are located in the middle of the slope. In each of the Instrumentation locations, at 5 ft (1.5 m), 10 ft (3 m), and 15 ft (5 m) depths, a moisture sensor, and a potential water sensor were installed. Additionally, a rain gauge and air temperature were installed at instrumentation 1 at Slope 6. The sensor installations photos are presented in Figure 4.59.

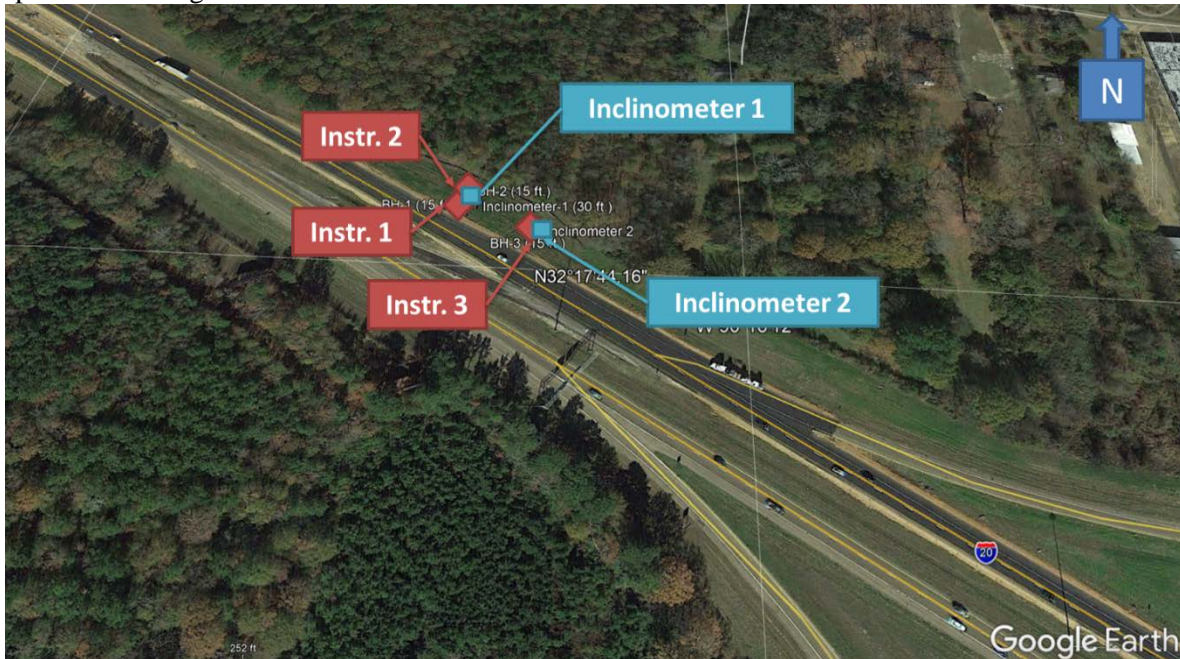


Figure 4.58 Instrumentation layout at Slope 6



Figure 4.59 Slope 6 sensor installation

The slope inclinometer installations are presented in Figure 4.60. The 30 ft slope inclinometer 1 was installed at the repaired section, whereas, Inclinometer 2 was installed at the as-built section of Slope 6.



Figure 4.60 Slope 6 slope inclinometer installation

4.7.1 Field Monitoring Results

4.7.1.1 Slope Movement Data

The horizontal movement data from the slope was observed using slope inclinometer measurements collected at every 2 ft. spacing along the slope inclinometer pipe. The collected inclinometer data was analyzed to determine the slope movement. The horizontal movement data from Inclinometer 1 at the repaired section and time-dependent movement at the surface of the slope are presented in Figure 4.61 and Figure 4.62, respectively. No significant movement was observed in the repaired section of Slope 6. The performance of this section is within a satisfactory level.

The horizontal movement data from Inclinometer 2 at the as-built section and time-dependent movement at the surface of the slope are presented in Figure 4.63 and Figure 4.64. Based on the horizontal movement data, the slope is experiencing a movement and has moved up to 3 inches at the slope surface, within the monitoring period. In addition, the depth of the slope movement is around 5 ft., which is shallow in nature. This section of the slope will require maintenance to repair the shallow slope failure.

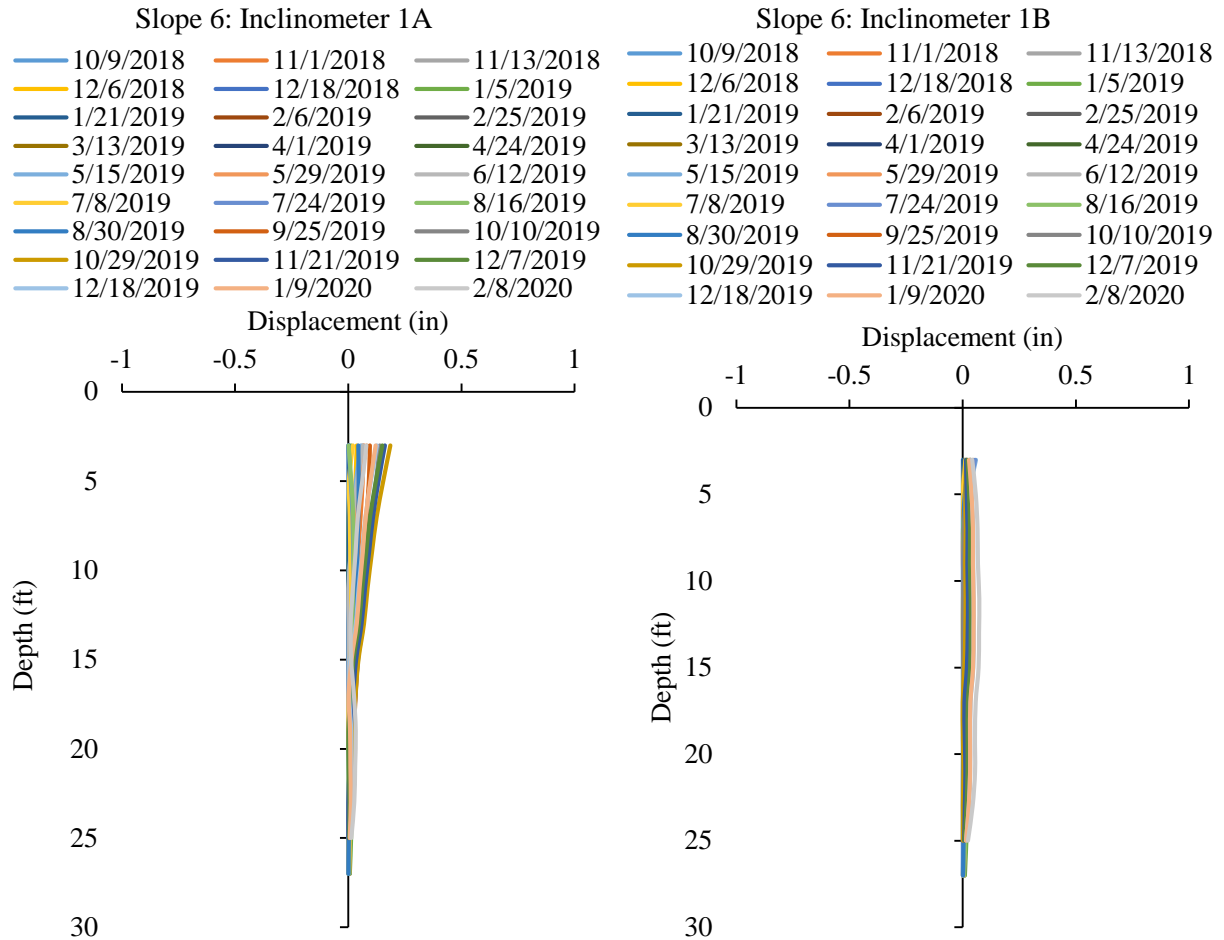


Figure 4.61 Horizontal displacements of the Inclinometer 1 at Slope 6

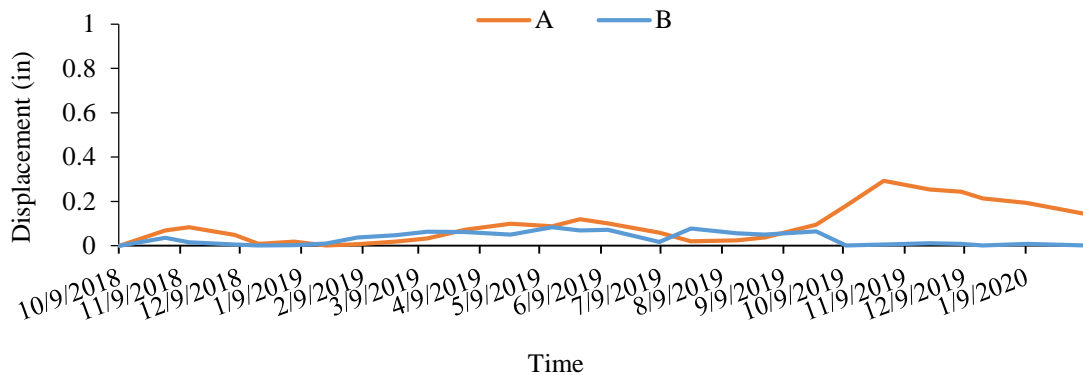


Figure 4.62 Variation of lateral deformation at the top of Inclinometer 1 at Slope 6

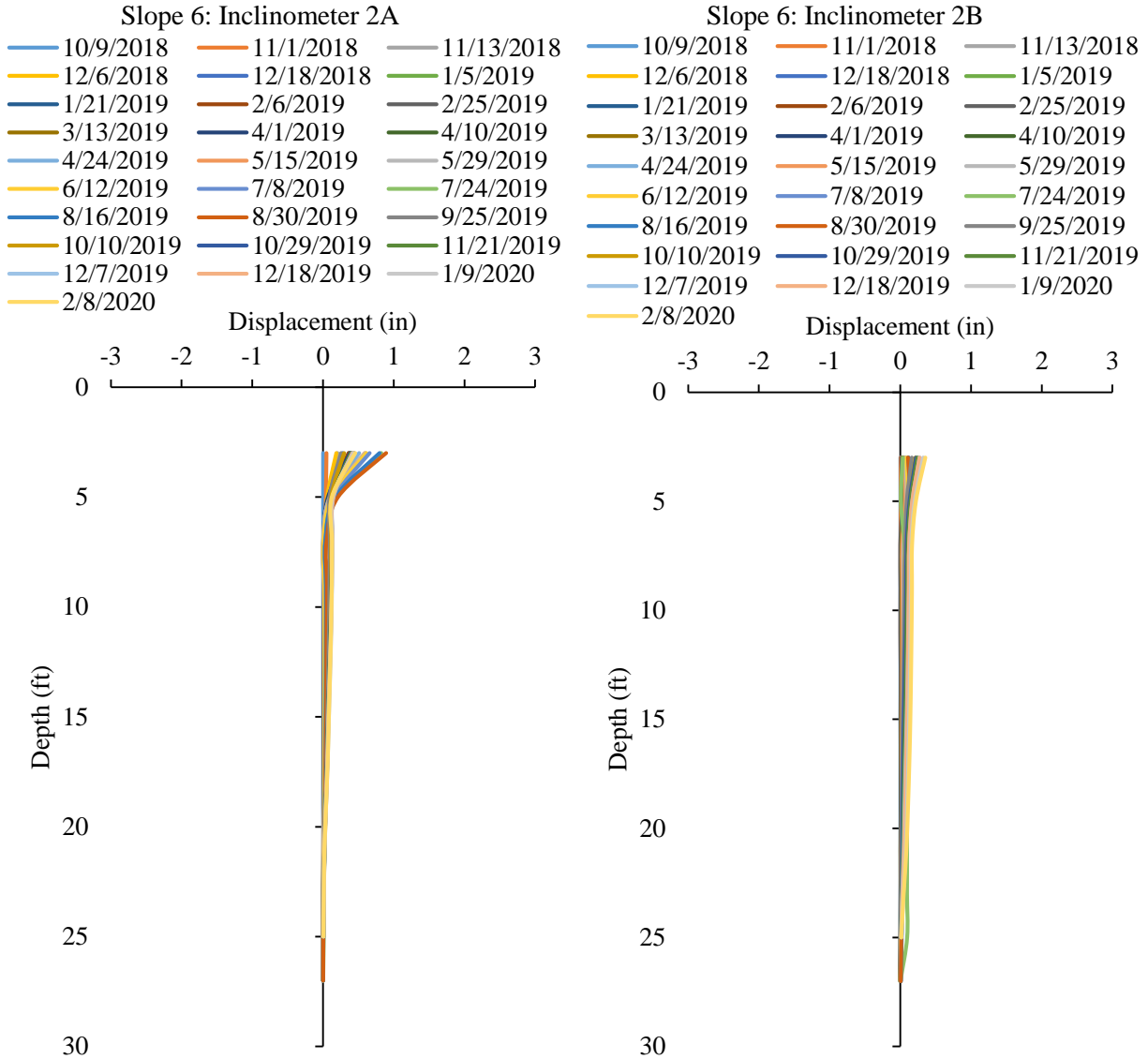


Figure 4.63 Horizontal displacements of the Inclinerometer 2 at Slope 6

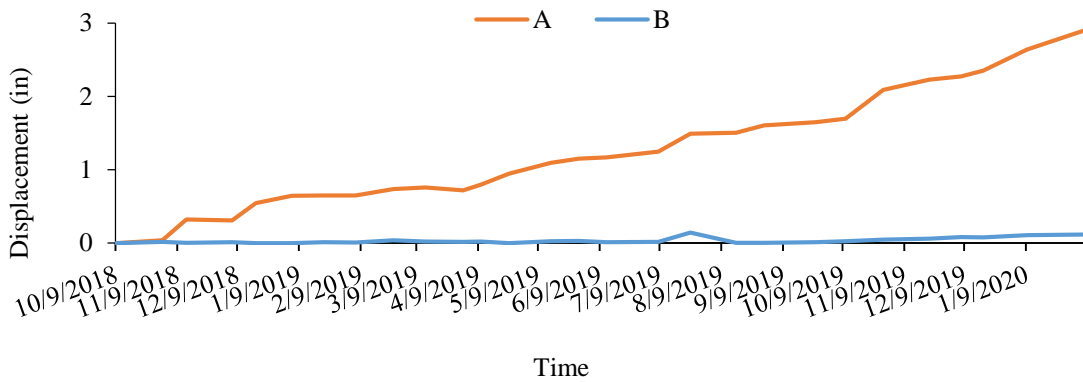


Figure 4.64 Variation of lateral deformation at the top of Inclinerometer 2 at Slope 6

4.7.1.2 Field Instrumentation Data

Variation of in situ matric suction profile and moisture content at 5 ft. (1.5 m), 10 ft. (3 m), and 15 ft. (5 m) depths with rainfall at Instrumentation 1, Instrumentation 2, and Instrumentation 3 are presented in Figure 4.65, Figure 4.66, and Figure 4.67, respectively. Based on the field monitoring results presented in Figure 4.65 from instrumentation 1, the matric suction has a high number for around three months, and then reached an equilibrium condition, which presents a low value (10 kPa) that also remain constant along the monitoring period. Similar to the matric suction variation, the volumetric moisture content remained constant over the last two years at instrumentation 1. As observed in other slopes, the constant low value at the matric suction and high consistent moisture content signify that the soil is likely close to a fully saturated condition. It is highly possible, there is a formation of perched water conditions at the slope.

Based on the instrumentation results presented in Figure 4.66 and Figure 4.67 at the middle of the slopes of both repaired sections and as-built sections indicates a similar matric suction variation like Figure 4.65 for the crest of the slope. However, in the volumetric moisture content, few peaks and drops were observed during summer 2019, which indicates the intrusion of the rainwater; however, the overall moisture content remains constant throughout the monitoring period. The constant moisture content and matric suction at the instrumentation 2 and instrumentation 3 attribute to the existence of the perched water condition of the slope. Exact Similar observation was made on Slope 3, which also experienced a shallow slide at the as-built section. The movement at the as-built section of the slope is taking place due to the formation of perched water with the top part of the slope. It is important to mention that the slope at the repair section is also experiencing a similar perched water zone; however, due to the repair, it is not experiencing any further movement.

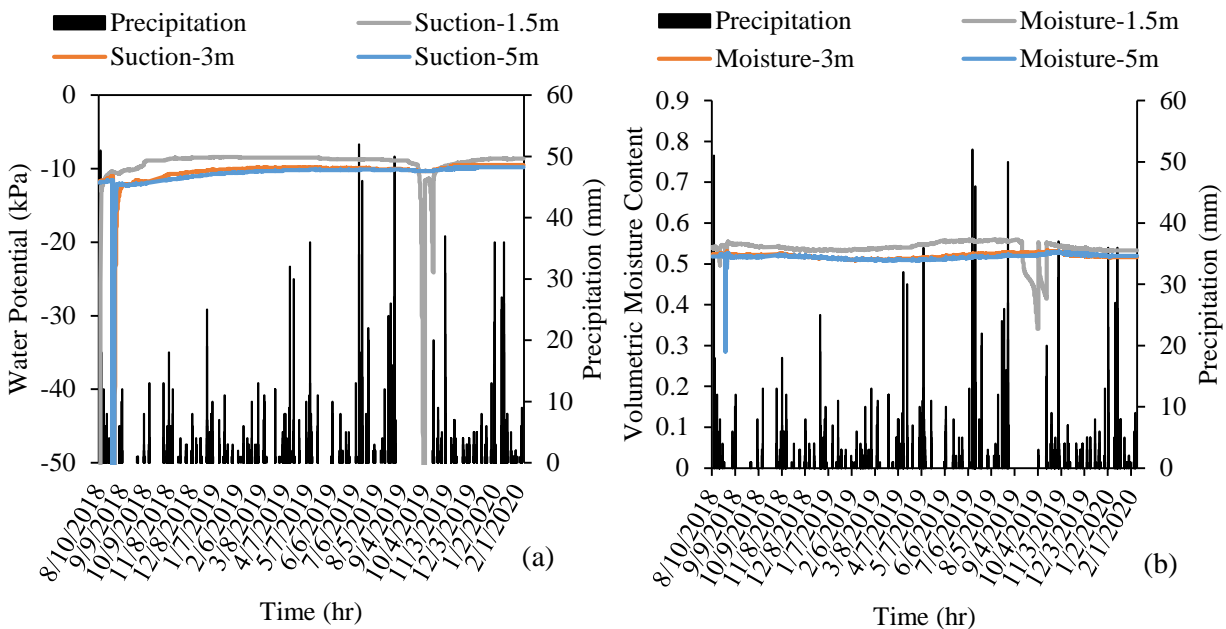


Figure 4.65 In situ variation of (a) matric suction (b) moisture content with rainfall across instrumentation 1 at Slope 6

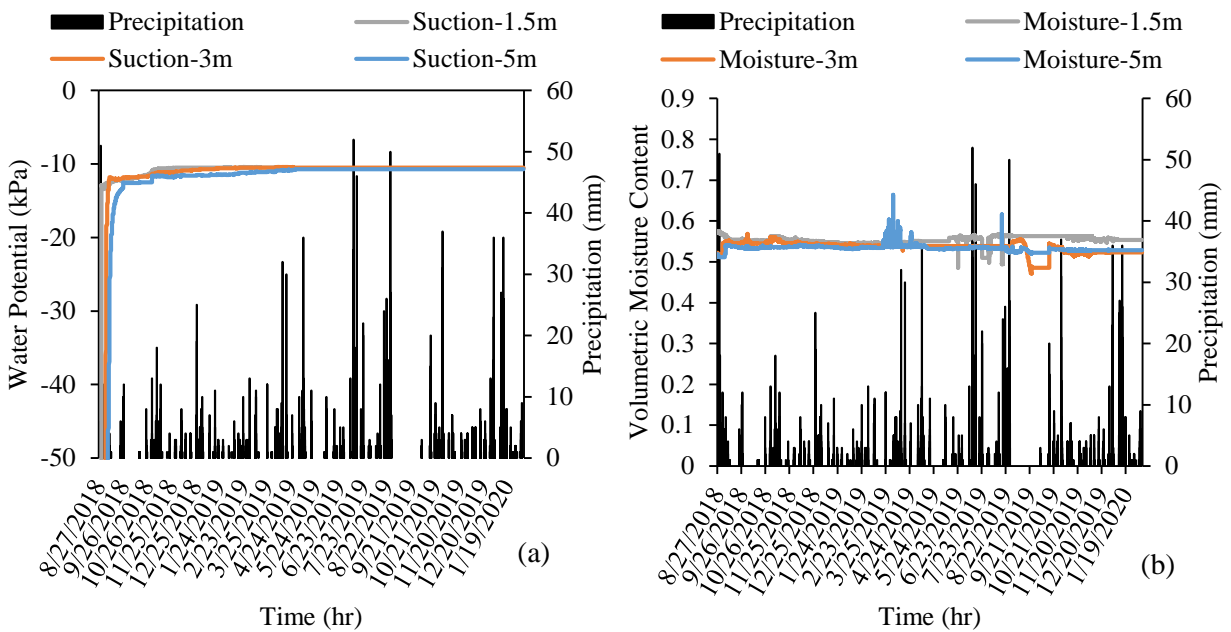


Figure 4.66 In situ variation of (a) matric suction (b) moisture content with rainfall across instrumentation 2 at Slope 6

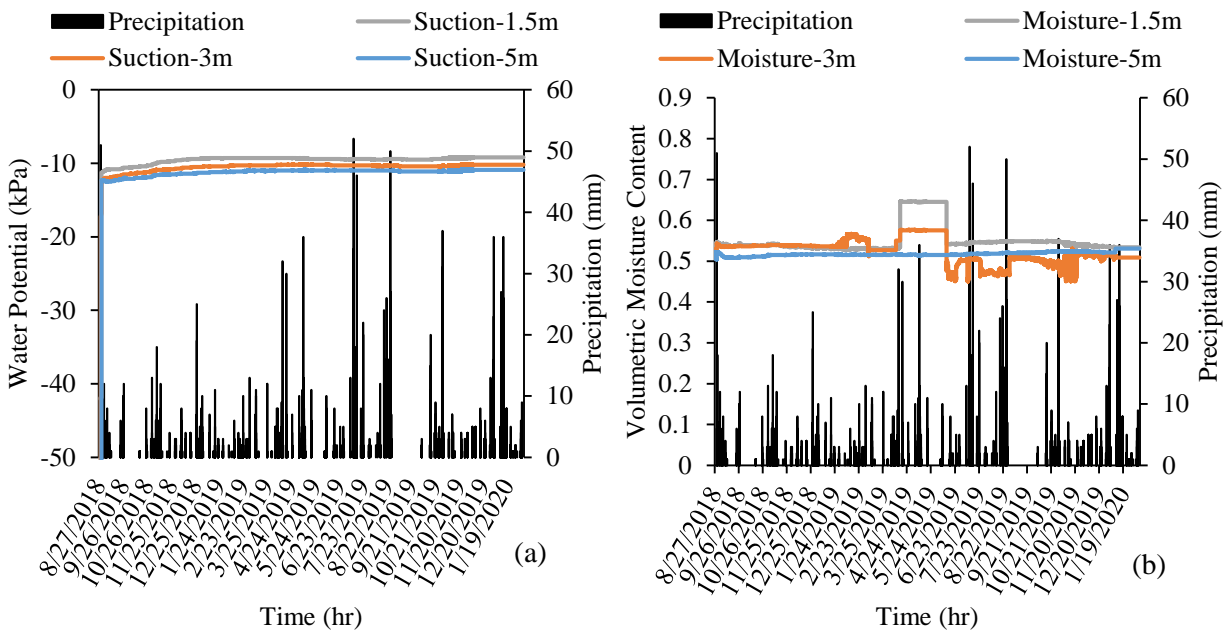
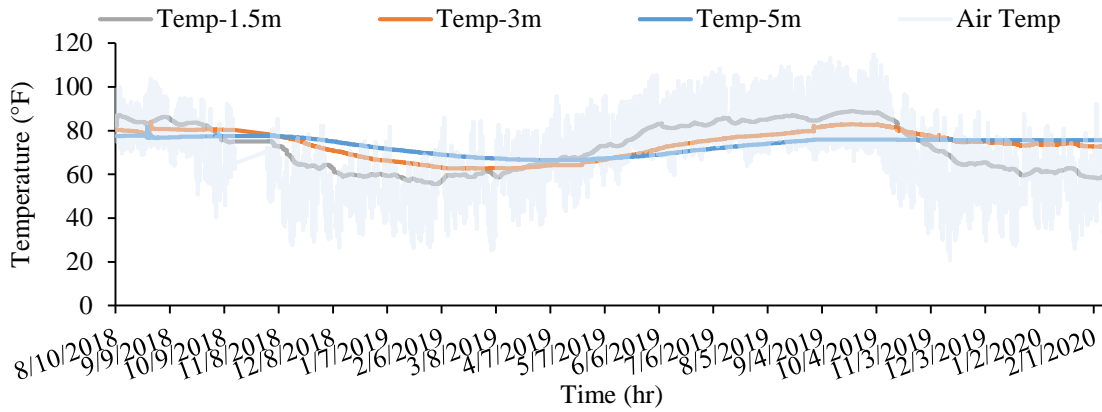
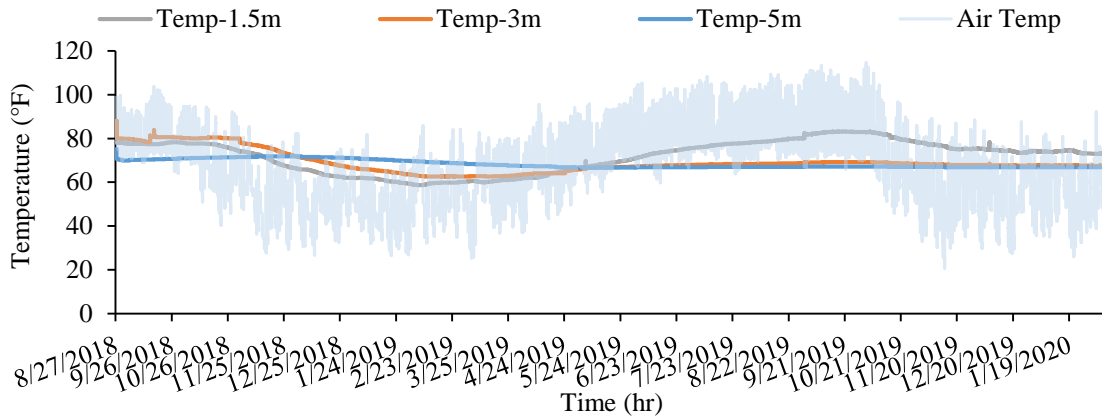


Figure 4.67 In situ variation of (a) matric suction (b) moisture content with rainfall across instrumentation 3 at Slope 6

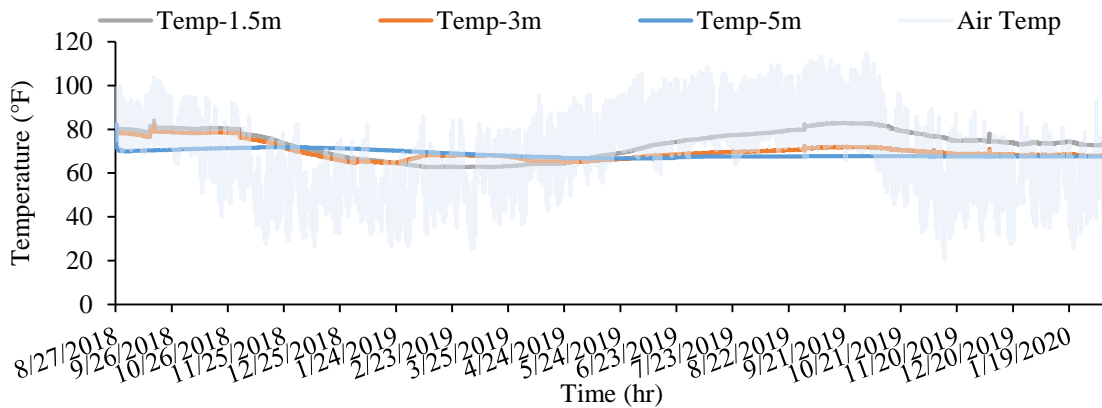
Figure 4.68 presents the in situ variations of soil and air temperature at instrumentation 1 to instrumentation 3 at Slope 5. Based on the temperature variation data, minor changes in the soil temperature at the deeper depth was observed, similar to other slopes. However, at a shallower depth, soil temperature varied with the changes in the air temperature.



(a)



(b)



(c)

Figure 4.68 Combined air and soil temperature variation at Slope 6 at (a) Instrumentation 1 (b) Instrumentation 2 (c) Instrumentation 3

4.8 I220S Ramp Toward I20E/US49S Highway Slope

An additional slope located along the exit from I220 South toward I20 East was repaired using H-piles and a slope inclinometer was installed to check the movement of the repaired area. JSU Team monitored the slope movement every two weeks. The variations of lateral deformation for slope 7 located on I220 South ramp toward US49 South are presented. The slope inclinometer at this slope is located in the repaired section. Figure 4.69 and Figure 4.70 illustrate the movement along with the inclinometer, which indicates no notable deformation in the slope.

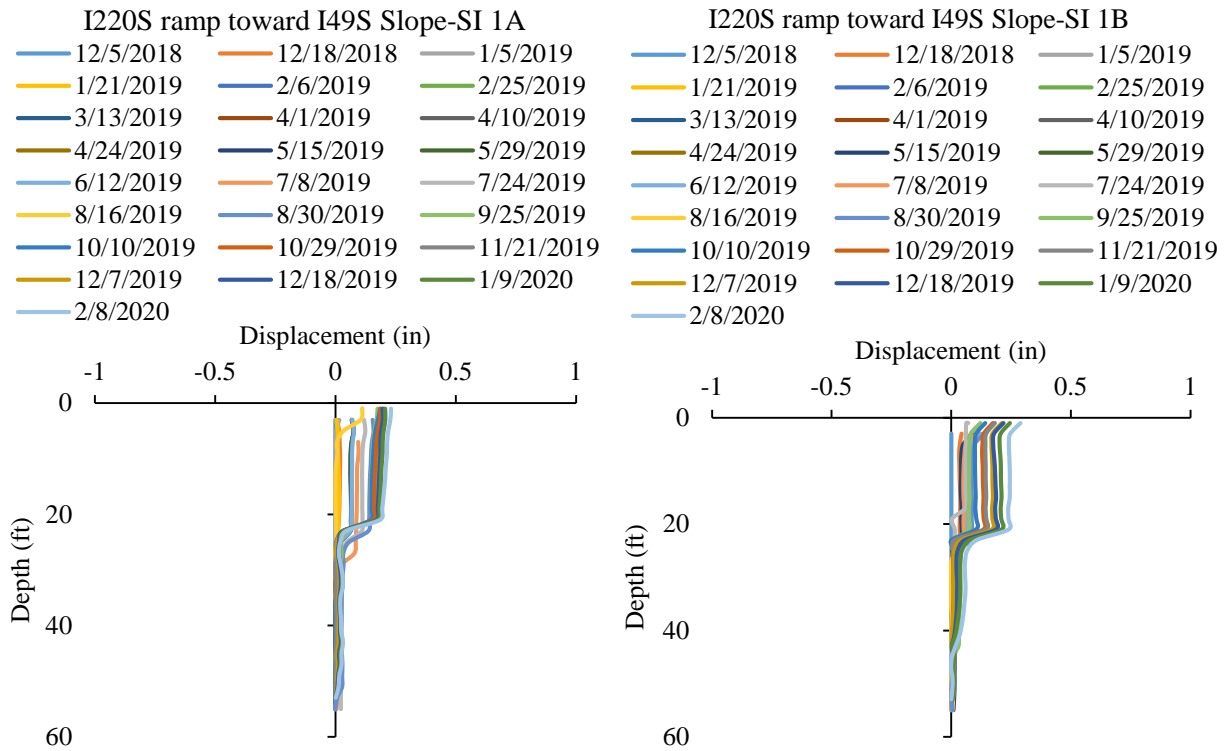


Figure 4.69 Horizontal Displacement at Slope 7

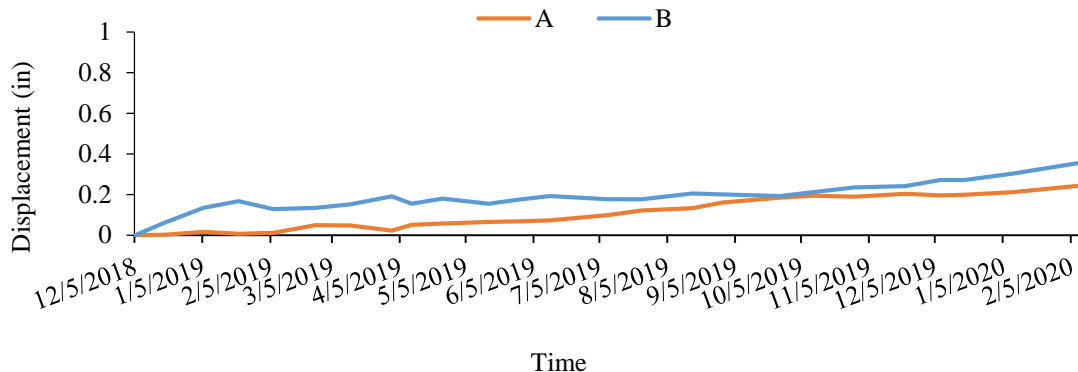


Figure 4.70 Variation of lateral deformation at Slope 7

4.9 Discussion

4.9.1 Determination of Active Zone

The depth of the seasonal moisture variation is known as the depth of the active zone. To assess the depth of the active zone, three highway slopes, Slope 1: I220N ramp toward I55N, Slope 2: Metro Center, and Slope 6: McRaven road was selected for this assessment.

4.9.1.1 I220N ramp toward I55N Highway Slope

The filed variation of the moisture content along with the depth of the crest and middle of the Slope 1 with wet-dry cycles due to the seasonal change is presented in Figure 4.71. It can be seen that the moisture variation is quite constant along with the depth, and the magnitude of variation decreased with an increase in depth with different wet-dry cycles.

The field variation of the matric suction along with the depth of the crest and middle of the I220N ramp toward I55N highway slopes with wet-dry cycles due to the seasonal change is presented in Figure 4.72. From the filed suction data of the wet-dry period from August 2018 to June 2019, it can be seen that the suction varied with the wet-dry cycle, however, the variation is critical at the dry period (September 2018) up to 3.5 m (12 ft.) depth. Therefore, the depth of the active zone for Slope 1 is considered as 12 ft. from the field instrumentation results.

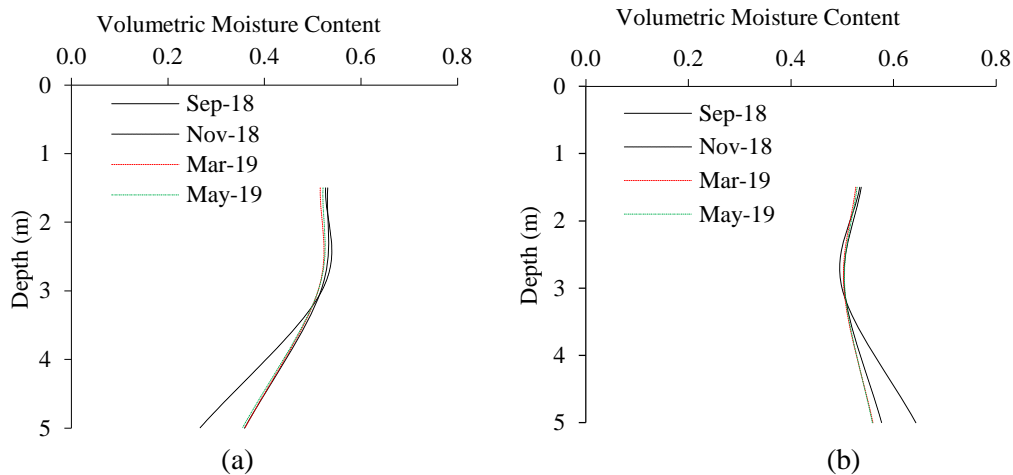


Figure 4.71 Moisture variation along with depth at Slope 1 (a) at the crest (b) at the middle of the slope

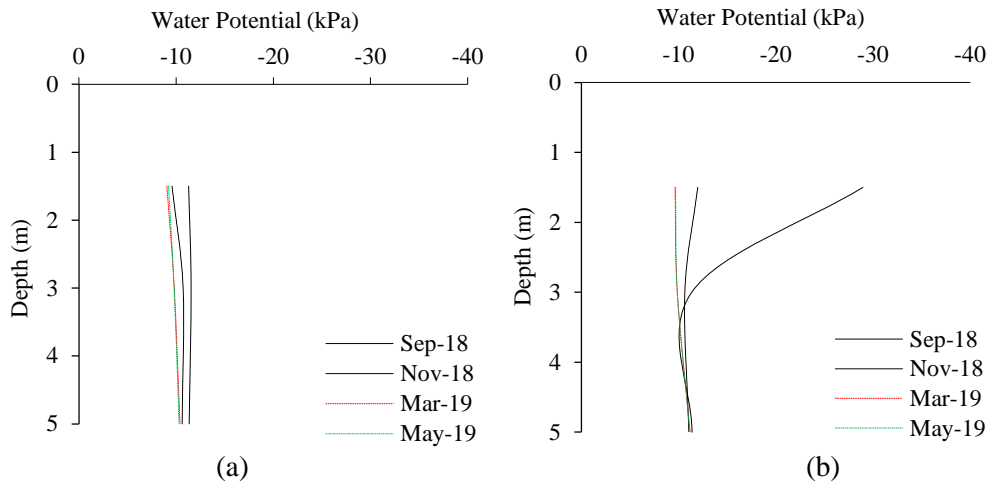


Figure 4.72 Suction variation along with depth at Slope 1 (a) at the crest (b) at the middle

4.9.1.2 Metro Center Highway Slope

The filed variation of the moisture content along with the depth of the crest and middle of Slope 2 with wet-dry cycles due to the seasonal change is presented in Figure 4.73. At the crest, during September 2018, high moisture content was observed at 10 ft. (3 m) depth, however, in the middle, this variation was not visible.

The matric suction variation along the depth of the slope is indicated in Figure 4.74. From the filed suction data of the wet-dry period, it can be observed that near the crest in Metro Center, the slope has experienced suction variation at 10 ft. (3 m) depth. Moreover, in the middle of the slope, suction variation was observed during September 2018, which continued up to 12 ft. (3.5 m) depth, similar to slope 1. Therefore, the depth of the active zone can be considered as 12 ft. depth.

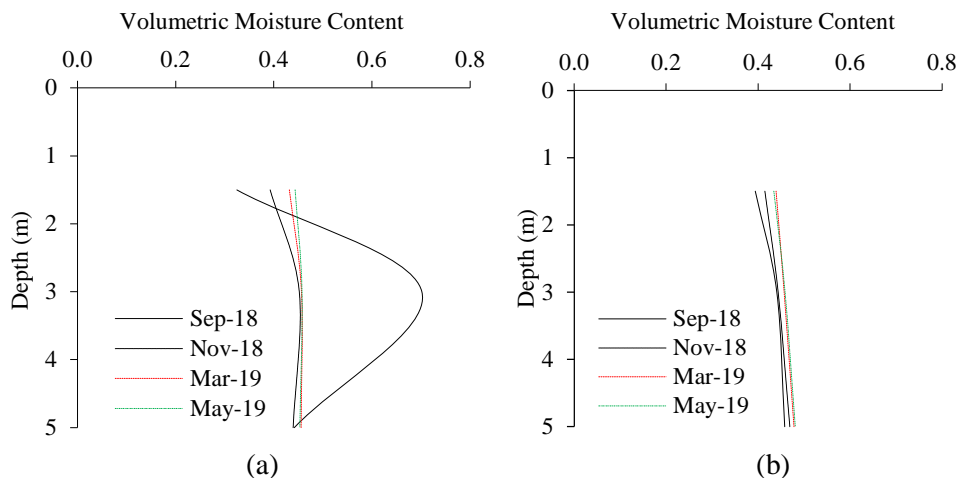


Figure 4.73 Moisture variation along with depth at Slope 2 (a) at the crest (b) at the middle of the slope

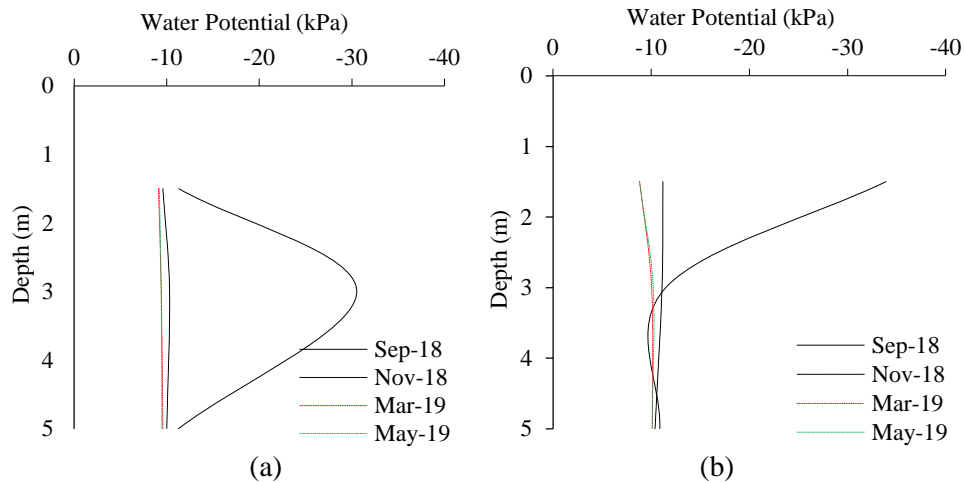


Figure 4.74 Suction variation along with depth at Slope 2 (a) at the crest (b) at the middle

4.9.1.3 McRaven Road Highway Slope

The field variation of the moisture content along with the depth of the crest and middle of Slope 6 with wet-dry cycles due to the seasonal change is presented in Figure 4.75. It can be observed that no significant variation of the moisture content along with the depth of the slope. The field variation of the matric suction along with the depth of the crest and middle of Slope 6 with wet-dry cycles due to the seasonal change is presented in Figure 4.76. The matric suction variation has shown a similar trend, where no major variation is observed.

Based on the field instrumentation results, it was indicated that a Perched water zone existing at Slope 6, which has a bathtub condition and does allowing any changes in the moisture content or matric suction. Therefore, no seasonal changes in the moisture content were observed in this slope.

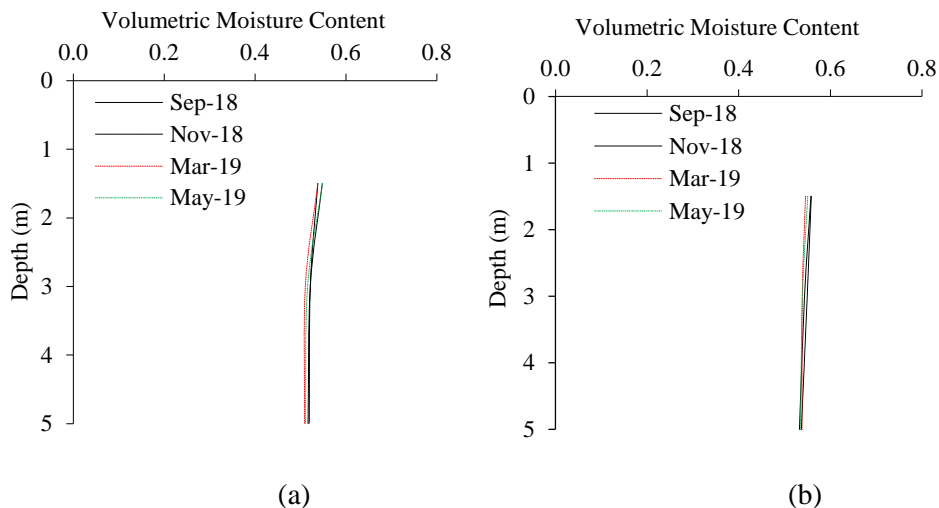


Figure 4.75 Moisture variation along with depth at Slope 6 (a) at the crest (b) at the middle of the slope

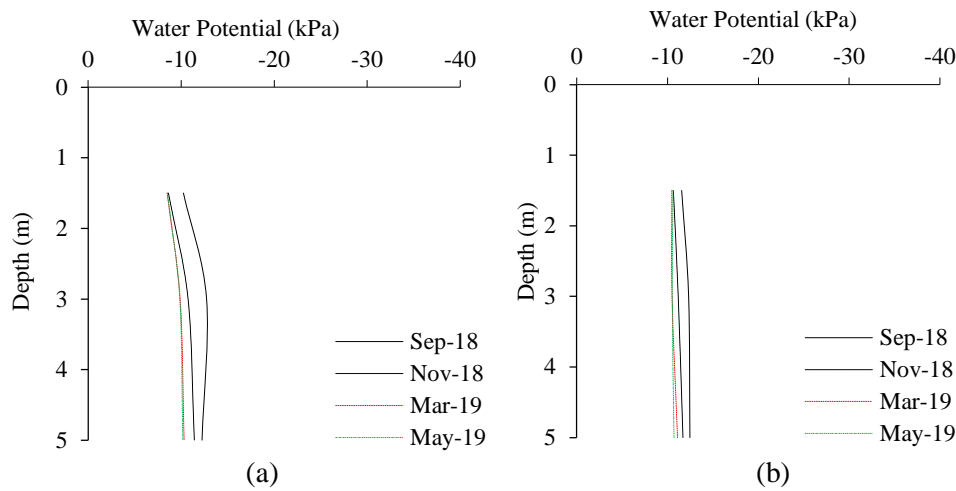


Figure 4.76 Suction variation along with depth at Slope 6 (c) at the crest (d) at the middle

Thus, comparing the variation of the moisture content and matric suction at these three slopes, it can be concluded that the depth of the active zone in Yazoo clay is around 12 ft. (3.5 m).

4.9.2 Field Soil Water Retention Curve (SWRC)

The soil water retention curve (SWRC) is crucial to explain the hydro-mechanical behavior of any soil in the unsaturated environment. There are numerous unknown factors in the field, and due to heterogeneity state, all sorts of indeterminate parameters may be included. As a result, it is anticipated that the parameters from the field curve could be more realistic. Field-based SWRC with field instrumentation was determined either in vegetated or non-vegetated soil as proposed by Alam et al., 2017 and Ahmed et al., 2017. In this study, a similar approach to obtain the field SWRC through the field instrumentation data was undertaken, and six SWRC curves were developed for each slope. Figure 4.77 to Figure 4.82 present the Field SWRC instrumentation data for the slope. The field SWRC obtained from instrumented highway slopes was developed individually. Separately, each slope SWRC parameters were fitted with the Van Genuchten approach (Genuchten, 1980) presented in equation (4.1), where ψ is soil matric suction, Θ is gravimetric moisture content, α and n are shape parameters, Θ_r is residual gravimetric moisture content, and Θ_s is saturated gravimetric moisture content.

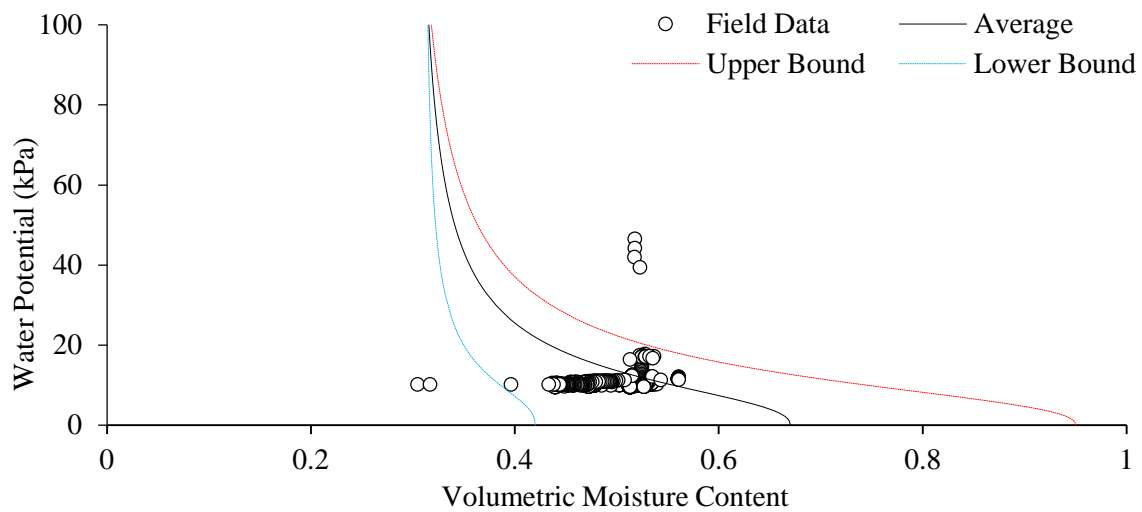
$$\theta(\psi) = \theta_r + \frac{\theta_s - \theta_r}{(1 + (\alpha|\psi|)^n)^{1-\frac{1}{n}}} \quad (4.1)$$

Table 4.4 presents the field SWRC fitted parameters. The saturated and residual gravimetric moisture content obtained from the filed SWRC found individually for each slope. The shape parameter values fitted with Van Genuchten equation found individually for each slope. All of the values tabulated in chapter 5 related to soil parameters input for the 3D Finite Element Method analysis were implemented in numerical analysis individually for each slope. Moreover, the SWRC plots for detailed slope sections are included in Appendix B. In this study, Table 4.4 values were used directly for fully softened Yazoo clay and weathered Yazoo clay soil layers. For other soil layers, parameters from the literature were used.

Table 4.4 Field Soil Water Retention Curve fitted parameters

Van Genuchten Parameters		I220N ramp toward I55N highway slope	Metro Center highway slope	Terry Road highway slope	McRaven Road highway slope
Shape Parameters	α	0.095	0.097	0.095	0.095
	n	2.4	0.47	1.9	0.45
	$m=1-1/n$	0.58	1.9	0.47	1.7
Soil Water Parameter	θ_r	0.3	0.21	0.25	0.19
	θ_s	0.67	0.6	0.61	0.58

Van Genuchten Parameters		Highland Drive highway slope	Sowell Road highway slope	Laboratory SWRC Curve (Nobahar et al., 2019)
Shape Parameters	α	0.095	0.096	0.0031
	n	1.7	1.6	2.75
	$m=1-1/n$	0.45	0.46	0.1
Soil Water Parameter	θ_r	0.19	0.19	0.018
	θ_s	0.58	0.096	0.41

**Figure 4.77** Field SWRC based on instrumentation data at Slope 1

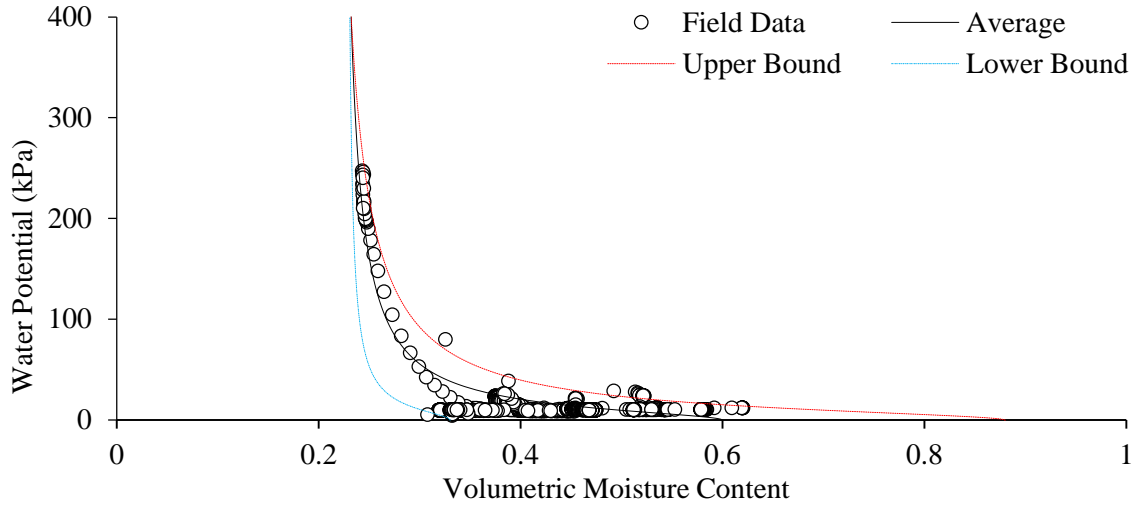


Figure 4.78 Field SWRC based on instrumentation data at Slope 2

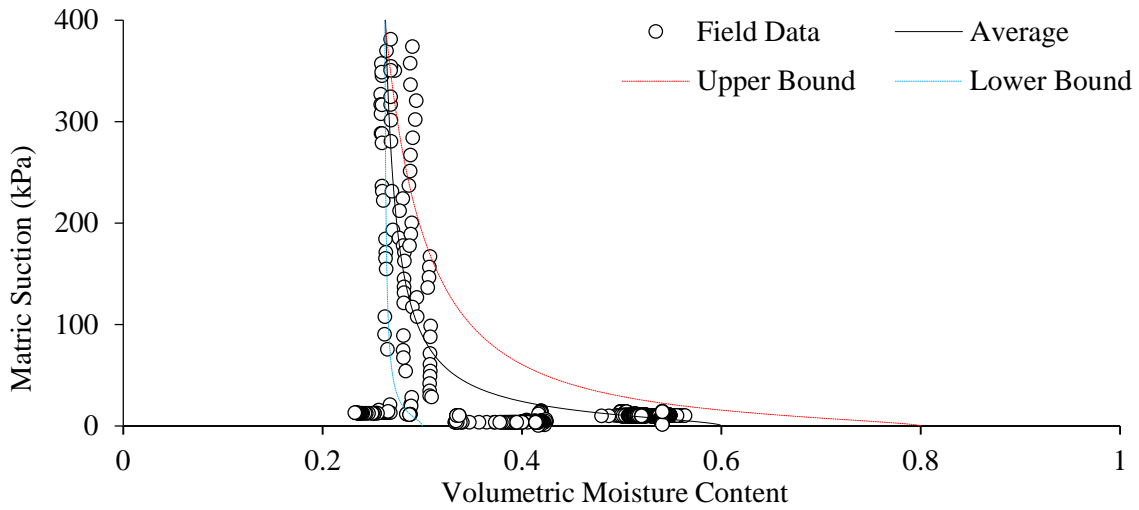


Figure 4.79 Field SWRC based on instrumentation data at Slope 3

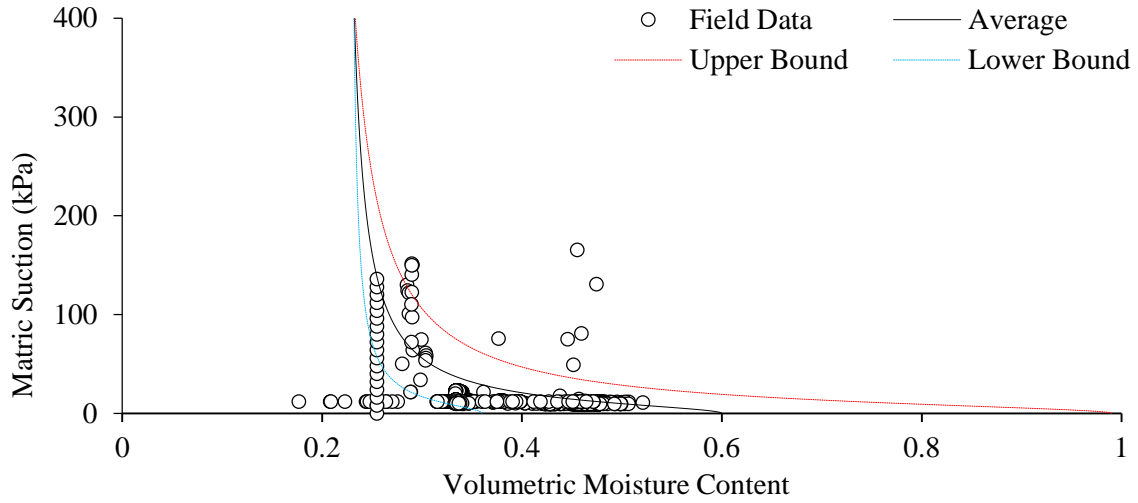


Figure 4.80 Field SWRC instrumentation data at Highland Drive highway slope

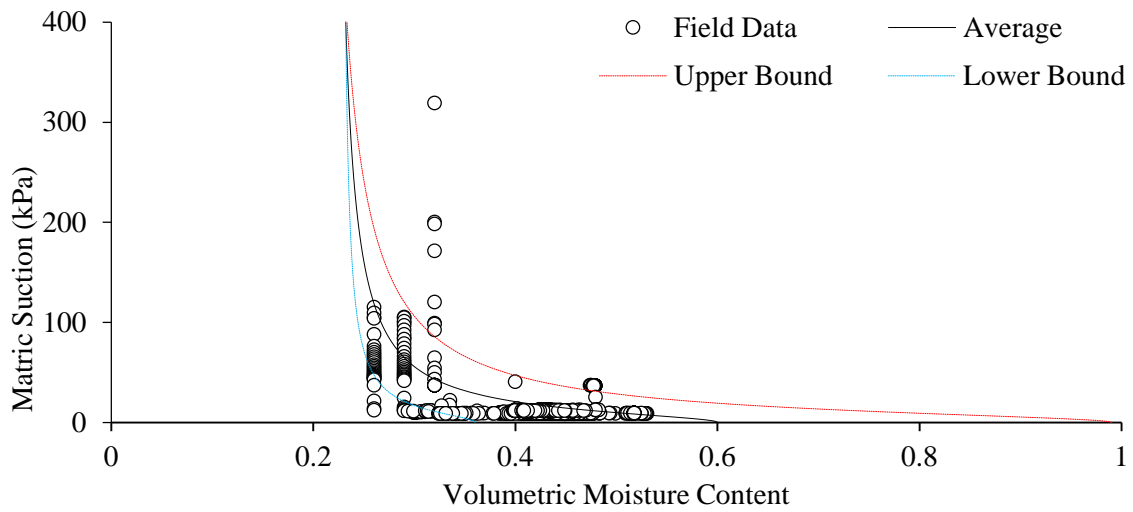


Figure 4.81 Field SWRC instrumentation data at Sowell Road highway slope

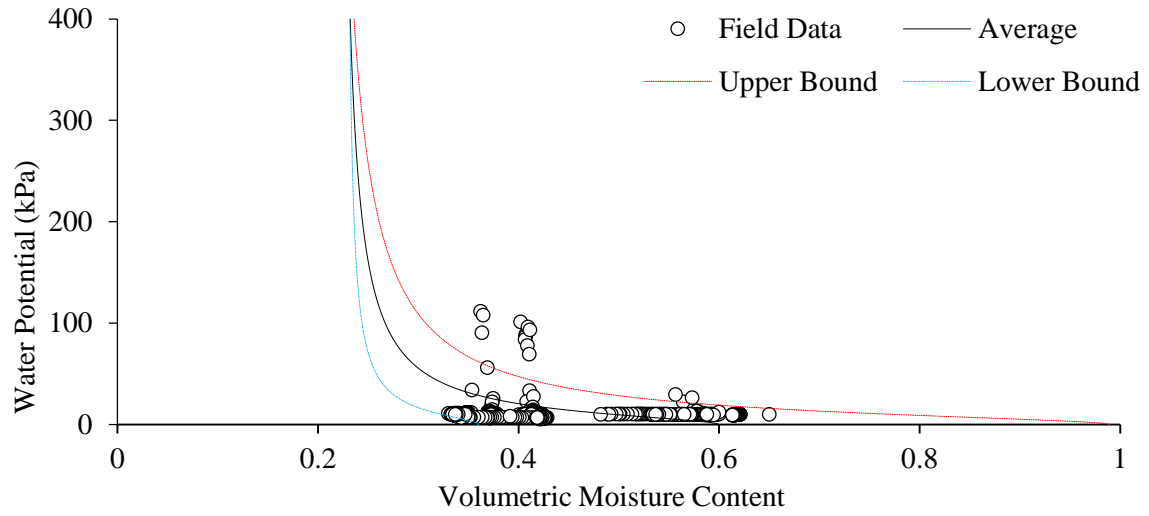


Figure 4.82 Field SWRC instrumentation data at McRaven Road highway slope

Chapter 5: NUMERICAL INVESTIGATION

5.1 Finite Element Method (FEM)

The slope stability analysis by elastoplastic finite element analysis (FEA) is an accurate, robust, and advanced method. The graphical presentation of the FEA program allows a better understanding of the failure mechanism, and the deformation analysis allows to evaluate the performance of the slope. During this study, 3D slope stability analyses were performed using the FEM program, Plaxis. The FEA was conducted to understand the infiltration behavior, and its effect on the stability of the slope, considering two different approaches, a. Flow Analysis and b. Coupled Flow Deformation Analysis.

5.1.1 Flow Analysis

The effect of rainfall on the moisture variation and matric suction of the slope was analyzed by performing unsaturated flow analysis. The flow analysis considered the following steps:

- a. Utilizing the CPT results (as described in Chapter 3) of the slopes to derive the in-situ soil parameters. The derived parameters further used in the FEA method using Plaxis. In addition to the flow parameters from the CPT results, unsaturated flow parameters of the Yazoo clay soil, based on the lab test were utilized in this study to model the effect of rainfall on the moisture variation of each slope.
- b. Perform the unsaturated flow analysis on each slope to evaluate the effect of rainfall on matric suction variation. The rainfall data was recorded for two years. The rainfall data was utilized as an input in the Finite Element Analysis.
- c. Utilizing the field performance and sensors result to calibrating the FEA model for unsaturated flow analysis to simulate the exact field behavior. Later, flow analysis was conducted in Plaxis with various intensities and durations based on PDS based IDF curve as a parametric study to determine the extent and the depth of the moisture variation within the highway slopes.

5.1.2 Coupled flow-deformation and safety Analysis

The performance and safety of the slope were analyzed with a combination of the unsaturated flow behavior to compare the field performance data. The Mohr-Coulomb soil model was utilized for deformation and stability analyses using 15 node triangular elements. The coupled flow deformation and safety analysis were performed considering the following steps:

- a. Utilizing the calibrated model from flow analysis for this phase. In addition, the shear strength properties of the soil were utilized based on the soil test data performed on the Yazoo clay, as presented in the Literature.
- b. Compare the deformation of slope from modeling results with the field performance data at different locations. Based on the comparison between the two, the soil model for finite element analysis calibrated with several iterations. The soil model was utilized to investigate the performance of the reinforced slope during the wet and dry periods with various slope and soil conditions.
- c. Conduct the FEM analysis of the slope to investigate the slope performance and safety at different rainfall period. Based on the flow analysis results, several critical rainfall periods were selected for the coupled flow-deformation analysis. With the selected rainfall period, analyses were performed in Plaxis to investigate the deformation and safety of the slope.

5.2 Slope 1: I220N Ramp Toward I55N Highway Slope

5.2.1 Flow Analysis

5.2.1.1 Model Development

The Finite Element Method (FEM) program PLAXIS 3D was used to conduct a fully flow analysis. A 15-node triangular element was used. The Mohr-Coulomb model is used to define the mechanistic behavior of soil, and the van Genuchten model is considered as the hydraulic model to define the infiltration/seepage behavior. The soil parameters were used in the numerical analysis using PLAXIS 3D, as shown in Table 5.1. The Poisson's ratio was considered to be 0.3. The precipitation amount that was used as an input for flow analysis is presented in Figure 5.1. The representative soil model for Slope 1 is presented in Figure 5.2. The global model boundary condition, as outlined in the figure, is defined as open flow along the vertical direction (Z-axis) and closed for horizontal direction (X-axis). The flow along the translation direction (Y-axis) is also considered a closed boundary. The initial depth of the water table was selected to be 8 ft. (2.43 m) below the ground surface based on observation on the field.

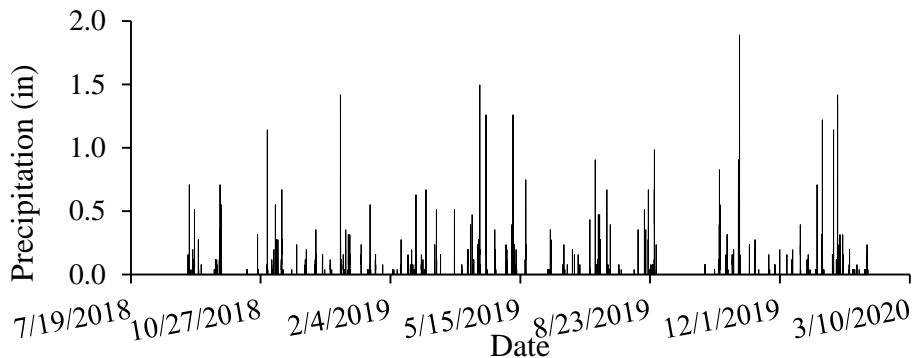


Figure 5.1 Natural daily precipitation input as a discharge function for Slope 1

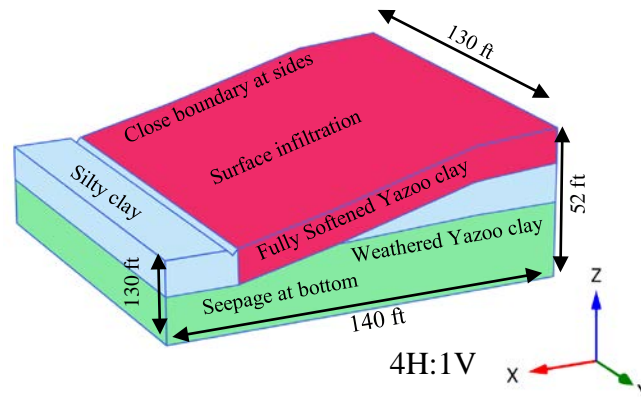


Figure 5.2 FEM soil model with the boundary conditions of Slope 1

Table 5.1 Soil parameters for FEM analysis

Parameter	Name	Unit	Fully softened Yazoo clay	Weathered Yazoo clay	Unweathered Yazoo clay	Silty clay
Bulk unit weight	γ_{unsat}	kN/m ³ (pcf)	19.7 (125.4)	20.2 (128.5)	19.9 (126.6)	19.6 (124.7)
Saturated unit weight	γ_{sat}	kN/m ³ (pcf)	21.2 (134.9)	21.1 (134.3)	19.9 (126.6)	20.5 (130.5)
Permeability	$k_x=k_y$ $=k_z$	cm/sec (ft/day)	0.0012 (1.23E-5)	3.06E-6 (0.0086)	3.06E-6 (0.0086)	3.06E-6 (0.0086)
Young's modulus	E	kN/m ² (psf)	4.70E3 (98.16E3)	7.10E3 (148.28E3)	9.50E3 (198.41E3)	4.30E3 (89.80E3)
Poisson's ratio	ν	-	0.3	0.3	0.25	0.3
Cohesion	C	kN/m ² (psf)	3.8 (79.3)	11.9 (248.5)	18.4 (384.2)	9.5 (198.4)
Friction angle	Φ	degree	19 °	19 °	20 °	20 °

5.2.1.2 Model Calibration

Figure 5.3 presents the field and numerical model comparison for a selected rainfall event of Gravimetric moisture content and matric suction at 1.5 m (4.9 ft) depth. Precipitation values were used for calibration of the model during periods of mid-August to mid-September 2018. Resulted Van Genuchten fitted parameters from field SWRC, as well as the permeability values from the literature, were utilized in flow numerical analyses. Nobahar et al., 2019 utilized a high vertical permeability value for the surficial soil layer at the slopes to simulate the impact of desiccation crack in the hydro-mechanical analysis. The high vertical permeability value as utilized by Nobahar et al., 2019 was adopted during this study for Weathered Yazoo clay. For other soil layers, the vertical and horizontal permeability values were considered same in all directions. Using this technique, the moisture and matric suction values obtained from numerical analysis found to be in very good agreement with field instrumentation results.

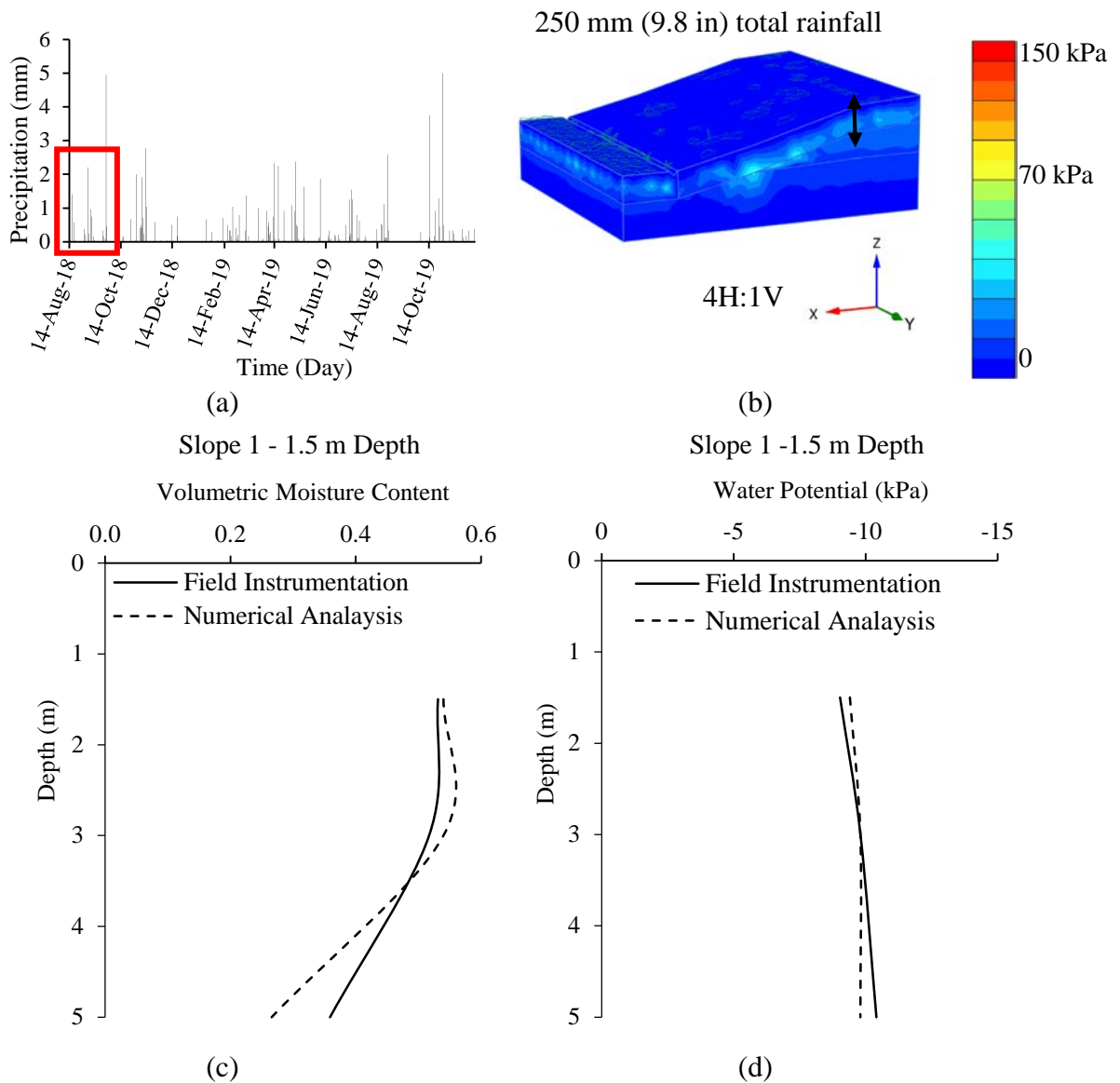


Figure 5.3 Field and numerical model comparison (a) Selected rainfall event (b) Numerical modeling (c) Vol. moisture content (d) Matric suction

5.2.2 FEM Flow Analysis Results

During the FEM analysis, the open boundary was used at the topsoil layer, whereas, the seepage boundary was used for the bottom soil layer, and the closed boundary was used for the sides of the soil model. The open boundary layer in Plaxis allows the formation of the seepage flow during the rainwater infiltration. The total daily real-time rainfall period (August 2018 to June 2019) was considered for the discharge function input for the flow analysis.

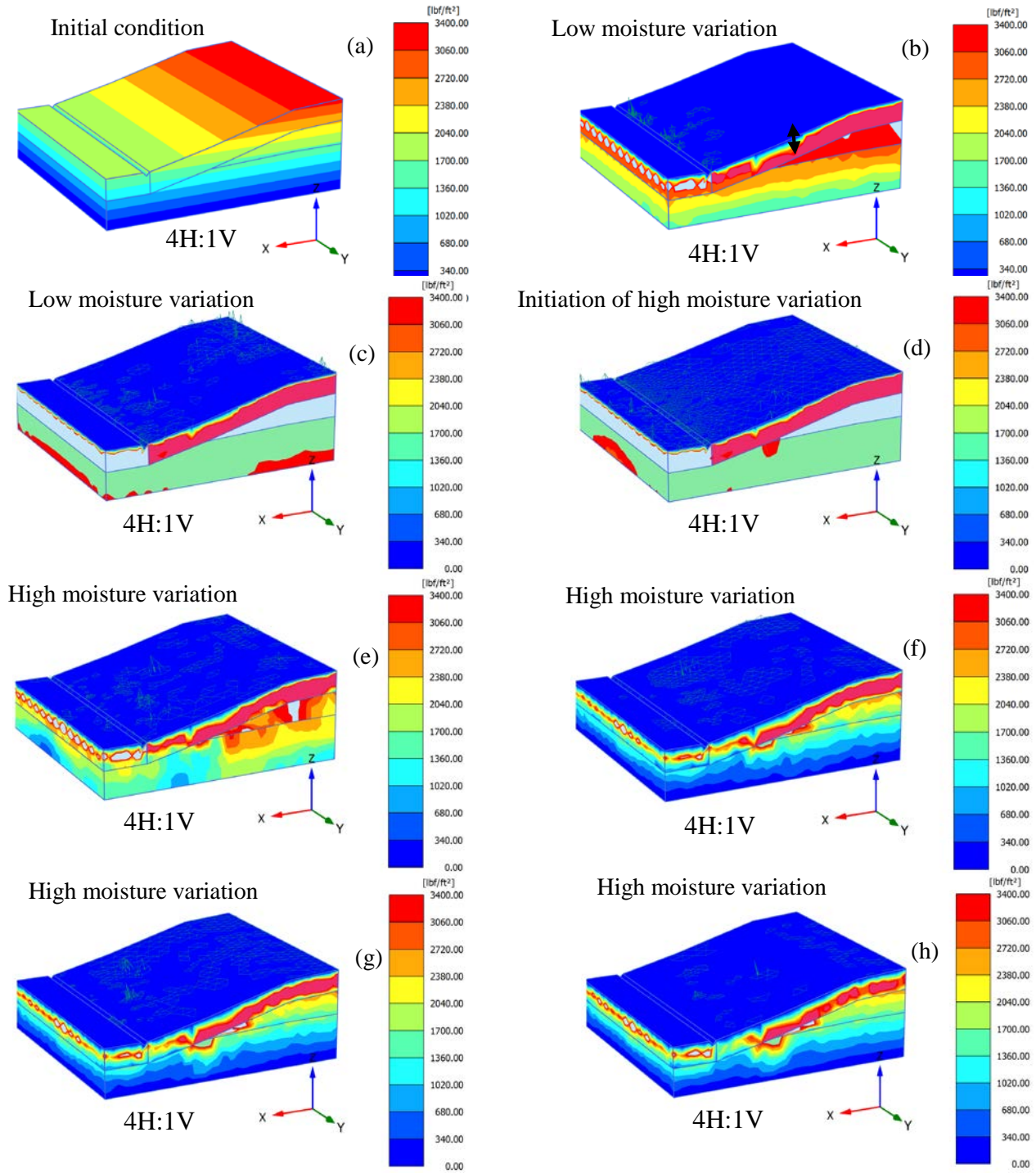


Figure 5.4 FEM flow analysis results (Depth of moisture variation profiles) for I220N Ramp Toward 155N highway slope for Max of 2 in (50.8 mm) daily rainfall (a) Before rainfall (b) 30 min after rainfall (c) 60 min after rainfall (d) 12 hrs after rainfall (e) 1 day after rainfall (f) 3 days after rainfall (g) 7 days after rainfall (h) 15 days after rainfall

Figure 5.4 presents the depth of moisture variation for fully softened Yazoo clay at the surficial layer with a maximum total rainfall volume of about 2 in (50.8 mm) for the Slope 1 which has a 4H:1V

slope ratio. Before any rainfall event, the primary value of suction was about 3400 psf (162.7 kPa), which dropped to a value of 2380 psf (113.9 kPa) after a one-day rainfall event. The suction immediately dropped at the top surficial soil layer after rainfall and continued for thirty days, representing the active wetting depth. The topsoil layer experienced a drop of moisture variation after the rainfall event and varied slightly after seven days of rainfall. Finally, after 30 days of the rainfall event, the matric suction dropped about 41.1% from the initial condition. The most critical moisture variation occurred at the topsoil layer (less than 12 ft (3.6 m)). In contrast, the change in suction continued several days to weeks post-rainfall to reach a steady value at the critical depth. The field monitoring results indicated the saturation of the slope during the time of the rainfall. The flow analysis results indicated similar behavior as observed in the field.

5.3 Slope 2: Metro Center Highway Slope

5.3.1 Coupled Flow-Deformation and Safety Analysis

5.3.1.1 Model Development

The FEM program Plaxis was used to conduct coupled flow-deformation analysis. In this technique, Plaxis analyzes the simultaneous development of deformations and pore pressures in saturated and partially saturated soils because of time-dependent changes in rainfall. When rainfall is applied to the slope, infiltration is generated and, consequently, pore water pressure is measured, and the stress profile is developed.

The model in PLAXIS makes use of the extended Mohr-Coulomb concept to describe the shear strength behavior of unsaturated soil (Fredlund et al., 1993). It is presented in equation (5.1). In Equation 5.1, C' are the cohesion at zero matric suction and zero normal stress, $(A - B_a)_f$ is the net normal stress on the failure plane at failure, ϕ' is the angle of internal friction associated with the net normal stress variable, $(B_a - C_w)_f$ is the matric suction at failure, and ϕ^b is the angle of internal friction angle that is associated with matric suction. The ϕ^b describes the rate of increase in shear strength relative to matric suction. The soil parameters, as presented in Table 5.2, were used in the numerical analysis.

$$\tau_f = C' + (A - B_a)_f \tan \phi' + (B_a - C_w)_f \tan \phi^b \quad (5.1)$$

Based on the material stiffness, Poisson's ratio was considered to be 0.3. The soil parameters for the numerical analysis in PLAXIS 2D are presented in Table 5.2. The soil model for this analysis is presented in Figure 5.5. During the numerical study, different shear strength values for the topsoil layer (weathered Yazoo clay in active zone) were utilized. 2D and 3D FEM analysis was conducted considering the following criteria:

- i. Flow behavior in 2D and 3D environment with Different intensity and Duration of Rainfall
- ii. Effect of Changes in the Shear Strength due to number of wet-dry cycles at the active zone of weathered Yazoo clay
- iii. Effect of Changes in the Shear Strength throughout the life of the slope from Peak, Fully Softened and Residual Shear Strength at the active zone of weathered Yazoo clay

The current study considered the depth of the active zone as 3.5 m (12 ft.) below the topsoil layer. Below the active zone, the shear strength of the Yazoo clay soil remains constant. The values of strength parameters selected for soil layer 2 and soil layer 3 were established from CPT test results. The different shear strength value for this analysis are presented in Table 5.3, and Table 5.4, which is discussed later in this chapter. The discharge function for the 3D coupled flow deformation analysis is presented in Figure 5.6. Later a parametric study was conducted to investigate changes in the shear strength and different intensity and duration of rainfall at different slope ratio (2H: 1V, 3H: 1V and 4H: 1V).

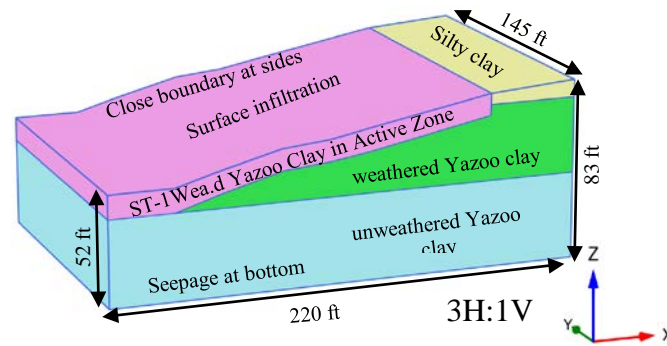


Figure 5.5 FEM soil model with the boundary conditions for Metro Center highway slope

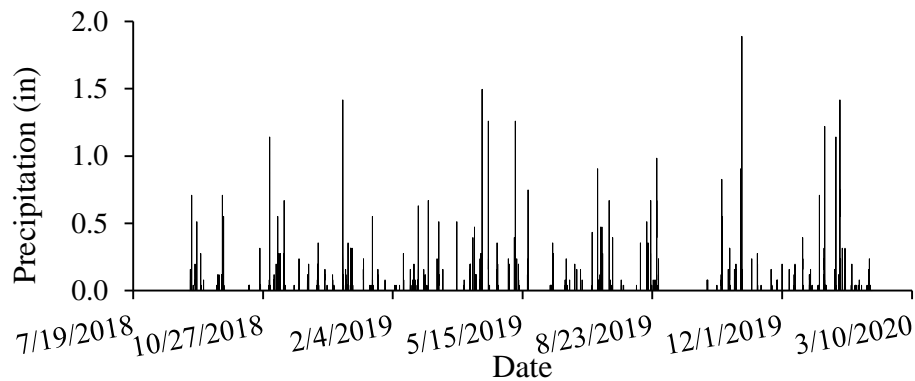


Figure 5.6 Natural daily precipitation input as a discharge function for Metro Center highway slope

Table 5.2 Soil parameters for FEM analysis

Parameter	Name	Unit	ST1- Weathered Yazoo clay in Active Zone	ST 2- Weathered Yazoo clay	ST 3- Unweathere d Yazoo clay	ST 4-Silty clay
Bulk unit weight	γ_{unsat}	kN/m ³ (pcf)	19.7 (125.4)	20.2 (128.5)	19.9 (126.6)	19.6 (124.7)
Saturated unit weight	γ_{sat}	kN/m ³ (pcf)	21.2 (134.9)	21.1 (134.3)	19.9 (126.6)	20.5 (130.5)
Permeability	$k_x=k_y=k_z$	cm/sec (ft/day)	0.0012 (1.23E-5)	3.06E-6 (0.0086)	3.06E-6 (0.0086)	3.06E-6 (0.0086)
Young's modulus	E	kN/m ² (psf)	4.70E3 (98.16E3)	7.10E3 (148.28E3)	9.50E3 (198.41E3)	4.30E3 (89.80E3)
Poisson's ratio	ν	-	0.3	0.3	0.25	0.3
Cohesion	C	kN/m ² (psf)	3.8 (79.3)	11.9 (248.5)	18.4 (384.2)	9.5 (198.4)
Friction angle	Φ	degree	19 °	19 °	20 °	20 °

5.3.2 FEM Flow Analysis Results

The variations in suction at the 3H: 1V slope for the initial phase, 30 min, 60 min, 12 hours, 1 day, 3 days, 7days, and 15 days' rainfall volumes are presented in Figure 5.7. As indicated, the suction

immediately dropped at the toe of the slope after rainfall and continued to drop during rainfall, representing the accumulation of water at the corresponding depth. It was also observed that the suction increase had continued for a few hours, even after the rainfall. It was also noticed that after a few days of rainfall, the suction increased, and the soil almost regained its original profile for the layer.

It can be seen from the mentioned Figure that before any rainfall event, the primary value of suction was about 3300 psf (140.7 kPa), which dropped to a value of 2000 psf (99.9 kPa) after a one-day rainfall event. The suction immediately dropped at the top surficial soil layer after rainfall and continued for thirty days, representing the active wetting depth. The topsoil layer experienced a drop of matric suction variation after the rainfall event and varied slightly after seven days of rainfall. Finally, after 30 days of the rainfall event, the matric suction variation dropped about 38.11%. The most critical matric suction variation occurred at the topsoil layer (less than 12 ft (3.6 m)). In contrast, the change in suction continued several days to weeks post-rainfall to reach a steady value. The field investigation results have shown a drop in the matric suction after the rainfall, as indicated in Chapter 4. Therefore, the numerical flow analysis results are in a good agreement with the observed field behavior.

The flow analysis was extended evaluate the effect of different intensity and duration of rainfall, based on PDS based Intensity-Duration-Frequency (IDF) curve. The details of the flow analysis is presented in the following section.

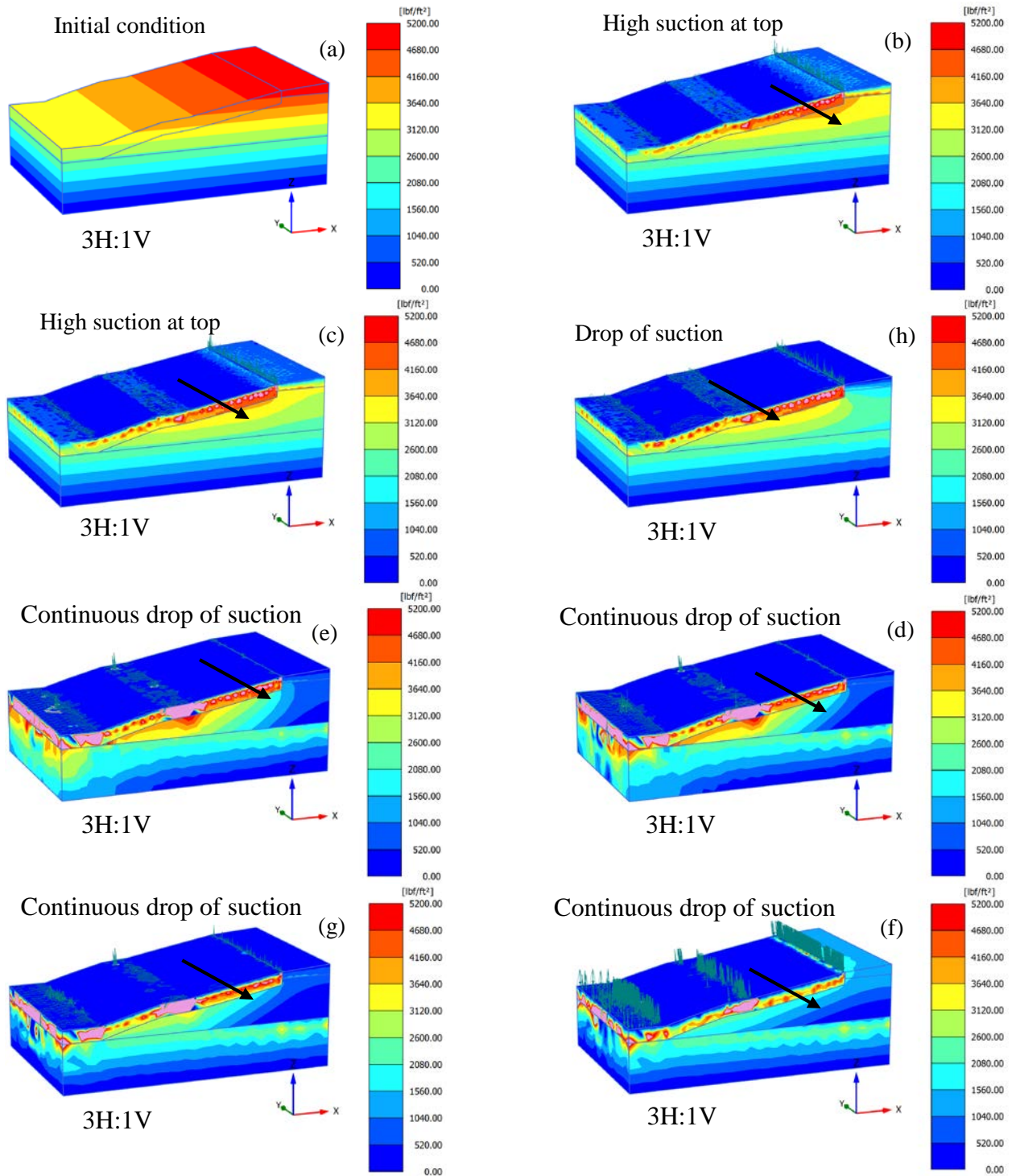


Figure 5.5 FEM flow analysis results (Depth of moisture variation profiles) for Metro Center highway slope for Max of 2 in (50.8 mm) daily rainfall (a) Prior to rainfall (b) 30 min after rainfall (c) 60 min after rainfall (d) 12 hrs after rainfall (e) 1 day after rainfall (f) 3 days after rainfall (g) 7 days after rainfall (h) 15 days after rainfall

Parametric Study on the Effect of Rainfall Intensity and Duration - The Partial Duration Series (PDS) based Intensity Duration and Frequency (IDF) curve of precipitation with a 100-year return period, based on the 2014 NOAA Atlas for Jackson, Mississippi (NOAA Daily Report, 2014), is utilized for the parametric study, as presented in Figure 5.8. Based on the NOAA database, different volumes of rainfall (70.8 mm (2.7 in) and 271.7 mm (10.6 in)) with different durations of rainfall (2 hrs. to 3 days) were selected based on the IDF curve for the area. Precipitation with different total rainfall volumes (70.8 mm (2.7 in) to 312.4 mm (12.2 in)) was applied to the soil model to assess the coupled flow-deformation behavior during rainfall. The flow through the topsoil was determined for each of the intensities, assuming rainfall durations lasted 30 min, 60 min, 2 hours, 6 hours, 12 hours, 1 day, and 3 days. The Van Genuchten model was used as the hydraulic model. Nobahar et al. (2019) developed the Soil Water Retention Curve (SWRC) curve for the Yazoo Clay in Mississippi. The Van Genuchten fitting parameters of the Yazoo Clay was utilized during this study. During the dry period, the highly plastic clay soil developed desiccation cracks, which might have significantly increased the permeability vertically in the active zone. However, due to the desiccation cracks, the permeability in the horizontal direction might not have any effect and could have remained unchanged (Khan et al., 2019, Nobahar et al., 2019). Yazoo Clay usually has significant cracks, which have been observed in the laboratory as well as in the field. The diameter of the cracks varies from 3 mm (0.118 in) (laboratory) to 304.8 mm (12 in) (field), where the boundary plays a significant role in defining the size of the cracks. Therefore, a high vertical permeability value of $k_v = 0.034$ cm/sec (96.37 ft/day) was used for the part mentioned above for each of the slopes (surficial soil layer at the slope) to simulate the effect of the desiccation crack. It should be noted that with the changes in the wet-dry cycles, the horizontal permeability of the clay soil also gets impacted. However, due to a lack of available data and literature on the change in the k_h of Yazoo Clay, a constant value of the k_h was considered, which also showed good agreement with the existing scenario of the slopes in Mississippi. The value for horizontal permeability was selected as $k_h = 3.06 \times 10^{-6}$ cm/sec (0.0086 ft/day). In other clay layers, the permeability for both the horizontal and vertical directions was selected as 3.06×10^{-6} cm/sec (0.0086 ft/day), respectively. The parametric study was extended on slope have 2H:1V, 3H:1V and 4H:1V slope ratio.

Figure 5.9 presents the suction profile variation of the slope made of Yazoo clay for different rainfall periods. In this analysis, the 3H:1V slope ration is considered. It should be noted that during the FEM analysis, the infiltration behavior was assigned at the topsoil layer, which allowed the ponding of water to simulate realistic behavior. From FEM analysis results, ponding exists in almost all surficial soil for the toe of the slope with different rainfall intensities. However, for the 12-hours and three days' rainfall intensities, ponding hardly can be found on the slope, due to the low intensity. Ponding decreased the amount of suction for the topsoil layer at the toe. Ponding of the water is very commonly visible at the failed slope sites in Mississippi.

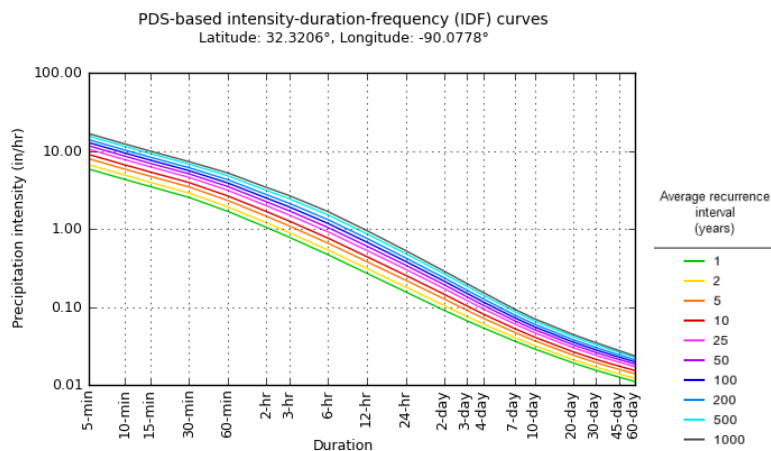


Figure 5.6 PDS based IDF curves of Jackson, Mississippi (NOAA, 2014)

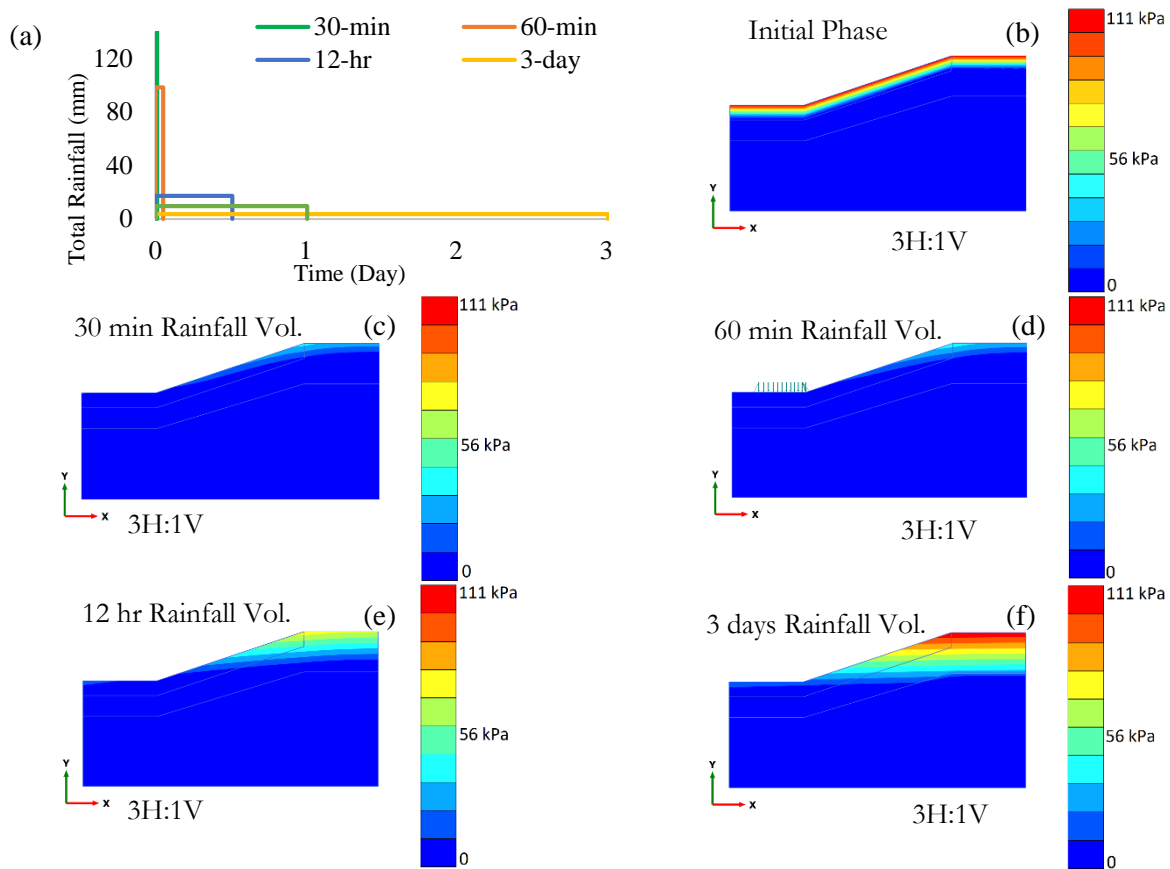


Figure 5.7 Suction profile variation of 3H:1V slope made of Yazoo clay (a) Flow functions to simulate the rainfall in FEM analysis (b) Suction profile before rainfall (c) Suction profile after rainfall-30 min (d) Suction profile after rainfall-60 min (e) Suction profile after rainfall-12 hours (f) Suction profile after rainfall-3 days

Figure 5.10 presents the suction variation for a rainfall volume of 234.1 mm (9.21 in) for the three slope ratios 2H:1V, 3H:1V, and 4H:1V respectively. Before any rainfall event, the primary value of suction was 30.6 kPa (4.43 psi). It decreased to a value of 23.9 kPa (3.46 psi) at the 2H:1V slope (21.8% decrease), to 13.4 kPa (1.94 psi) at the 3H:1V slope (52% decrease) and to 6.7 kPa (0.97 psi) at the 4H:1V slope (41.6% decrease) after a 1-day rainfall event with about 234.1 mm (9.21 in) of total rainfall volume. Based on the FEM analysis results depicted in Figure 5.10, the suction value dropped with the milder slope ratio, name the slope ratio. The suction immediately dropped at the top after rainfall and continued to drop for two days, representing the accumulation of water at the corresponding depth near the crest. After 7 days, still, the suction continued to drop. The suction decreased by about 58% from initial conditions to 7 days of rainfall. As observed, the critical section of the slope, which experienced the most amount of variation in suction, is the crest of the slope for the 2H:1V slope ratio, whereas, in milder slope ratios, the variation occurred from middle to the crest of the slope.

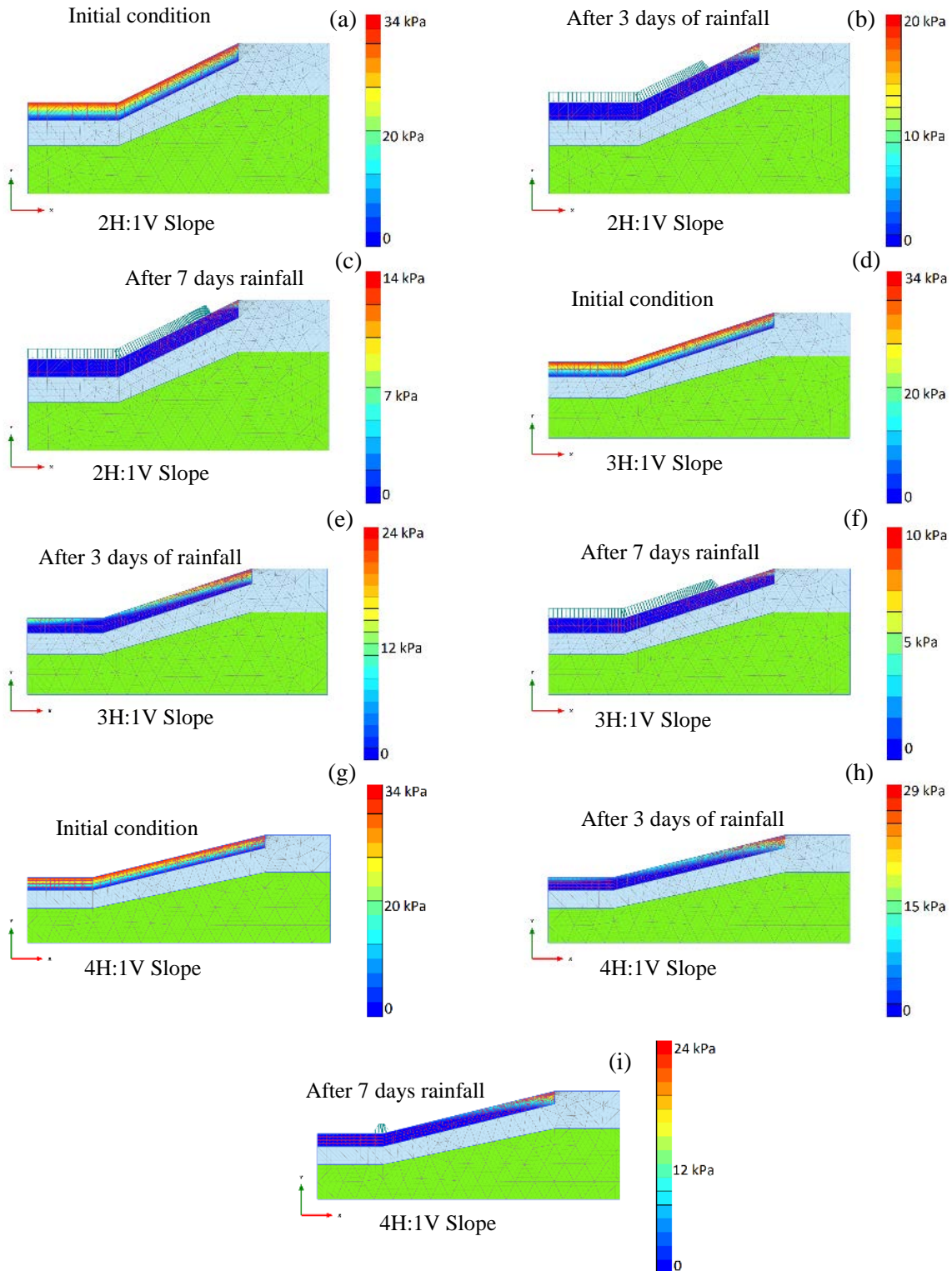


Figure 5.8 Suction variation for total rainfall amount of 4.7 in with fully softened shear strength, 2H:1V slope (a) Before rainfall (b) After 3 days rainfall (c) After 7 days rainfall, 3H:1V slope (d) Before rainfall (e) After 3 days rainfall (f) After 7 days rainfall, 4H:1V slope (g) Before rainfall (h) After 3 days rainfall (i) After 7 days rainfall

It was also observed that the variation in suction showed a 45% increase from the 2H:1V slope to the 4H:1V for 234 mm (9.21 in) of rain after 3 days of steady rainfall. Similarly, the same trend was observed and resulted in about a 70% rise in suction from steepest to the mildest slope ratio (2H:1V to 4H:1V). Consequently, for a high range of suction, the crest of the slope is very susceptible to soil suction variation.

The variations of change in suction near the crest, with a fully softened shear strength, for the topsoil layer with two total rainfall amounts, are presented in Figure 5.11. The change of suction refers to the change from the initial suction value before rainfall to the change after a given rainfall duration. Figure 5.11 shows various rainfall durations with a 100-year return period with a total rainfall amount of 234.1 mm (9.21 in), considered as high rainfall and 98.5 mm (3.87 in) considered as low rainfall. The suction was observed to drop significantly with a higher intensity and longer duration rainfall. Moreover, the change in suction was more significant at depths of 1 to 2 meters (39.3 to 78.7 in) beneath the topsoil layer with a low amount of total rainfall when compared to high total rainfall amounts. Based on the FEM analysis results, the critical suction variation zone was observed near the crest, topsoil layer, within the bounds of about 2 meters (6.5 ft).

Consequently, for the observed suction change, the study investigated the surficial layer and the zone close to the crest. The drop of suction was instantaneous near the crest for different-rainfall amounts and durations for the three slope ratios, as depicted in Figure 5.11(a) to Figure 5.11 (f). The constant values of suction at the crest, in Figure 5.11(b) and Figure 5.11 (e), indicated that the percolated water could not drain from the slope due to the very low permeability of the highly plastic clay soil. Furthermore, based on the FEM analysis results, it was observed that suction variation increased as the slope ratio became milder, or close to the crest. For instance, the suction initiated at the early time of rainfall (234.1 mm (9.21 in) total rainfall) is about -120 kPa, -150 kPa, and -170 kPa for 2H:1V, 3H:1V and 4H:1V slopes respectively. Similar trends are also observed for the slope ratios with a low rainfall amount (98.5 mm (3.87 in) total rainfall).

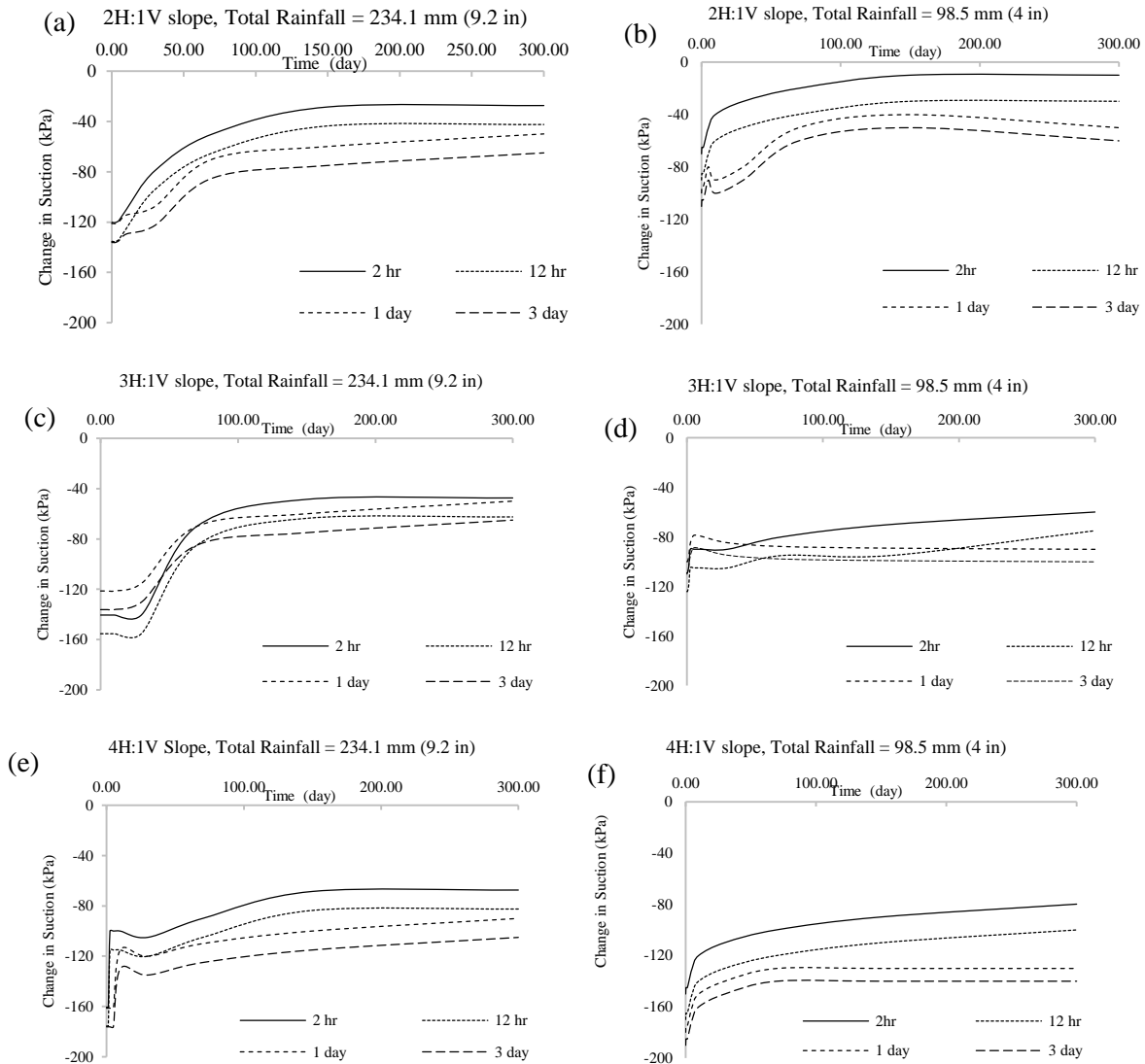


Figure 5.9 Variation of change in suction near the crest with Fully Softened Shear Strength at topsoil layer (a) with 234.1 mm (9.2 in) total rainfall of the slope 2H:1V (c) with 234.1 mm (9.2 in) total rainfall of the slope 3H:1V (e) with 234.1 mm (9.2 in) total rainfall of the slope 4H:1V (b) with 98.5 mm (4 in) total rainfall of the slope 2H:1V (d) with 98.5 mm (4 in) total rainfall of the slope 3H:1V (f) with 98.5 mm (4 in) total rainfall of the slope 4H:1V

The variations of change in suction at the crest, middle and toe of the slope at topsoil layer for a 100-year return period with two total rainfall amounts (98.5 mm (3.87 in) and 234.1 mm (9.21 in) total rainfall amounts) are presented in Figure 5.12. The variations were due to similar rainfall intensity in Figure 5.12. The maximum change in suction was observed in 2H:1V slope within 100 days in almost all three zones of the slope (crest, middle, and toe). Moreover, the change in suction was more significant at milder slope ratios due to longer periods of high rainfall intensity. The change in suction was not substantial at the middle or toe of the slope.

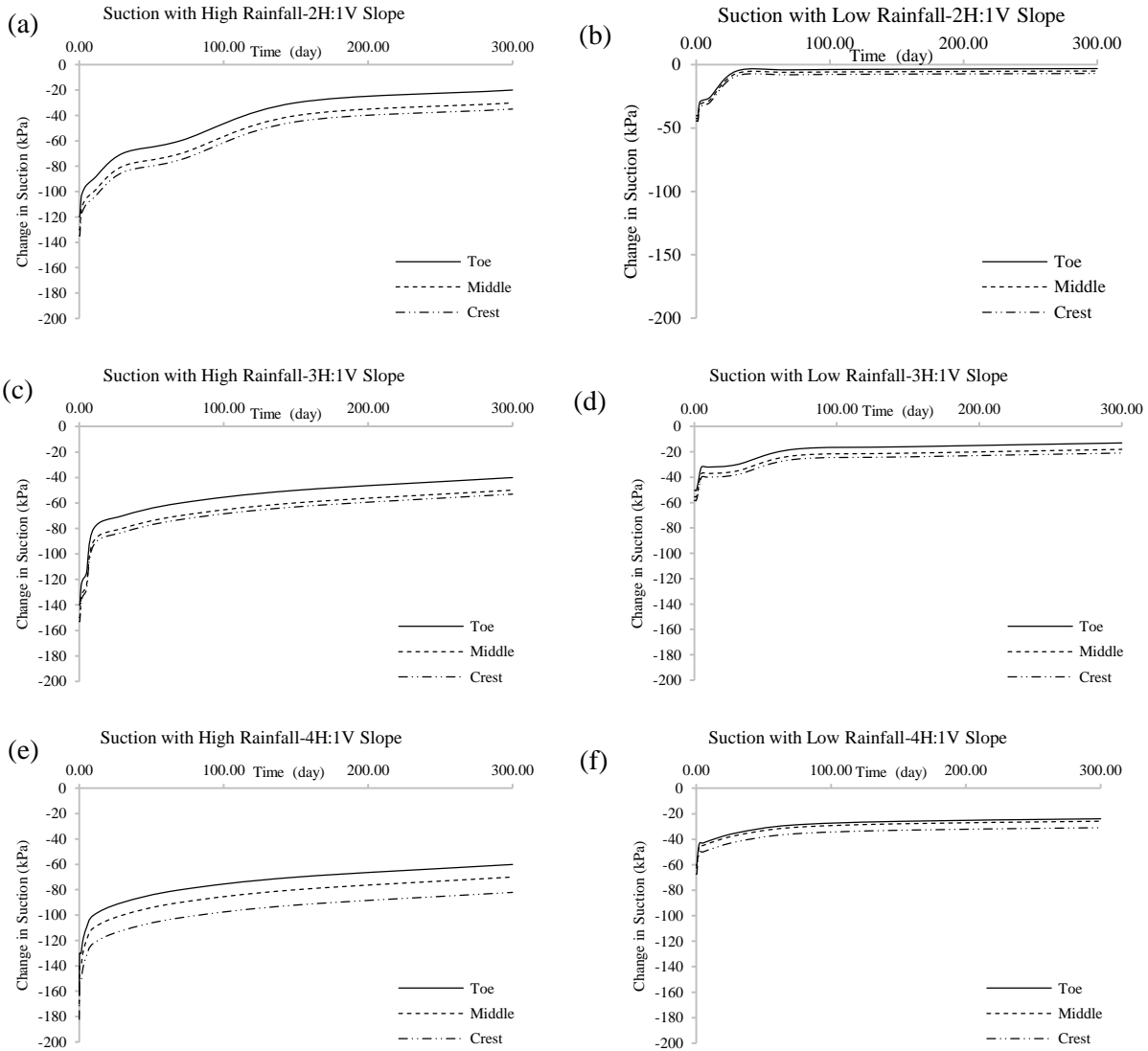


Figure 5.10 Change in suction at the crest, middle, and toe of the slope with Fully Softened Shear Strength at topsoil layer (a) with 234.1 mm (9.2 in) total rainfall of the slope 2H:1V (c) with 234.1 mm (9.2 in) total rainfall of the slope 3H:1V (e) with 234.1 mm (9.2 in) total rainfall of the slope 4H:1V (b) with 98.5 mm (4 in) total rainfall of the slope 2H:1V (d) with 98.5 mm (4 in) total rainfall of the slope 3H:1V (f) with 98.5 mm (4 in) total rainfall of the slope 4H:1V

5.3.3 Stability Analysis

The FEM program PLAXIS 2D was used to conduct coupled flow-deformation analysis, which analyzes the simultaneous development of deformations and pore pressures in saturated and partially saturated soils. The developed stress profile from coupled flow deformation analysis is used as an initial condition to conduct the stability analysis and determine the factor of safety of the slope. In Plaxis, the strength reduction analysis or phi-c reduction analysis is performed to calculate the factor of safety.

5.3.4 FEM Stability Analysis Results

In the shear strength reduction method, the factor of safety of a slope is defined as the factor in which the original shear strength parameters can be reduced to bring the slope to the point of failure (Griffith and

Lane, 1999). During this study, stability analysis was conducted considering the unsaturated moisture and matric suction variation of the soil, as investigated by the fully-coupled flow analysis. Time-dependent hydro-mechanical behavior of the soil is described in a coupled format, taking both deformation and groundwater flow into account, in which mixed equations of displacement and pore pressure, are solved simultaneously. Based on the material stiffness, Poisson's ratio and Young's Modulus were 0.3 and 4,788 kN/m² (120,000 psf). During this study, different shear strength values for the topsoil layer were utilized, considering three different cases in the active zone.

The factor of safety of the slope was determined using the phi-c reduction method in Plaxis, which is alternately known as the shear strength reduction analysis. In the shear strength reduction method, the factor of safety of the slope is defined as the number by which the original shear strength parameters must be divided in order to bring the slope to the point of failure. In Plaxis, the shear strength parameters $\tan \phi$ and c of the soil are successively reduced until failure of the slope occurs to determine the failure shear strength. The reduced strength parameters c'_f and ϕ'_f are defined in Equation 5.2 and Equation 5.3, as suggested by Griffiths and Lane (1999).

$$c'_f = \frac{c}{FS} \quad (5.2)$$

$$\phi'_f = \arctan\left(\frac{\tan \phi}{FS}\right) \quad (5.3)$$

Where, c is available cohesion of soil, c'_f is cohesion at failure, ϕ is available friction angle, ϕ'_f is friction angle at failure, and FS is the Factor of Safety.

The finite element analysis was conducted considering the effect of different rainfalls and changes in the shear strength at the top soil layer. The analysis results are presented in Two major category:

1. Effect of Wet-Dry Cycles at 2 different rainfall conditions.
2. Effect of Changes in the Shear Strength from Peak, Fully Soften, and Residual Conditions with the presence of different intensity and duration of rainfall.

5.3.4.1 Effect of Wet-Dry Cycles on the Stability of Highway Slope

The slope made by Yazoo clay has very high shear strength, which get softened over the period of time, as the soil is exposed to different number of wet-dry cycles. The finite element modeling is extended to investigate the effect of the changes in shear strength as the soil is exposed to different number of wet-dry cycles. To investigate this effect, at the topsoil layer, the shear strength of the soil is utilized from the study performed by Khan et al., 2019, as presented in Table 5.3. The other soil properties and geometry remained the same as presented in Figure 5.6 and Table 5.2. During this analysis, four different cases of stability condition were analyzed, considered Case I as the as-built condition, Case II as the slope subjected to 3 numbers of wet-dry cycles, Case III as the slope subjected to 5 numbers of wet-dry cycles and Case IV as slope subjected to 7 numbers of wet-dry cycles.

Table 5.3 Wet-Dry Cycle Shear Strength Values for Yazoo clay (Soil 1 in Table 5.2)

Case	Wet-Dry Cycles	Cohesion kPa (psf)	Friction angle (deg.)
I	0N	18.44 (385)	20.34
II	3N	5.98 (124)	21.99
III	5N	4.79 (100)	20.87
IV	7N	4.31 (90)	18.42

The slip surface for the 126.2 mm (4.9 in) rainfall volume of the 3H: 1V slope within four cases is presented in Figure 5.13. As presented in Figure 5.13, the deformation contours are presented. During the

phi-c reduction analysis in Plaxis 2D, at the failure strength, the factor of safety of the soil is determined. Besides the determination of the soil strength, the FEM package calculates displacement at the soil body. The displaced area represents the failure area (deformation contour), and the edge of displaced soil is presenting the slip surface of the slope. Based on the FEM results, it can also be observed that the factor of safety changed with different rainfall durations.

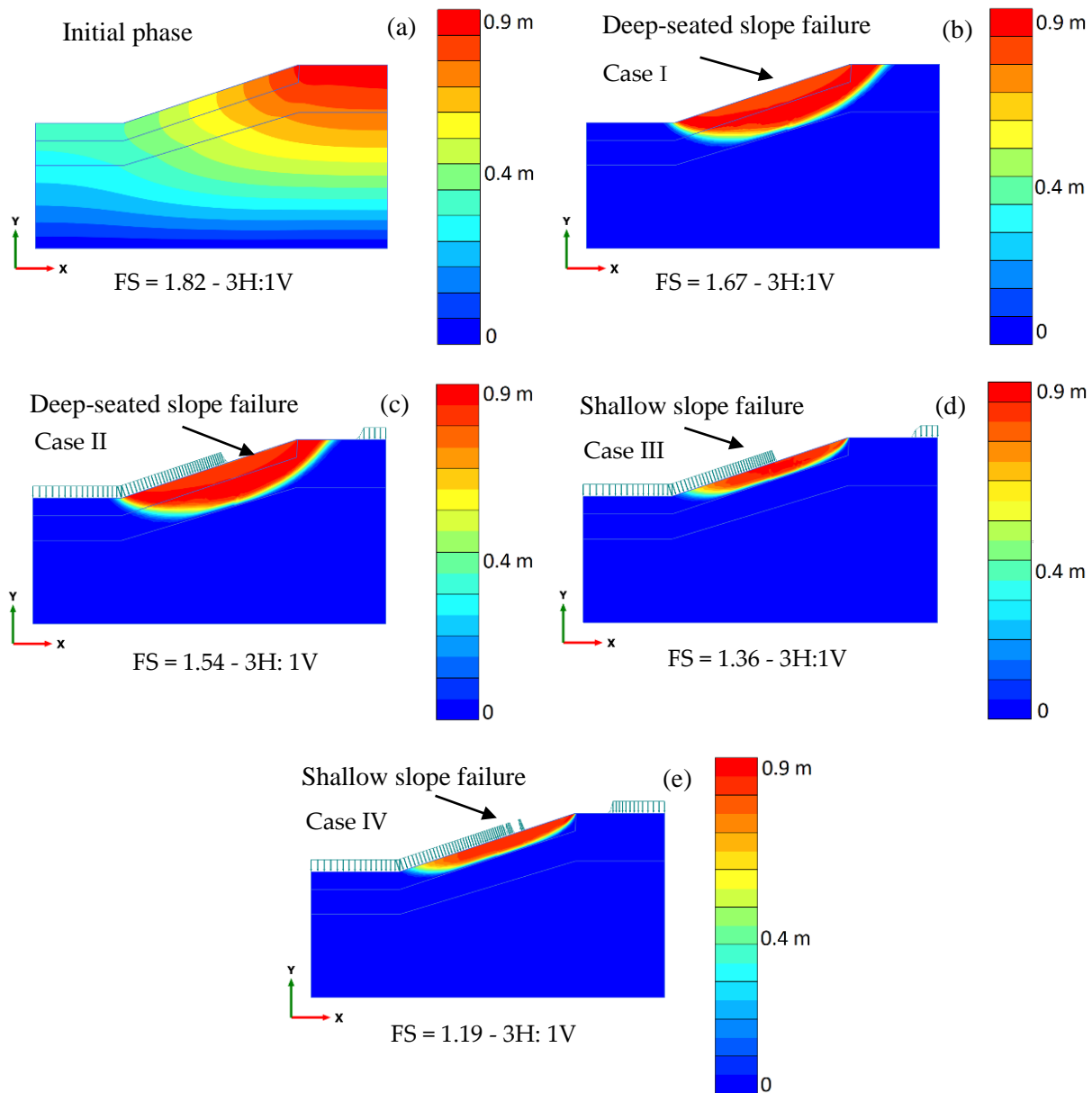


Figure 5.11 Change in factor of safety for 4.7 in/hr. (126.2 mm/hr.) with 2 hours of rainfall (a) before rainfall (b) Case I (c) Case II (d) Case III (e) Case IV

Figure 5.14 shows the change in the slip failure surface for Case IV (7 numbers of wet-dry cycles). In this part, the soil shear strength is with seven wet and dry cycles, and the factor of safety varied from 1.28 to 1.2. As shown, the soil strength in the top layer with seven cycles of wet and dry decreased and was very susceptible to failure. Therefore, the slope failure took place due to the reduction in shear strength with an increased number of wet and dry cycles at the steep part of the slope.

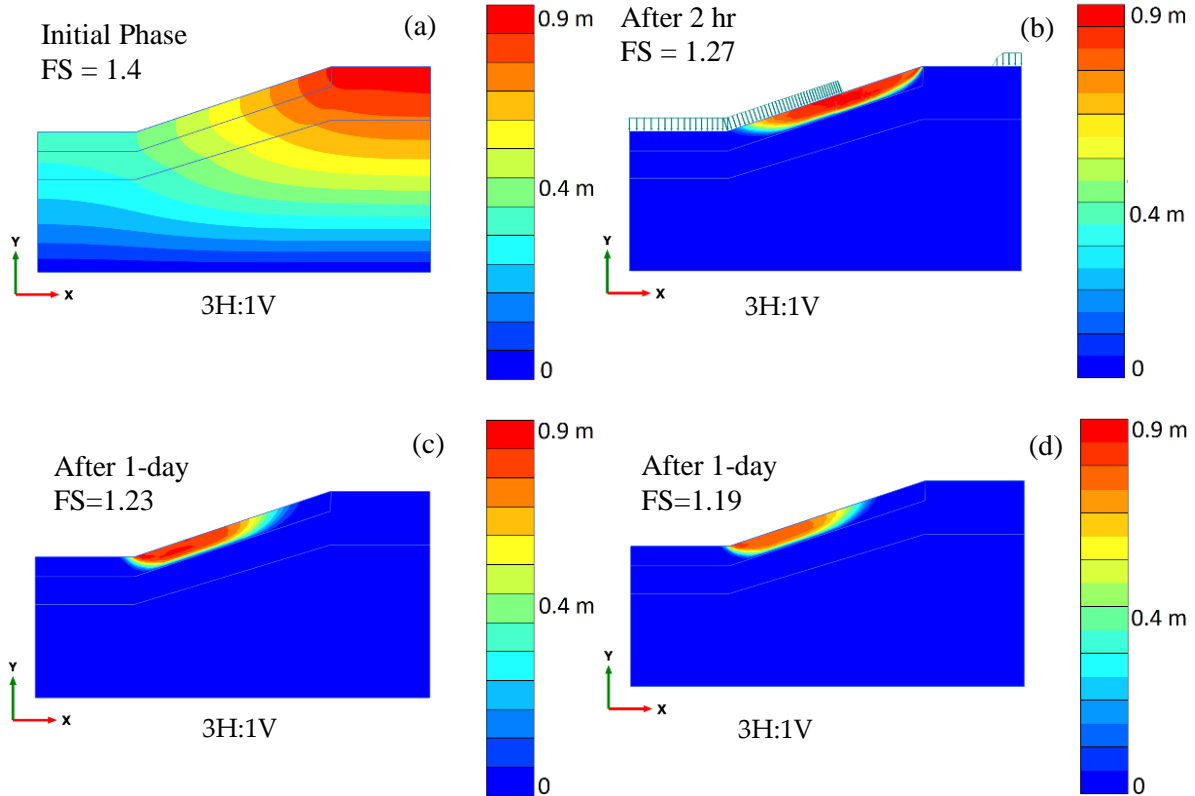


Figure 5.12 Changes in factor of safety for 4.7 in/hr. (126.2 mm/hr.) with 2 hours of rainfall (a) prior to rainfall (b) 2 hours rainfall duration (c) after 1-day (d) after 3-day

The factor of safety for the 3H: 1V slope with consideration of the mentioned four cases is presented in Figure 5.15. The Figure mentioned above shows the progressive variation of the factor of safety for Case I to Case IV. The failure surface was observed to be deep-seated in Case I and shallow in Cases II to IV, which is due to the progressive change in the shear strength due to the repeated wet-dry cycles. As the rainfall influenced the matric suction value at the topsoil, a significant change in the factor of safety occurred, leading to shallow slip surface failure. The factor of safety considering the effect of two total rainfall periods of Rainfall Volume (RV)= 126.2 mm (2 hours) and RV = 271.7 mm (3 days) reduced from 1.7 to 1.2 and 1.68 to 1.02 respectively considering the effect of the 7th wet-dry cycles at the topsoil. Consequently, it can be observed that the factor of safety reached a critical value after the topsoil layer shear strength was replaced with the seven wet and dry cycle's value with higher total rainfall. It is also observed that at dry state with 7 wet-dry cycles, the slopes are stable (FS = 1.4). However, the slope will fail at the presence of consistent 3 days of rainfall after 7N of wet-dry cycles.

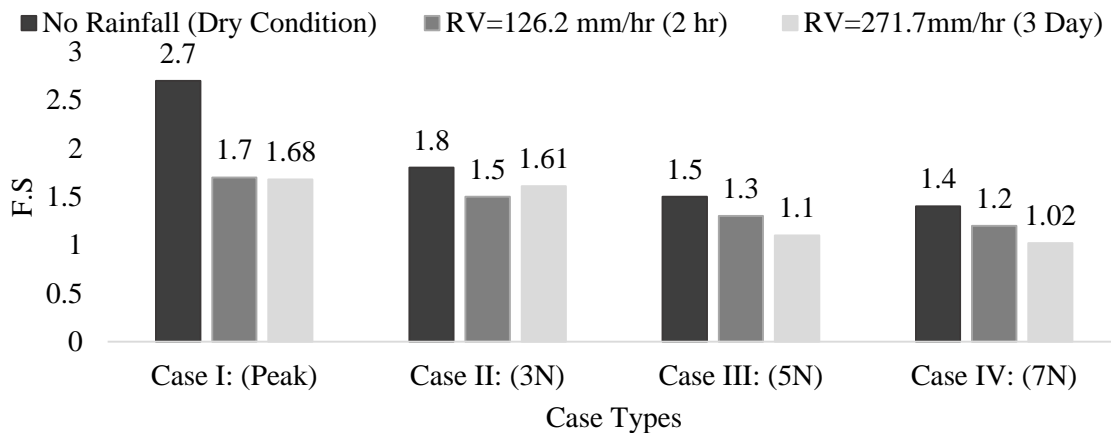


Figure 5.13 Change in the factor of safety

5.3.4.2 Effect of Changes in Shear Strength on the Stability of Highway Slope

The stability analysis results for the slopes with fully softened shear strengths was analyzed with 234.1 mm (9.21 in) of rainfall and is presented in Figure 5.17. It should be noted that shear strength value, as presented in Table 5.4, was utilized for the top layer, whereas other parameters are presented in Table 5.2.

Table 5.4 Variation in shear strength of Yazoo clay

Soil Layer	Case 1 Peak Shear Strength	Case 2 Fully Softened Shear Strength	Case 3 Residual Shear Strength
Topsoil Layer	c = 18.4 kPa φ = 20.2 deg.	c = 10.8 kPa φ = 18.6 deg.	c = 5.45 kPa φ = 12.8 deg.

From the FEM analysis results, it can be noted that the factor of safety is decreasing with the steeper slope ratios. The factor of safety reached a minimum value of 1.56, with 234.1 mm (9.21 in) of rainfall (after 7 days). The initial factors of safety for three slope ratios (2H:1V, 3H:1V, and 4H:1V) with 234.1 mm (9.21 in) total rainfall applied were 1.8, 2.3, and 2.8, respectively. Figure 5.16 presents the slope stability analysis results for three slope ratios (2H:1V, 3H:1V, and 4H:1V). Three different shear strengths of Yazoo clay were utilized at the topsoil layer with three different slope ratios to evaluate the progressive change in the stability of the slope. The depth of the active zone was 3.5 m (12 ft.) near the crest. Based on result observations, the three slope ratios experienced a shallow slope failure condition and showing a deduction in their stabilities. A friction angle-cohesion reduction analysis was conducted, and results indicated that the factor of safety of the slope reduced to 1.15, 1.38, and 1.77 for the 2H:1V, 3H: V, and 4H:1V slopes, respectively. The failure plane of the slopes is illustrated in Figure 5.16. The saturation at the surficial soil layer played an important role in this analysis, and as a result, an almost 40% reduction in the factor of safety was observed.

The variation of change in the factor of safety with different rainfall volumes for peak shear strength and three slope ratios are presented in Figure 5.17. It should be noted that the variation of change in the factors of safety, due to eight rainfall intensities at 100-year return periods for the three slopes, have a similar trend in which the stability of the slope reduced progressively over time. Based on the previously mentioned figure, the change in the factor of safety was more significant at the initial rainfall period, whereas the safety factor started decreasing with the milder slope. The factor of safety was observed to be higher with peak shear strength for the milder slope (4H:1V) than the steeper slope (2H:1V).

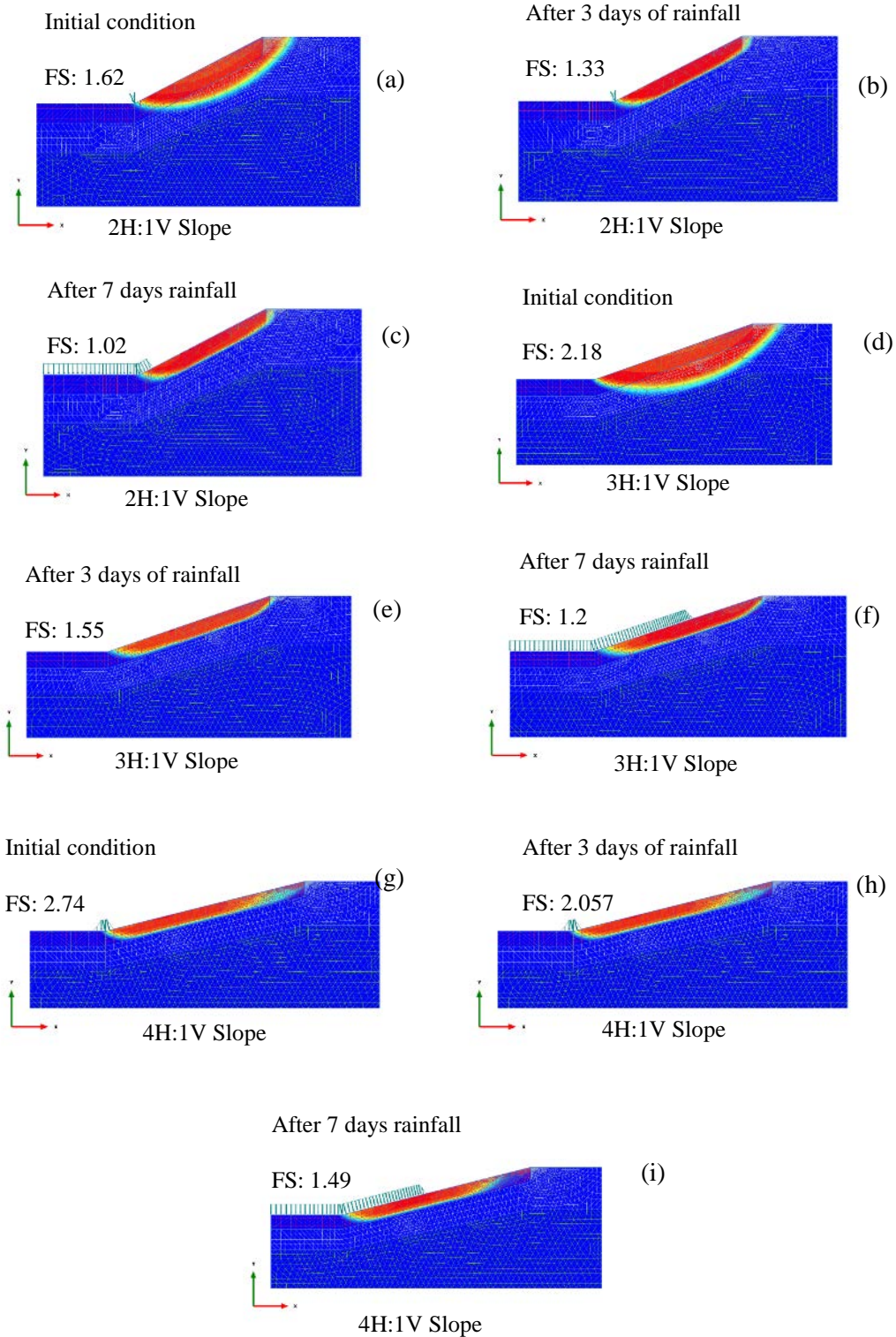


Figure 5.14 Slip surface for total rainfall amount of 4.7 in for fully softened shear strength, 2H:1V slope (a) Prior to rainfall (b) After 3 days rainfall (c) After 7 days rainfall, 3H:1V slope (d) Prior to rainfall (e) After 3 days rainfall (f) After 7 days rainfall, 4H:1V slope (g) Prior to rainfall (h) After 3 days rainfall (i) After 7 days rainfall

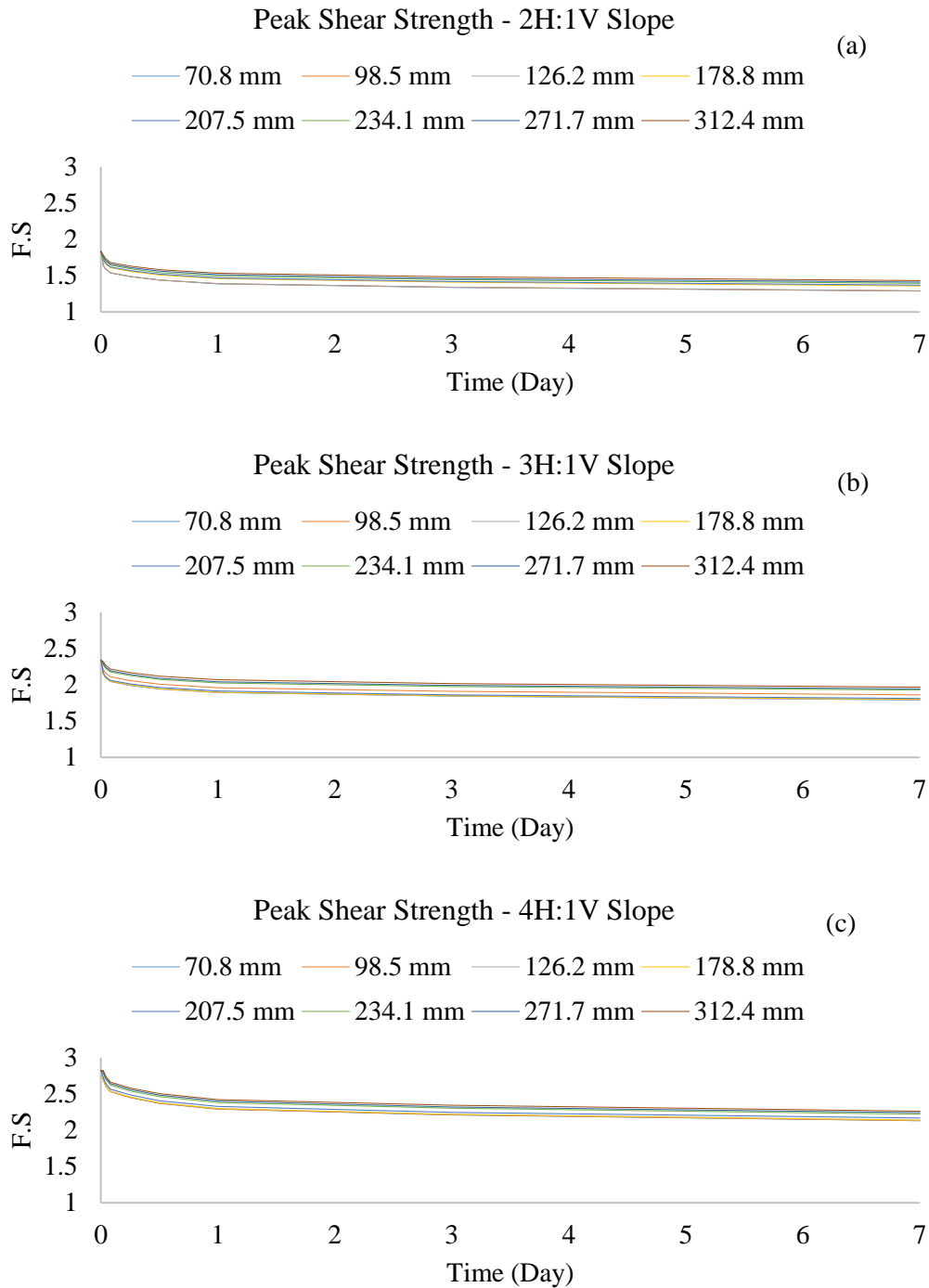


Figure 5.15 Change in the factor of safety with different total rainfall for peak shear strength
(a) 2H:1V slope (b) 3H:1V slope (c) 4H:1V slope

The variation of change in the factor of safety for the three slope ratios with different total rainfall intensities at fully softened shear strength is presented in Figure 5.18. Both the 3H:1V and 4H:1V slopes, with fully softened shear strengths, are stable after one day of about 312.4 mm (12.29 in) of rainfall.

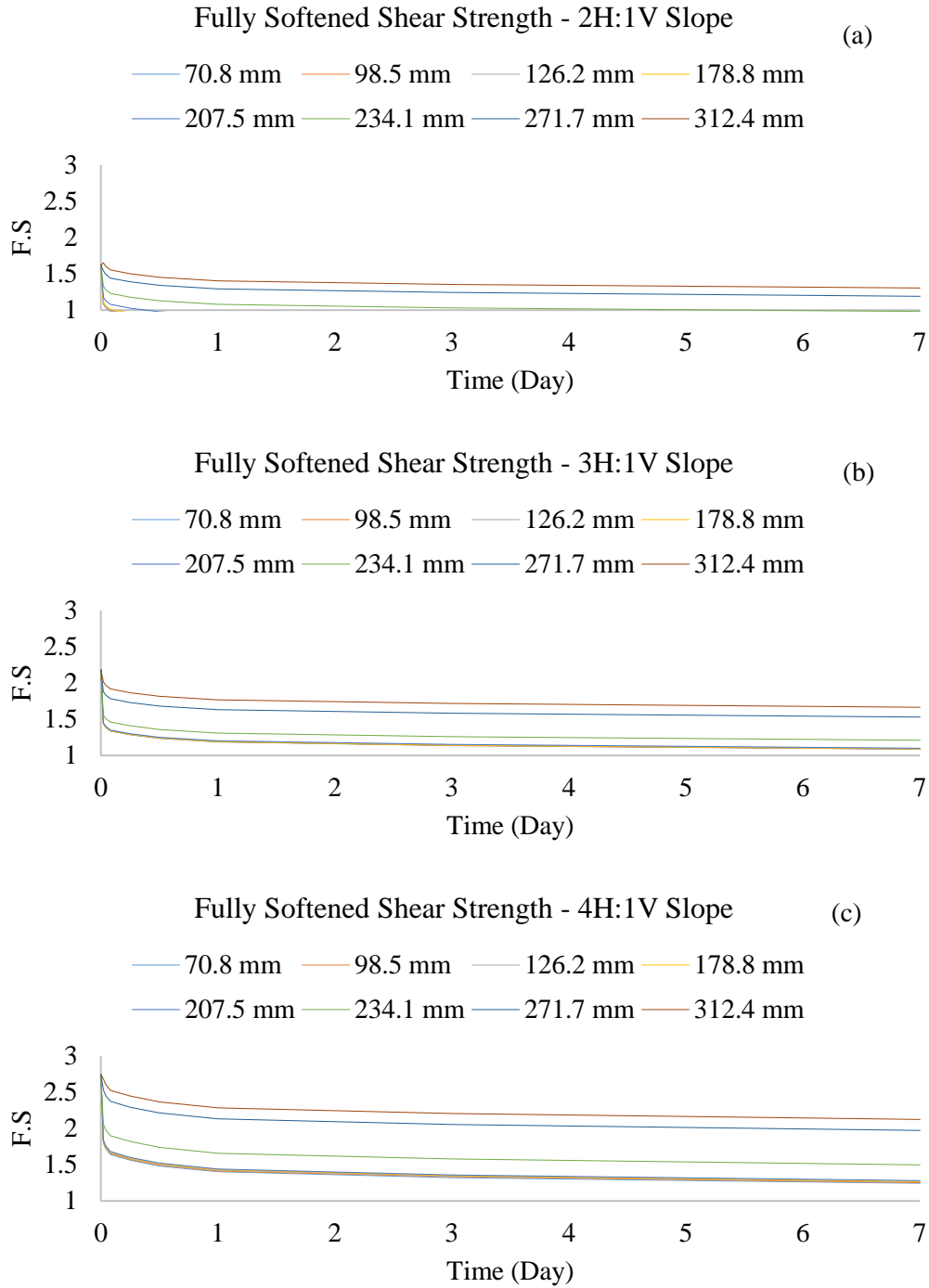


Figure 5.16 Change in the factor of safety with different total rainfall for fully softened shear strength
 (a) 2H: 1V slope (b) 3H: 1V slope (c) 4H: 1V slope

The variation of change in the factor of safety with different total rainfall volumes for residual shear strength and two slope ratios are presented in Figure 5.19. Based on the analysis, it can be observed that only the 4H:1V slope with residual shear strength, may be stable after one day of about 234.1 mm (9.21 in) of rainfall. The reason for such a stability observation is defined in Table 5.5. The coupled flow-deformation and stability results are presented in Figure 5.17 to Figure 5.19, which indicated that the interdependency of the rainfall volume, coupled with the infiltration pattern, influences not only the development of the perched water zone but also the changes in the factor of safety for the slope.

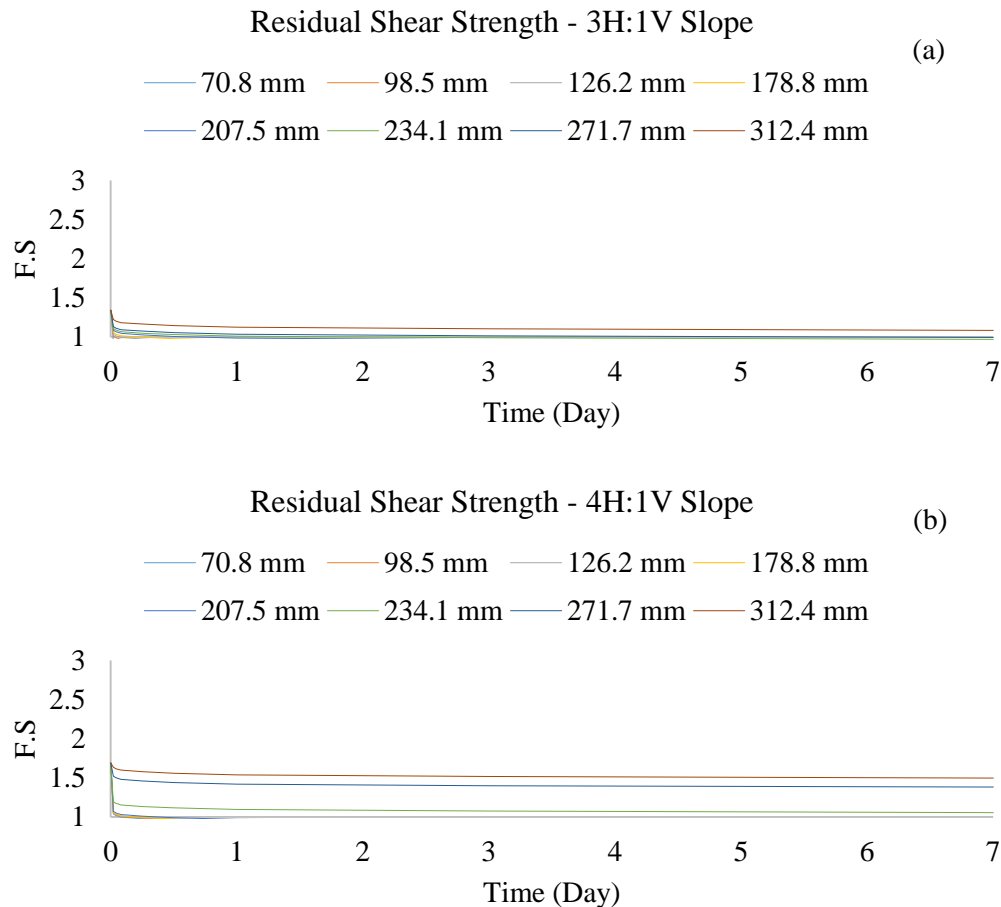


Figure 5.17 Change in the factor of safety with different total rainfall for residual shear strength

(a) 3H: 1V slope (b) 4H: 1V slope

5.4 Slope 3: Terry Road Highway Slope

5.4.1 Flow Analysis

5.4.1.1 Model Development

For the flow analysis for slope 3, PLAXIS 3D was used to conduct flow analysis. Similar to other slopes, 15-node triangular elements were used, which provide fourth order interpolation for displacements, while the numerical integration involved twelve Gauss points in Plaxis. The Van Genuchten model is considered as the hydraulic model. The model in PLAXIS makes use of the extended Mohr-Coulomb concept to describe the shear strength behavior of unsaturated soil (Fredlund et al., 1993). The discharge

function and representative soil model for this analysis are presented in Figure 5.20 and Figure 5.21. The boundary condition (Figure 5.21) is infiltration for topsoil, which allows simulating water ponding on the topsoil level. At the horizontal ground surface boundaries, the full precipitation is specified by the value of recharge (q). At inclined ground surface boundaries such as in slope with an angle α with respect to the horizontal plane, the recharge is applied as perpendicular to the inclined boundary with a magnitude of $q\cos(\alpha)$. When the resulting pore water pressure due to the precipitation has increased over the groundwater surface, ponding is considered in Plaxis. In that scenario, the software automatically changes the ponding water as a constant head boundary. During the dry period, the highly plastic clay soil develops desiccation cracks. It might have significantly increased permeability along the vertical direction of the topsoil at the active zone. However, due to the desiccation crack, the permeability along the horizontal direction might have did not affect and could have remained unchanged (Khan et al., 2017). Therefore, a high vertical permeability value was used for the aforementioned top part for each one of slopes to simulate the effect of the desiccation crack, as suggested by Khan et al., 2017. In other clay layers, the permeability for both horizontal and vertical directions was selected as the same. The water table was placed at 3 m, below the ground surface.

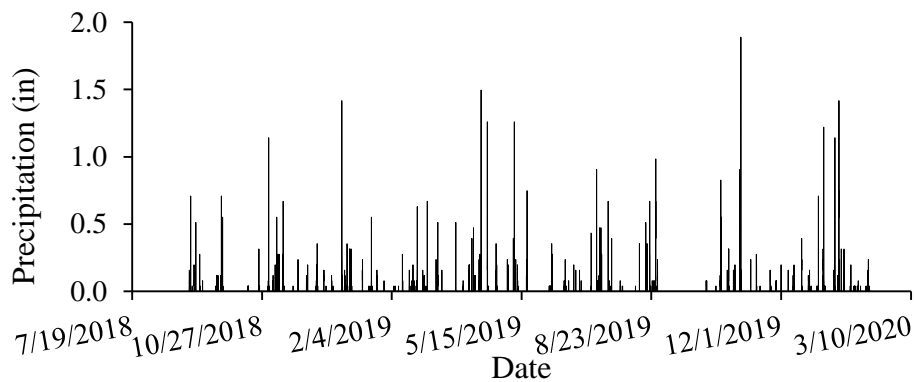


Figure 5.18 Natural daily precipitation input as a discharge function for Terry Road highway slope

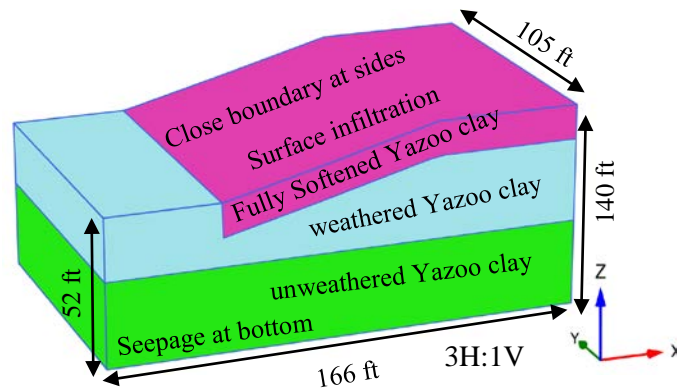


Figure 5.19 FEM soil model with the boundary conditions for Terry road highway slope

Table 5.3 Soil parameters for FEM analysis

Parameter	Name	Unit	Fully Softened in Active Zone	Weathered Yazoo	Unweathered Yazoo
Bulk unit weight	γ_{unsat}	lb/ft ³	126	125.9	127.3
Saturated unit weight	γ_{sat}	lb/ft ³	135	134.9	127.3
Horizontal permeability	$k_z=k_x$	Ft/day (cm/sec)	0.0012 (1.23E-5)	5.50E-07 (1.98e-10)	5.50E-07 (1.98e-10)
Vertical permeability	k_y	Ft/day (cm/sec)	0.0012 (1.23E-5)	5.50E-07 (1.98e-10)	5.50E-07 (1.98e-10)
Residual water content	$\Theta_{\text{res}}=S_{\text{res}}$	-	0.018	0.018	0.018
Saturated water content	$\Theta_{\text{sat}}=S_{\text{sat}}$	-	0.41	0.41	0.41
Cohesion	C	psf (kN/m ²)	25 (1.1)	248.5 (11.9)	384.2 (18.3)
Friction angle	Φ	degree	12 °	19 °	20 °
Van Genuchten fitting parameter	n	-	2.7	2.7	2.7
	α	1/ft	0.0008	0.0008	0.0008
	m	-	0.095	0.095	0.095

5.4.1.2 FEM Flow Analysis Results

Figure 5.22 illustrates the depth of moisture variation for the surficial soil layer with a maximum total rainfall volume of about 2 in (50.8 mm) for the site slope 3 with a 3H:1V slope ratio. The initial amount of suction at the top surficial soil layer was about 3200 psf (153.2 kPa) prior to the rainfall event. Change in moisture dropped immediately at the crest of the slope after one-day rainfall. The matric suction reduced about 70% at the topsoil layer at the middle and toe of the slope after 7 days of rainfall as compared to the crest of the slope. It is also noticed that after a thirty-days of progressive rainfall, the suction decreased, which had taken place due to the water ponding at the top for the mentioned slope. It is observed the suction remarkably decreased by about 42.3 % after one-day rainfall. The suction observed to drop significantly with higher intensity and longer duration of rainfall. It can be noted that the change in suction was more significant at shallower depths. The suction variation took only about one month to become very low in amount and remain unchanged. It was also observed that the drop of suction was instantaneous at the depth for different rainfall intensities and durations, and the suction decrease had continued for thirty days after rainfall. The constant value of suction indicated that the percolated water could not drain out from the slope due to the very low permeability of the high plasticity Yazoo clay soil. The maximum change in suction was observed up to 3 m depth at the crest and middle of the slope for the daily total rainfall. The change in the suction was slightly substantial at the toe of the slope. The flow analysis results using FEM analysis were supported by the field investigation as presented in Chapter 4.

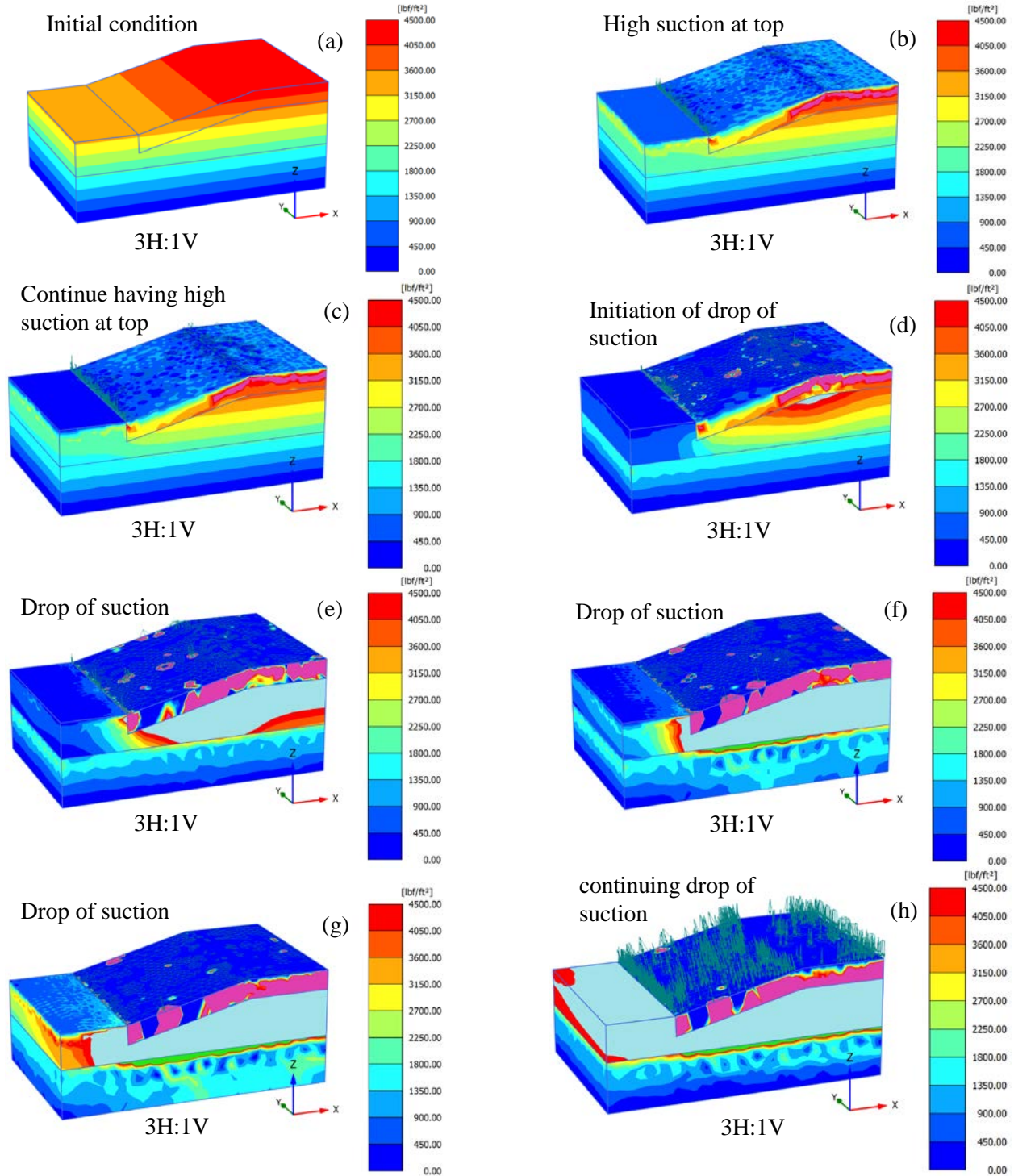


Figure 5.20 FEM flow analysis results (Depth of moisture variation profiles) for Slope 3 for Max of 2 in (50.8 mm) daily rainfall (a) Prior to rainfall (b) 30 min after rainfall (c) 60 min after rainfall (d) 12 hrs after rainfall (e) 1 day after rainfall (f) 3 days after rainfall (g) 7 days after rainfall (h) 15 days after rainfall

5.4.2 Comparison of Flow Analysis Results between Slope 1, Slope 3 and Slope 6

The flow analysis results for Slope 1, Slope 3, and Slope 6 are further analyzed to investigate the effect of the wet-dry cycles as well as the effect of the wet period and dry period in the infiltration behavior. Based on the flow analysis results for Slope 1, Slope 3, and Slope 6, as presented in Figure 5.4, Figure 5.22 and Figure 5.38 (presented later in this chapter), the variation of matric suction along the depth of the slopes is presented in Figure 5.23.

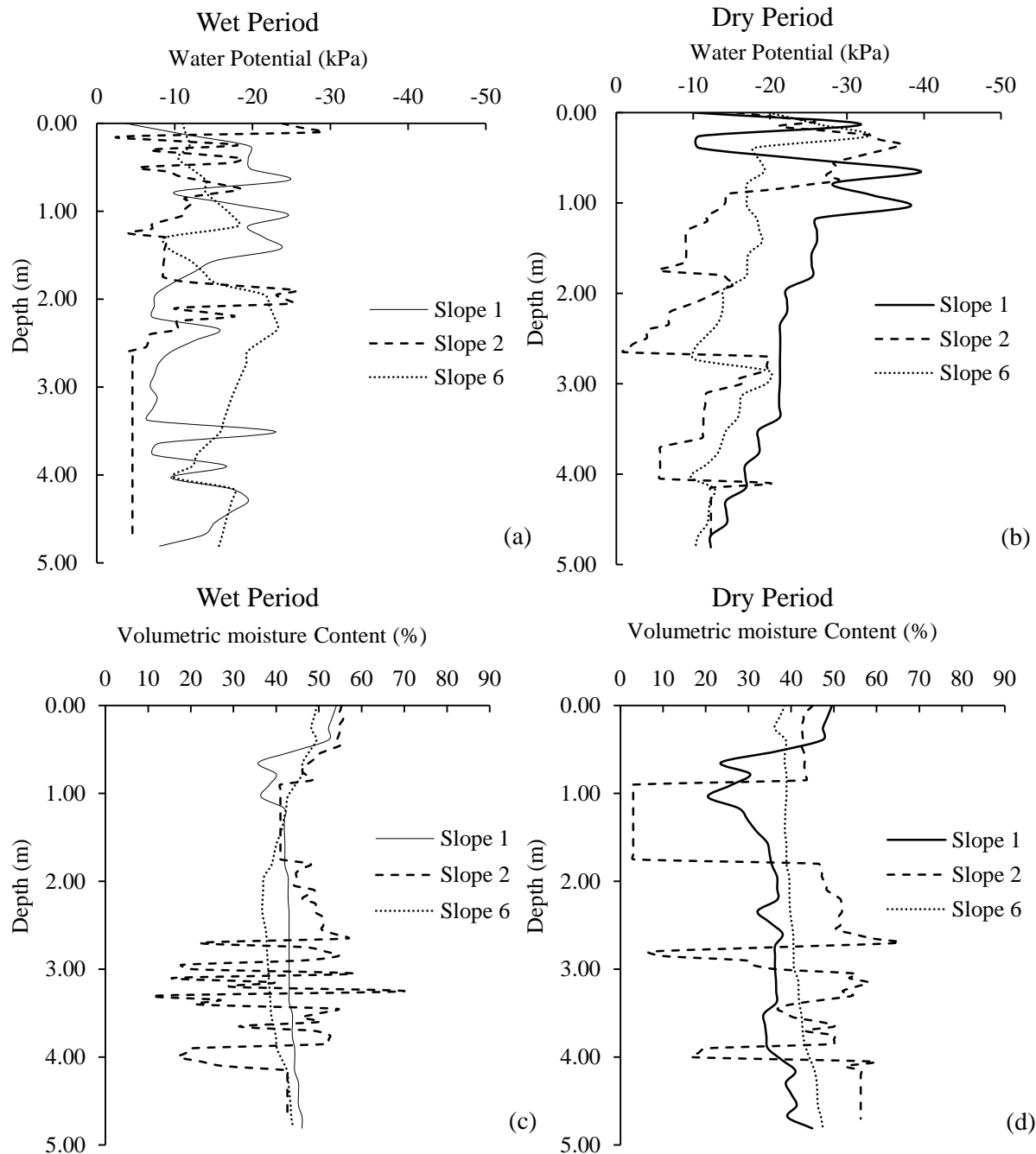


Figure 5.21 Numerical variation of matric suction (a) Wet period (b) Dry period, Numerical variation of moisture content (c) Wet period (d) Dry period at Slope 1, Slope 3, and Slope 6

Figure 5.23 presents the numerical variation of both matric suction and soil moisture along with active depth for the three slopes for both wet and dry season. It can be observed that the matric suction shows an increase and more fluctuations in the values in the very shallow depths in the dry period. The trend of matric suction variation is almost similar in all three slopes. Unlike suction values, in soil moisture variation plots (Figure 5.23(c) and Figure 5.23 (d)), the moisture content values decreased in the summertime in shallower depths. However, the bottom of the wetting depth experienced more changes. While some of this may be due to soil movement at that zone, some are probably due to perched water zone development.

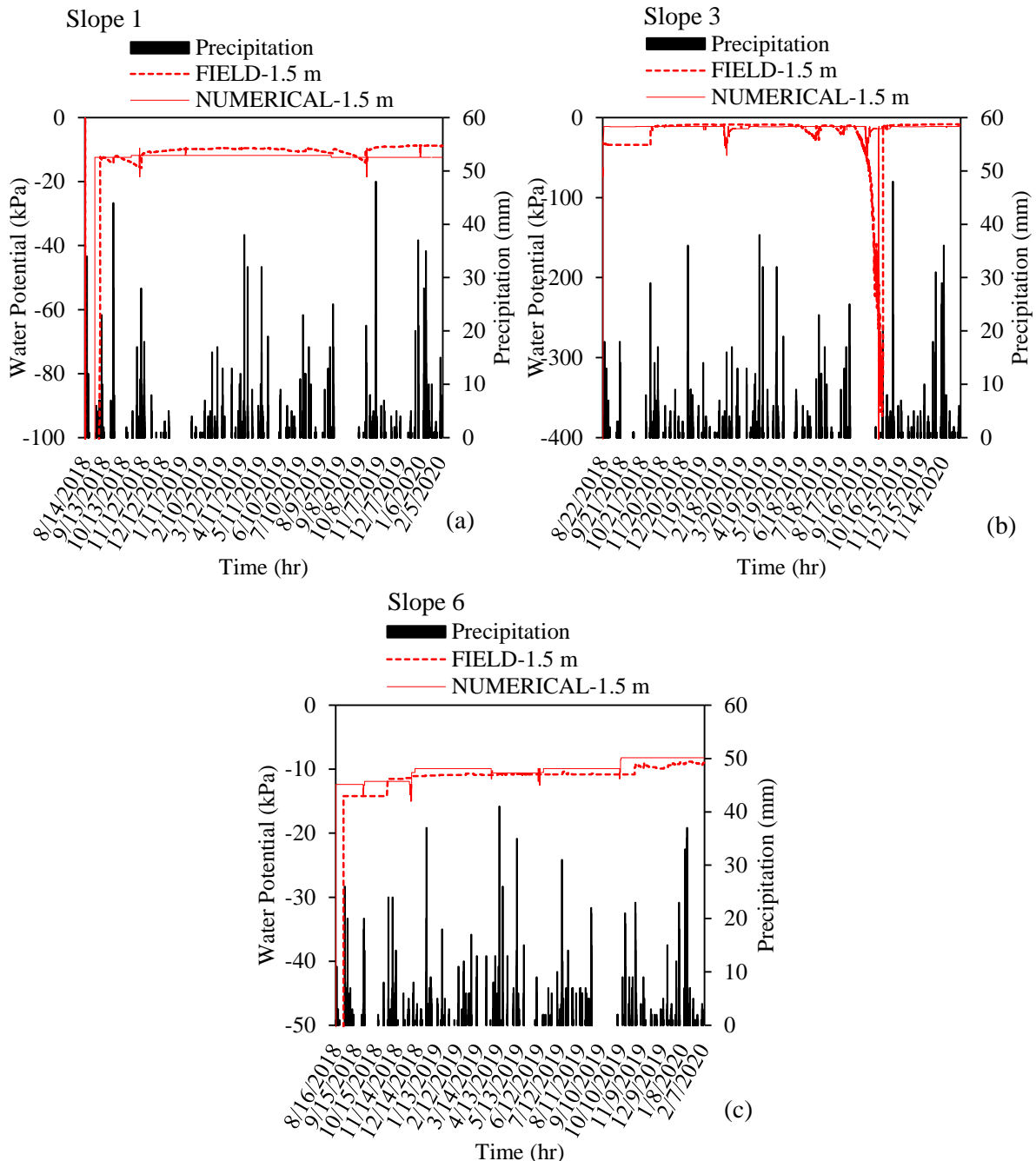


Figure 5.22 Field-Numerical Modeling comparison (a) Slope 1 (b) Slope 3 (c) Slope 6

Figure 5.24 presents the suction variation comparison between field and numerical modeling for the three slopes at instrumentation 2. It can be seen that a close trend resulted from the numerical analysis based on model calibration. It should be noted that the suction increase was followed the filed trend numerically due to the low natural daily precipitation occurred in early November 2019.

Hossain et al., 2015 conducted a study on an earth slope constructed on Texas expansive clay in Midlothian, Texas. In this study, the depth of moisture variation zone, in addition to in situ infiltration behavior with different precipitation patterns, was investigated. During this study, the author instrumented the site slope with a rain gauge, moisture, and suction sensor over a period of 4 years. The study reported that the wetted depth extends up to 3.6 m (11.8 ft), and the highest rainwater penetration occurred at the crest of the slope. The field monitoring data in this study also indicated that the total daily rainfall infiltration experienced a delay due to prolonged rainfall with low intensity. In comparison with the current study, the field and the numerical analysis results indicate an active zone depth extends up to 2 m (6.5 ft) in highway slopes of Yazoo expansive clay. Moreover, a long-delayed precipitation infiltration was observed in both the FEM analysis and the field instrumentation results.

5.4.3 Stability Analysis

During this study, stability analysis was conducted considering the unsaturated moisture and matric suction variation of the soil, as investigated by the fully coupled flow analysis in Slope 3. In this analysis, time-dependent hydro-mechanical behavior of the soil is described in a coupled format, taking both deformation and groundwater flow into account, in which mixed equations of displacement and pore pressure, are solved simultaneously. Based on the effective stress, pore water pressure, and matric suction profile developed by coupled-flow deformation analysis, the factor of safety of the slope was determined using the phi-c reduction method in Plaxis 3D, which is alternately known as the shear strength reduction analysis.

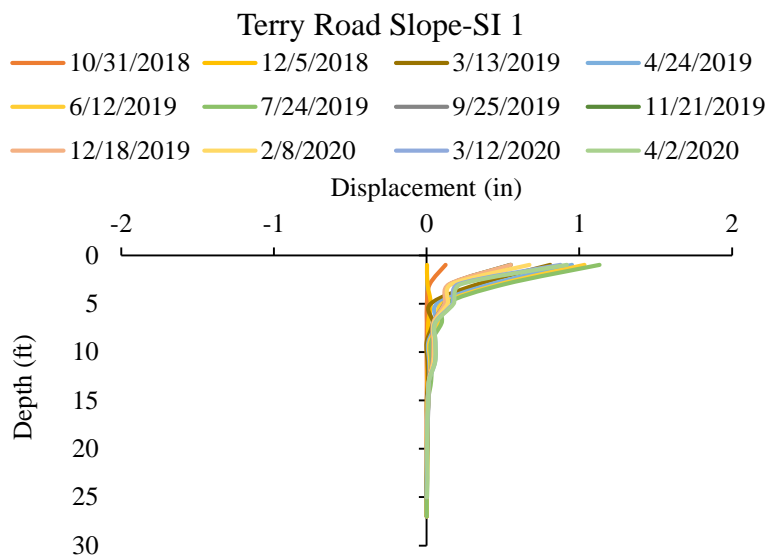


Figure 5.25 Horizontal deformations of slope 3 at the as-built section

The slope 3 has faced consistent movement throughout the monitoring period, as presented in Figure 5.25. Based on the field monitoring results, the slope is moving as it experienced a high rainfall period. During this analysis, the actual rainfall from field instrumentation was utilized as an input. However, such analysis requires significant computation power, and time for the analysis is extremely time-consuming. As a result, an alternative analysis was performed, where the effect of the total rainfall (120 inches) was used as an input within a short period of time, and then the changes of the factor of safety were evaluated at a different time period. The stability analysis results followed by coupled-flow deformation analysis is

presented in Figure 5.26, which indicated a consistent drop in the factor of safety (from 1.19 to 1.1) of the slope with progressive rainfall. It should be noted that for this analysis, the back-analysis cohesion and friction angle was utilized, as indicated in Table 5.5.

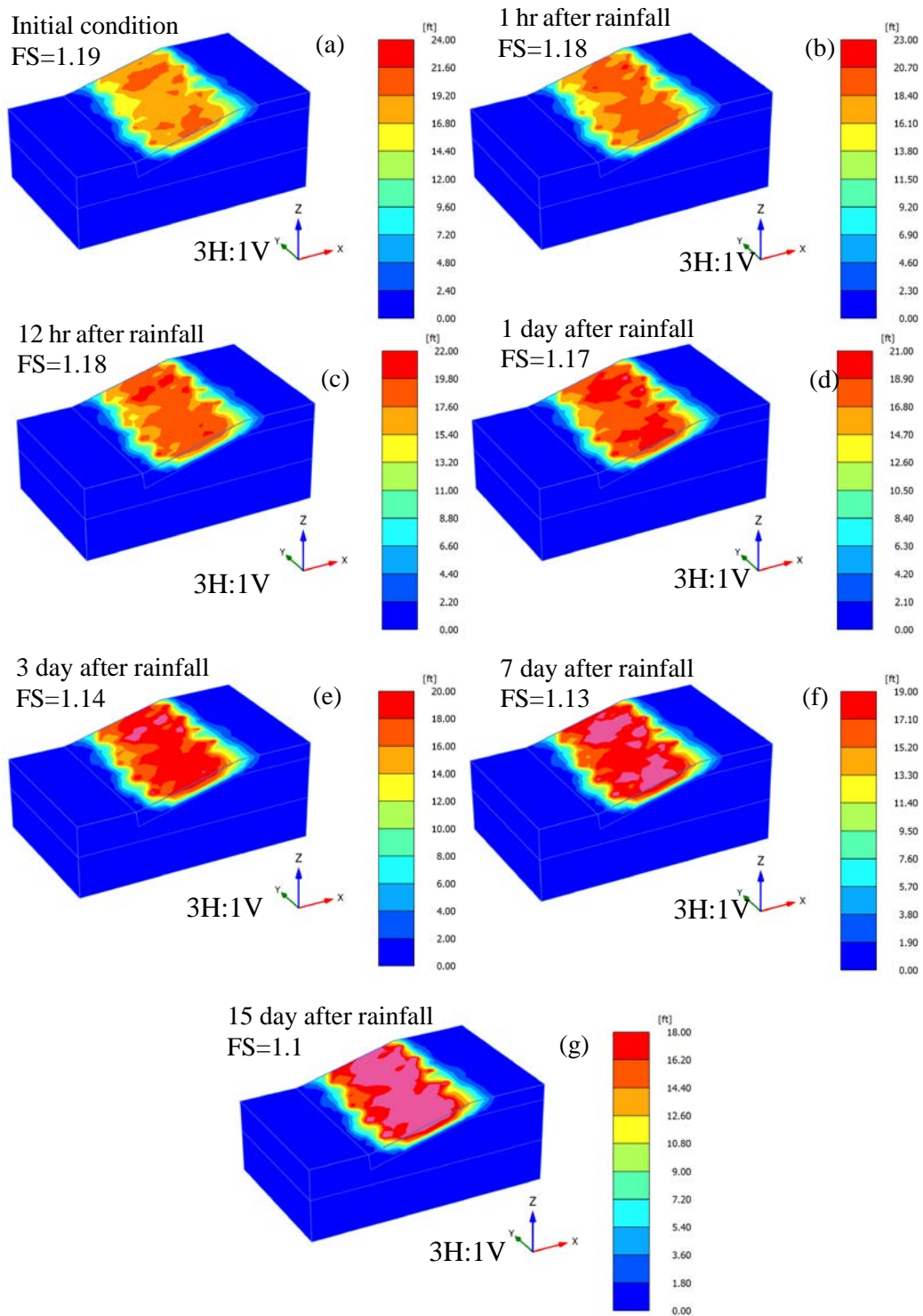


Figure 5.26 Variation in slip surface for the critical total natural rainfall amount of 120 inches (3048 mm) throughout the monitoring period of Slope 3 (a) Prior to rainfall (b) 1 hr. after rainfall (c) 12 hrs. after rainfall (d) 1 day after rainfall (e) 3 days after rainfall (f) 1 day after rainfall (g) 15 days after rainfall

5.5 Slope 4: Highland Drive Highway Slope

5.5.1 Flow Analysis

5.5.1.1 Model Development

The Finite Element Method (FEM) program PLAXIS 3D was used to conduct a fully flow analysis. A 15-node triangular element was used. The Mohr-Coulomb model is used to define the mechanistic behavior of soil, and the van Genuchten model is considered as the hydraulic model to define the infiltration/seepage behavior. The soil parameters were used in the numerical analysis using PLAXIS 3D, as shown in Table 5.6. Based on the soil properties, Poisson's ratio was considered to be 0.3. The discharge function and representative soil model are presented in Figure 5.27 and Figure 5.28 for Slope 4. The global model boundary condition, as outlined in the figure, is defined as open flow along the vertical direction (Z-axis) and closed for horizontal direction (X-axis). However, the flow along the translation direction (Y-axis) is also considered a closed boundary. The initial depth of the water table was selected to be 8 ft (2.43 m) below the ground surface based on observation on the field.

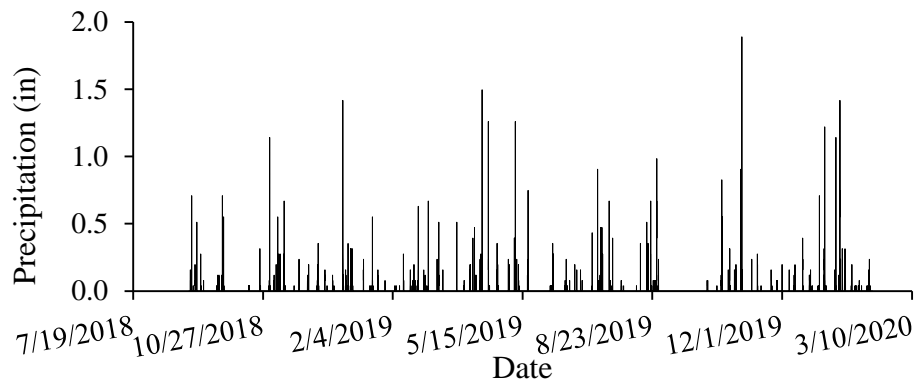


Figure 5.27 Natural daily precipitation input as a discharge function for Highland Drive highway slope

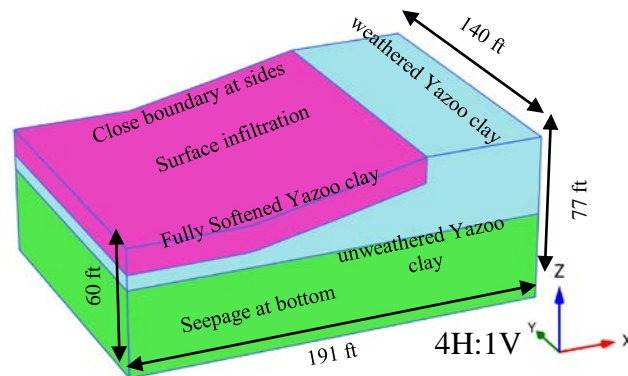


Figure 5.28 FEM soil model with the boundary conditions for Highland Drive highway slope

Table 5. 4 Soil parameters for FEM analysis

Parameter	Name	Unit	Soil 1 (Fully Softened)	Soil 2 (Weathered Yazoo)	Soil 3 (Unweathered Yazoo)
Bulk unit weight	γ_{unsat}	lb/ft ³	126	125	127.3
Saturated unit weight	γ_{sat}	lb/ft ³	135	134	127.3
Horizontal permeability	$K_z=k_x$	Ft/day (cm/sec)	0.0012 (1.23E-5)	5.50E-07 (1.98e-10)	5.50E-07 (1.98e-10)
Vertical permeability	k_y	Ft/day (cm/sec)	0.0012 (1.23E-5)	5.50E-07 (1.98e-10)	5.50E-07 (1.98e-10)
Residual water content	$\Theta_{\text{res}}=S_{\text{res}}$	-	0.018	0.018	0.018
Saturated water content	$\Theta_{\text{sat}}=S_{\text{sat}}$	-	0.41	0.41	0.41
Van Genuchten fitting parameter	n	-	2.7	2.7	2.7
	α	1/ft	0.0008	0.0008	0.0008
	m	-	0.095	0.095	0.095

5.5.1.2 FEM Flow Analysis Results

During the FEM analysis, the infiltration and open boundary were used at the topsoil layer, the seepage boundary was used for the bottom soil layer, and the closed boundary was used for the sides of the soil model. The model conditions for a groundwater flow calculation can be defined at the extreme boundaries of the model. The open boundary layer in Plaxis allows the formation of the seepage travel pass during the infiltration at the upstream of the shells. The groundwater level was located at the ground surface as reported during the site investigation to define the initial unsaturated condition. The total daily real-time rainfall period (August 2018 to June 2019) was considered for the discharge function input for the flow analysis to simulate the failure condition.

Figure 5.29 presents the depth of moisture variation for fully softened Yazoo clay at the surficial layer with a maximum total rainfall volume of about 2 in (50.8 mm) for the site slope 1 with a 4H:1V slope ratio. It can be seen from the mentioned Figure that before any rainfall event, the primary value of suction was about 3200 psf (135.7 kPa), which dropped to a value of 1984.5 psf (105.9 kPa) after a one-day rainfall event. The suction immediately dropped at the top surficial soil layer after rainfall and continued for thirty days, representing the active wetting depth. The topsoil layer experienced a drop of moisture variation after the rainfall event and varied slightly after seven days of rainfall.

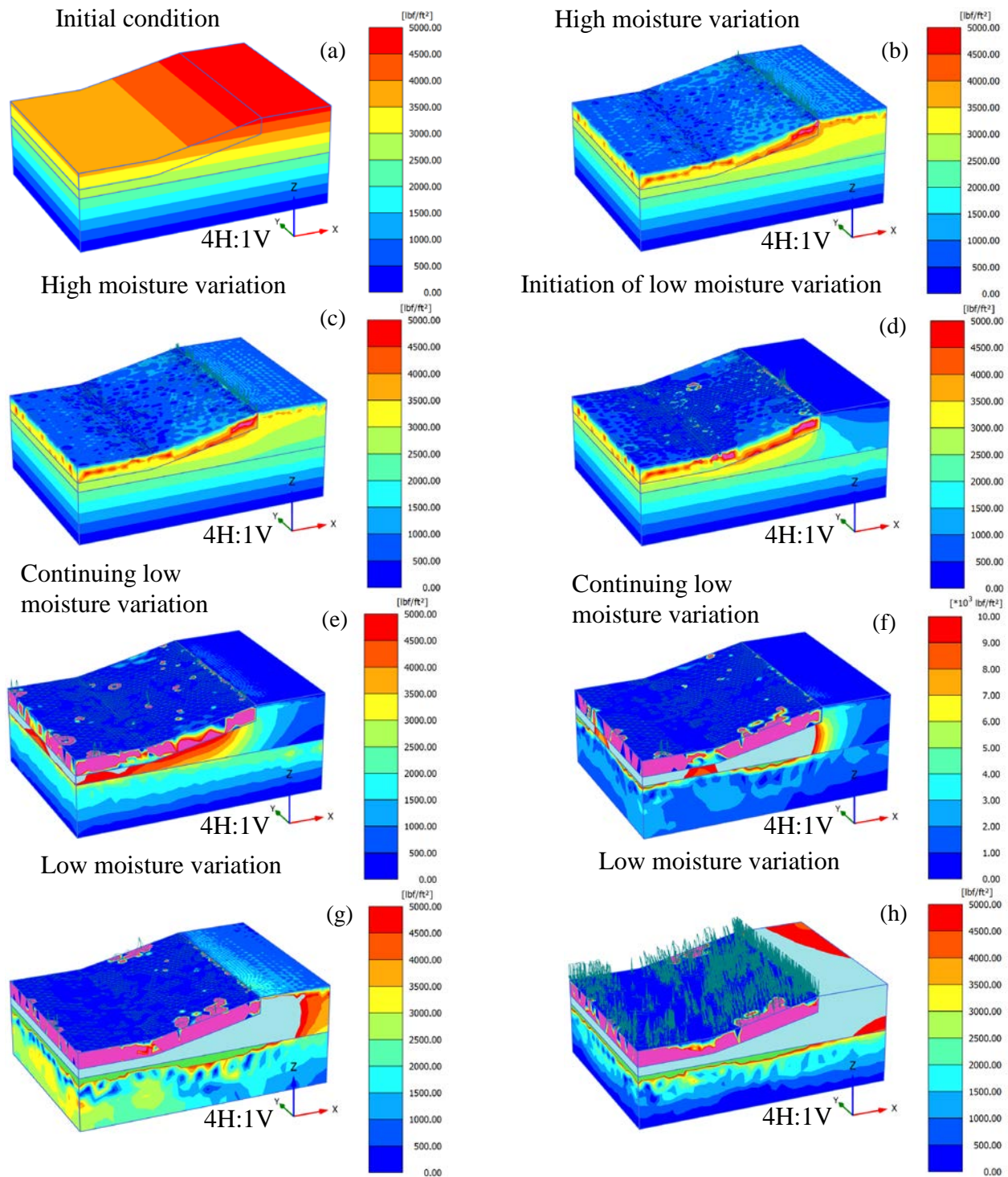


Figure 5.29 FEM flow analysis results (Depth of moisture variation profiles) for Highland Drive highway slope for Max of 2 in (50.8 mm) daily rainfall (a) Before rainfall (b) 30 min after rainfall (c) 60 min after rainfall (d) 12 hrs after rainfall (e) 1 day after rainfall (f) 3 days after rainfall (g) 7 days after rainfall (h) 15 days after rainfall

Finally, after 30 days of the rainfall event, the moisture variation dropped by about 35.1%. It can be seen that the most critical moisture variation occurred at the topsoil layer (less than 12 ft (3.6 m)). In contrast,

the change in suction continued several days to weeks post-rainfall to reach a steady value at the critical depth.

5.6 Sowell Road Highway Slope

5.6.1 Field Investigation Results

The reinforced section of this slope has experienced a shallow slide. As presented in Chapter 4, the inclinometer at the reinforced section had a significant movement after about three months after monitoring the stabilized slope. The slope experienced approximately 0.09 ft (3 cm) horizontal displacement, which led to shallow slope failure, as presented in Figure 5.30. It should be noted that the depth of the failure is about 13.1 ft (4 m).

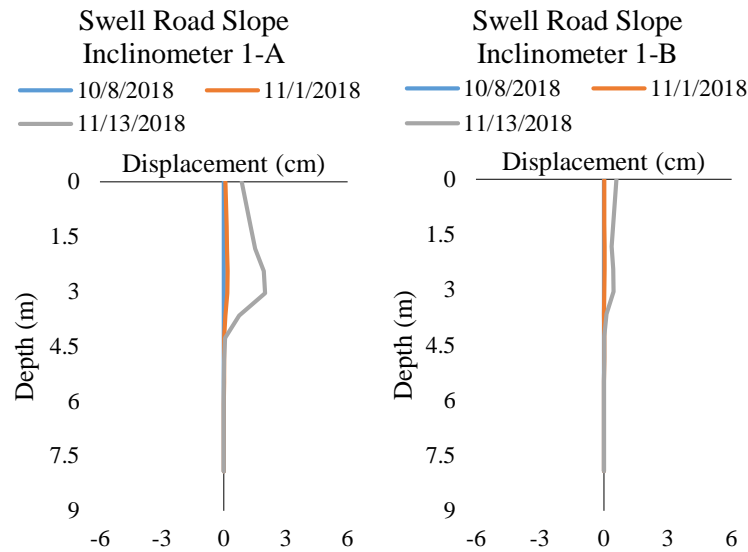


Figure 5.30 Horizontal displacements of slope inclinometer at the reinforced section of the Slope 5

According to the obtained field instrumentation results, the change in moisture content and daily rainfall distribution at the crest, middle, and toe of the Sowell road slope at three different depths 5 ft (1.5 m), 10 ft (3 m), and 15 ft (5 m) at instrumentation 1, 2, and 3 from September 2018 to April 2019 are depicted in Figure 5.31. For this study, the concentration is on the period of November 2018 to the past, due to the time of failure.

Variation of moisture content at the crest of the slope- Variation of in situ moisture content with daily rainfall data at the crest of the slope at three different depths 5 ft (1.5 m), 10 ft (3 m), and 15 ft (5 m) is presented in Figure 5.31(a). The initial moisture content was comparatively low. It is observed that the moisture content recorded initially as 0.28, 0.38, and 0.48 at the crest and middle of the slope, respectively, during the installation time. Afterward, total precipitation of 1.31 ft (402 mm) was observed in three months between early September to late November 2018, with the highest precipitation of about 0.05 ft (18 mm) during the rainfall events in late September and late October 2018. Consequently, the moisture content increased to about 0.45 at the crest and middle of the slope and 0.53 at the toe of the slope. It can be seen that the average moisture content variation is about 0.36 in average, and it is considered to be the lowest in the amount in comparison to the change in moisture at 10 ft (3 m) and 15 ft (5 m) in the period between early September to early November 2018 as it was expected. The change in moisture experienced an increase due to a high amount of rainfall and started decreasing with daily rainfall disappearing approximately at all three depths. It is seen that the average change in moisture with about 0.38 at 10 ft (3 m) stands between the upper and lower depths. It is important to recognize that the change in moisture with

about 0.45 on average seated at the top at 15 ft (5 m) in comparison to the other depths, and it is more susceptible to the precipitation. The observed behavior could be attributed to the existence of water accumulation or excess water percolation.

Variation of moisture content at the middle of the slope- Figure 5.31(b) illustrates the moisture content variation at the middle of the slope at three different depths 5 ft (1.5 m), 10 ft (3 m), and 15 ft (5 m). Unlike the moisture variation at the crest, during the relatively wet fall of 2018, the moisture content at 1.5 m depth showed an increase and decrease of about 0.8 to 1.0, and it is exposing the most fluctuation among the other depths as it was expected (Figure 5.31(c)). In contrast, the moisture variation at deeper depths shows a monotonous change with total daily rainfall variation. It should be noted that this behavior was attributed to the soil type (Yazoo clay) in which low infiltration with slight variations in addition to longer time occurred at deeper depths. Nobahar et al., 2020 also reported considerable variation in infiltration and matric suction at deeper depth in highly plastic clay soil (Yazoo clay). It also observed that the average moisture content at 10 ft (3 m) remained with the highest in amount (0.48).

Variation of moisture content at the toe of the slope- The in-situ moisture variation at the toe of the slope at three different depths 5 ft (1.5 m), 10 ft (3 m), and 15 ft (5 m) is depicted in Figure 5.31(c). At the time of precipitation, the toe of the slope absorbing the highest amount of moisture. In effect, the average moisture variation at the toe of the slope maintained the highest moisture content (about 0.5) (Figure 5.31(c)). In contrast to the expected behavior, it is observed that the change in moisture at 5 ft (1.5) seats in the middle of the other two depths (10 ft (3 m) and 15 ft (5 m)).

The moisture variation at the toe of the slope at 5 ft (1.5 m) reached its maximum up to about 0.5 in comparison to the middle and the crest of the slope (Figure 5.31). It should be noted that it was expected the moisture variation had fluctuations at 5 ft (1.5 m), unlike the deeper depths in which the variation of the moisture remains almost steady at 10 ft (3 m) and 15 ft (5 m) (Figure 5.31). The average amount of moisture content decreased from the toe to the middle and to the crest of the slope (Figure 5.31). A similar trend of the moisture variation was also observed at the deeper depths. As a result, probably the most significant aspect of the data monitoring results is that the variation of moisture is steady, with minor fluctuations in the wet fall. Particularly, the soil is trying to keep its natural moisture content.

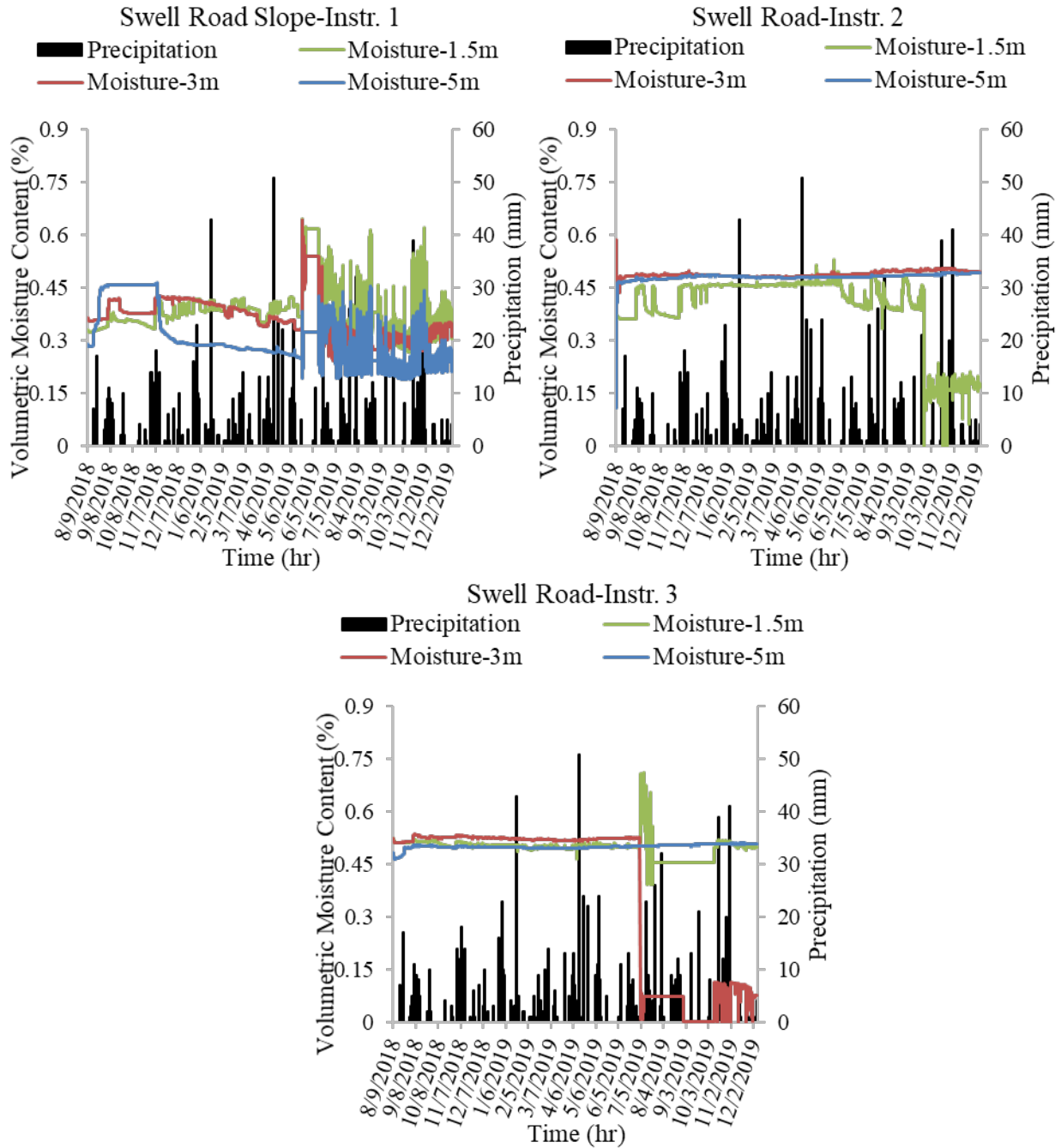


Figure 5.31 Moisture variation with time (a) at the crest of the slope (b) at the middle of the slope (c) at the toe of the slope at Sowell Road Highway slope

5.6.2 Coupled Hydro-Mechanical and Stability Analysis

The soil parameters were used in the numerical analysis using PLAXIS 3D, as shown in Table 5.7. The soil parameters were obtained from existing soil test reports. Precipitation of prolonged total rainfall was applied to the soil model to assess the deformation behavior during rainfall by daily rainfall distribution presented in Figure 5.34(g). The representative soil model is presented in Figure 5.32. It should be noted that the repaired area of Slope 5 has HP14x73 at the middle of the slope and two layers of uniaxial geo-grid

reinforcement after the H-piles up to the toe of the slope. The analysis was carried out for fully coupled flow deformation concentrating on the surficial soil layer reinforced with HP 14x73 at 3 ft (0.91 m) spacing, and HP 14x73 along with two layers of uniaxial geogrids, as presented in Figure 5.33. The boundary condition, as outlined in the mentioned figure, is infiltration at the top, closed at sides, and seepage at the bottom of the soil layer. Based on the material stiffness, Poisson's ratio was 0.3.

Furthermore, although it has been identified that the coefficient of permeability is a function of matric suction, and it is not constant in unsaturated soils, determination of it requires time and effort. Therefore, further investigation is needed in this matter. Yet, for ease of analysis, static permeability values considered. Based on the cone penetration test carried out in this project, spatially, the planar and vertical values are determined as k_x , k_y , and k_z , respectively, in which it is assumed to be the same in all directions. The detailed permeability values are presented in Table 5.6. For this analysis, the depth of the water table was defined as a distance from the ground surface to the water table. The initial depth of the water table was selected to be 8 ft (2.43 m) below the ground surface based on typical groundwater conditions in Jackson, Mississippi, USA. Figure 5.32 presents the soil types for the soil model.

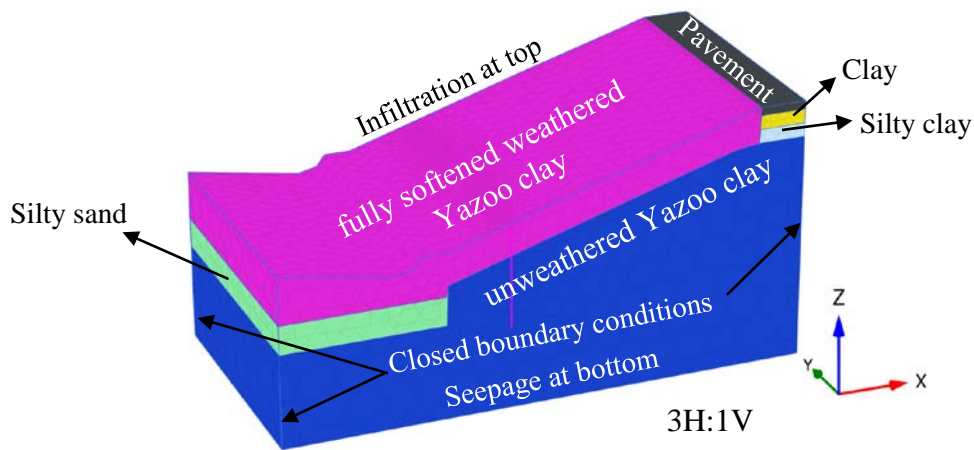


Figure 5.32 Boundary conditions for the soil flow-deformation model of Slope 5

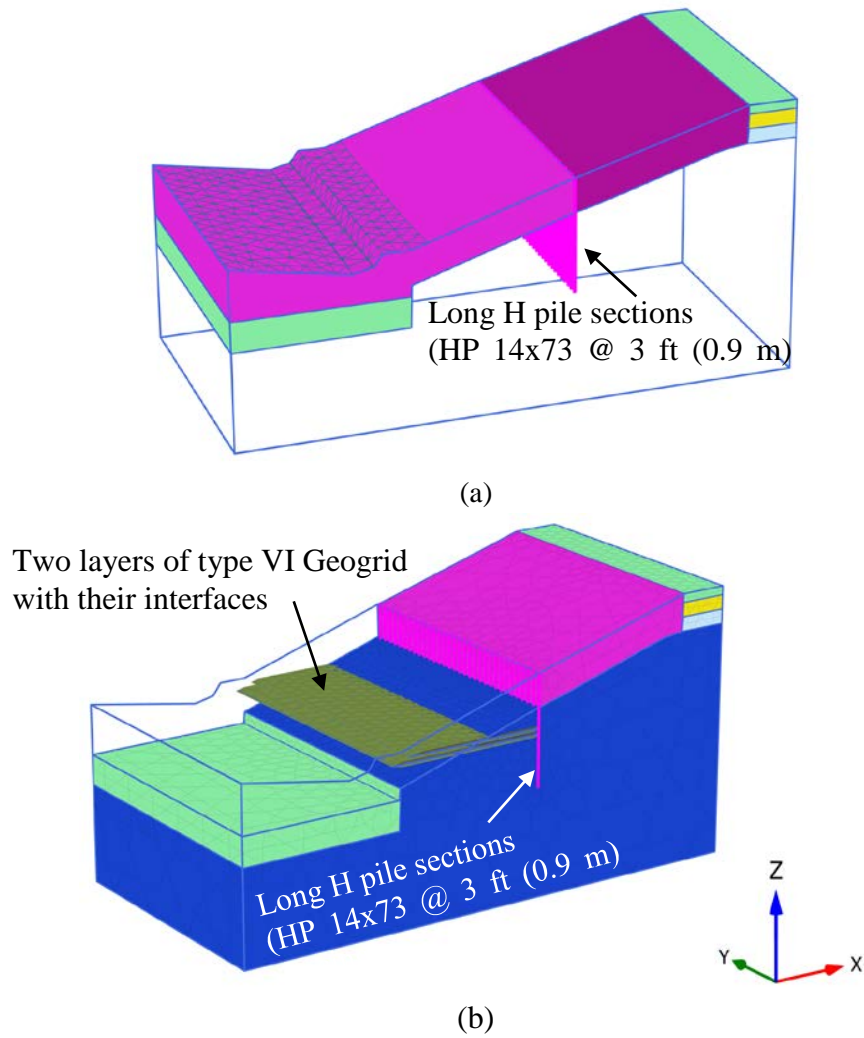


Figure 5.33 The geometry and pile description of the repaired section of slope 5, a. With only HP 14x73 and b. Combination of HP 14x73 and two layers of Uniaxial Geogrid.

Table 5.5 Soil parameters for FEM analysis

Parameter	Name	Unit	pavement	clay	Silty clay	Fully softened weathered Yazoo clay	unweathered Yazoo clay	Silty sand
Bulk unit weight	γ_{unsat}	Pcf (kN/m ³)	171.9 (27)	125.9 (19.7)	125.9 (19.7)	128 (20.1)	127.3 (19.9)	120.9 (18.9)
Saturated unit weight	γ_{sat}	Pcf (kN/m ³)	171.9 (27)	134.9 (21.1)	134.9 (21.1)	136 (21.3)	127.3 (19.9)	130.9 (20.5)
Permeability	$k_x=k_y=k_z$	Ft/day (cm/sec)	0	4.3E-6 (1.5E-9)	8.93E-7 (3.1E-10)	0.0006 (2.11E-7)	4.8E-8 (1.7E-10)	4.37E-6 (1.5E-9)
Young's modulus	E	Psf (kN/m ²)	647.4E6 (30.9E6)	150.0E3 (7.1E3)	180.5E3 (8.6E3)	100.0E3 (4.7E3)	200.0E3 (9.5E3)	180.0E3 (8.6E3)
Poisson's ratio	ν	-	-	0.3	0.25	0.3	0.25	0.3
Residual water content	Θ_{res}	-	-	0.018	0.018	0.018	0.018	
Saturated water content	Θ_{sat}	-	-	0.41	0.41	0.41	0.41	
Van Genuchten fitting parameter	n	-	-	2.75	2.75	2.75	2.75	
(Nobahar et al., 2019)	α	1/m	-	0.0031	0.0031	0.0031	0.0031	
Cohesion	C	Psf (kN/m ²)	-	100 (4.7)	110 (5.2)	37 (1.7)	250 (11.9)	60 (2.8)
Friction angle	Φ	degree	-	23 °	25 °	15 °	15 °	30 °

Figure 5.34 presents the suction variation for fully softened Yazoo clay at the surficial layer with a maximum total rainfall volume of 25 mm (98 in) for the Sowell road with a 3H:1V slope ratio. It can be seen from the mentioned Figure that before any rainfall event, the primary value of suction was about 1000 psf (47.88 kPa) which dropped to a value of 600 psf (28.72 kPa), 500 psf (23.94 kPa), 350 psf (16.75 kPa), 300 psf (14.36 kPa), 200 psf (9.57 kPa) after one, two, three, four, and five-months rainfall event. The suction immediately dropped at the top surficial soil layer after rainfall and continued for five months, representing the accumulation of water at the corresponding depth. It is observed that in a fall period, the suction remarkably decreased by about 80 %. The suction observed to drop significantly with higher intensity and longer duration of rainfall. It can be noted that the change in suction was more significant at shallower depths. The suction variation took several months to become very low in amount and remain

unchanged. The constant value of suction indicated that the percolated water could not drain out from the slope due to the very low permeability of the high plasticity Yazoo clay soil. The maximum change in suction was observed up to 6 ft (1.8 m) depth at the crest and middle of the slope for the daily total rainfall. The change in the suction was no substantial at the toe of the slope. The flow analysis results using FEM analysis were supported by the field investigation in the current study.

The topsoil, particularly in the upper middle, failed in November 2018 after a prolonged period of abnormally low rainfall conditions continued by a rainfall event (Figure 5.34(g)). The existence of shrinkage cracks allowed for easy rainwater intrusion at the slope upper-middle in the top few feet immediately after rainfall. The low permeability of the highly plastic Yazoo clay likely prevented the downward movement of the water, creating a perched water zone near the middle of the slope. Hence, the slope stability analysis of the slope was extended to consider a slip surface near the middle of the slope.

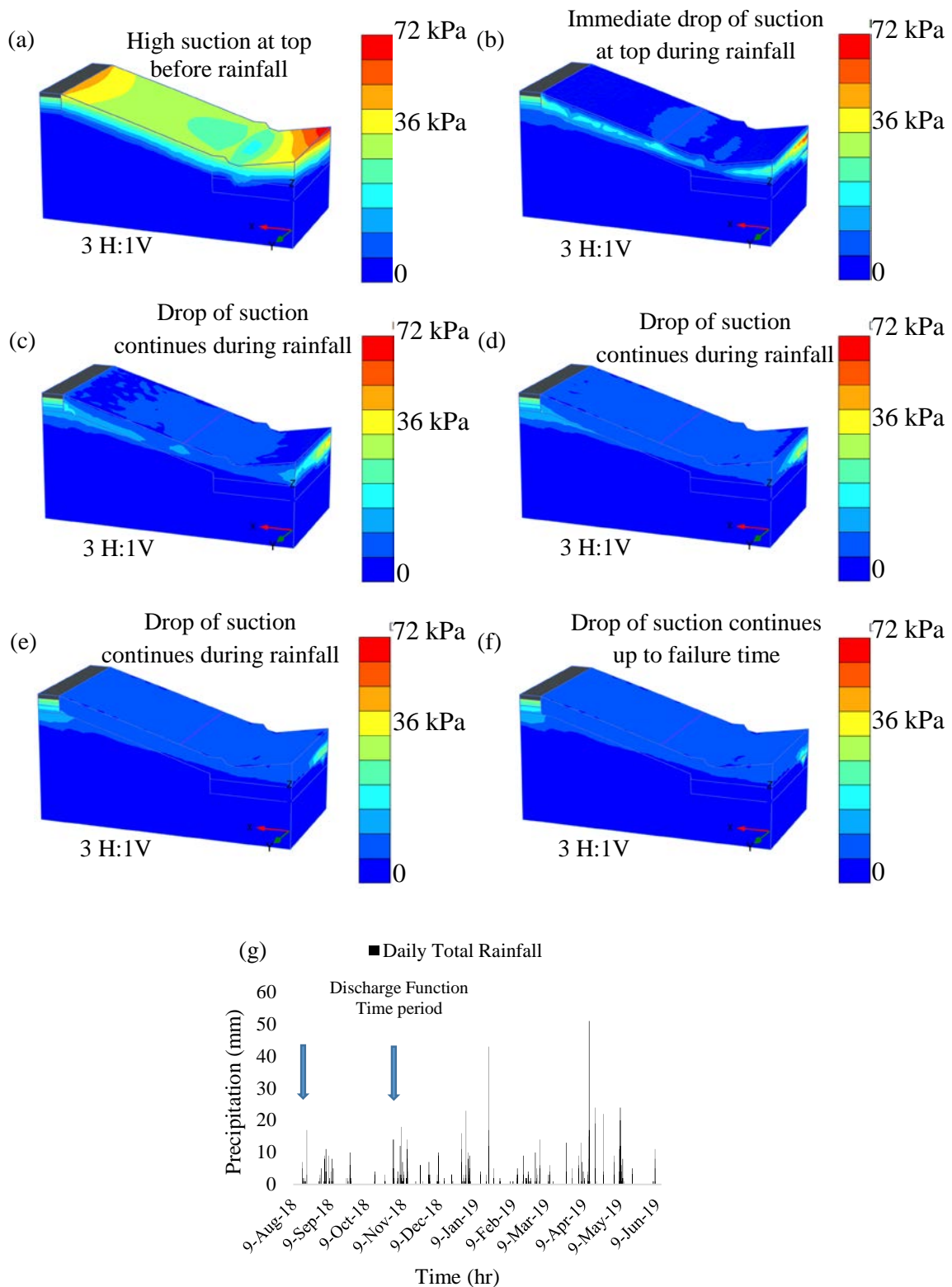


Figure 5.34 Suction profile for 25 mm (98 in) total rainfall amount (a) Before rainfall (b) 120 days before failure (c) 90 days before failure (d) 60 days before failure (e) 30 days before failure (f) at time of failure (g) Discharge function period as input for FEM flow analysis

5.6.3 Stability Analysis Results

The slope stability analysis was conducted using the soil model presented in Figure 5.33. In addition, based on the existing project data, the 40 ft. long (12.19 m) H-piles and two row of uniaxial geogrid were applied at the exact location at the slope to simulate the observed field movement and calculate the factor of safety of the slope. During the stability analysis, the moisture variation, matric suction variation and pore water pressure profile which was developed under the coupled flow deformation analysis (Figure 5.34 (f)) was used as an input condition. The stability analysis was conducted using strength reduction method in Plaxis 3D. The stability analysis results indicated that the factor of safety of the slope was 1.1 when considering the moisture profile at time of the failure as observed in the field with the presence of H-piles and two layers of the uniaxial geogrid. However, the slip surface of the slope was similar as it is observed in field, where the failure surface initiate beyond the H-pile. Since the slipping surface of the slope was observed at the location of the Geogrid, there is always a consideration of the placement and development of the interaction between the soil and geogrid. Another stability analysis was conducted with H-pile but no geogrid, where the factor of safety was observed as 0.98. The stability analysis results for both cases are presented in Figure 5.35.

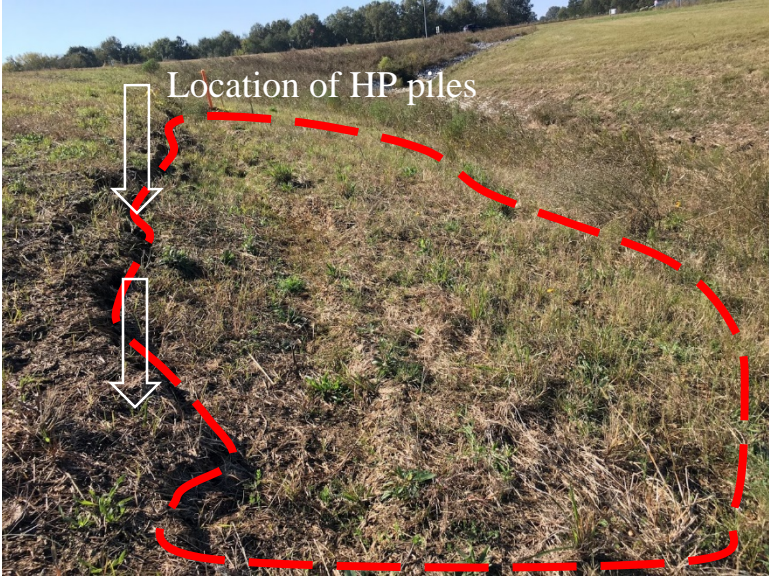
It should be noted that the slip surface with or without the Geogrid matches the same however the factor of safety varied between 1.1 and 0.98. Therefore, it is obvious that the expected interaction between the soil and Geogrid didn't exist during the time of the failure. This might have happened due to placing poor backfill soil (highly plastic Yazoo clay) at the location of the Geogrid, instead of B9-6 soil (LL 46 and PI 26) as required by the designer. To determine the interaction between the Geogrid and highly plastic Yazoo clay during the time of failure, additional analysis was conducted.

5.6.4 Effect of Uniaxial Geogrid- Soil Interaction

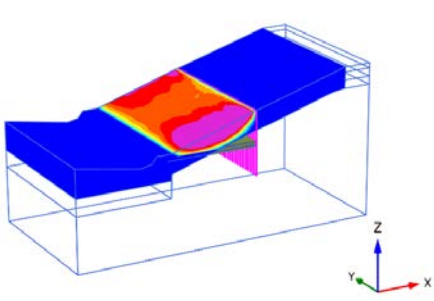
The type VI uniaxial Geogrid was modeled as geotextile with maximum Ultimate Tensile Strength of 7000 lb/ft (967.7 kg/m). The roughness of the soil-structure interaction is modeled by using appropriate strength reduction factor (ξ_{int}) for the interface element. This factor correlates the surrounding soil strength in terms of cohesion and friction angle to the structure interface strength in terms of adhesion and material friction (Goodman and Taylor and Brekke, 1968; Van Langen and Vermeer, 1991).

Different values of ξ_{int} have been considered in this analysis to investigate the impact of interface strength on the factor of safety of the slope. When the interface between the soil and the geogrid (soil-structure interaction) reduces its strength with respect to the strength in the surrounding soil, the interface becomes weaker and more flexible than the surrounding soil. Subsequently, relative displacement parallel and perpendicular to the interface may be occur. Consequently, the ξ_{int} value will become below one, in this condition. Researchers have investigated the effective interaction between expansive soils and geogrid (Xu et al., 2004; Zornberg and Gupta, 2008; Zornberg et al., 2008; Dessouky et al., 2012; Al-Omari et al., 2016). Figure 13 presents the changes in slip surface with consideration of different interface strengths between the surficial Yazoo clay soil and the Geogrid reinforcement.

Zornberg et al. (2008) concluded based on the field assessment that geogrid reinforcement can reduced the crack developments effectively. Dessouky et al. (2012) also found that the geogrid can increase both lateral and vertical stiffness of the base layer soil based on the site evaluations. The Yazoo clay at the failed area has a liquid limit of 88 with a plasticity index of 54, as well as the soil was observed very saturated during the time of the monitoring. At high moisture content, and possibly with the presence of the perched water condition, the Yazoo clay loses it's strength and becomes very soft. As a result, a very weak interaction between the soil and Geogrid is expected. As presented in Figure 5.36, the factor of safety of the slope is very close to 1.03 with the strength reduction factor $\xi_{int} = 0.3$ appear to be case when the sliding has occurred.

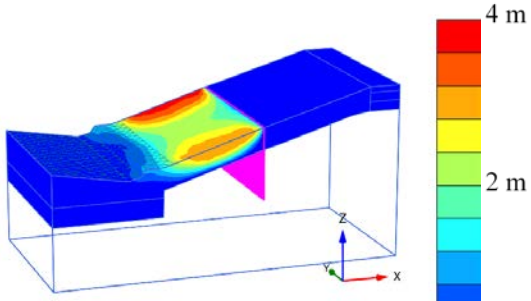


(a)



Factor of Safety: 1.1

(b)



Factor of Safety: 0.98

(c)

Figure 5.35 Stability Analysis results (a) H-pile and two layers of uniaxial Geogrid, and (b) Only H-pile.

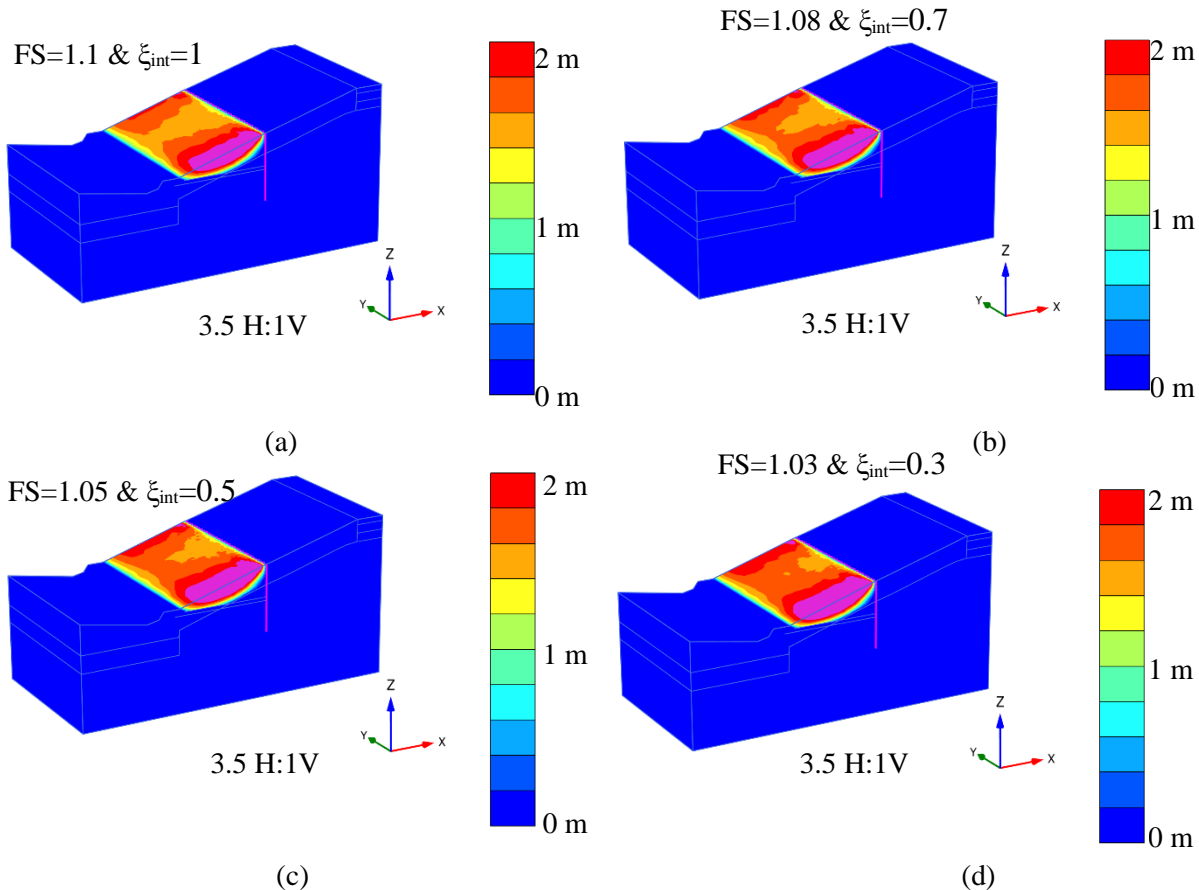


Figure 5.36 Variations in slip surface with different interface strengths for 3.5H:1V slope ratio at Sowell road highway slope (a) $\xi_{int}=1$ (b) $\xi_{int}=0.7$ (c) $\xi_{int}=0.5$ (d) $\xi_{int}=0.3$

5.7 McRaven Road Highway Slope

5.7.1 Flow Analysis

5.7.1.1 Model Development

The Finite Element Method (FEM) program PLAXIS 3D was used to conduct a fully flow analysis. A 15-node triangular element was used. The Mohr-Coulomb model is used to define the mechanistic behavior of soil, and the van Genuchten model is considered as the hydraulic model to define the infiltration/seepage behavior. The soil parameters were used in the numerical analysis using PLAXIS 3D, as shown in Table 5.8. The soil parameters were obtained, conducted at each site slope at the crest, middle, and toe of the slope at three different depths of 9.1 m (29.8 ft), 7.6 m (24.9 ft), and 6 m (19.6 ft) respectively. Based on the soil properties, Poisson's ratio was considered to be 0.3. The discharge function and representative soil model are presented in Figure 5.37 for the three selected site slopes. The global model boundary condition, as outlined in the figure, is defined as open flow along the vertical direction (Z-axis) and closed for horizontal direction (X-axis). However, the flow along the translation direction (Y-axis) is also considered a closed boundary. The initial depth of the water table was selected to be 8 ft (2.43 m) below the ground surface based on observation on the field.

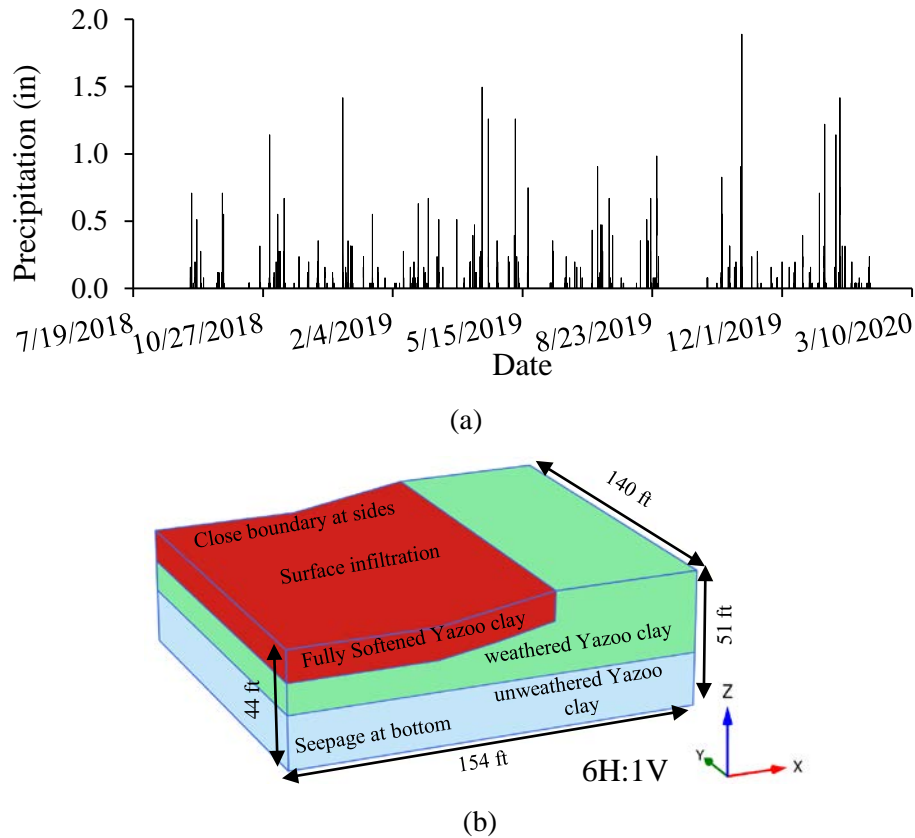


Figure 5.37 (a) Natural daily precipitation input as a discharge function for McRaven Road highway slope, and (b) FEM soil model with the boundary conditions for McRaven road highway slope

Table 5. 6 Soil parameters for FEM analysis

Parameter	Name	Unit	Fully softened Yazoo clay	Weathered Yazoo clay	Unweathered Yazoo clay	Silty clay
Bulk unit weight	γ_{unsat}	kN/m ³ (pcf)	19.7 (125.4)	20.2 (128.5)	19.9 (126.6)	19.6 (124.7)
Saturated unit weight	γ_{sat}	kN/m ³ (pcf)	21.2 (134.9)	21.1 (134.3)	19.9 (126.6)	20.5 (130.5)
Permeability	$k_x=k_y=k_z$	cm/sec (ft/day)	0.0012 (1.23E-5)	3.06E-6 (0.0086)	3.06E-6 (0.0086)	3.06E-6 (0.0086)
Young's modulus	E	kN/m ² (psf)	4.70E3 (98.16E3)	7.10E3 (148.28E3)	9.50E3 (198.41E3)	4.30E3 (89.80E3)
Poisson's ratio	ν	-	0.3	0.3	0.25	0.3
Cohesion	C	kN/m ² (psf)	0.62 (13)	11.9 (248.5)	18.4 (384.2)	9.5 (198.4)
Friction angle	Φ	degree	6 °	19 °	20 °	20 °

5.7.1.2 FEM Flow Analysis Results

During the FEM analysis, the infiltration and open boundary were used at the topsoil layer, the seepage boundary was used for the bottom soil layer, and the closed boundary was used for the sides of the

soil model. The model conditions for a groundwater flow calculation can be defined at the extreme boundaries of the model. The open boundary layer in Plaxis allows the formation of the seepage travel pass during the infiltration at the upstream of the shells. The groundwater level was located at the ground surface as reported during the site investigation to define the initial unsaturated condition. The total daily real-time rainfall period (August 2018 to June 2019) was considered for the discharge function input for the flow analysis to simulate the failure condition.

Figure 5.38 presents the depth of moisture variation for fully softened Yazoo clay at the surficial layer with a maximum total rainfall volume of about 2 in (50.8 mm) for Slope 6 with a 6H:1V slope ratio. It can be observed that before any rainfall event, the primary value of suction was about 3000 psf (112.7 kPa), which dropped to a value of 1380 psf (65.9 kPa) after a one-day rainfall event. The suction immediately dropped at the top surficial soil layer after rainfall and continued for thirty days, representing the active wetting depth. The topsoil layer experienced a drop of moisture variation after the rainfall event and varied slightly after seven days of rainfall. Finally, after 30 days of the rainfall event, the moisture variation dropped about 21.1%. It can be seen that the most critical moisture variation occurred at the topsoil layer (less than 12 ft. (3.6 m)). In addition, the change in suction continued several days to weeks post-rainfall to reach a steady value at the critical depth.

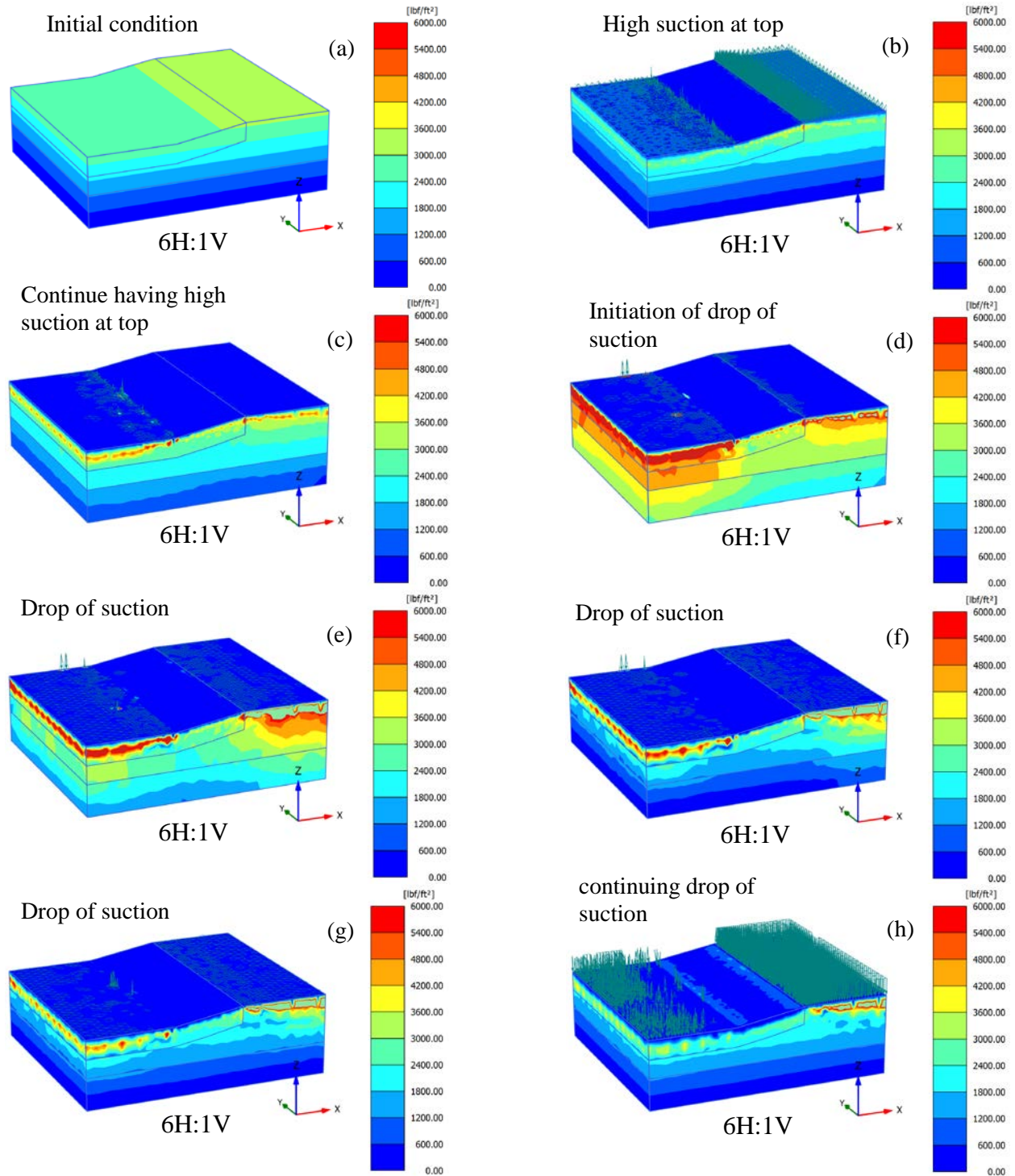


Figure 5.38 FEM flow analysis results (Depth of moisture variation profiles) for McRaven road highway slope for Max of 2 in (50.8 mm) daily rainfall (a) Prior to rainfall (b) 30 min after rainfall (c) 60 min after rainfall (d) 12 hrs after rainfall (e) 1 day after rainfall (f) 3 days after rainfall (g) 7 days after rainfall (h) 15 days after rainfall

5.7.2 Stability Analysis

During this study, stability analysis was conducted considering the unsaturated moisture and matric suction variation of the soil, as investigated by the fully coupled flow analysis in Slope 6. In this analysis, time-dependent hydro-mechanical behavior of the soil is described in a coupled format, taking both deformation and groundwater flow into account, in which mixed equations of displacement and pore pressure, are solved simultaneously. Based on the effective stress, pore water pressure, and matric suction profile developed by coupled-flow deformation analysis, the factor of safety of the slope was determined using the phi-c reduction method in Plaxis 3D, which is alternately known as the shear strength reduction analysis.

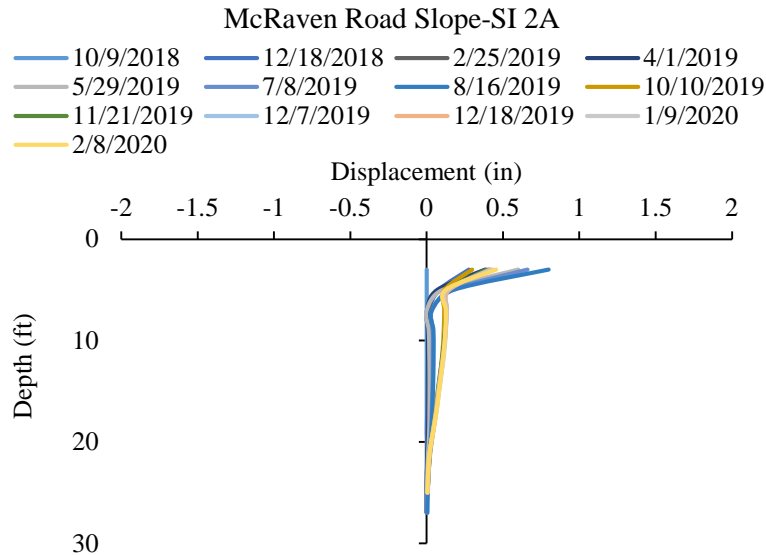


Figure 5.39 Horizontal deformations of slope 6 at the as-built section

The slope 6 has faced consistent movement throughout the monitoring period, as presented in Figure 5.39. Based on the field monitoring results, it can be seen that the slope is moving as it experienced a high rainfall period. During this analysis, the actual rainfall from field instrumentation was utilized as an input. However, such analysis requires significant computation power, and time for the analysis is extremely time-consuming. As a result, an alternative analysis was performed, where the effect of the total rainfall (120 inches) was used as an input within a short period of time, and then the changes of the factor of safety were evaluated at a different time period. The stability analysis results followed by coupled-flow deformation analysis is presented in Figure 5.40, which indicated a consistent drop in the factor of safety (from 1.15 to 1.09) of the slope with progressive rainfall. It should be noted that for this analysis, the back-analysis cohesion and friction angle was utilized, as indicated in Table 5.8.

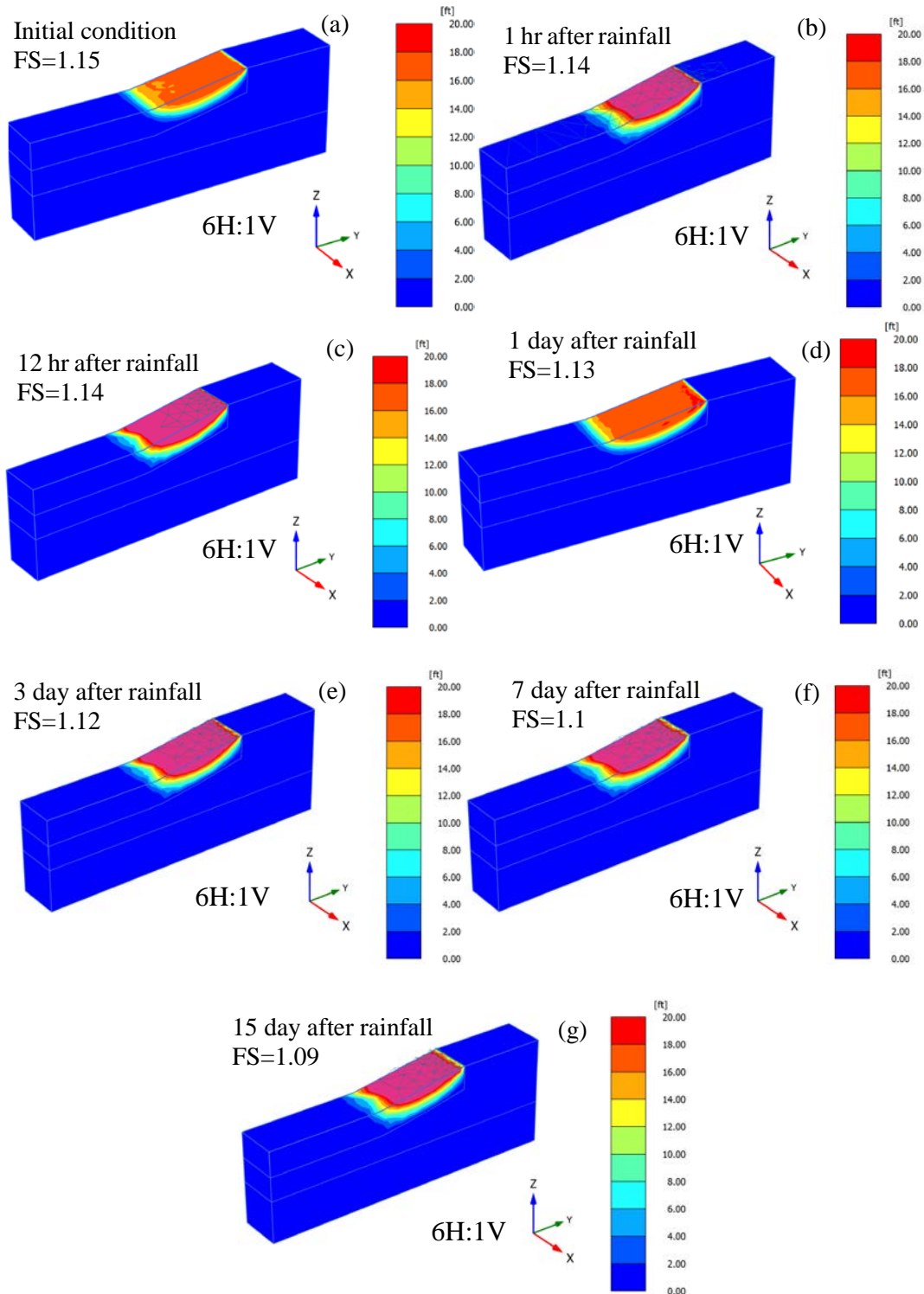


Figure 5.40 Variation in slip surface for the critical total natural rainfall amount of 120 inches (3048 mm) throughout the monitoring period of Slope 6 (a) Prior to rainfall (b) 1 hr. after rainfall (c) 12 hrs. after rainfall (d) 1 day after rainfall (e) 3 days after rainfall (f) 1 day after rainfall (g) 15 days after rainfall

Chapter 6: CONCLUSIONS

6.1 Conclusion

Slope failures are frequent in highway embankments on expansive Yazoo clay in Mississippi due to the rainfall and climatic variation. The objective of the current study was to investigate the infiltration behavior of the slope on expansive Yazoo clay during rainfall using field monitoring and evaluate its impact on the safety of the slope. Six repaired highway slopes were instrumented comprehensively to monitor the moisture content, matric suction, and temperature variation, and the movement of the slope. Besides field monitoring, numerical modeling using the Finite Element Method (FEM) was conducted to evaluate the effect of different frequency and duration of rainfall (based on historical rainfall data of Mississippi) on the infiltration and corresponding change in the factor of safety of the highway slope. Finally, the field monitoring data and FEM analysis results were combined to evaluate the performance of the repaired slope.

6.2 Major Findings

The major findings of the study are summarized in the following:

- I. Based on the field monitoring results, volumetric moisture content was observed almost constant throughout all six slopes. Certain peaks and drops in the moisture content were observed during the summertime, which happened because of the shrinkage/desiccation cracks that increase the vertical permeability and allow more infiltration during early fall. The infiltrated water stayed in the slope, which eventually creates a perched water condition.
- II. The matric suction variation along the highway slopes also remained constant, similar to the constant moisture content variation. Moreover, once the matric suction variation reached to an equilibrium condition, a very low value (10 kPa) was observed for all slope throughout the monitoring period, which indicated the soil within the slopes are almost fully saturated condition. It is another indication that there exists a perched water zone in the highway slopes.
- III. The existence of the perched water condition within the highway slopes makes the condition vulnerable. The portion of the slopes that is repaired with reinforcement (such as H-pile) resisted any sliding. However, the section of the slopes that has no reinforcement or any other means of repair technique has shown the shallow sliding movement in Slope 3 (Terry Road) and Slope 6 (McRaven Road). Moreover, the Slope 5 (Sowell Road) has already experienced a sliding movement up to 12 ft. depth beyond the H-pile reinforcement. However, in most cases, the expected failure depth is within shallow (5-7 ft.) depth.
- IV. The flow analysis and coupled flow deformation analysis results from the extensive numerical study are in good agreement with the field instrumentation results. The flow analysis results indicated at moisture variation up to 10-12 ft. deep, whereas from the field instrumentation, the depth of the moisture variation was observed as 12 ft. Therefore, based on this study, the depth of the active zone within the Yazoo clay can be considered as 12 ft.
- V. Based on the numerical analysis results, two scenarios can be defined for Yazoo Clay in terms of seasonal variations, summer, and late fall. Parameters such as permeability, rainfall intensity, rainfall duration, infiltration, and surface runoff may impact the accumulation of residual water that can have a significant influence on shallow slope failure. In the summertime, with high rainfall intensity and short rainfall duration, the slope may experience high permeability and low surface runoff, which may increase the infiltration at the surficial soil level and increase the perched water development rate. In contrast, with low rainfall intensity and long rainfall duration, the residual water may not form very rapidly. In late fall, even with high rainfall intensity and short rainfall duration, the residual water may be slightly impacted due to the slow infiltration process. Similarly, at the same seasonal time, the same trend may result in low

rainfall intensity and long rainfall duration. The interdependency of the rainfall, permeability, and development of perched water conditions are summarized in Table 6.1.

Table 6.1 Development of perched water conditions

Seasonal Variation	Soil Vertical Permeability	Rainfall Intensity	Rainfall Duration	Infiltration	Percolation	Surface Runoff	Residual Water (Perched Water)
Summer to Early Fall	High	High	Short	Slow	Slow	High	Low
		Low	Long	Rapid	Slow	Low	High
Late Fall to Early Summer	Low	High	Short	Slow	Slow	Rapid	Low
		Low	Long	Slow	Slow	Low	Low

- VI. It is evident from the literature that the variation in numbers of the wet-dry cycles increases the void ratio of Yazoo clay. With the changes in the void ratio of the Yazoo clay, the shear strength of the soil, especially the cohesion, dropped significantly. With 7 numbers of wet-dry cycles, a 77% drop in cohesion was observed. The stability analysis of slope made of Yazoo clay with a different number of wet-dry cycle shear strengths on the topsoil decreased from 2.7 to 1.4 as the number of wet-dry cycle increases. Considering the effect of two rainfall periods of 126.2 mm in 2 hours' period and 271.7 mm at 3 days' period, the factor of safety reduced from 1.7 to 1.2 and 1.68 to 1.02 respectively considering the effect of the 3, 5 and 7 numbers of wet-dry cycles at the topsoil. It is observed that the factor of safety reached a critical value, which is a coupled effect of the changes in the shear strength due to 7 numbers of wet-dry cycles and saturation due to sustained rainfall for 3 days.
- VII. The effect of the progressive change in shear strength due to the softening behavior of the expansive Yazoo clay with a combination of rainfall creates the most vulnerable situation for 2H: 1V slopes at fully softened shear strength with the presence of rainfall [126.2 mm (4.96 in) to 312.4 mm (12.2 in)]. On the other hand, 3H: 1V and 4H: 1V slopes are subjected to failure with the presence of rainfall at a residual state.
- VIII. Based on the study, it is very likely that any slopes made of Yazoo clay or High-Volume Clay (HVC) in Mississippi have a perched water zone within the top 10-12 ft. after few years down the line of construction. Moreover, the shear strength of the clay is likely to be in between the fully soften to residual state based on the number of wet-dry cycles it has been subjected to. To stabilize the landslides on Yazoo clay, an introduction of the drainage layer along the slipping surface will drain out the water and reduce the possibility of development of the perched water zone. Moreover, the slope should be reinforced to increase the resistance along the slipping plane, which will also provide resistance due to the softening behavior of Yazoo and HVC clay. It is highly recommended to consider a perched water zone in the slope stability analysis of any slope made of Yazoo/HVC clay. Moreover, adding drainage layer and reinforcing elements (such as short piles, Recycled Plastic pins, or other proven techniques to repair shallow slope failure) can be an effective technique to stabilize the landslides on Yazoo clay.

REFERENCES

- Ahmed, A., Hossain, M. D. S., and Khan, M. S. (2017). "Unsaturated Hydraulic Properties and Suction Variation on a Pavement Subgrade Over Expansive Soil." Transportation Research Board 97th Annual Meeting Transportation Research Board, Issue 18-04297.
- Alam, J. B., Hossain, M. S., Ahmed, A., and Khan, M. S. (2017). "Comparison of deep percolation of flat and slope section vegetated lysimeters using field soil water characteristic curve." Proc. Second Pan-American Conference on Unsaturated Soils, Geo-Institute of ASCE, Dallas, TX.
- Alonso, E.; Romero, E.; Hoffmann, C.; Garcia-Escudero, E. (2005). "Expansive bentonite-sand mixtures in cyclic controlled-suction drying and wetting." Eng. Geol. 2005, 81, 213–226.
- ASTM D3080/D3080M-11, Standard Test Method for Direct Shear Test of Soils Under Consolidated Drained Conditions; ASTM International: West Conshohocken, PA, USA, 2011.
- Bishop, A. W., Green, G. E., Garga, V. K., Andresen, A., and Brown, J. D. (1971). "A new ring shear apparatus and its application to the measurement of residual strength." Géotechnique, 21(4), 273–328.
- BS 5930, (1981). "Code of practice for site investigations." British Standard Institution, London.
- Carter, M., and Bentley, S., P. (1991). Correlations of soil properties, Pentech.
- Chabrillat, S., Goetz, A.F., Krosley, L., Olsen, H.W. (2002). "Use of hyperspectral images in the identification and mapping of expansive clay soils and the role of spatial resolution." Remote Sens. Environ. 82 (2), 431–445.
- Charles, L. (2008). "Geotechnical aspects of buildings on expansive soils in Kibaha, Tanzania." Doctoral Thesis, Division of Soil and Rock Mechanics, Department of Civil and Architectural Engineering, Royal Institute of Technology Stockholm, Sweden.
- Chleborad, A., F., Diehl, S., F., and Cannon, S., H. (2008). "Geotechnical properties of selected material from the slumgullion landslide."
- D. G. Fredlund, N. R. Morgenstern, R. A. Widger (1978). "The shear strength of unsaturated soils." Canadian Geotechnical Journal, 1978, 15:313-321.
- Das, B.M. (2013). "Advanced Soil Mechanics." CRC Press, Boca Raton, FL.
- De Freitas MH, Mannion WG, 2007, A biostratigraphy for the London Clay in London, Conference on Stiff Sedimentary Clays - Genesis and Engineering Behaviour, Publisher: ICE PUBLISHING, Pages: 91-99, ISSN: 0016-8505
- Douglas, S. C., and Dunlap, G. T. (2000). "Light commercial construction on Yazoo clay." Proc., 2nd Forensic Congress, ASCE, Reston, Va., 607–616. Edition. PTI Manual, Phoenix, Arizona.
- Douglas, S. C., and Dunlap, G. T. (2000). "Light commercial construction on Yazoo clay." Proc., 2nd Forensic Congress, ASCE, Reston, Va., 607–616.
- Duncan, J. M., and Wright, S. T. (2005). "Soil strength and slope stability." Wiley, New Jersey.
- Fourie, A. B. (1996). "Predicting rainfall-induced slope instability." Proc. Inst. Civ. Eng. Geotech. Eng., 119(4), 211–218.
- Fredlund, D. G., Xing, A., Fredlund, M. D., and Barbour, S. L. (1996). "The relationship of unsaturated soil shear strength to the soil–water characteristic curve." In Canadian Geotechnical Journal, Vol 33, pp. 440–448.
- Fredlund, D. G., and Rahardjo, H. (1993). "Soil Mechanics for unsaturated soils." Wiley, Singapore.
- G. Mesri and A. F. Cepeda-Diaz. (1986). "Residual shear strength of clays and shales." Géotechnique 1986 36:2, 269-274.
- Gan, J. K. M., Fredlund, D. G., and Rahardjo, H. (1988). "Determination of the Shear-Strength Parameters of An Unsaturated Soil Using the Direct Shear Test." Canadian Geotechnical Journal, v. 25, no. 3, p. 500-510.

- Genuchten, V. (1980). "A closed-formed equation for predicting the hydraulic conductivity of unsaturated soils." *Soil Sci.*
- Griffiths, D. V., Lane, P. A. (1999). "Slope stability analysis by finite elements. *Geotechnique* 49 (3).
- Hamilton, J. J. (1966). "Swelling and Shrinking Subsoils." *Canadian Building Digest* 84, Ottawa, Canada.
- Hensen, E.J., Smit, B. (2002). "Why clays swell." *J. Phys. Chem.* 106 (49), 12664–12667.
- Heydinger, A. G. (2003). "Evaluation of seasonal effects on subgrade soils." *Transp. Res. Rec.*, 1821(1), 47-55.
- Hight, D.W., Gasparre, A., Nishimura, S., Minh, N.A., Jardine, R.J., and Coop, M.R. (2007). "Characteristics of the London Clay from Terminal 5 site at Heathrow Airport," *Geotechnique* 57(1), pp. 3 – 18.
- Holtz, R. D., and Kovacs, W. D. (1981). *An Introduction to Geotechnical Engineering*, Prentice-Hall, Englewood Cliffs, NJ, 733 pp
- Hossain, J., Hossain, M. S., and Hoyos, L. R. (2013). "Effect of rainfall on stability of unsaturated earth slope constructed on expansive clay." *Geocongress*. American Society of Civil Engineers, San Diego, CA.
- Hossain, J., Khan, M. S., Hossain, M. S., and Ahmed, A. (2015). "Determination of Active Zone in Expansive Clay in North Texas through Field Instrumentation." *Proc. 95th annual meeting of Transportation Research Board*, Washington D.C.
- Hossain, J., Khan, M.S., Hossain, M.S. and Ahmed, A. (2016) "Determination of Active Zone in Expansive Clay in North Texas through Field Instrumentation," *Proc. 95th Annual Meeting of Transportation Research Board*, January 10-14, 2016, Washington, DC, USA.
- <http://pubs.usgs.gov/bul/b2130/Chapter11.html>, December, 23rd.
- Johnson, L. D. (1973). "Properties of expansive clay soils, Jackson field test section study", Report 1, Misc. Paper S-73-28, U.S. Army Engineer Waterways Experiment Station, Vicksburg, Mississippi.
- Jones, L., D., and Jefferson, I. (2012). "Problematic soils and site investigation." In *ICE manual of Geotechnical Engineering*, volume 1, *Geotechnical Engineering Principles*, pp. 413-441.
- Jones, L.D. and Terrington, R. (2011). "Modelling volume change potential in the London Clay," *Quarterly Journal of Engineering Geology and Hydrogeology*, Vol 44, pp. 109 – 122.
- Jotsankasa, A., and Mairaing, W. (2010). "Suction-Monitored Direct Shear Testing of Residual Soils from Landslide-Prone Areas." In *Journal of Geotechnical and Geoenvironmental Engineering*, Vol 136(3), pp. 533-537.
- Kayyal, M.K. and Wright, S.G. (1991). "Investigation of Long-Term Strength Properties of Paris and Beaumont Clays in Earth Embankments." *Center for Transportation Research*, Research Report 1195-2F.
- Khan, M. S., Hossain, S., Ahmed, A., & Faysal, M. (2017). Investigation of a shallow slope failure on expansive clay in Texas. *Engineering Geology*, 219, 118-129.
- Khan, M.S., Hossain, M.S., Ahmed, A. and Faysal, M. (2016), "Investigation of a shallow slope failure on expansive clay in Texas", *Eng. Geol.*, <http://dx.doi.org/0.1016/j.enggeo.2016.10.004>
- Khan, M.S., Ivoke, J. and Nobahar, M. (2019). "Coupled Effect of Wet-Dry Cycles and Rainfall on Highway slope made of Yazoo Clay." *Geosciences*, Open Access Journal by MDPI, ISSN 2076-3263, Manuscript ID 504447, April 28th, 9(8), 341.
- Kim, Y. K., and Lee, S. R. L. (2010). "Field infiltration characteristics of natural rainfall in compacted roadside slopes." In *Journal of Geotechnical and Geoenvironmental Engineering*, Vol 136(1), 358, pp. 248-252.
- Kovacevic, N., Hight, D.W. and Potts, D.M. (2007). "Predicting the stand-up time of temporary London Clay slopes at Terminal 5, Heathrow Airport," *Geotechnique* 57(1), pp. 63 – 74.
- Kutschke, W. G. and Vallejo, L. E. (2010). "Failure analysis of an instrumented stiff clay slope." *GeoFlorida*, ASCE.

- Lee Jr, L. T. (2012). “State Study 151 and 236: Yazoo Clay Investigation.” MDOT State Study 236, US Army Corps of Engineers.
- Lee Jr, L. T. (2012). “State Study 151 and 236: Yazoo Clay Investigation” (No. FHWA/MS-DOT-RD-11-236).
- Lee, Jr, Landris, T. (2012). “State Study 151 and 236: Yazoo Clay Investigation.” MDOT State Study 236, US Army Corps of Engineers.
- Lim, T. T., Rahardjo, H., Chang, M. F., and Fredlund, D. G. (1996). “Effect of rainfall on matric suction in a residual soil slope.” In *Canadian Geotechnical Journal*, Vol 33, pp. 618-628.
- Loehr, J. E., and Bowders, J. J. (2007). “Slope stabilization using recycled plastic pins—Phase III.” Final Rep. RI98-007D, Missouri Dept. of Transportation, Jefferson City, MO.
- Loehr, J. E., Fennessey, T. W., and Bowders, J. J. (2007). “Stabilization of surficial slides using recycled plastic reinforcement.” *Transportation Research Record* 1989, Transportation Research Board, Washington, DC.
- Lucian, C. (2008). “Geotechnical aspects of buildings on expansive soils in Kibaha, Tanzania,” Ph.D. Thesis, Division of Soil and Rock Mechanics Department of Civil and Architectural Engineering Royal Institute of Technology Stockholm, Sweden, 196 pp.
- Martin, R. V. (2007). “Sample, describe, and map Yazoo Clay,” Unpublished Report of Mississippi Dept. of Transportation, MDoT Study 151, Jackson, MS.
- Melinda, F., Rahardjo, H., Han, K. K., and Leong, E. C. (2004). “Shear strength of compacted soil under infiltration condition. In *Journal of Geotechnical and Geoenvironmental Engineering*, Vol 130 (8), pp.807-817.
- Mesri, G. and Cepeda-Diaz, F. (1986). “Residual shear strength of clays and shales.” *Géotechnique*, 36(2), 269–274.
- Mesri, G. and Shahien, M. (2003). “Residual shear strength mobilized in first-time slope.” *Journal of Geotechnical and Geoenvironmental Engineering*, Vol. 129, Issue 1.
- Mitchell, J. K. (1993). *Fundamentals of Soil Behavior*, 3rd ed., John Wiley, New York.
- National Academies of Sciences, Engineering, and Medicine. 2007. *Cone Penetrating Testing*. Washington, DC: The National Academies Press.
- National Oceanic and Atmospheric Administration Daily Climate Report. (2014), <https://hdsc.nws.noaa.gov/hdsc/pfds/pfds_map_cont.html?bkmrk=ms> (Apr. 21, 2017)
- Nelson, J.; Miller, J.D. *Expansive Soils: Problems and Practice in Foundation and Pavement Engineering*; John Wiley & Sons, Inc.: Hoboken, NJ, USA, 1992.
- Nobahar M., Khan M.S., Ivoke J., Amini F. (2019). “Impact of Rainfall Variation on Slope made of Expansive Yazoo Clay Soil in Mississippi.” *Transportation Infrastructure Geotechnology*, Springer US, Online ISSN 2196-7210, July 27th. <https://doi.org/10.1007/s40515-019-00083-w>
- Nobahar, M., Khan, M. S., and Ivoke, J. (2020). “Combined Effect of Rainfall and Shear strength on the Stability of Highway Embankments made of Yazoo Clay in Mississippi.” *Journal of Geotechnical and Geological Engineering*, Springer US, Online ISSN 0960-3182, Jan 9th.
- Redus, J. F. (1962). “Experiences with expansive clay in Jackson, Miss.,” *Moisture, Density, Swelling and Swell Pressure Relationships*, Highway Research Board Bulletin No. 313, pp 40 - 46.
- Robertson, P., K., and Cabal, K., L. (2015). “Guide to Cone penetration Testing for geotechnical Engineering.” *Gregg Drilling and Testing, INC.*, 6th edition.
- Rogers, L.E. and Wright, S. G. (1986). “The effect of Wetting and Drying on the Long-Term Shear Strength Parameters for Compacted Beaumont Clay”. Research Rep. 436-2F, Center for Transportation Research, University of Texas at Austin, 1986.
- Rosenbalm, D., and Zapata, C., E. (2017). “Effect of wetting and drying cycles on the behavior of compacted expansive soils.” *Journal of Materials in Civil Engineering* Vol. 29, Issue 1 (January 2017).
- Seed, H. B., Mitchell, J. K. and Chan, C. K., (1960). “The strength of compacted cohesive soils.” *Journal of the Soil Mechanics and Foundations Division, ASCE, Soil Mechanics and foundation division*, vol. 88, No. SM-3, pp. 53-87.

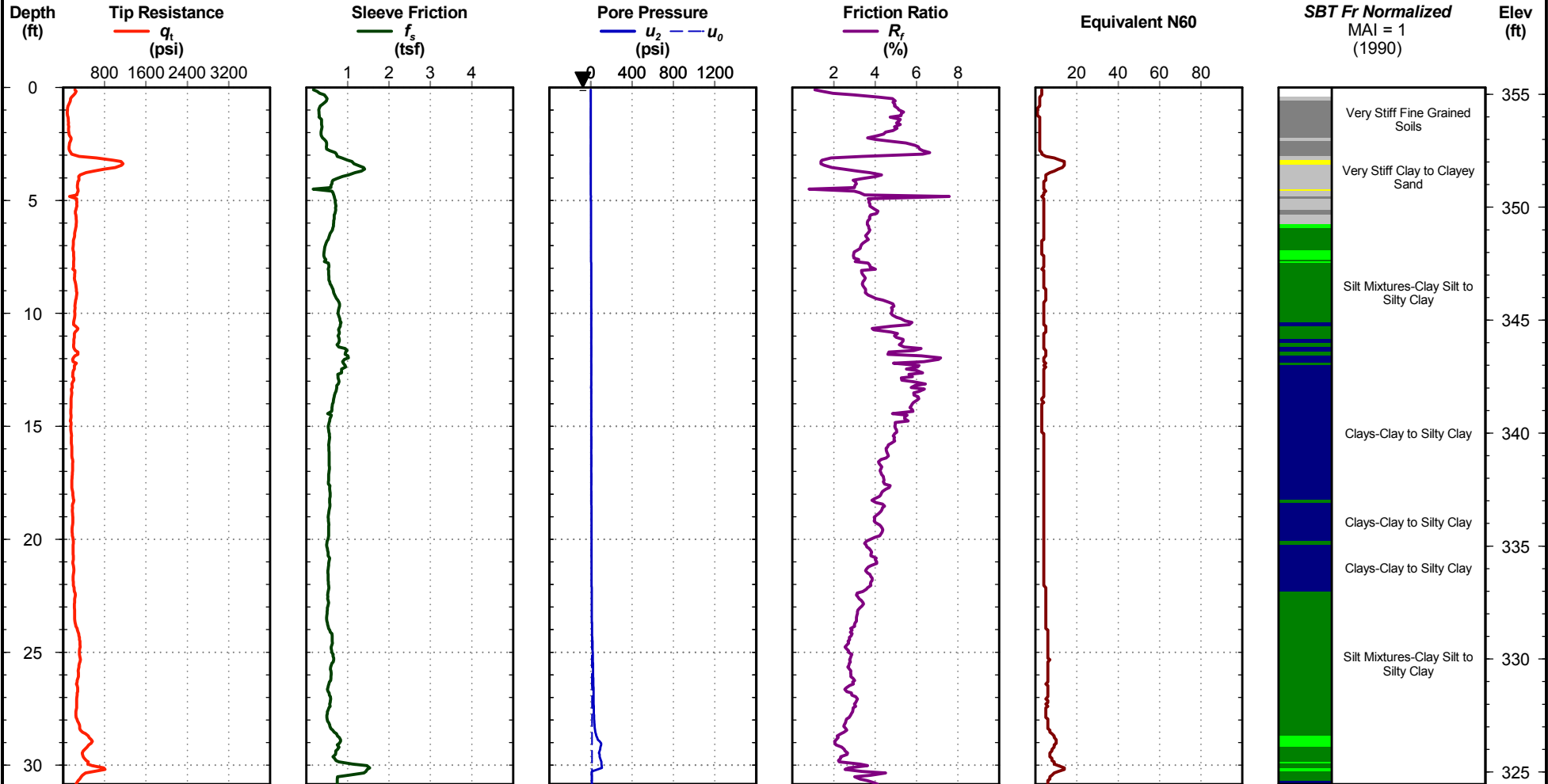
- Skempton, A.W. (1964). “Long-term stability of clay slopes.” *Géotechnique*, 14(2), 77–101.
- Skempton, A.W. (1977). “Slope Stability of Cuttings in Brown London Clay.” In *Proceedings of Ninth International Conference on Soil Mechanics and Foundation Engineering*, Tokyo, Vol. 3, 261-270.
- Skempton, A.W. (1984). “Slope Stability of Cuttings in Brown London Clay.” In *Proc. of Ninth International Conference on Soil Mechanics and Foundation Engineering*, Tokyo, Vol. 3, 261-270.
- Taylor, A.C. (2005). “Mineralogy and engineering properties of the Yazoo clay formation”, Jackson Group, Master’s Thesis, Mississippi State University.
- Tourtelot, H., A. (1973). “Regional geochemical investigations.” *Front Range Urban Corridor*, Colorado, Geological Society of America, v. 5, no. 6, p. 520-521.
- Tripathy, S.; Rao, K.S.; Fredlund, D.G. Water content—Void ratio swell-shrink paths of compacted expansive soils. *Can. Geotech. J.* 2002, 39, 938–959.
- US Army Corps of Engineers (USACE). 1970. *Laboratory soils manual*. EM 1110-2-1906. Vicksburg, MS:US Army Corps of Engineers Waterways Experiment Station.
- Van Der Merwe, D. H. (1964). “The prediction of heave from the plasticity index and percentage clay fraction of soils,” *Civil Engineer in South Africa* 6(6), pp. 103- 107.
- Weaver, C., C. (1989). “Clays, muds, and shales.” *Development in sedimentology* 44, Elsevier Science.
- Wright, S. G. (2005). “Evaluation of Soil Shear Strengths for Slope and Retaining Wall Stability Analyses with Emphasis on High plasticity Clays.” Federal Highway Administration, Washington, D.C, FHWA/TX-06/5-1874-01-1.
- Zapata, C.E.; Andrei, D.; Witczak, M.W.; Houston, W.N. Incorporation of Environmental Effects in Pavement Design. *Road Mater. Pavement Des.* 2007, 8, 667–693.
- Zhan, L, and Ng, C., W., W., and Fredlund, D., G. (2007). “Field study of rainfall infiltration into a grassed unsaturated expansive soil slope.” *Canadian Geotechnical Journal* 44(4):392-408.
- Zornberg, J.G., J. Kuhn, and Wright, S. (2007). “Determination of Field Suction Values, Hydraulic Properties and Shear Strength in High PI Clays.” Research Rep. 0-5202-1, Center for Transportation Research, the University of Texas at Austin.

APPENDIX A
CONE PENETRATION TEST (CPT) RESULTS

Project #: 18-1106-0004
Date: Apr. 30, 2018

Northing:
Easting:

Elevation: 355.3
Filename: slope 1c-1A.cpt



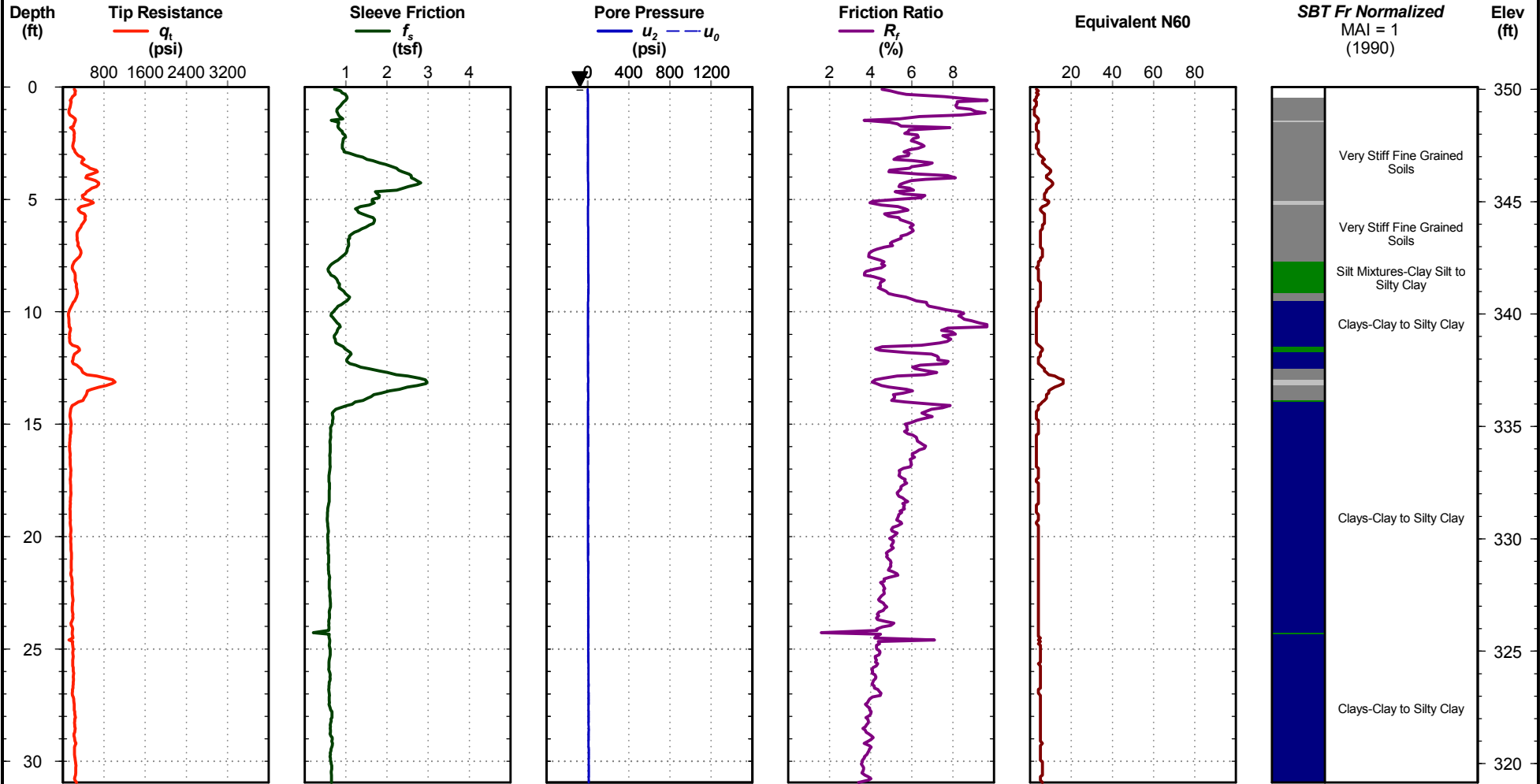
- | | | |
|--|--|---|
| 1 - Sensitive, Fine Grained Soils | 4 - Silt Mixtures-Clay Silt to Silty Clay | 7 - Gravelly Sand to Sand |
| 2 - Organic Soils, Peats | 5 - Sand Mixtures-Silty Sand to Sandy Silt | 8 - Very Stiff Clay to Clayey Sand |
| 3 - Clays-Clay to Silty Clay | 6 - Sands-Clean Sand to Silty Sand | 9 - Very Stiff Fine Grained Soils |

slope 1 c-1

Project #: 18-1106-0004
Date: Apr. 30, 2018

Northing:
Easting:

Elevation: 350.1
Filename: slope 1c-2A.cpt



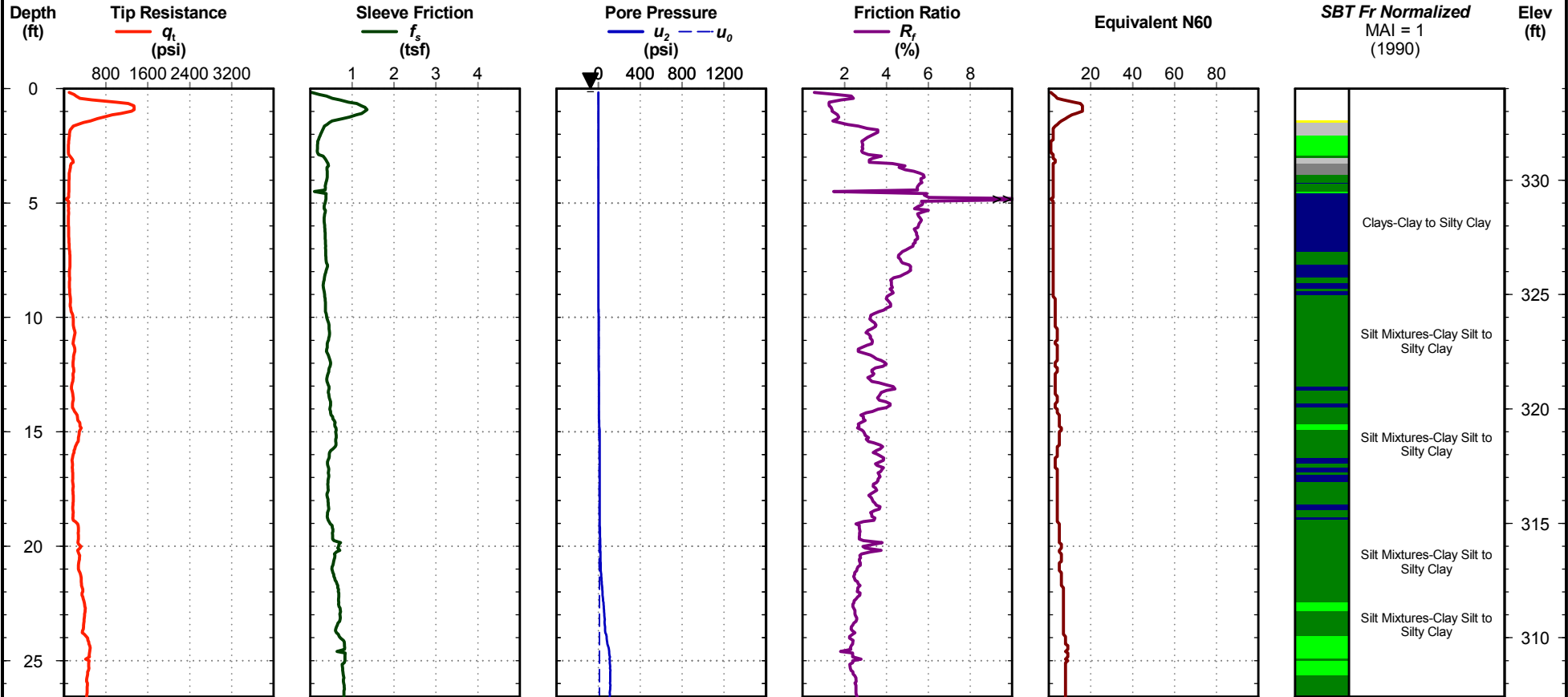
- | | | |
|--|--|---|
| 1 - Sensitive, Fine Grained Soils | 4 - Silt Mixtures-Clay Silt to Silty Clay | 7 - Gravelly Sand to Sand |
| 2 - Organic Soils, Peats | 5 - Sand Mixtures-Silty Sand to Sandy Silt | 8 - Very Stiff Clay to Clayey Sand |
| 3 - Clays-Clay to Silty Clay | 6 - Sands-Clean Sand to Silty Sand | 9 - Very Stiff Fine Grained Soils |

slope 1 c-2

Project #: 18-1106-0004
Date: Apr. 30, 2018

Northing:
Easting:

Elevation: 334
Filename: slope 1c-3A.cpt



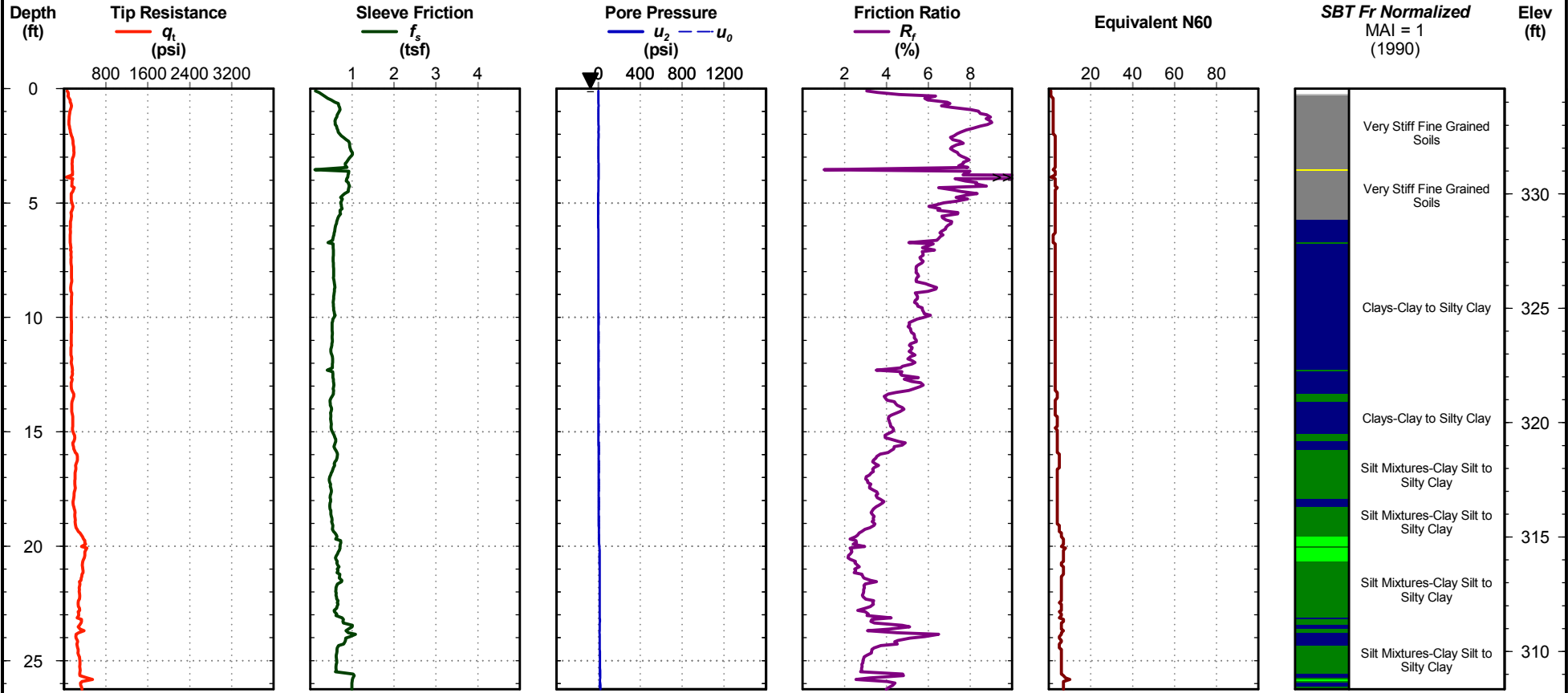
- | | | |
|--|--|---|
| 1 - Sensitive, Fine Grained Soils | 4 - Silt Mixtures-Clay Silt to Silty Clay | 7 - Gravelly Sand to Sand |
| 2 - Organic Soils, Peats | 5 - Sand Mixtures-Silty Sand to Sandy Silt | 8 - Very Stiff Clay to Clayey Sand |
| 3 - Clays-Clay to Silty Clay | 6 - Sands-Clean Sand to Silty Sand | 9 - Very Stiff Fine Grained Soils |

slope 1 c-3

Project #: 18-1106-0004
Date: Apr. 30, 2018

Northing:
Easting:

Elevation: 334.6
Filename: slope 1c-4A.cpt



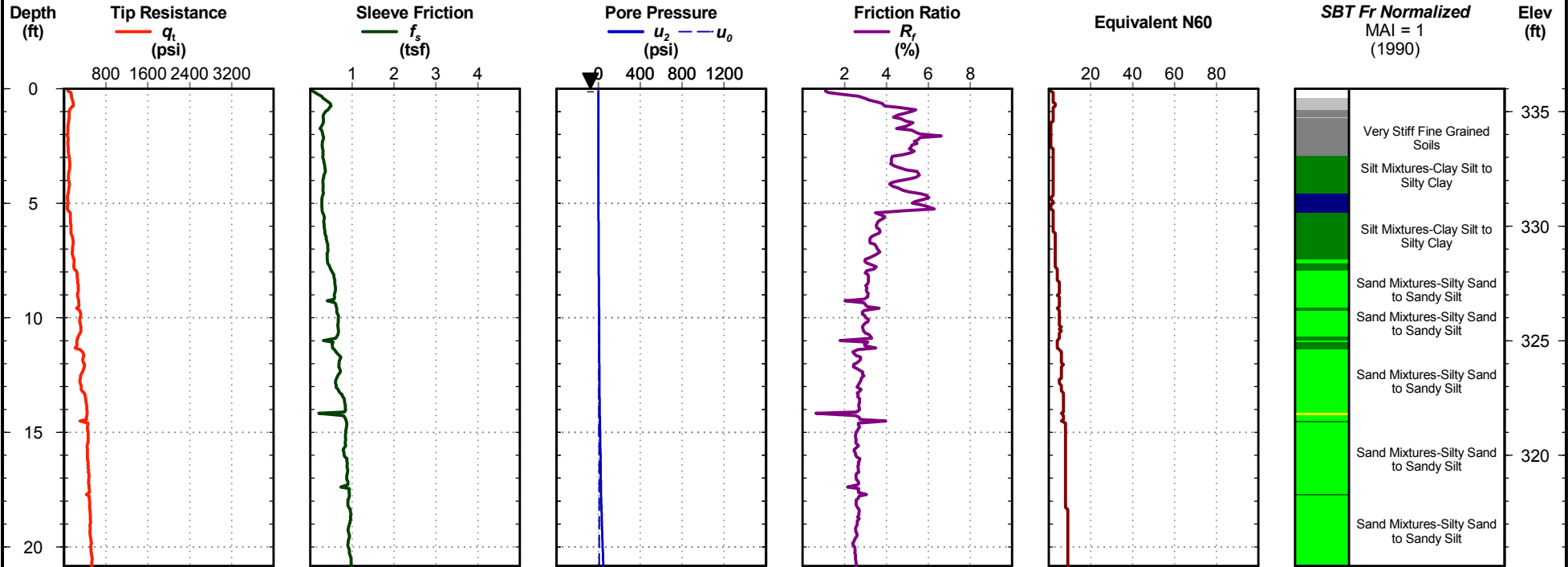
- 1 - Sensitive, Fine Grained Soils
- 4 - Silt Mixtures-Clay Silt to Silty Clay
- 7 - Gravelly Sand to Sand
- 2 - Organic Soils, Peats
- 5 - Sand Mixtures-Silty Sand to Sandy Silt
- 8 - Very Stiff Clay to Clayey Sand
- 3 - Clays-Clay to Silty Clay
- 6 - Sands-Clean Sand to Silty Sand
- 9 - Very Stiff Fine Grained Soils

slope 1 c-4

Project #: 18-1106-0004
Date: Apr. 30, 2018

Northing:
Easting:

Elevation: 336
Filename: slope 1c-5A.cpt



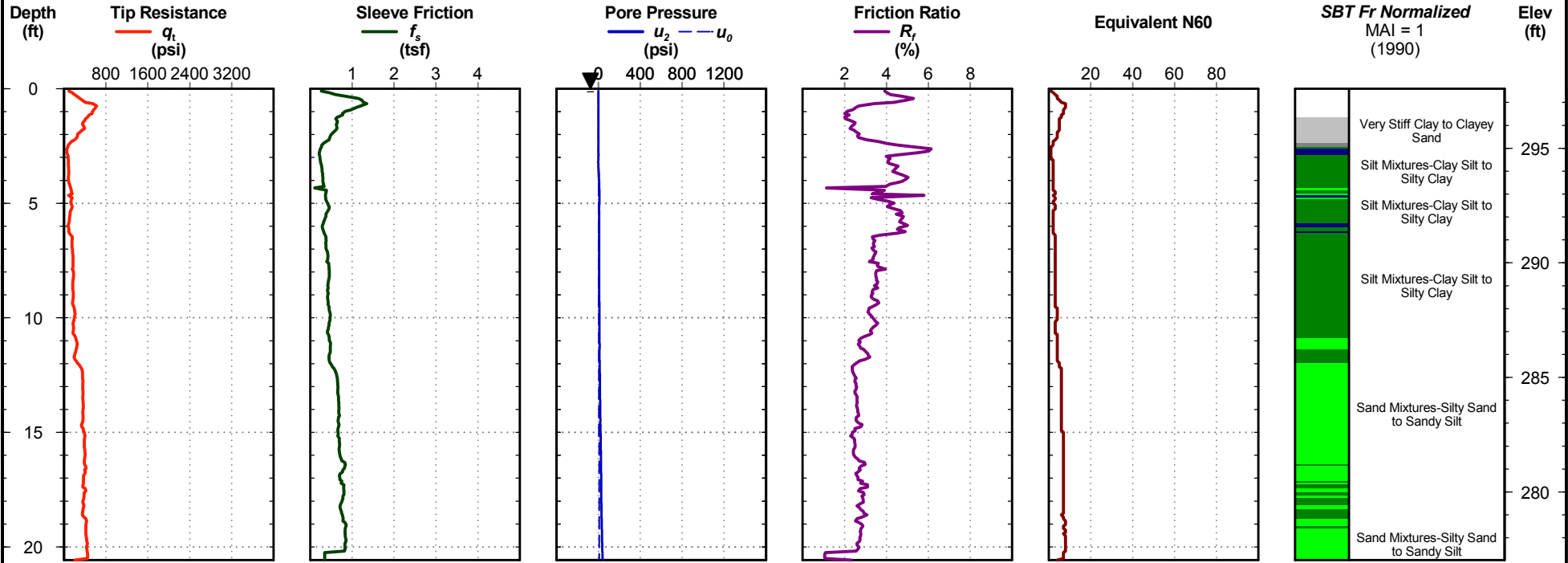
- | | | |
|--|--|---|
| ■ 1 - Sensitive, Fine Grained Soils | ■ 4 - Silt Mixtures-Clay Silt to Silty Clay | ■ 7 - Gravelly Sand to Sand |
| ■ 2 - Organic Soils, Peats | ■ 5 - Sand Mixtures-Silty Sand to Sandy Silt | ■ 8 - Very Stiff Clay to Clayey Sand |
| ■ 3 - Clays-Clay to Silty Clay | ■ 6 - Sands-Clean Sand to Silty Sand | ■ 9 - Very Stiff Fine Grained Soils |

slope 1 c-5

Project #: 18-1106-0004
Date: Apr. 30, 2018

Northing:
Easting:

Elevation: 297.6
Filename: slope 1c-6A[1].cpt



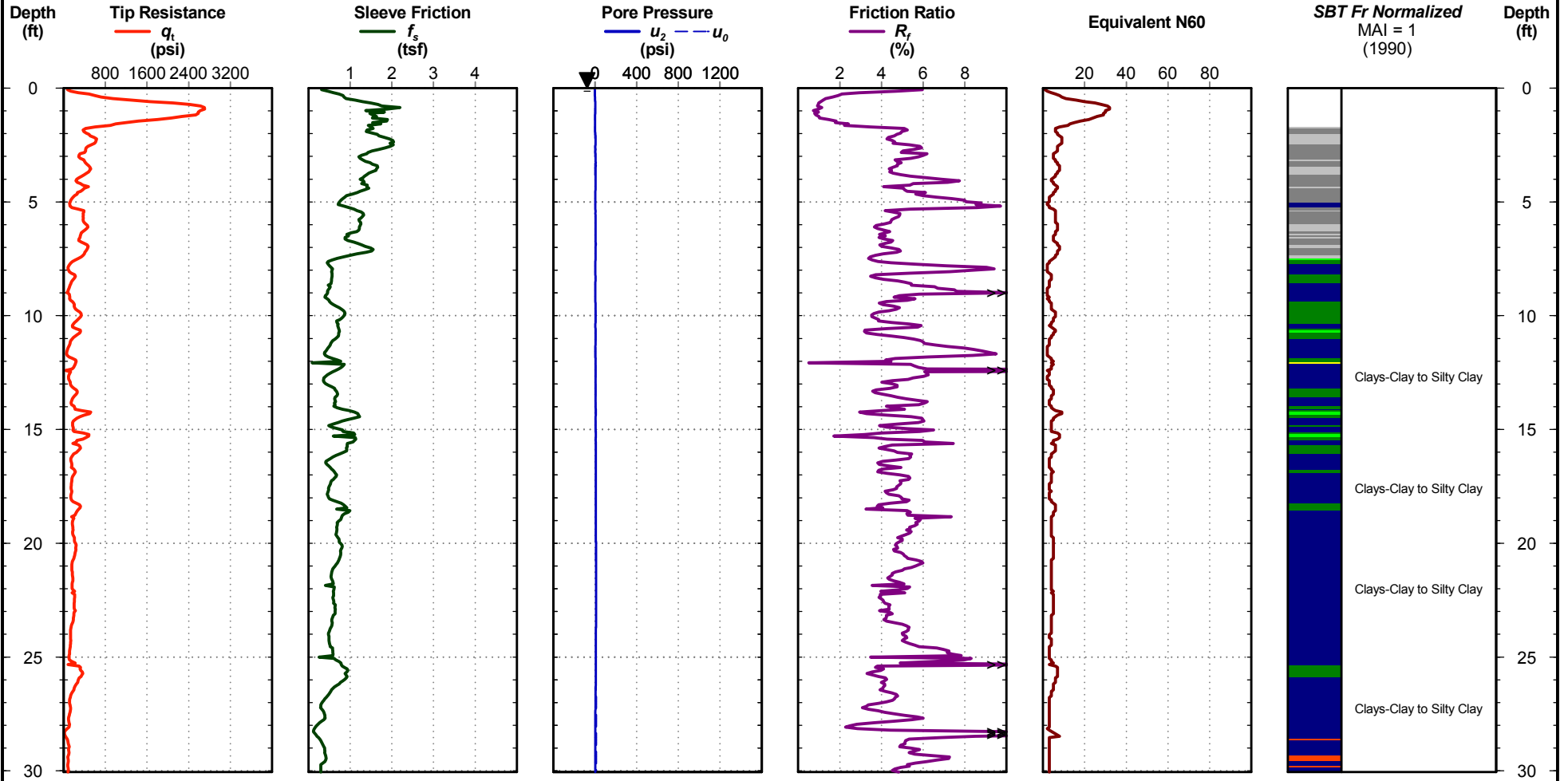
- | | | |
|--|--|---|
| 1 - Sensitive, Fine Grained Soils | 4 - Silt Mixtures-Clay Silt to Silty Clay | 7 - Gravelly Sand to Sand |
| 2 - Organic Soils, Peats | 5 - Sand Mixtures-Silty Sand to Sandy Silt | 8 - Very Stiff Clay to Clayey Sand |
| 3 - Clays-Clay to Silty Clay | 6 - Sands-Clean Sand to Silty Sand | 9 - Very Stiff Fine Grained Soils |

slope 1 c-6

Project #: 18-1106-0004
Date: May 23, 2018

Northing:
Easting:

Elevation:
Filename: Metro Center CPT-2A.cpt



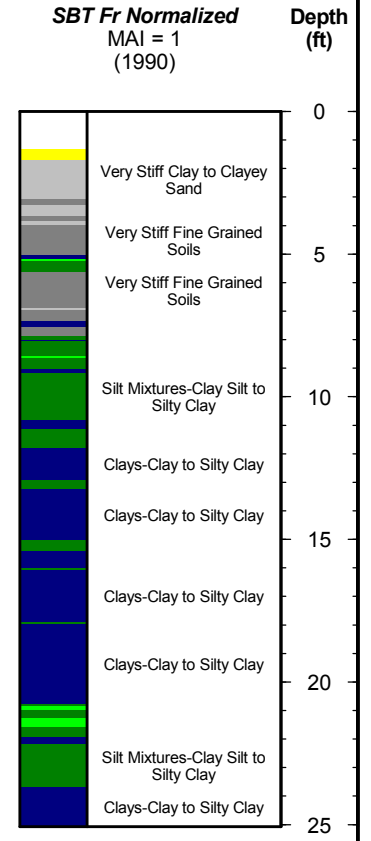
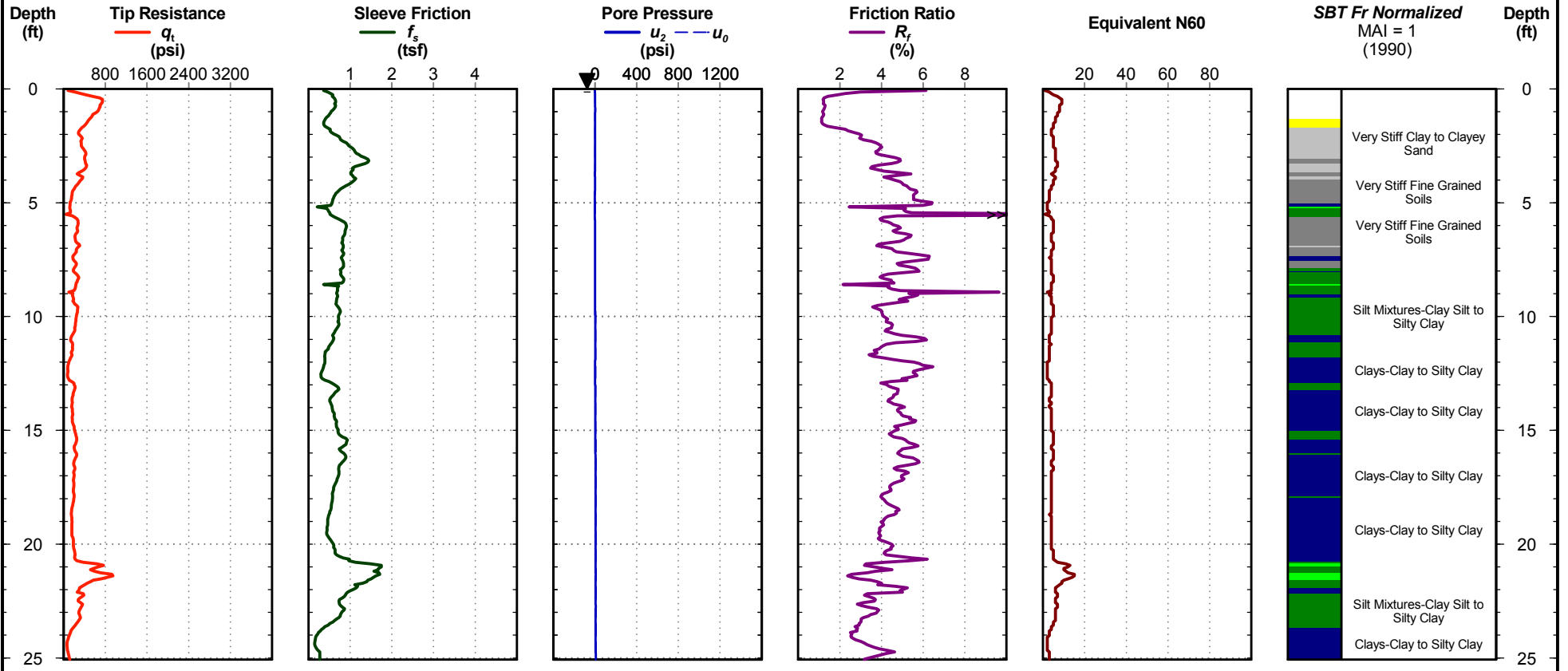
- | | | |
|--|--|---|
| 1 - Sensitive, Fine Grained Soils | 4 - Silt Mixtures-Clay Silt to Silty Clay | 7 - Gravelly Sand to Sand |
| 2 - Organic Soils, Peats | 5 - Sand Mixtures-Silty Sand to Sandy Silt | 8 - Very Stiff Clay to Clayey Sand |
| 3 - Clays-Clay to Silty Clay | 6 - Sands-Clean Sand to Silty Sand | 9 - Very Stiff Fine Grained Soils |

slope 2 c-2

Project #: 18-1106-0004
Date: May. 23, 2018

Northing:
Easting:

Elevation:
Filename: Metro Center CPT-4A.cpt

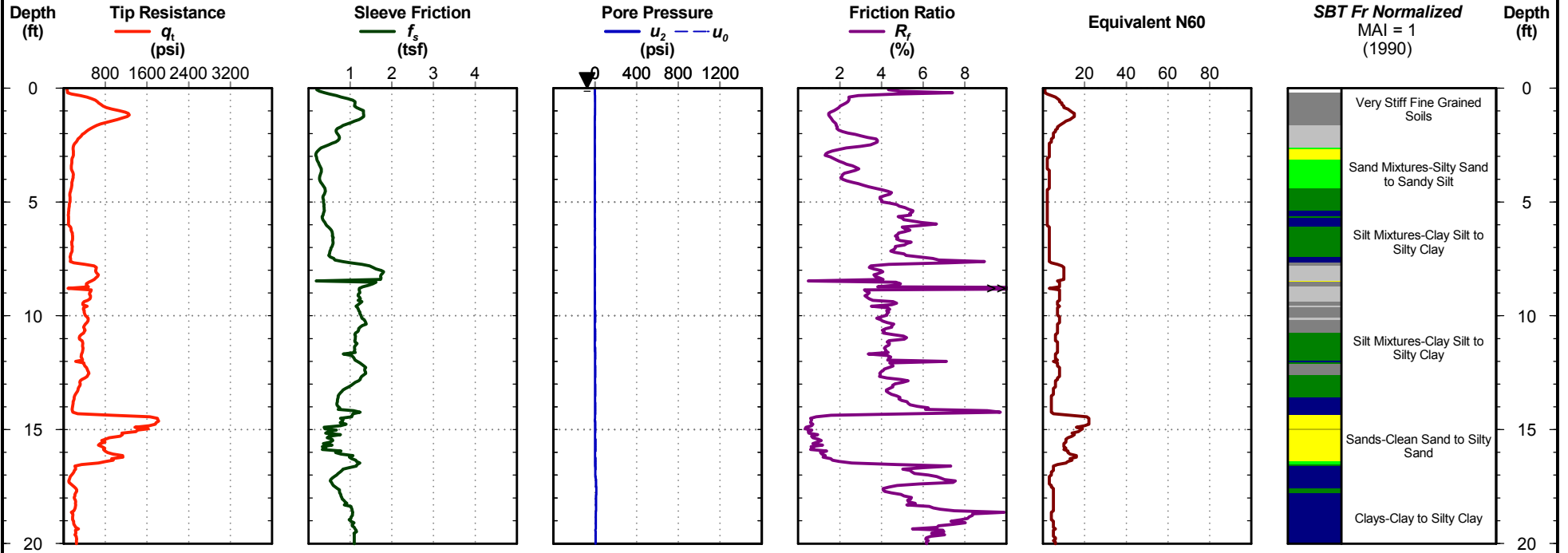


- | | | |
|--|--|---|
| ■ 1 - Sensitive, Fine Grained Soils | ■ 4 - Silt Mixtures-Clay Silt to Silty Clay | ■ 7 - Gravelly Sand to Sand |
| ■ 2 - Organic Soils, Peats | ■ 5 - Sand Mixtures-Silty Sand to Sandy Silt | ■ 8 - Very Stiff Clay to Clayey Sand |
| ■ 3 - Clays-Clay to Silty Clay | ■ 6 - Sands-Clean Sand to Silty Sand | ■ 9 - Very Stiff Fine Grained Soils |

Project #: 18-1106-0004
Date: May. 23, 2018

Northing:
Easting:

Elevation:
Filename: Metro Center CPT-5A.cpt



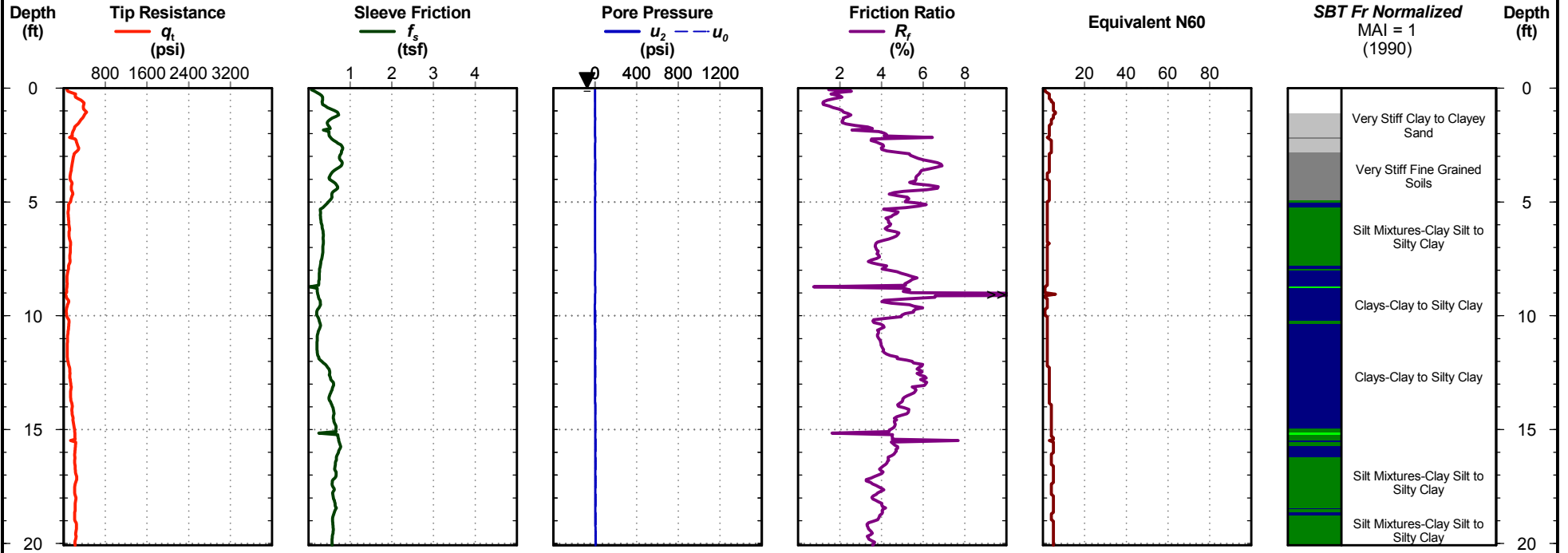
- | | | |
|--|--|---|
| 1 - Sensitive, Fine Grained Soils | 4 - Silt Mixtures-Clay Silt to Silty Clay | 7 - Gravelly Sand to Sand |
| 2 - Organic Soils, Peats | 5 - Sand Mixtures-Silty Sand to Sandy Silt | 8 - Very Stiff Clay to Clayey Sand |
| 3 - Clays-Clay to Silty Clay | 6 - Sands-Clean Sand to Silty Sand | 9 - Very Stiff Fine Grained Soils |

slope 2 c-5

Project #: 18-1106-0004
Date: May. 23, 2018

Northing:
Easting:

Elevation:
Filename: Metro Center CPT-6A.cpt

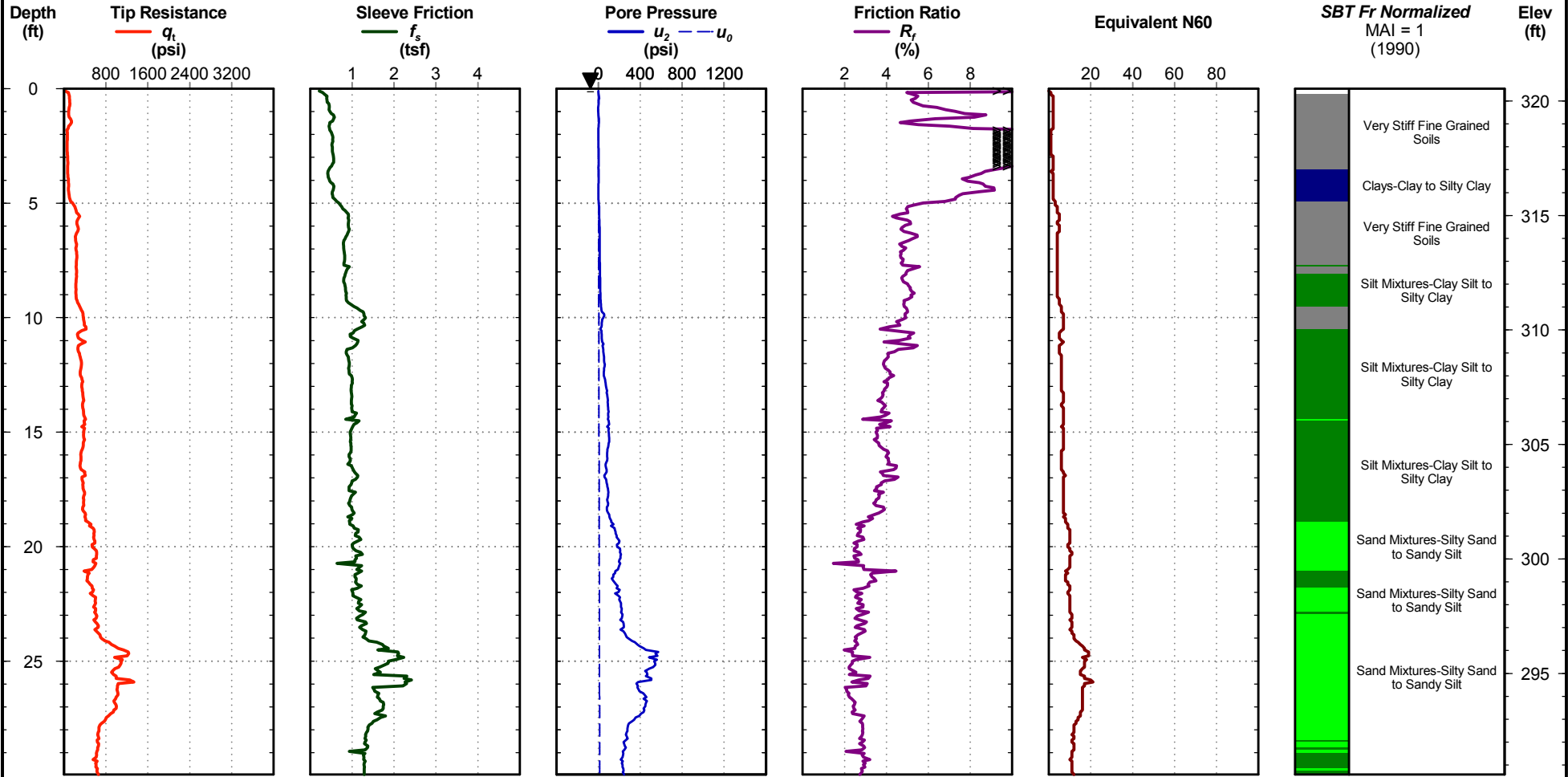


- | | | |
|--|--|---|
| 1 - Sensitive, Fine Grained Soils | 4 - Silt Mixtures-Clay Silt to Silty Clay | 7 - Gravelly Sand to Sand |
| 2 - Organic Soils, Peats | 5 - Sand Mixtures-Silty Sand to Sandy Silt | 8 - Very Stiff Clay to Clayey Sand |
| 3 - Clays-Clay to Silty Clay | 6 - Sands-Clean Sand to Silty Sand | 9 - Very Stiff Fine Grained Soils |

Project #: 18-1106-0004
Date: Apr. 28, 2018

Northing:
Easting:

Elevation: 320.5381
Filename: slope 3c-1A.cpt



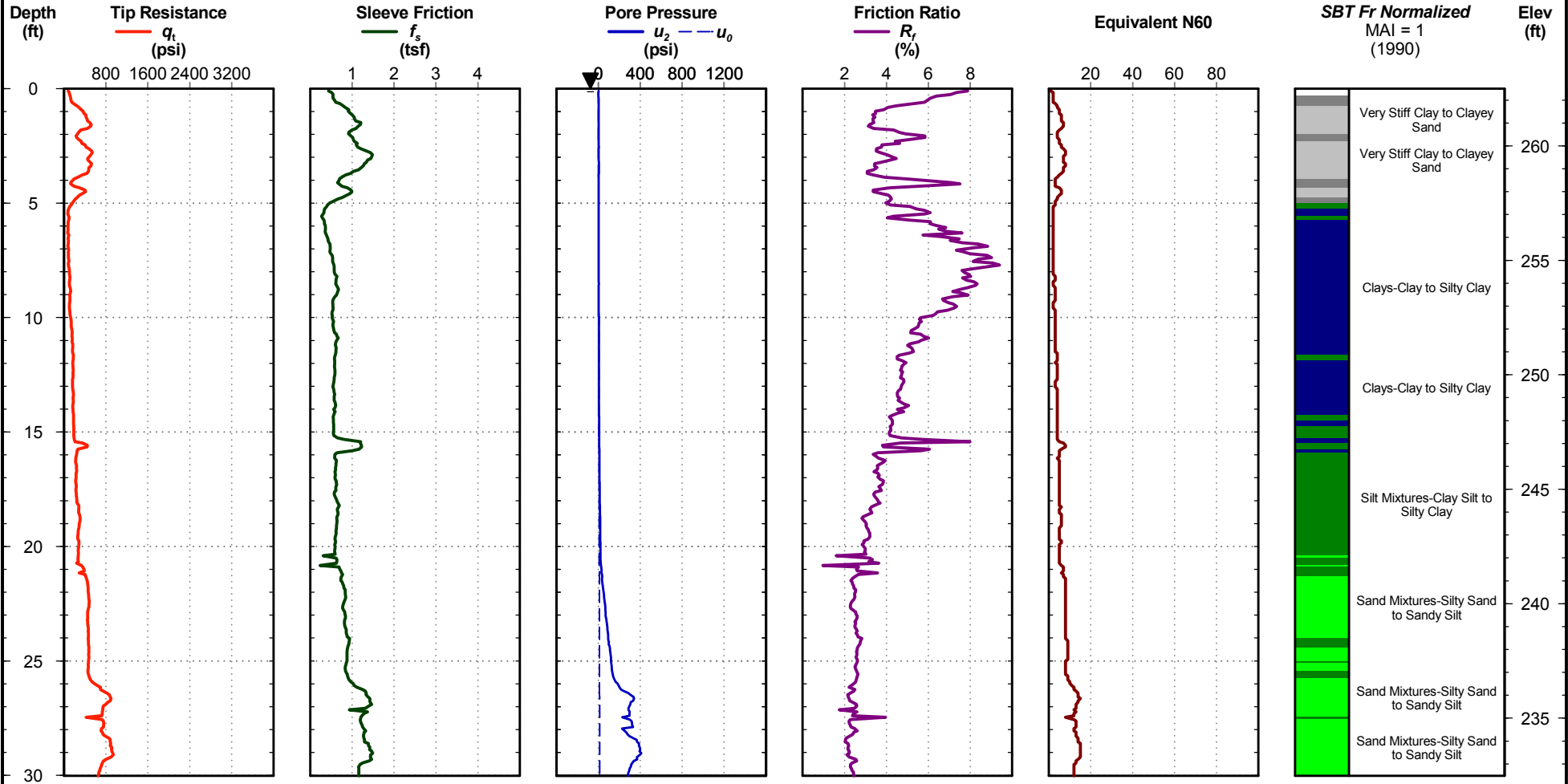
- 1 - Sensitive, Fine Grained Soils
- 4 - Silt Mixtures-Clay Silt to Silty Clay
- 7 - Gravelly Sand to Sand
- 2 - Organic Soils, Peats
- 5 - Sand Mixtures-Silty Sand to Sandy Silt
- 8 - Very Stiff Clay to Clayey Sand
- 3 - Clays-Clay to Silty Clay
- 6 - Sands-Clean Sand to Silty Sand
- 9 - Very Stiff Fine Grained Soils

slope 3 c-1

Project #: 18-1106-0004
Date: Apr. 28, 2018

Northing:
Easting:

Elevation: 262.5
Filename: slope 3c-2A.cpt



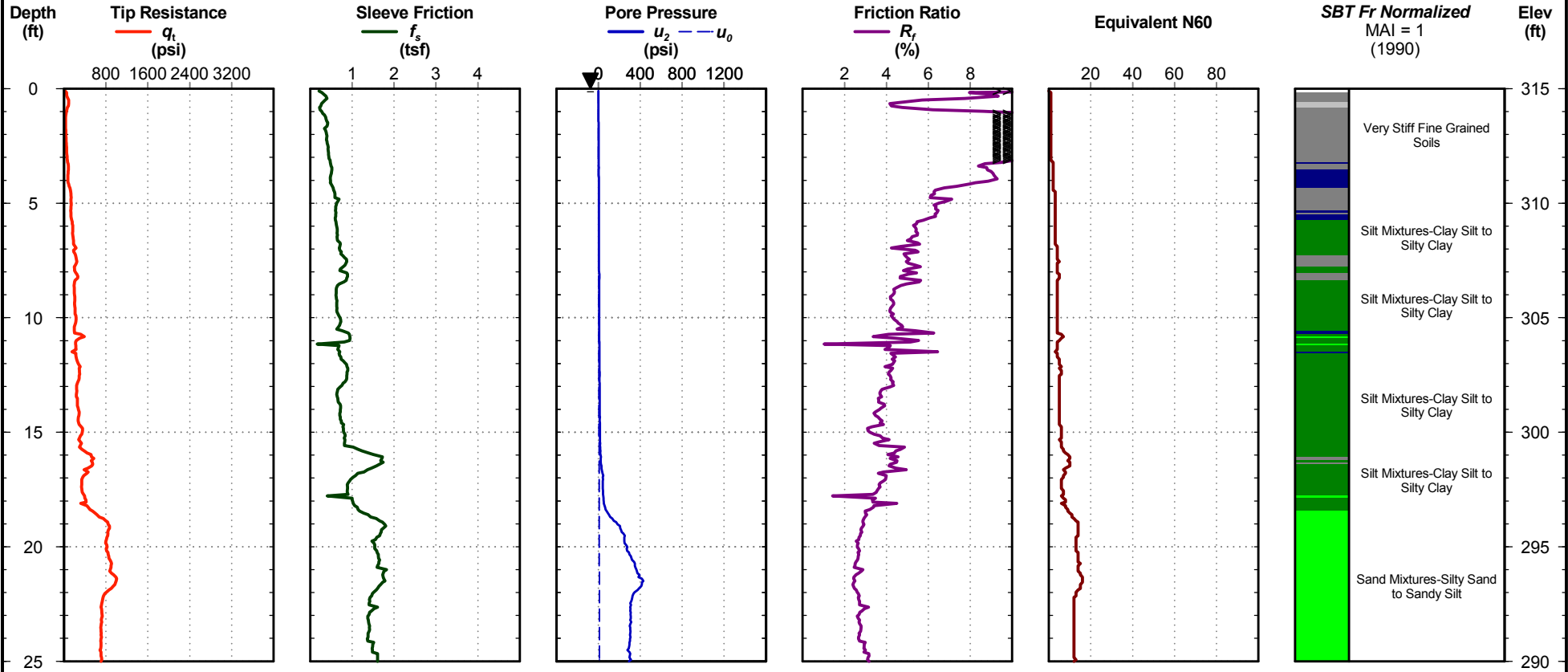
- | | | |
|--|--|--|
| ■ 1 - Sensitive, Fine Grained Soils | ■ 4 - Silt Mixtures-Clay Silt to Silty Clay | ■ 7 - Gravelly Sand to Sand |
| ■ 2 - Organic Soils, Peats | ■ 5 - Sand Mixtures-Silty Sand to Sandy Silt | ■ 8 - Very Stiff Clay to Clayey Sand |
| ■ 3 - Clays-Clay to Silty Clay | ■ 6 - Sands-Clean Sand to Silty Sand | ■ 9 - Very Stiff Fine Grained Soils |

slope 3 c-2

Project #: 18-1106-0004
Date: Apr. 28, 2018

Northing:
Easting:

Elevation: 315
Filename: slope 3c-3A.cpt



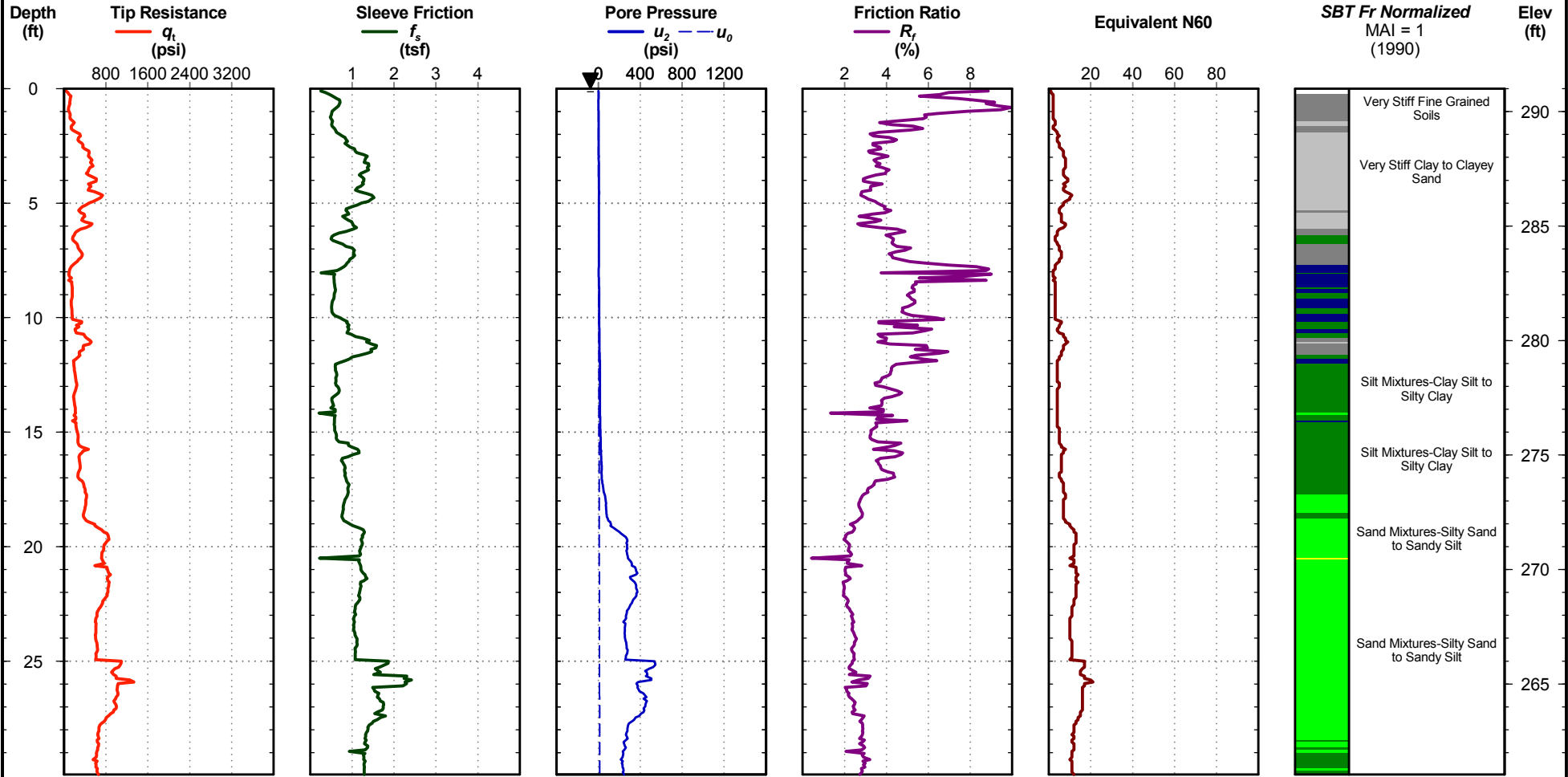
- | | | |
|--|--|---|
| 1 - Sensitive, Fine Grained Soils | 4 - Silt Mixtures-Clay Silt to Silty Clay | 7 - Gravelly Sand to Sand |
| 2 - Organic Soils, Peats | 5 - Sand Mixtures-Silty Sand to Sandy Silt | 8 - Very Stiff Clay to Clayey Sand |
| 3 - Clays-Clay to Silty Clay | 6 - Sands-Clean Sand to Silty Sand | 9 - Very Stiff Fine Grained Soils |

slope 3 c-3

Project #: 18-1106-0004
Date: Apr. 28, 2018

Northing:
Easting:

Elevation: 291
Filename: slope 3c-4A.cpt



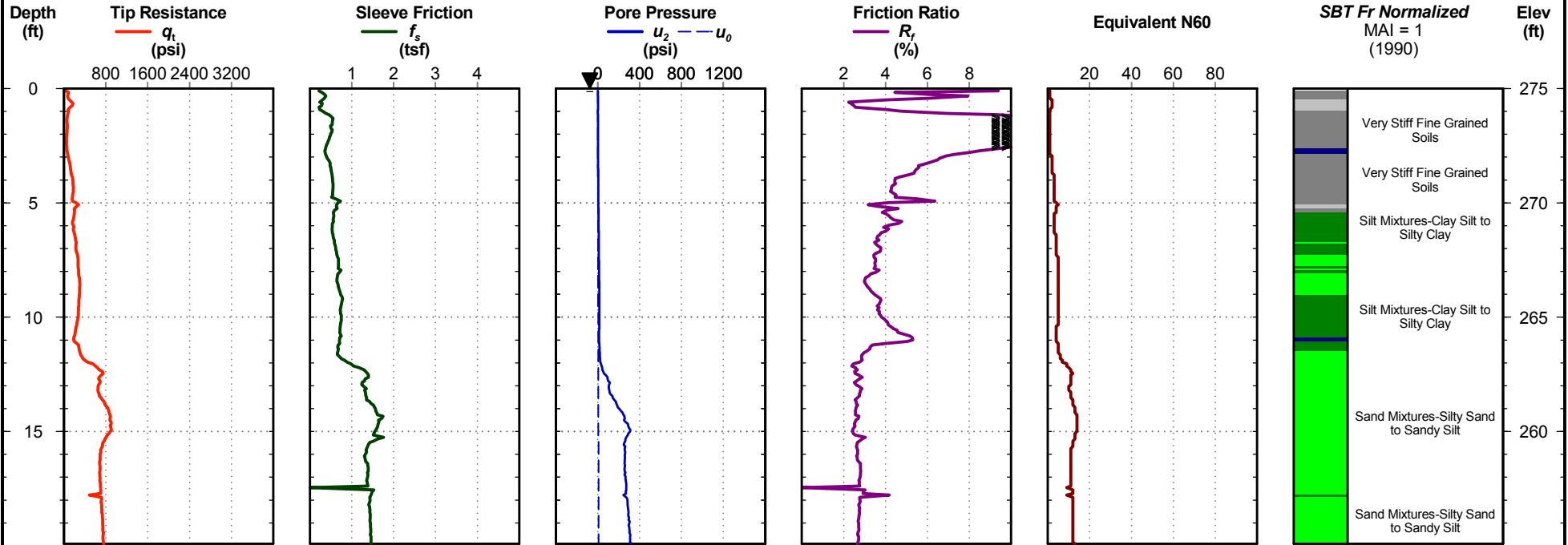
- | | | |
|--|--|---|
| ■ 1 - Sensitive, Fine Grained Soils | ■ 4 - Silt Mixtures-Clay Silt to Silty Clay | ■ 7 - Gravelly Sand to Sand |
| ■ 2 - Organic Soils, Peats | ■ 5 - Sand Mixtures-Silty Sand to Sandy Silt | ■ 8 - Very Stiff Clay to Clayey Sand |
| ■ 3 - Clays-Clay to Silty Clay | ■ 6 - Sands-Clean Sand to Silty Sand | ■ 9 - Very Stiff Fine Grained Soils |

slope 3 c-4

Project #: 18-1106-0004
Date: Apr. 28, 2018

Northing:
Easting:

Elevation: 275
Filename: slope 3c-5A.cpt



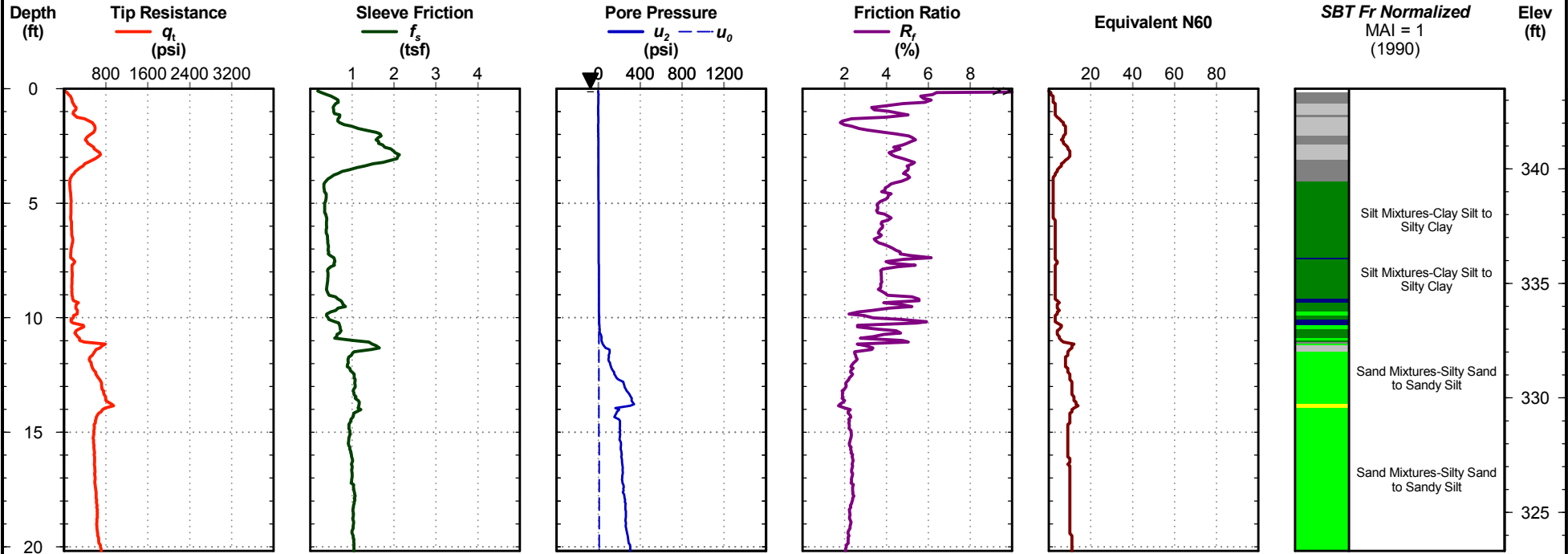
- | | | |
|--|--|---|
| 1 - Sensitive, Fine Grained Soils | 4 - Silt Mixtures-Clay Silt to Silty Clay | 7 - Gravelly Sand to Sand |
| 2 - Organic Soils, Peats | 5 - Sand Mixtures-Silty Sand to Sandy Silt | 8 - Very Stiff Clay to Clayey Sand |
| 3 - Clays-Clay to Silty Clay | 6 - Sands-Clean Sand to Silty Sand | 9 - Very Stiff Fine Grained Soils |

slope 3 c-5

Project #: 18-1106-0004
Date: Apr. 28, 2018

Northing:
Easting:

Elevation: 343.5
Filename: slope 3c-6A.cpt



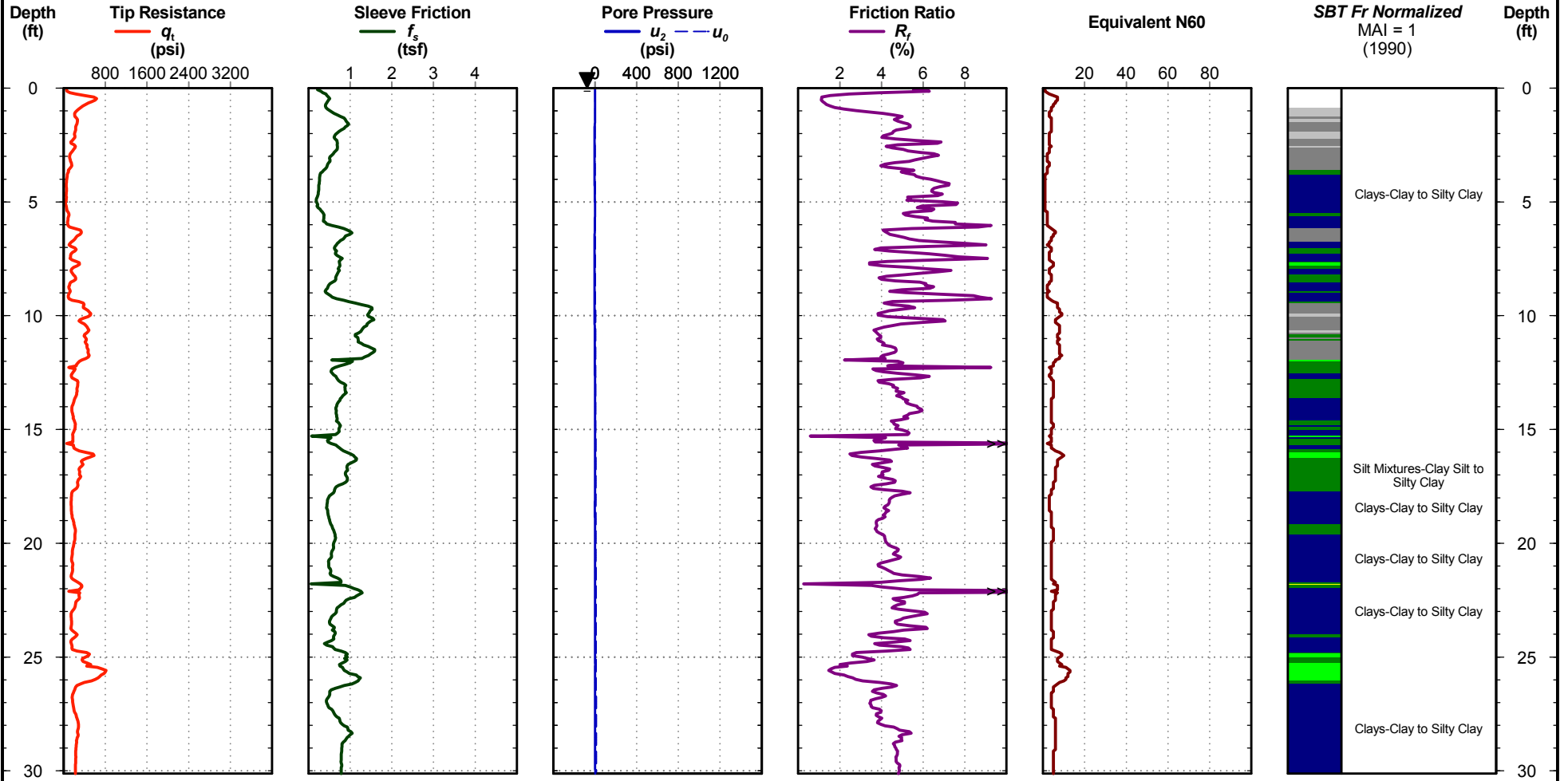
- | | | |
|--|--|---|
| 1 - Sensitive, Fine Grained Soils | 4 - Silt Mixtures-Clay Silt to Silty Clay | 7 - Gravelly Sand to Sand |
| 2 - Organic Soils, Peats | 5 - Sand Mixtures-Silty Sand to Sandy Silt | 8 - Very Stiff Clay to Clayey Sand |
| 3 - Clays-Clay to Silty Clay | 6 - Sands-Clean Sand to Silty Sand | 9 - Very Stiff Fine Grained Soils |

slope 3 c-6

Project #: 18-1106-0004
Date: May. 23, 2018

Northing:
Easting:

Elevation:
Filename: Slope 4 CPT-1A.cpt



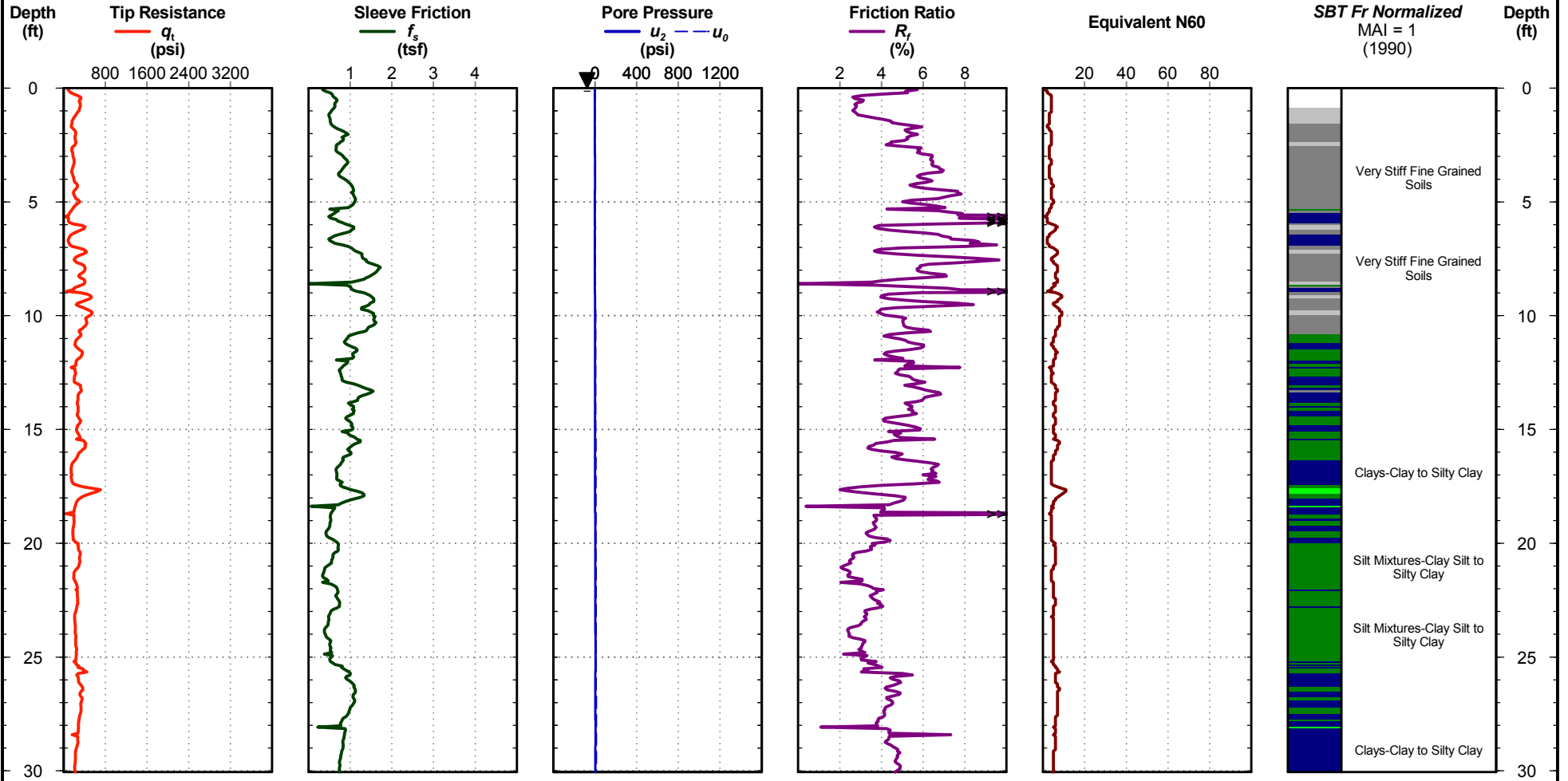
- | | | |
|--|--|---|
| 1 - Sensitive, Fine Grained Soils | 4 - Silt Mixtures-Clay Silt to Silty Clay | 7 - Gravelly Sand to Sand |
| 2 - Organic Soils, Peats | 5 - Sand Mixtures-Silty Sand to Sandy Silt | 8 - Very Stiff Clay to Clayey Sand |
| 3 - Clays-Clay to Silty Clay | 6 - Sands-Clean Sand to Silty Sand | 9 - Very Stiff Fine Grained Soils |

slope 4 c-1

Project #: 18-1106-0004
Date: May. 23, 2018

Northing:
Easting:

Elevation:
Filename: Slope 4 CPT-2A.cpt



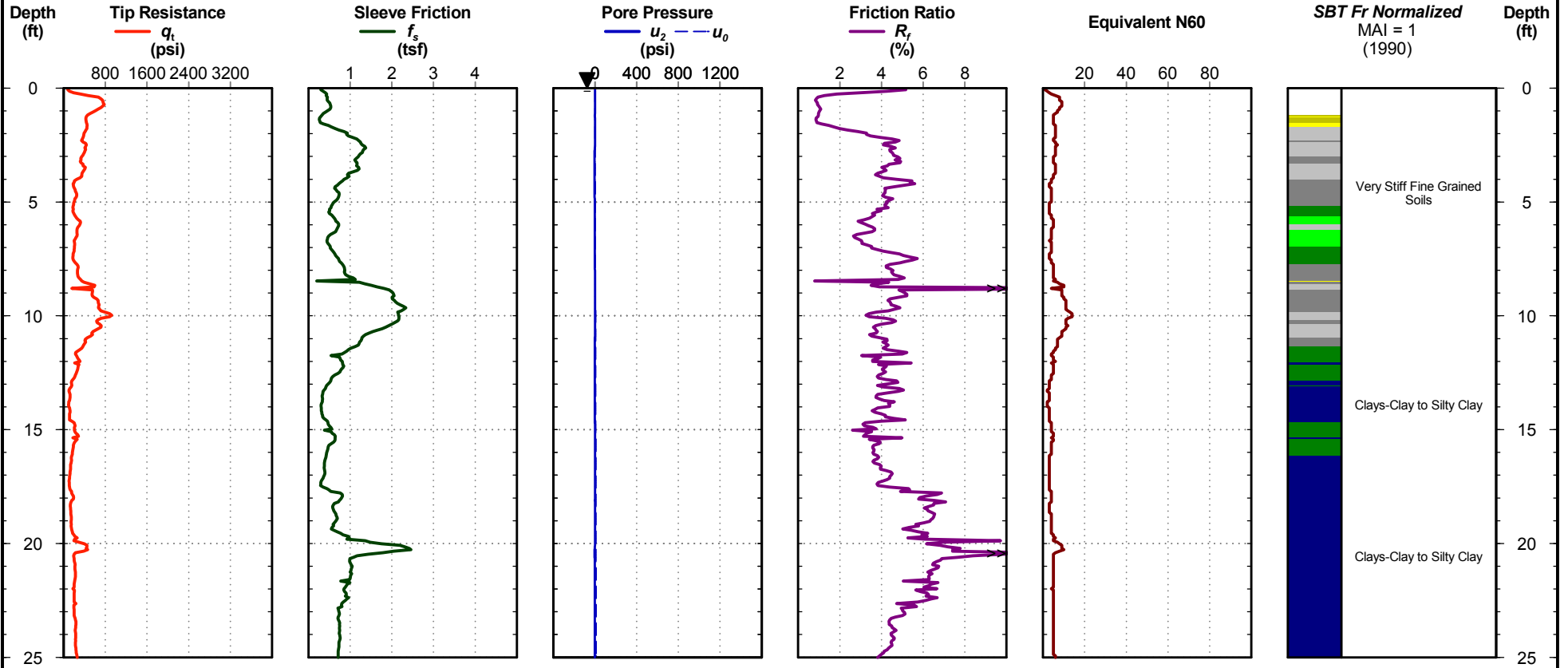
- | | | |
|--|--|---|
| 1 - Sensitive, Fine Grained Soils | 4 - Silt Mixtures-Clay Silt to Silty Clay | 7 - Gravelly Sand to Sand |
| 2 - Organic Soils, Peats | 5 - Sand Mixtures-Silty Sand to Sandy Silt | 8 - Very Stiff Clay to Clayey Sand |
| 3 - Clays-Clay to Silty Clay | 6 - Sands-Clean Sand to Silty Sand | 9 - Very Stiff Fine Grained Soils |

slope 4 c-2

Project #: 18-1106-0004
Date: May. 23, 2018

Northing:
Easting:

Elevation:
Filename: Slope 4 CPT-3A.cpt



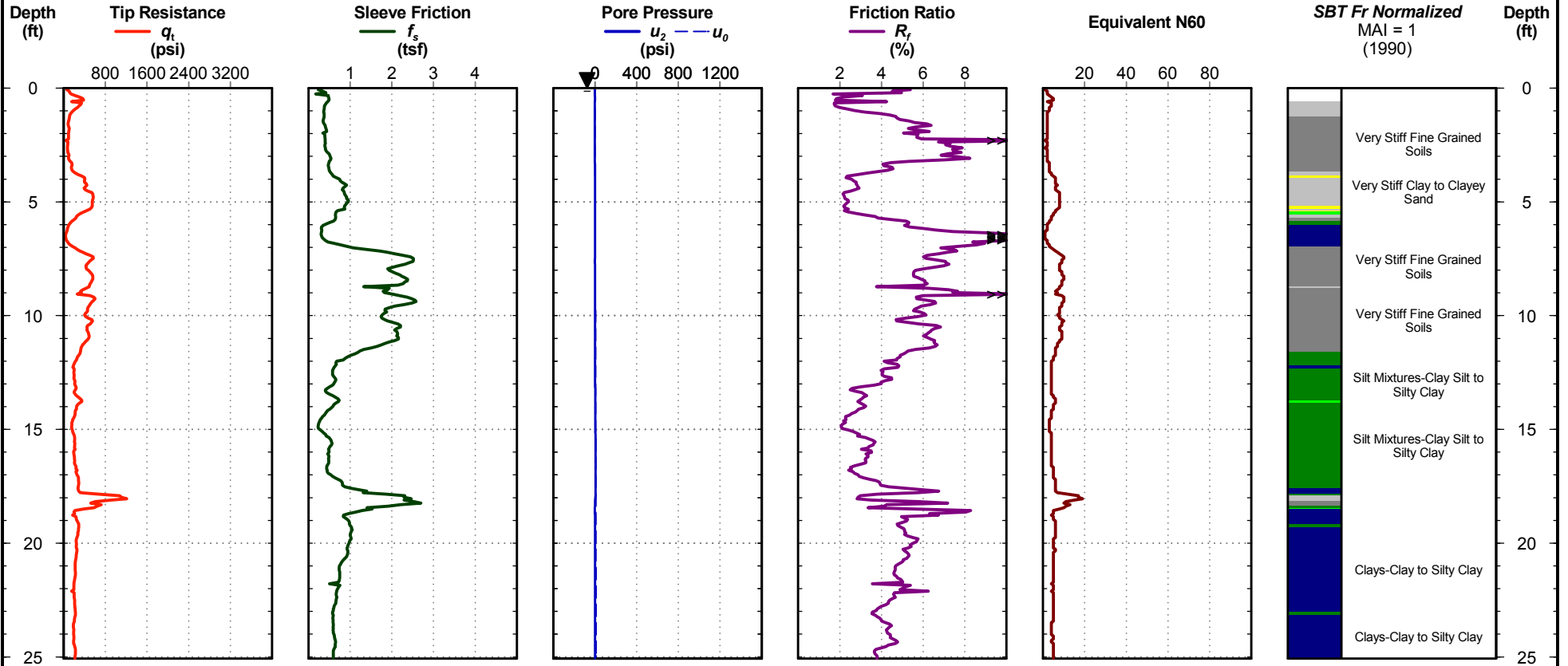
- | | | |
|--|--|---|
| 1 - Sensitive, Fine Grained Soils | 4 - Silt Mixtures-Clay Silt to Silty Clay | 7 - Gravelly Sand to Sand |
| 2 - Organic Soils, Peats | 5 - Sand Mixtures-Silty Sand to Sandy Silt | 8 - Very Stiff Clay to Clayey Sand |
| 3 - Clays-Clay to Silty Clay | 6 - Sands-Clean Sand to Silty Sand | 9 - Very Stiff Fine Grained Soils |

slope 4 c-3

Project #: 18-1106-0004
Date: May. 23, 2018

Northing:
Easting:

Elevation:
Filename: Slope 4 CPT-4A.cpt



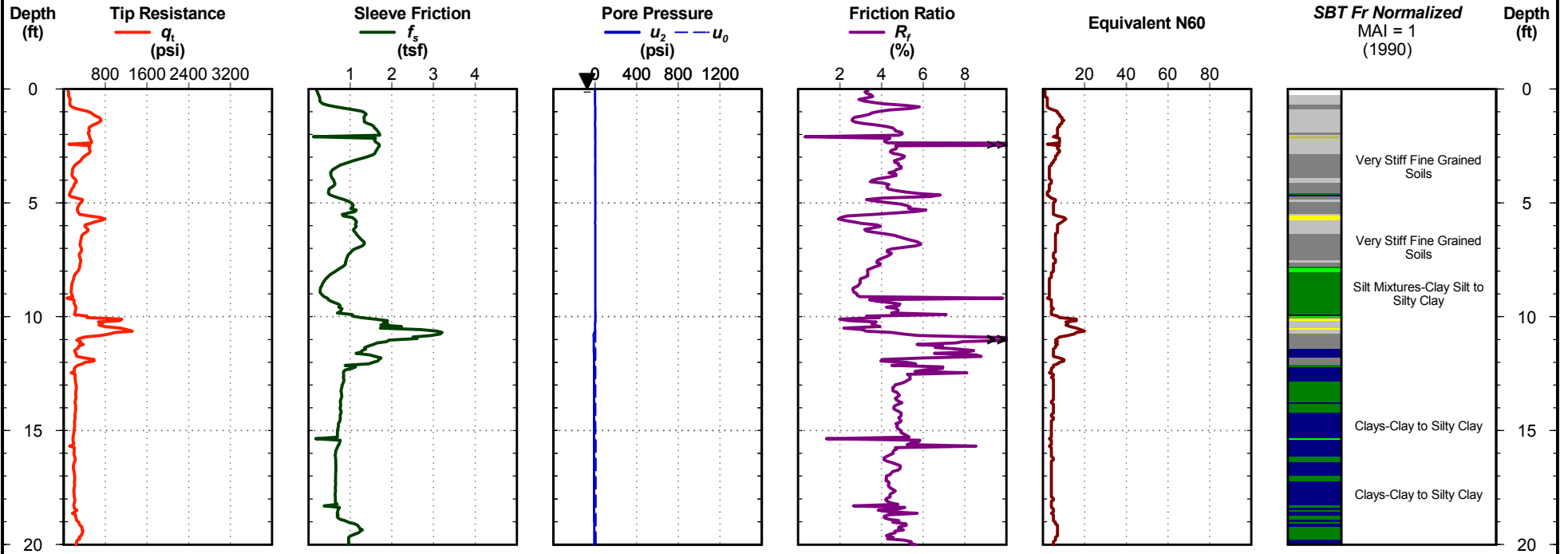
- | | | |
|--|--|---|
| 1 - Sensitive, Fine Grained Soils | 4 - Silt Mixtures-Clay Silt to Silty Clay | 7 - Gravelly Sand to Sand |
| 2 - Organic Soils, Peats | 5 - Sand Mixtures-Silty Sand to Sandy Silt | 8 - Very Stiff Clay to Clayey Sand |
| 3 - Clays-Clay to Silty Clay | 6 - Sands-Clean Sand to Silty Sand | 9 - Very Stiff Fine Grained Soils |

slope 4 c-4

Project #: 18-1106-0004
Date: May. 23, 2018

Northing:
Easting:

Elevation:
Filename: Slope 4 CPT-5A.cpt



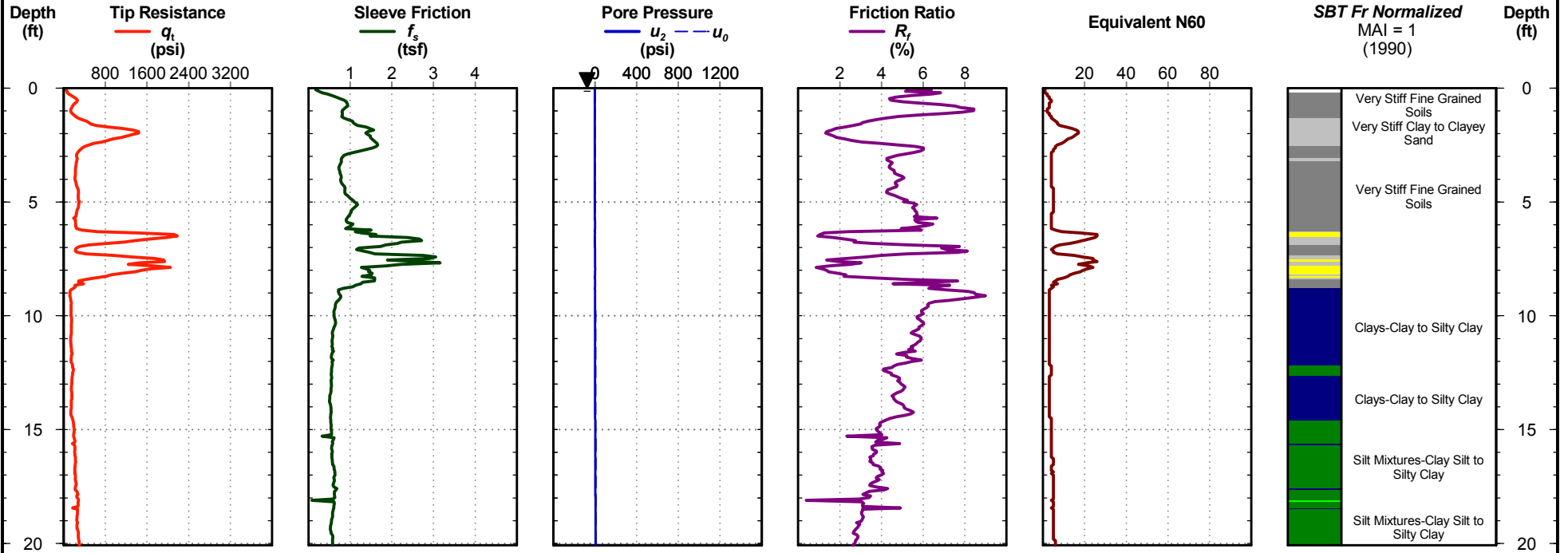
- | | | |
|--|--|---|
| ■ 1 - Sensitive, Fine Grained Soils | ■ 4 - Silt Mixtures-Clay Silt to Silty Clay | ■ 7 - Gravelly Sand to Sand |
| ■ 2 - Organic Soils, Peats | ■ 5 - Sand Mixtures-Silty Sand to Sandy Silt | ■ 8 - Very Stiff Clay to Clayey Sand |
| ■ 3 - Clays-Clay to Silty Clay | ■ 6 - Sands-Clean Sand to Silty Sand | ■ 9 - Very Stiff Fine Grained Soils |

slope 4 c-5

Project #: 18-1106-0004
Date: May. 23, 2018

Northing:
Easting:

Elevation:
Filename: Slope 4 CPT-6A.cpt



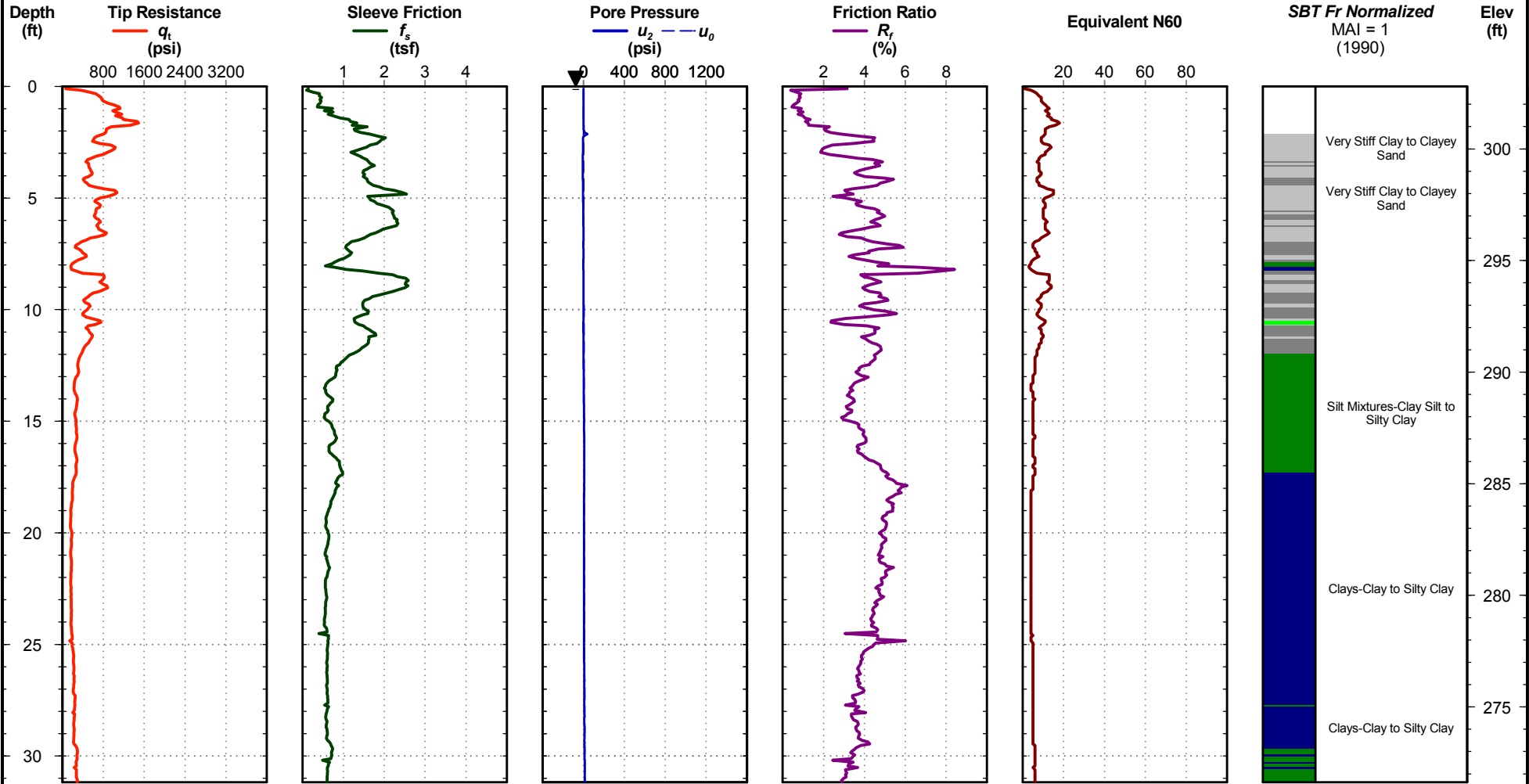
- 1 - Sensitive, Fine Grained Soils
- 4 - Silt Mixtures-Clay Silt to Silty Clay
- 7 - Gravelly Sand to Sand
- 2 - Organic Soils, Peats
- 5 - Sand Mixtures-Silty Sand to Sandy Silt
- 8 - Very Stiff Clay to Clayey Sand
- 3 - Clays-Clay to Silty Clay
- 6 - Sands-Clean Sand to Silty Sand
- 9 - Very Stiff Fine Grained Soils

slope 4 c-6

Project #: 18-1106-0004
Date: May. 1, 2018

Northing:
Easting:

Elevation: 302.8
Filename: slope 5c-1A[1].cpt



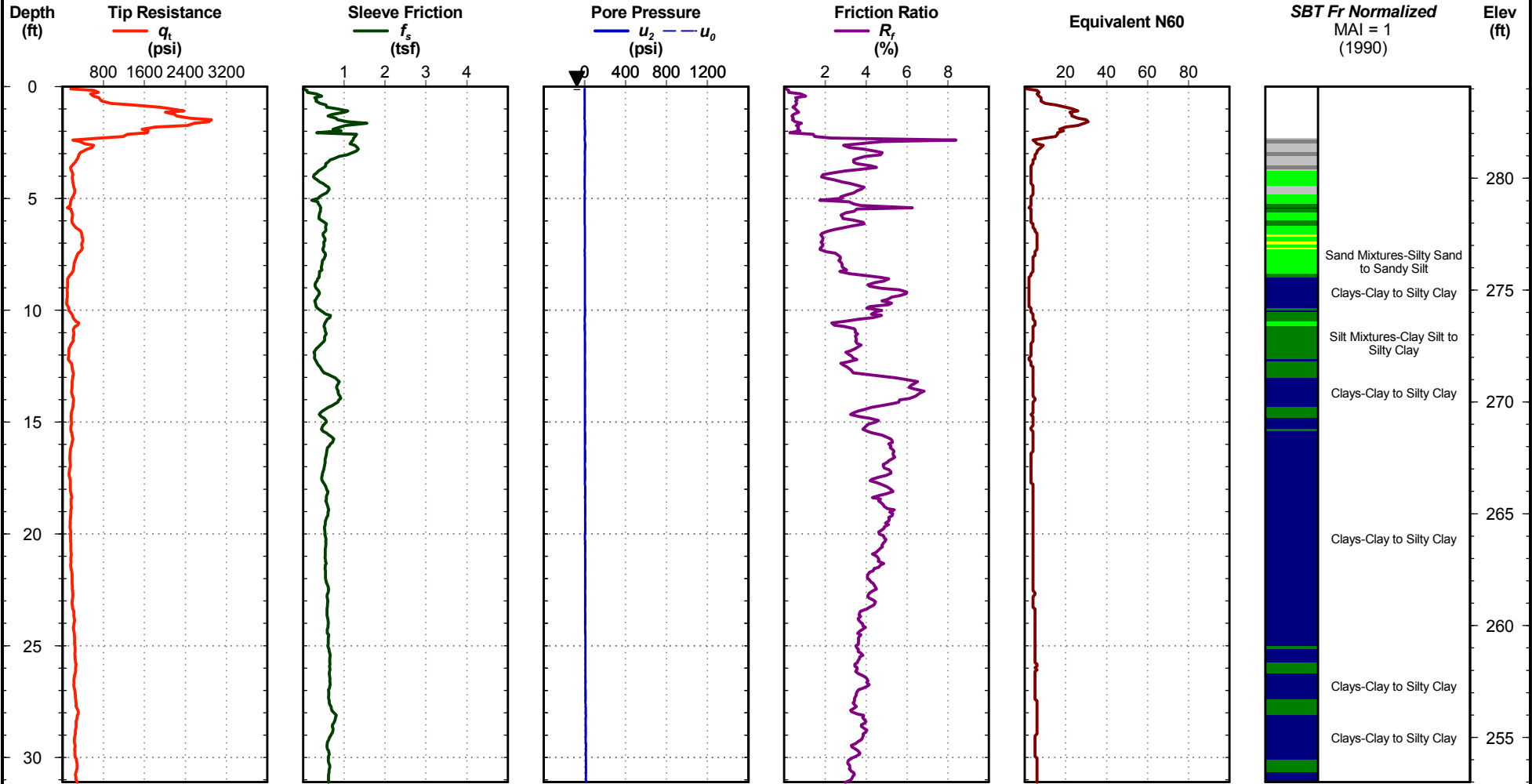
- | | | |
|--|--|---|
| 1 - Sensitive, Fine Grained Soils | 4 - Silt Mixtures-Clay Silt to Silty Clay | 7 - Gravelly Sand to Sand |
| 2 - Organic Soils, Peats | 5 - Sand Mixtures-Silty Sand to Sandy Silt | 8 - Very Stiff Clay to Clayey Sand |
| 3 - Clays-Clay to Silty Clay | 6 - Sands-Clean Sand to Silty Sand | 9 - Very Stiff Fine Grained Soils |

slope 5 c-1

Project #: 18-1106-0004
Date: May. 1, 2018

Northing:
Easting:

Elevation: 284.1
Filename: slope 5c-2A[1].cpt



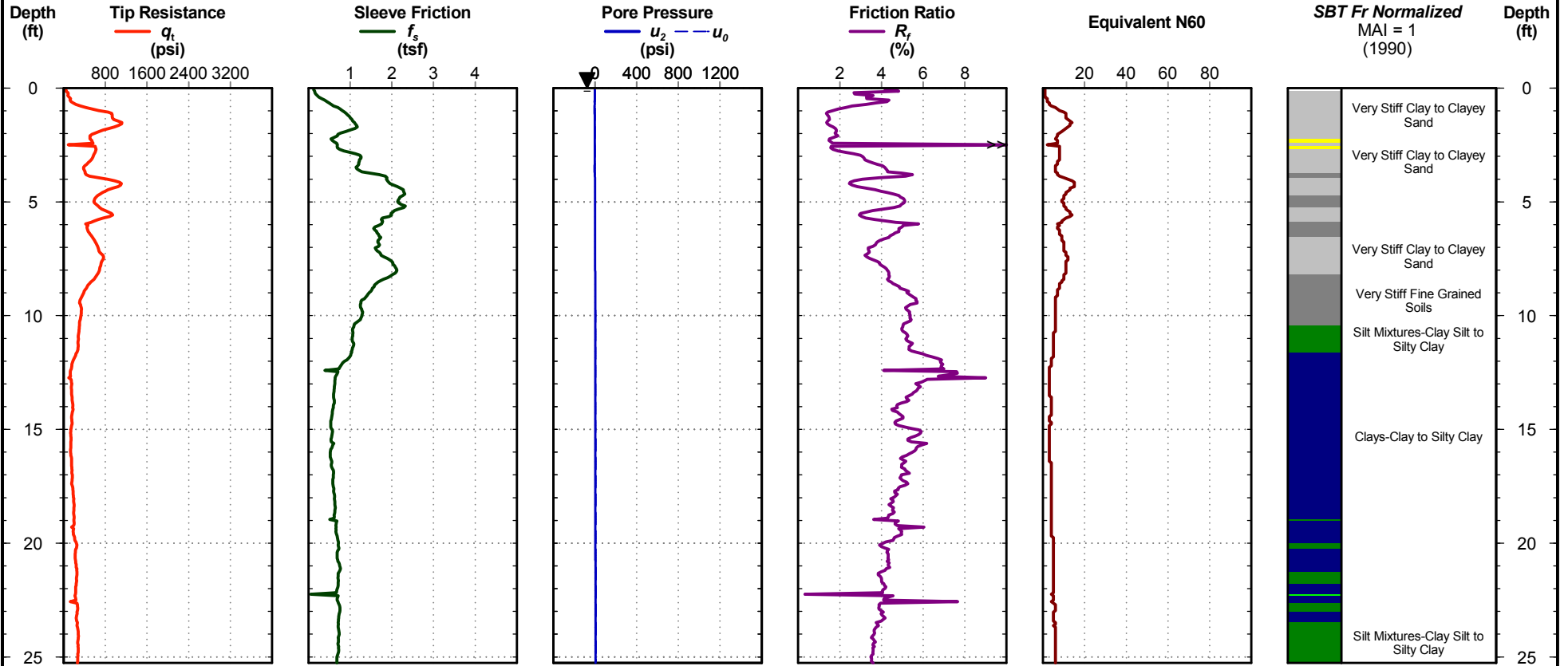
- | | | |
|--|--|---|
| 1 - Sensitive, Fine Grained Soils | 4 - Silt Mixtures-Clay Silt to Silty Clay | 7 - Gravelly Sand to Sand |
| 2 - Organic Soils, Peats | 5 - Sand Mixtures-Silty Sand to Sandy Silt | 8 - Very Stiff Clay to Clayey Sand |
| 3 - Clays-Clay to Silty Clay | 6 - Sands-Clean Sand to Silty Sand | 9 - Very Stiff Fine Grained Soils |

slope 5 c-2

Project #: 18-1106-0004
Date: May. 23, 2018

Northing:
Easting:

Elevation:
Filename: Slope 5 CPT-3A.cpt



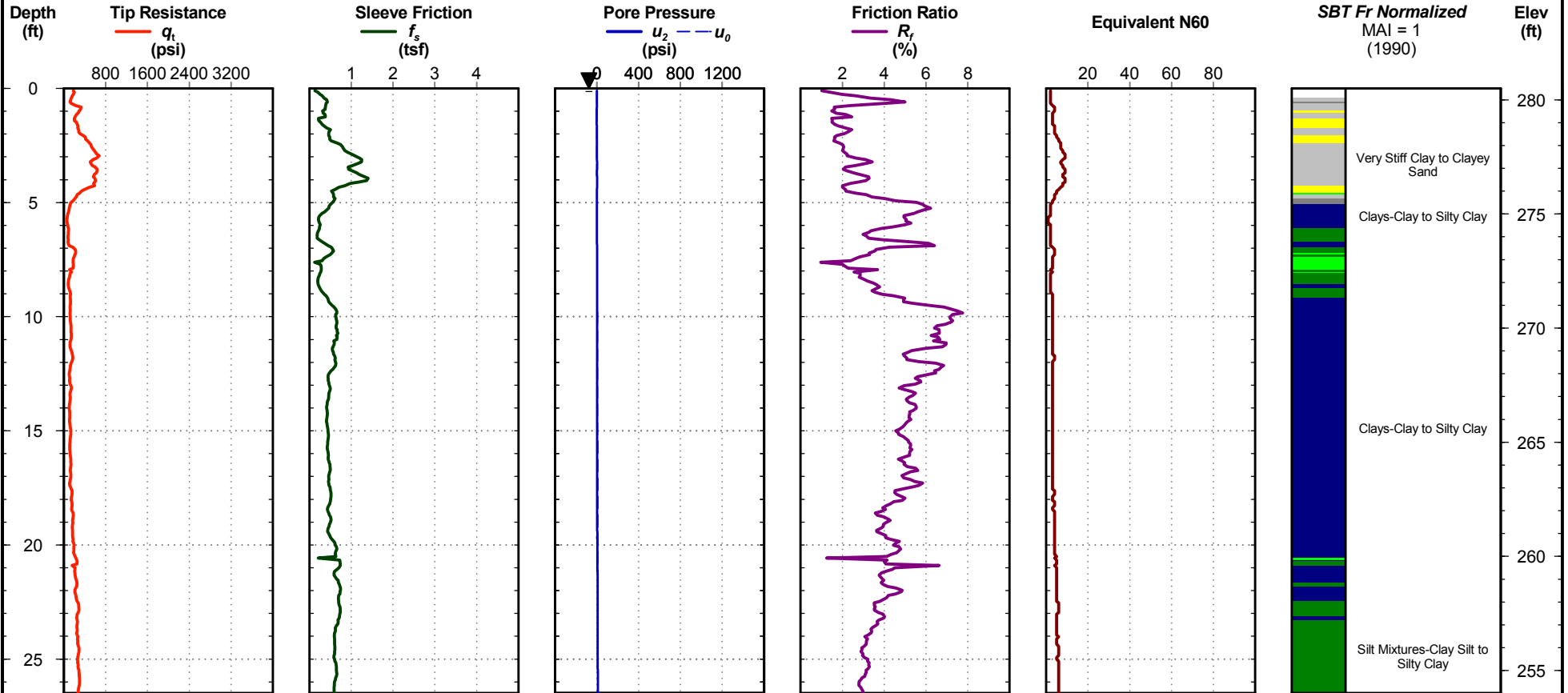
- 1 - Sensitive, Fine Grained Soils
- 4 - Silt Mixtures-Clay Silt to Silty Clay
- 7 - Gravelly Sand to Sand
- 2 - Organic Soils, Peats
- 5 - Sand Mixtures-Silty Sand to Sandy Silt
- 8 - Very Stiff Clay to Clayey Sand
- 3 - Clays-Clay to Silty Clay
- 6 - Sands-Clean Sand to Silty Sand
- 9 - Very Stiff Fine Grained Soils

slope 5 c-3

Project #: 18-1106-0004
Date: May. 1, 2018

Northing:
Easting:

Elevation: 280.5
Filename: slope 5c-4A[1].cpt



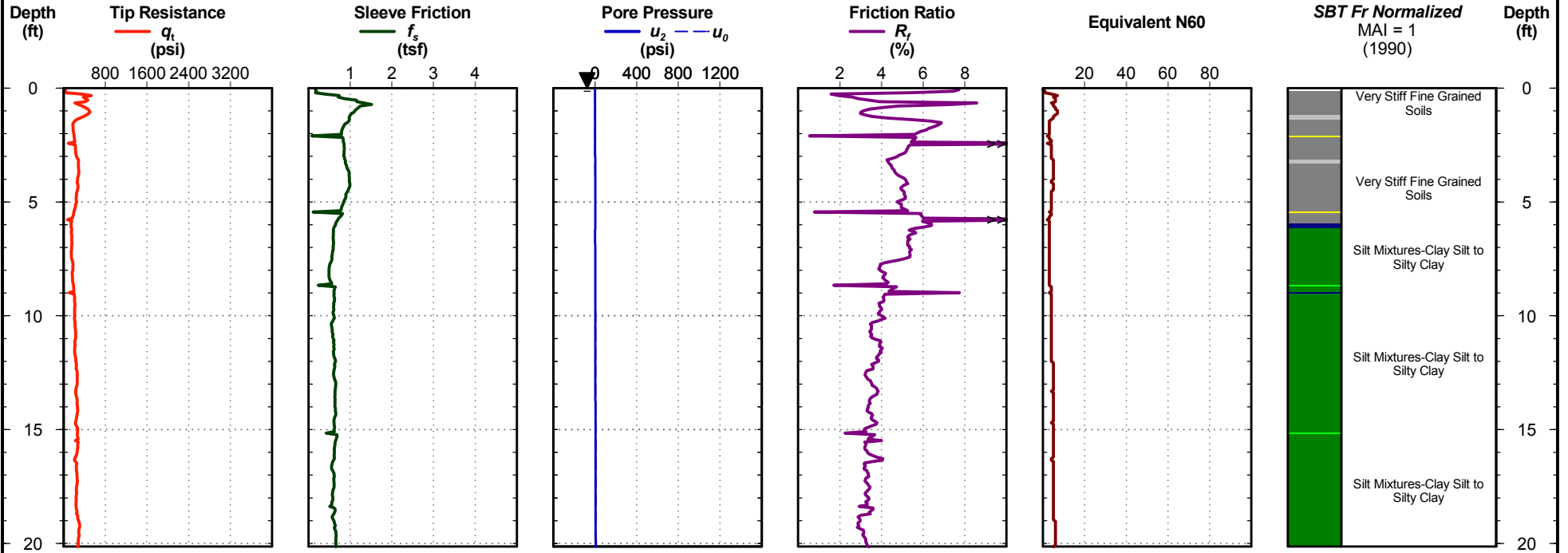
- | | | |
|--|--|---|
| ■ 1 - Sensitive, Fine Grained Soils | ■ 4 - Silt Mixtures-Clay Silt to Silty Clay | ■ 7 - Gravelly Sand to Sand |
| ■ 2 - Organic Soils, Peats | ■ 5 - Sand Mixtures-Silty Sand to Sandy Silt | ■ 8 - Very Stiff Clay to Clayey Sand |
| ■ 3 - Clays-Clay to Silty Clay | ■ 6 - Sands-Clean Sand to Silty Sand | ■ 9 - Very Stiff Fine Grained Soils |

slope 5 c-4

Project #: 18-1106-0004
Date: May. 23, 2018

Northing:
Easting:

Elevation:
Filename: Slope 5 CPT-5A.cpt



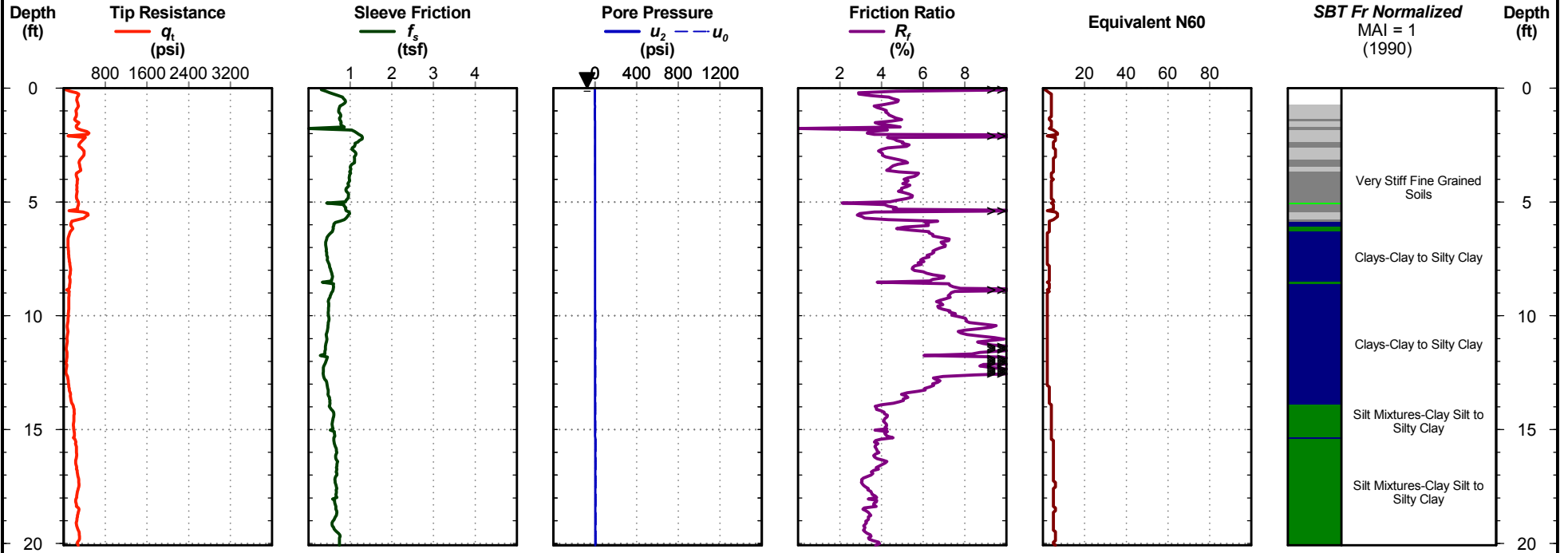
- | | | |
|--|--|---|
| 1 - Sensitive, Fine Grained Soils | 4 - Silt Mixtures-Clay Silt to Silty Clay | 7 - Gravelly Sand to Sand |
| 2 - Organic Soils, Peats | 5 - Sand Mixtures-Silty Sand to Sandy Silt | 8 - Very Stiff Clay to Clayey Sand |
| 3 - Clays-Clay to Silty Clay | 6 - Sands-Clean Sand to Silty Sand | 9 - Very Stiff Fine Grained Soils |

slope 5 c-5

Project #: 18-1106-0004
Date: May 23, 2018

Northing:
Easting:

Elevation:
Filename: Slope 5 CPT-6A.cpt

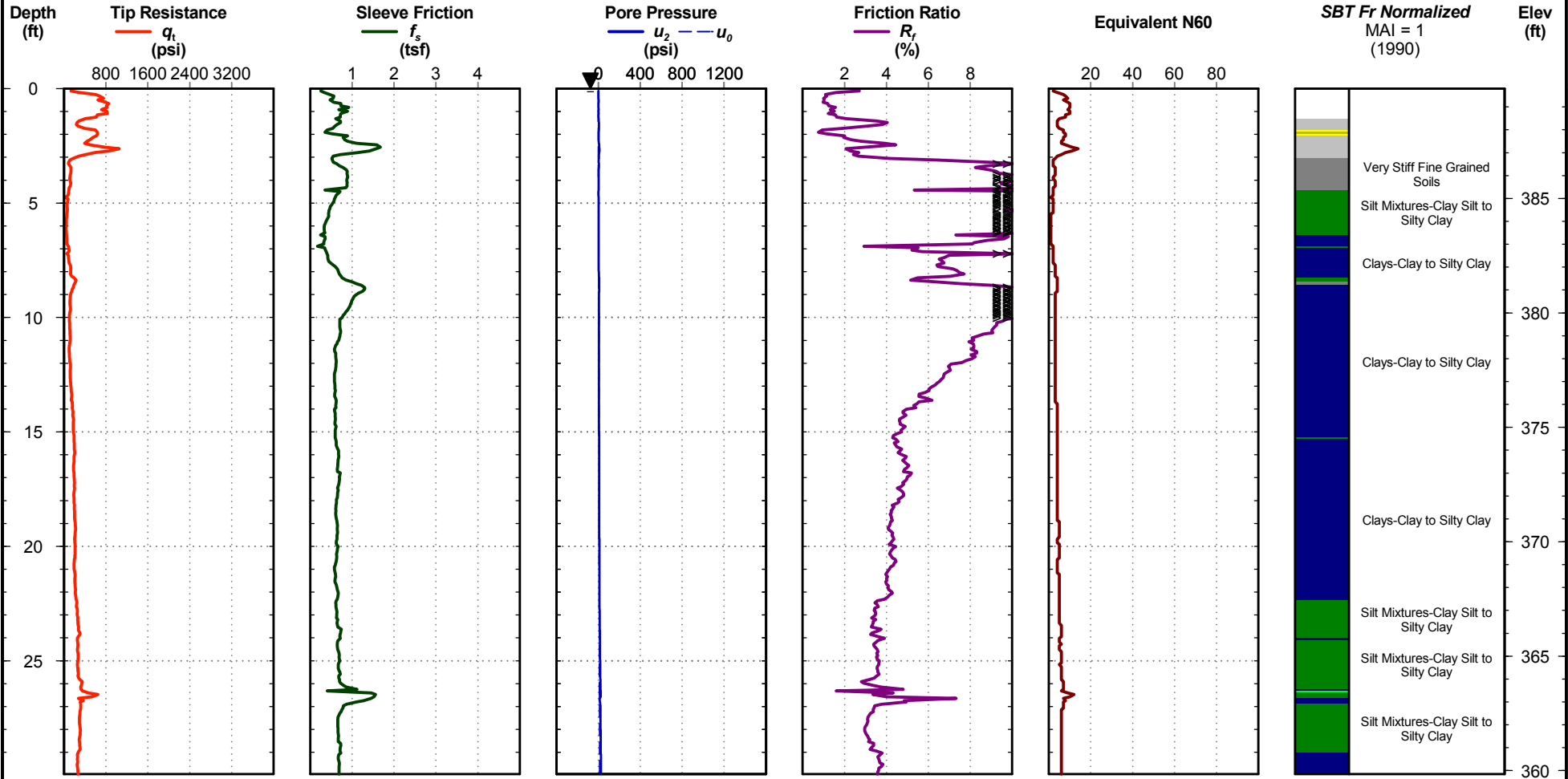


- | | | |
|--|--|---|
| ■ 1 - Sensitive, Fine Grained Soils | ■ 4 - Silt Mixtures-Clay Silt to Silty Clay | ■ 7 - Gravelly Sand to Sand |
| ■ 2 - Organic Soils, Peats | ■ 5 - Sand Mixtures-Silty Sand to Sandy Silt | ■ 8 - Very Stiff Clay to Clayey Sand |
| ■ 3 - Clays-Clay to Silty Clay | ■ 6 - Sands-Clean Sand to Silty Sand | ■ 9 - Very Stiff Fine Grained Soils |

Project #: 18-1106-0004
Date: Apr. 30, 2018

Northing:
Easting:

Elevation: 389.8
Filename: slope 6c-2A.cpt



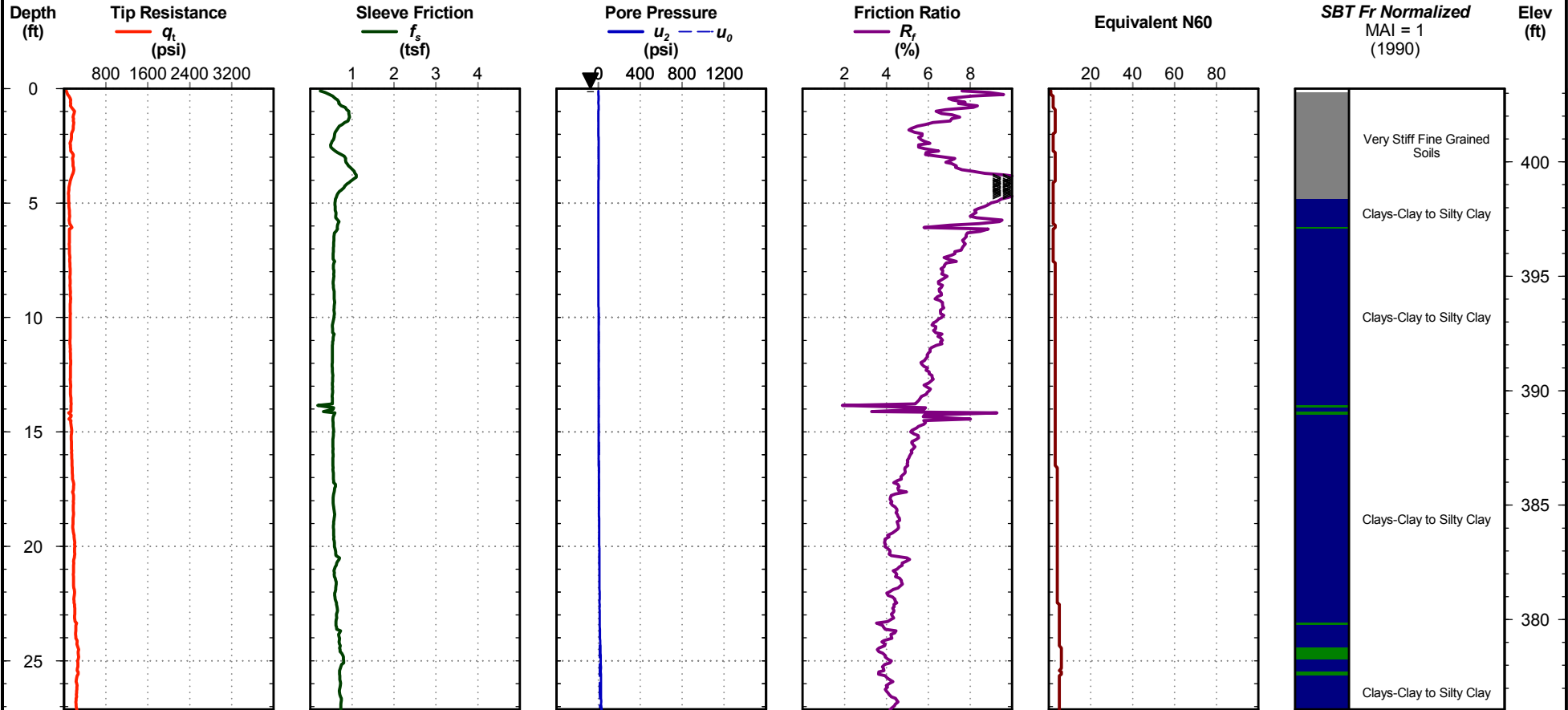
- 1 - Sensitive, Fine Grained Soils
- 4 - Silt Mixtures-Clay Silt to Silty Clay
- 7 - Gravelly Sand to Sand
- 2 - Organic Soils, Peats
- 5 - Sand Mixtures-Silty Sand to Sandy Silt
- 8 - Very Stiff Clay to Clayey Sand
- 3 - Clays-Clay to Silty Clay
- 6 - Sands-Clean Sand to Silty Sand
- 9 - Very Stiff Fine Grained Soils

slope 6 c-2

Project #: 18-1106-0004
Date: Apr. 30, 2018

Northing:
Easting:

Elevation: 403.2
Filename: slope 6c-3A.cpt



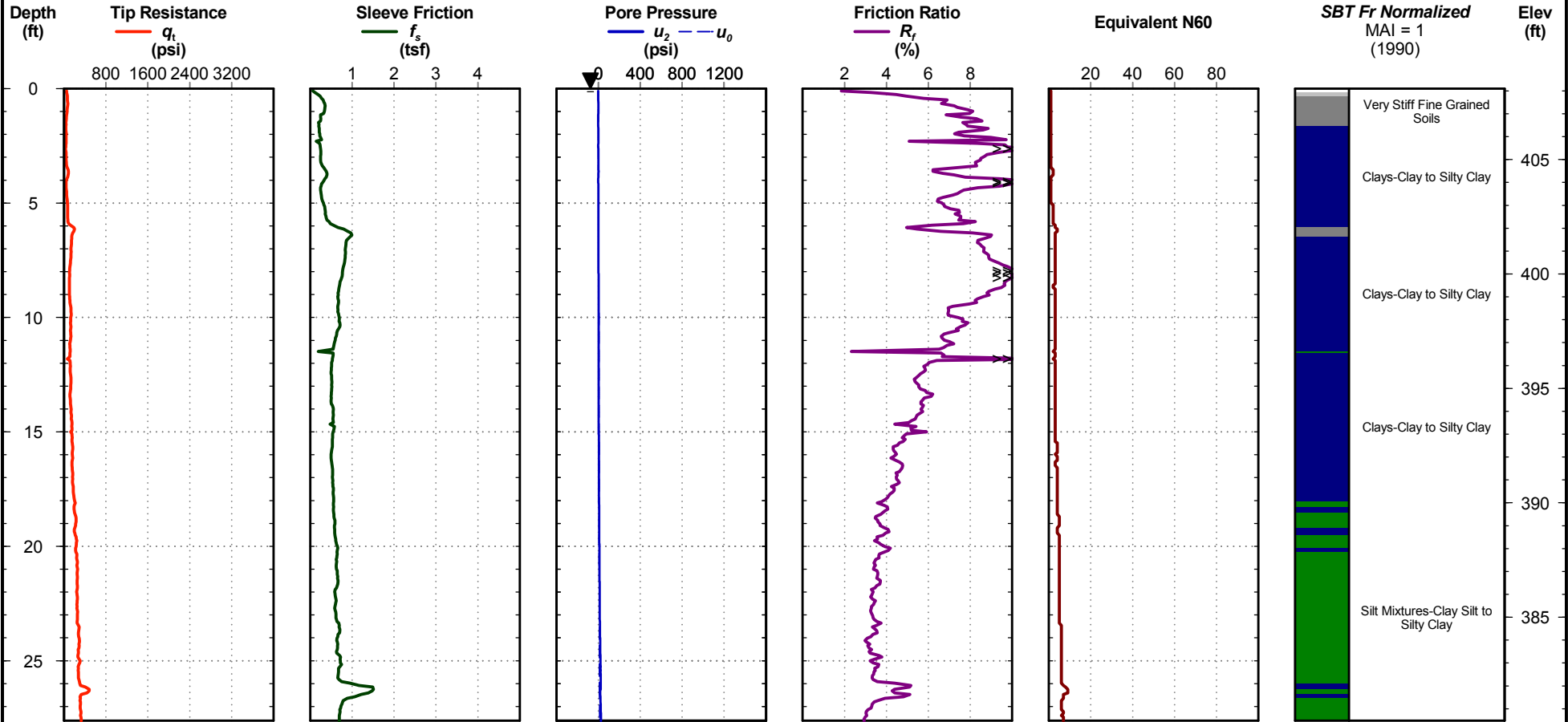
- | | | |
|--|--|---|
| ■ 1 - Sensitive, Fine Grained Soils | ■ 4 - Silt Mixtures-Clay Silt to Silty Clay | ■ 7 - Gravelly Sand to Sand |
| ■ 2 - Organic Soils, Peats | ■ 5 - Sand Mixtures-Silty Sand to Sandy Silt | ■ 8 - Very Stiff Clay to Clayey Sand |
| ■ 3 - Clays-Clay to Silty Clay | ■ 6 - Sands-Clean Sand to Silty Sand | ■ 9 - Very Stiff Fine Grained Soils |

slope 6 c-3

Project #: 18-1106-0004
Date: Apr. 30, 2018

Northing:
Easting:

Elevation: 408.1
Filename: slope 6c-4A.cpt



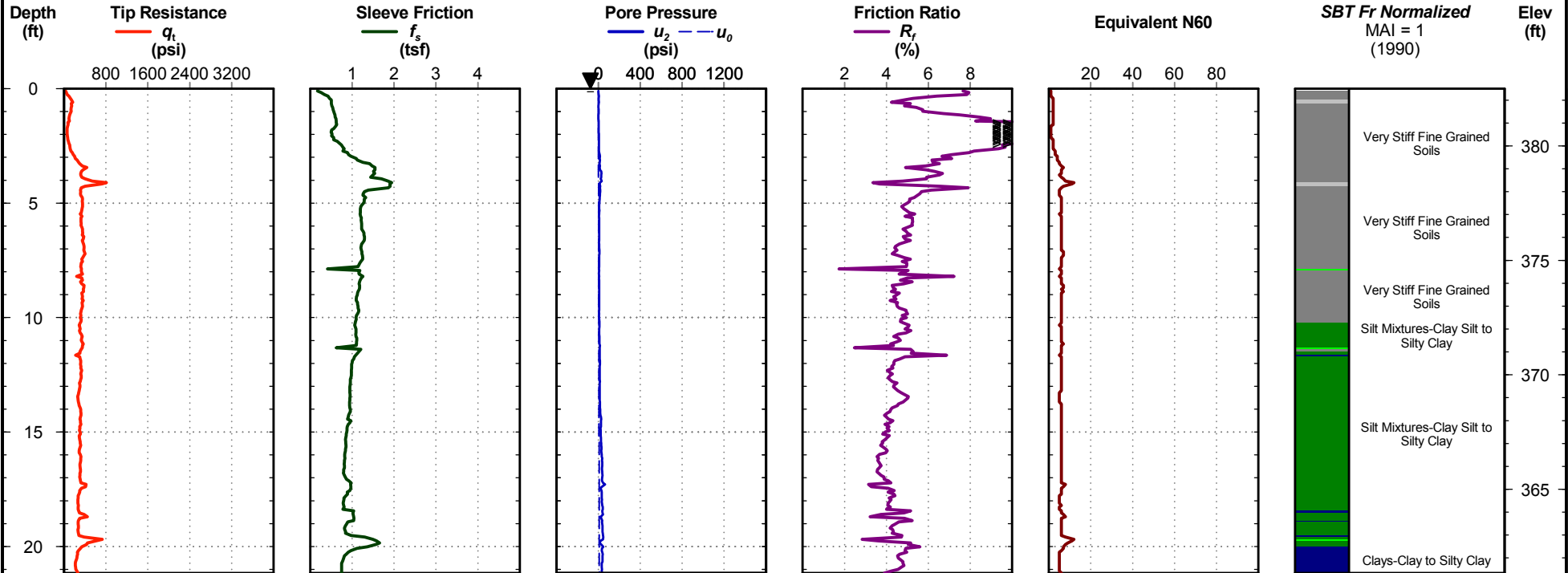
- | | | |
|--|--|---|
| ■ 1 - Sensitive, Fine Grained Soils | ■ 4 - Silt Mixtures-Clay Silt to Silty Clay | ■ 7 - Gravelly Sand to Sand |
| ■ 2 - Organic Soils, Peats | ■ 5 - Sand Mixtures-Silty Sand to Sandy Silt | ■ 8 - Very Stiff Clay to Clayey Sand |
| ■ 3 - Clays-Clay to Silty Clay | ■ 6 - Sands-Clean Sand to Silty Sand | ■ 9 - Very Stiff Fine Grained Soils |

slope 6 c-4

Project #: 18-1106-0004
Date: Apr. 30, 2018

Northing:
Easting:

Elevation: 382.5
Filename: slope 6c-5A.cpt



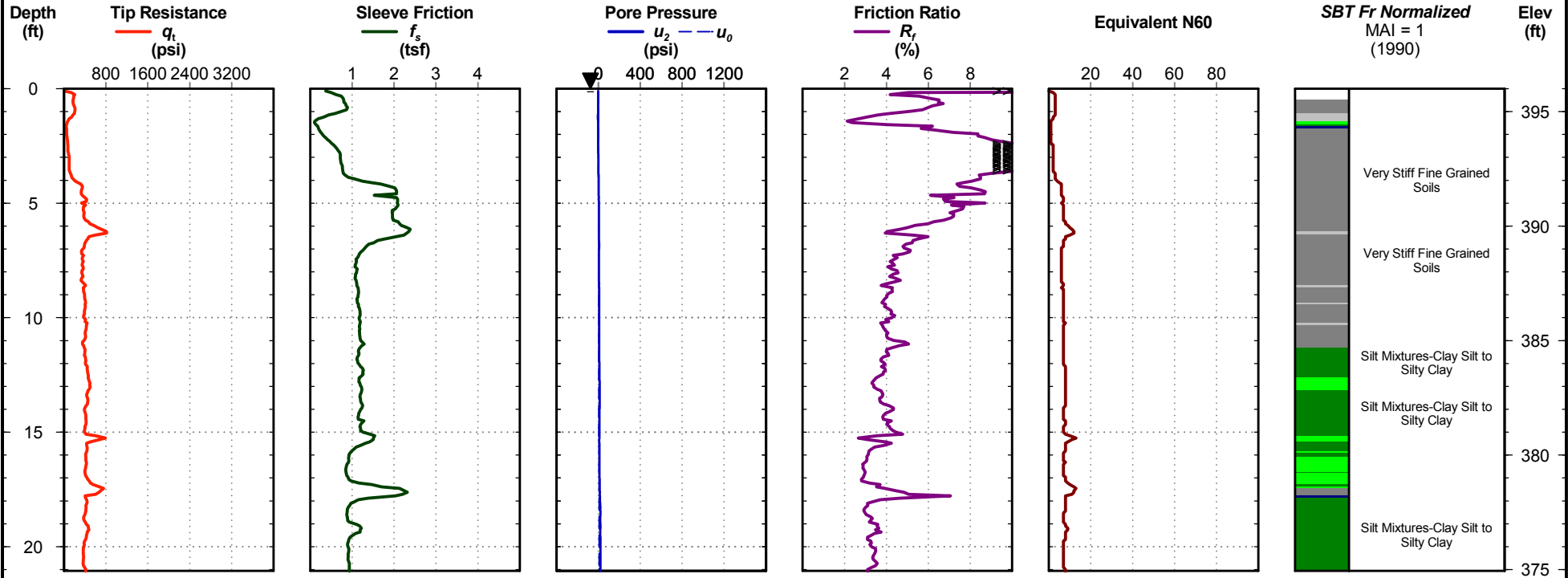
- | | | |
|--|--|---|
| 1 - Sensitive, Fine Grained Soils | 4 - Silt Mixtures-Clay Silt to Silty Clay | 7 - Gravelly Sand to Sand |
| 2 - Organic Soils, Peats | 5 - Sand Mixtures-Silty Sand to Sandy Silt | 8 - Very Stiff Clay to Clayey Sand |
| 3 - Clays-Clay to Silty Clay | 6 - Sands-Clean Sand to Silty Sand | 9 - Very Stiff Fine Grained Soils |

slope 6 c-5

Project #: 18-1106-0004
Date: Apr. 30, 2018

Northing:
Easting:

Elevation: 396
Filename: slope 6c-6A.cpt



- | | | |
|--|--|---|
| ■ 1 - Sensitive, Fine Grained Soils | ■ 4 - Silt Mixtures-Clay Silt to Silty Clay | ■ 7 - Gravelly Sand to Sand |
| ■ 2 - Organic Soils, Peats | ■ 5 - Sand Mixtures-Silty Sand to Sandy Silt | ■ 8 - Very Stiff Clay to Clayey Sand |
| ■ 3 - Clays-Clay to Silty Clay | ■ 6 - Sands-Clean Sand to Silty Sand | ■ 9 - Very Stiff Fine Grained Soils |

slope 6 c-6

APPENDIX B
FIELD SWRC INSTRUMENTATION DATA

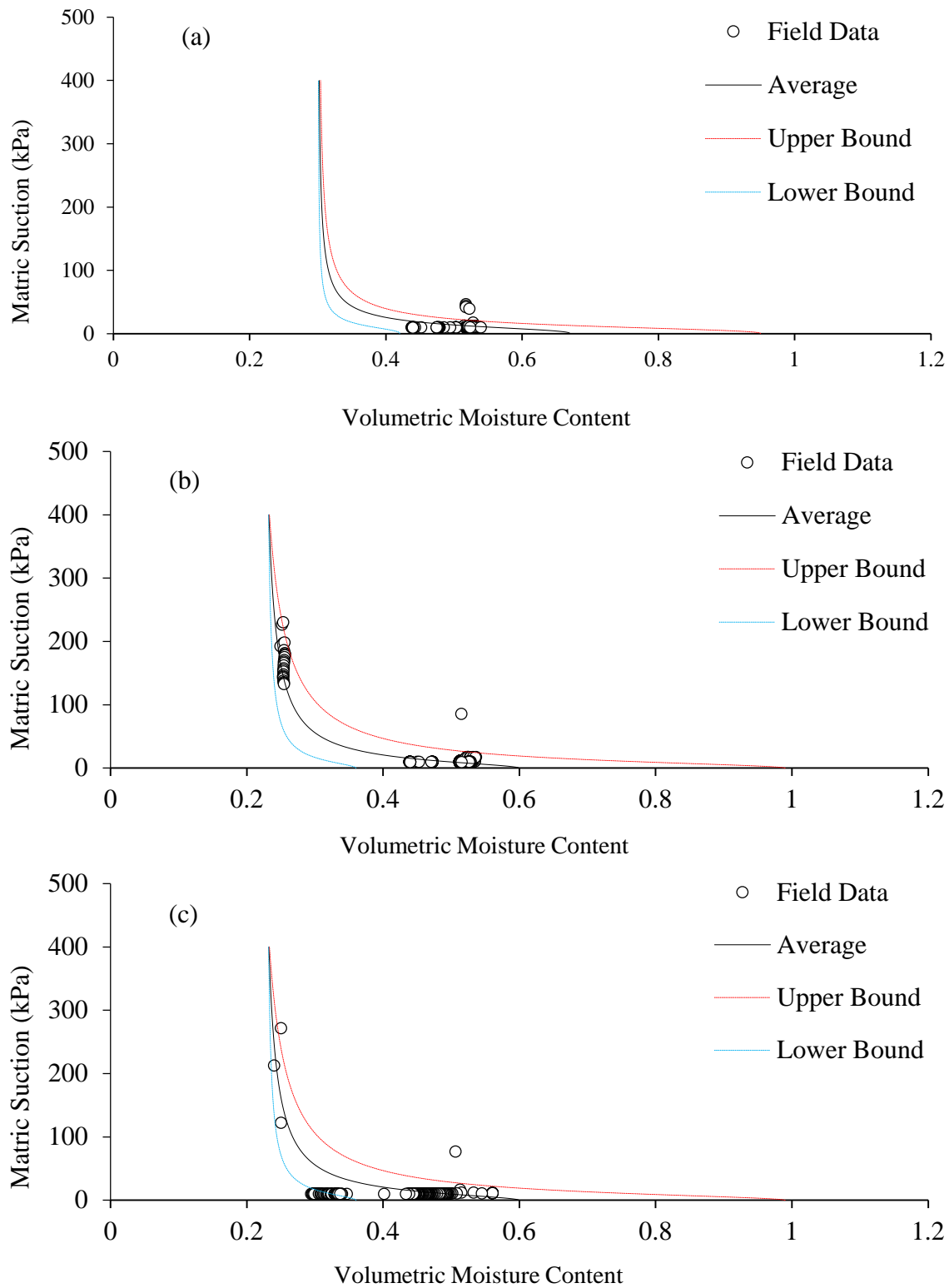


Figure B. 1 Field SWRC instrumentation data for I220N ramp toward I55 Slope (a) At instr.1 (b) At instr.2 (c) At instr.3

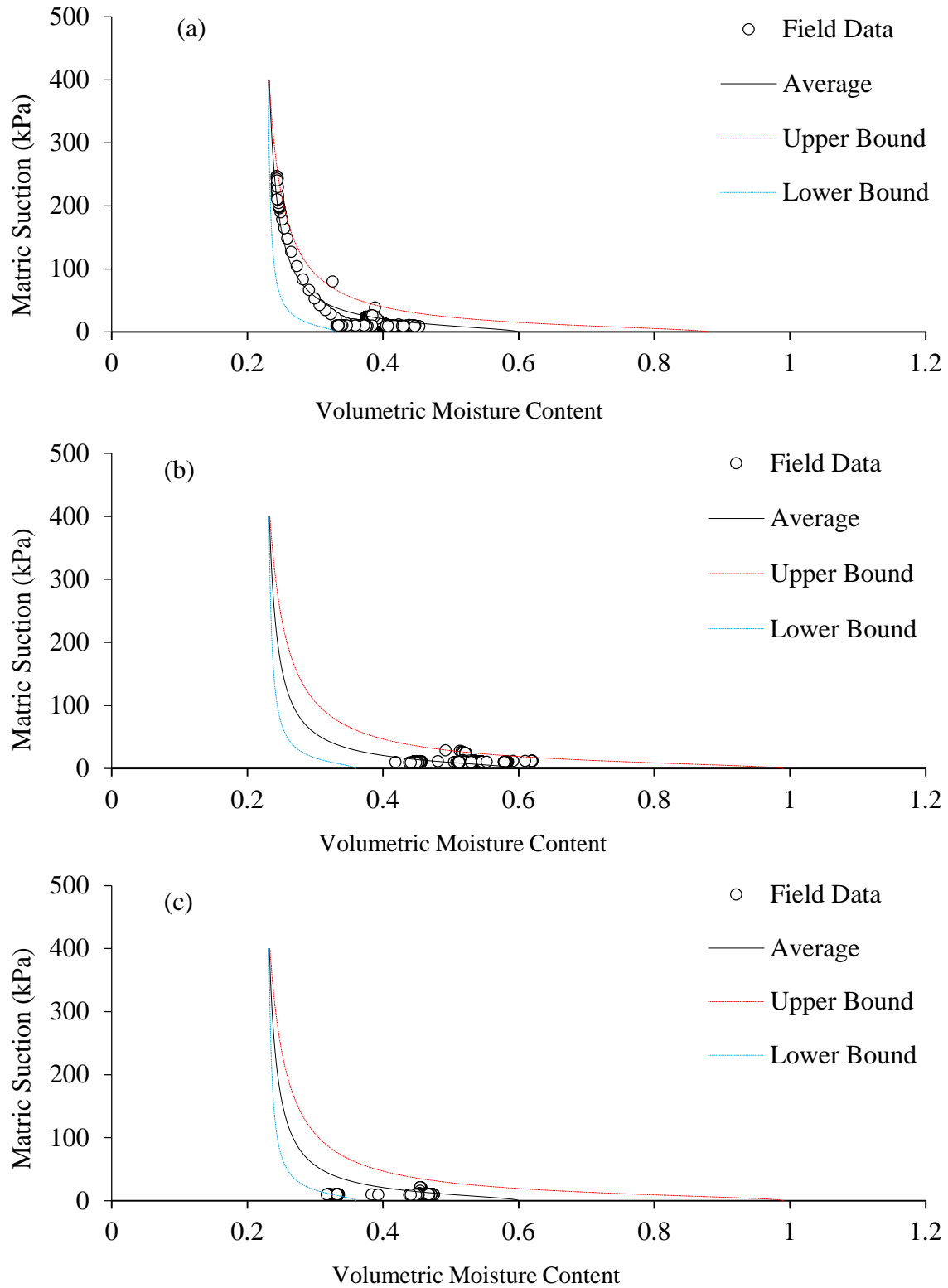


Figure B. 2 Field SWRC instrumentation data for Metro Center Slope (a) At instr.1 (b) At instr.2 (c) At instr.3

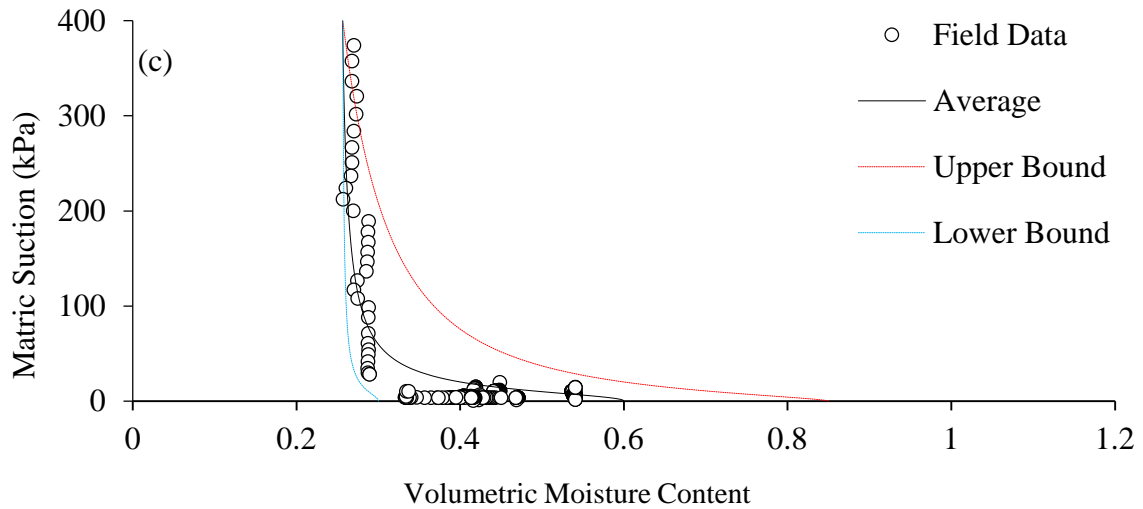
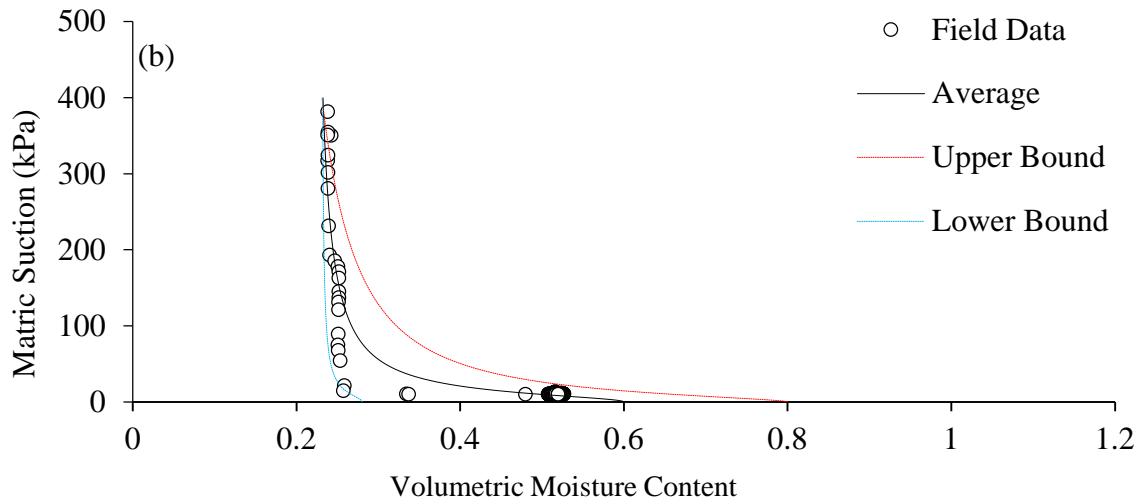
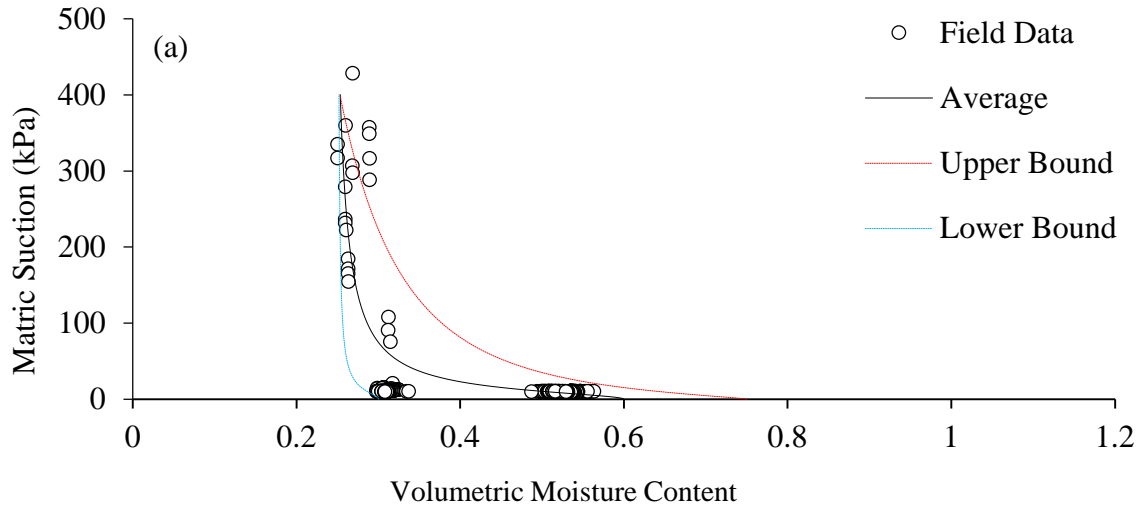


Figure B. 3 Field SWRC instrumentation data for Terry Road Slope (a) At instr.1 (b) At instr.2 (c) At instr.3

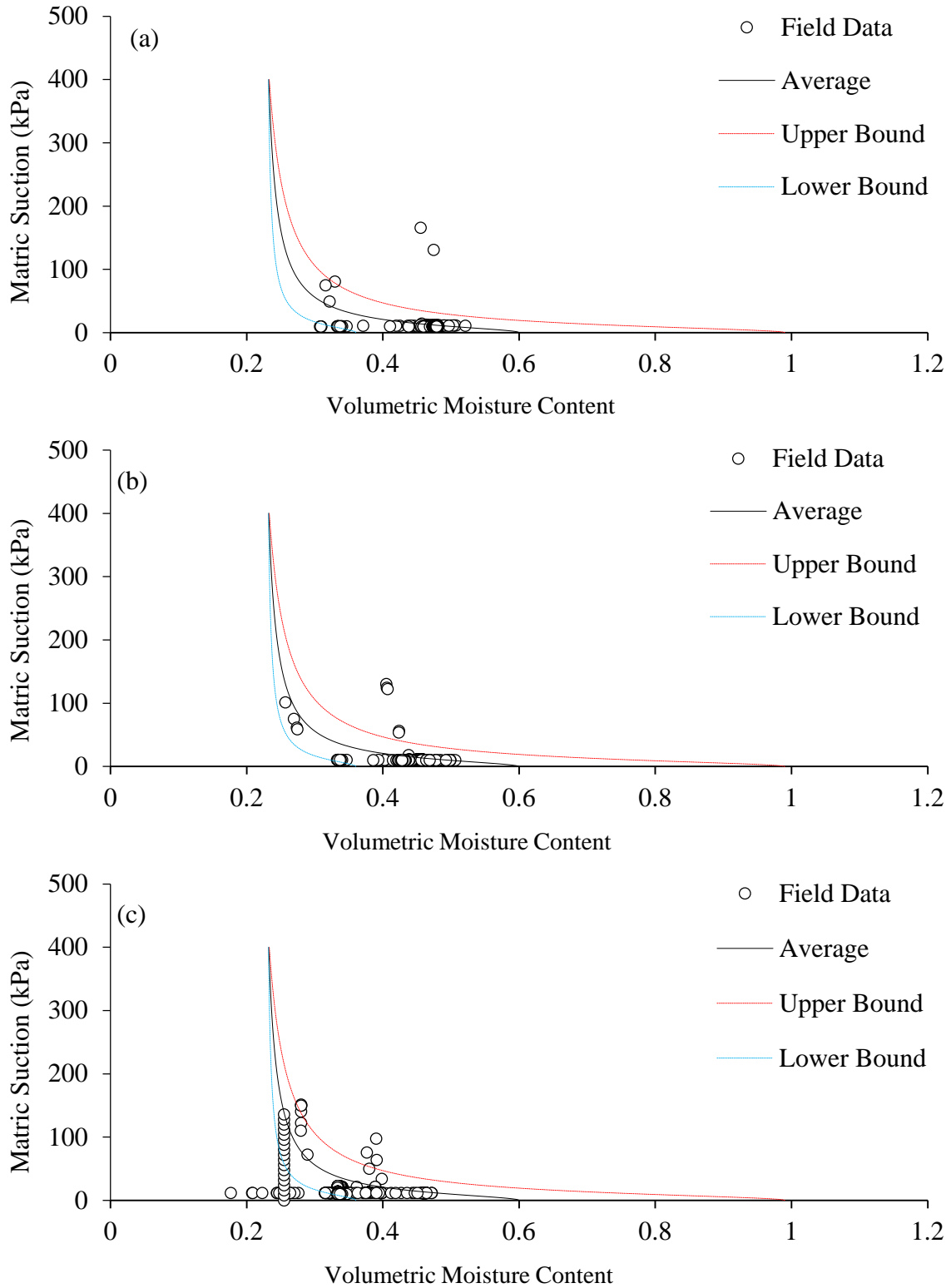


Figure B. 4 Field SWRC instrumentation data for Highland Drive Slope (a) At instr.1 (b) At instr.2 (c) At instr.3

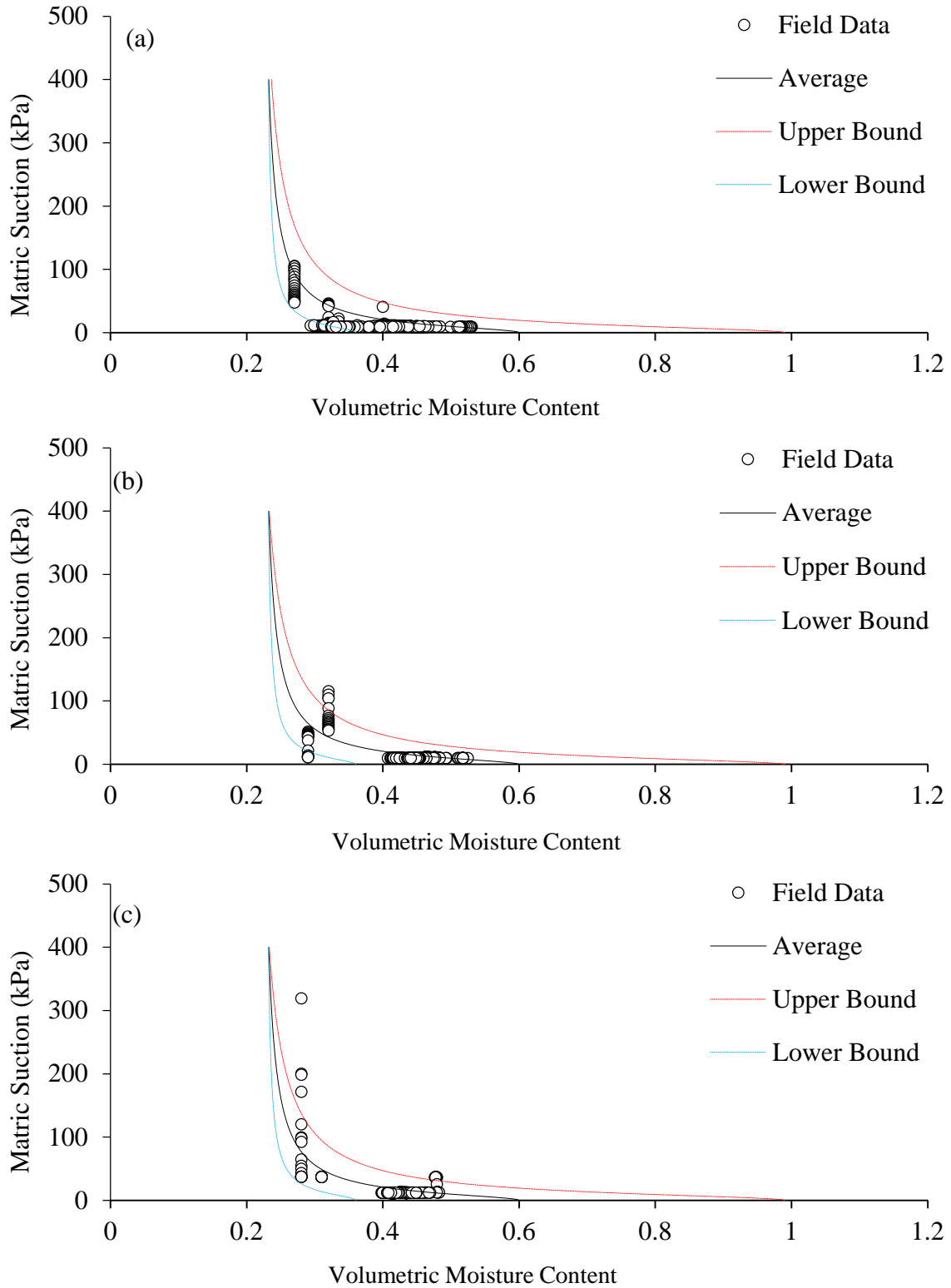


Figure B. 5 Field SWRC instrumentation data for Sowell Road Slope (a) At instr.1 (b) At instr.2 (c) At instr.3

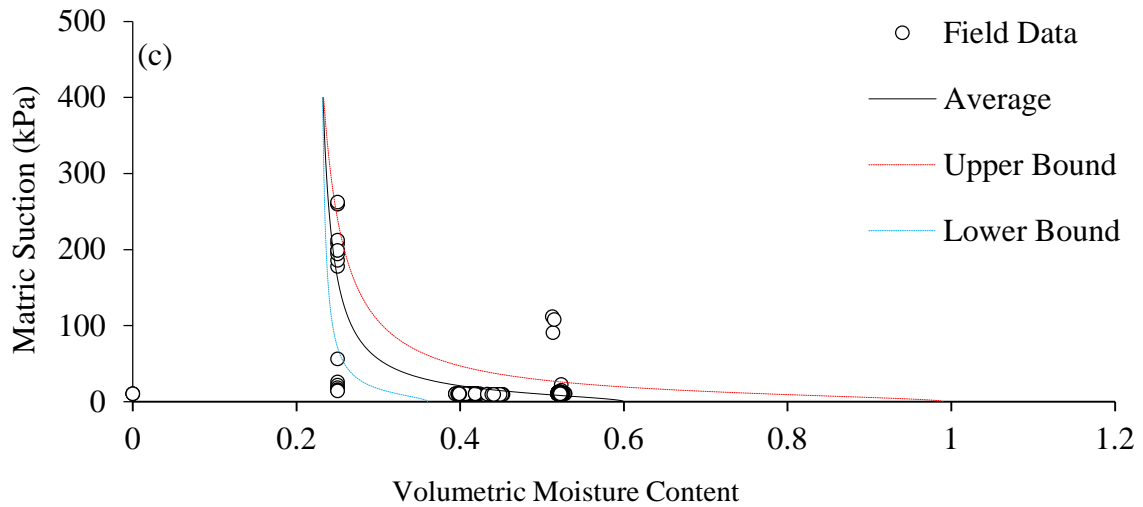
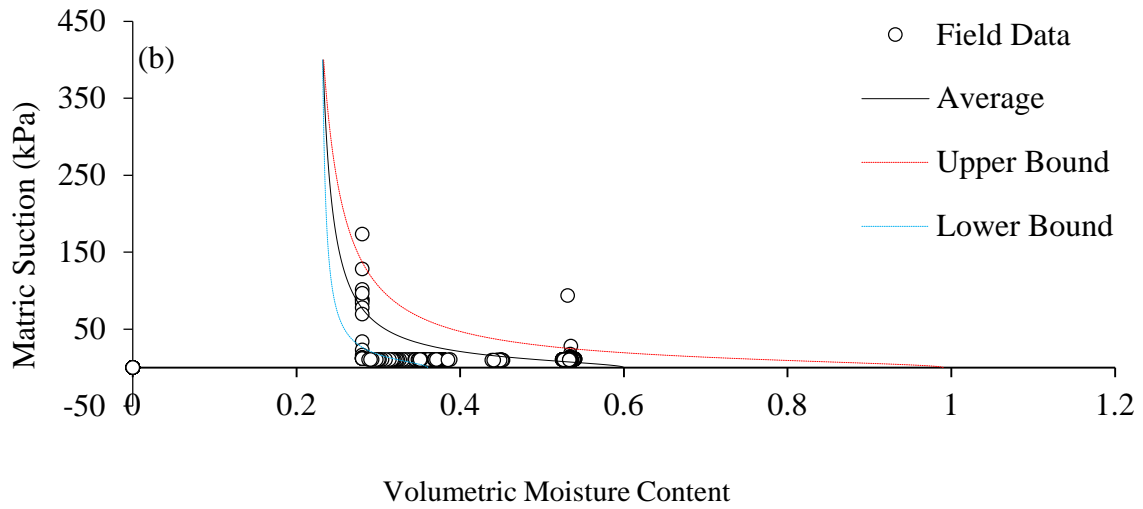
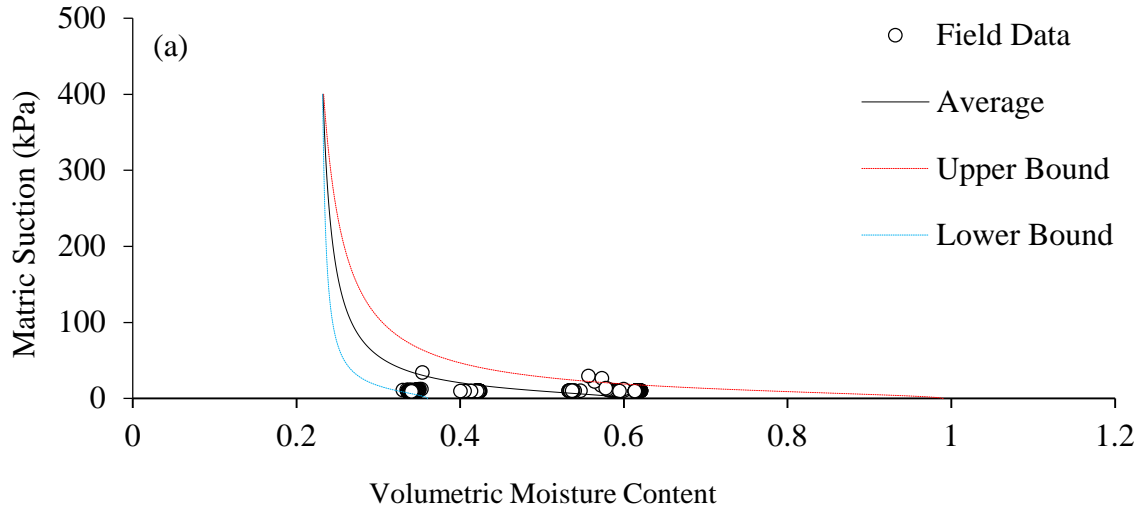


Figure B. 6 Field SWRC instrumentation data for McRaven Road Slope (a) At instr.1 (b) At instr.2 (c) At instr.3

Table B. 1 Field Soil Water Retention Curve fitted parameters

Van Genuchten Parameters		Slope 1 Instr.1	Slope 1 Instr.2	Slope 1 Instr.3	Nobahar et al., 2019
Shape Parameters	α	0.095	0.095	0.095	0.0031
	n	2.4	1.7	1.7	2.75
	$m=1-1/n$	0.58	0.45	0.45	0.1
Soil Water Parameter	θ_r	0.3	0.19	0.19	0.018
	θ_s	0.67	0.58	0.58	0.41

Table B. 2 Field Soil Water Retention Curve fitted parameters

Van Genuchten Parameters		Slope 2 Instr.1	Slope 2 Instr.2	Slope 2 Instr.3	Nobahar et al., 2019
Shape Parameters	α	0.097	0.095	0.095	0.0031
	n	1.9	1.7	1.7	2.75
	$m=1-1/n$	0.47	0.45	0.45	0.1
Soil Water Parameter	θ_r	0.21	0.19	0.19	0.018
	θ_s	0.6	0.58	0.58	0.41

Table B. 3 Field Soil Water Retention Curve fitted parameters

Van Genuchten Parameters		Slope 3 Instr.1	Slope 3 Instr.2	Slope 3 Instr.3	Nobahar et al., 2019
Shape Parameters	α	0.097	0.097	0.097	0.0031
	n	1.9	1.9	2.1	2.75
	$m=1-1/n$	0.47	0.47	0.52	0.1
Soil Water Parameter	θ_r	0.24	0.21	0.25	0.018
	θ_s	0.6	0.6	0.6	0.41

Table B. 4 Field Soil Water Retention Curve fitted parameters

Van Genuchten Parameters		Slope 4 Instr.1	Slope 4 Instr.2	Slope 4 Instr.3	Nobahar et al., 2019
Shape Parameters	α	0.095	0.095	0.095	0.0031
	n	1.7	1.7	1.7	2.75
	$m=1-1/n$	0.45	0.45	0.45	0.1
Soil Water Parameter	θ_r	0.19	0.19	0.19	0.018
	θ_s	0.58	0.58	0.58	0.41

Table B. 5 Field Soil Water Retention Curve fitted parameters

Van Genuchten Parameters		Slope 5 Instr.1	Slope 5 Instr.2	Slope 5 Instr.3	Nobahar et al., 2019
Shape Parameters	α	0.096	0.096	0.096	0.0031
	n	1.6	1.6	1.6	2.75
	$m=1-1/n$	0.46	0.46	0.44	0.1
Soil Water Parameter	θ_r	0.19	0.19	0.19	0.018
	θ_s	0.59	0.59	0.6	0.41

Table B. 6 Field Soil Water Retention Curve fitted parameters

Van Genuchten Parameters		Slope 6 Instr.1	Slope 6 Instr.2	Slope 6 Instr.3	Nobahar et al., 2019
Shape Parameters	α	0.095	0.095	0.095	0.0031
	n	1.7	1.7	1.7	2.75
	$m=1-1/n$	0.45	0.45	0.46	0.1
Soil Water Parameter	θ_r	0.19	0.19	0.19	0.018
	θ_s	0.58	0.58	0.61	0.41